nagra
National Cooperative for the
Disposal of Radioactive Waste

TECHNICAL REPORT 93-47

Grimsel Test Site

Developments in Hydrotesting, Fluid Logging and Combined Salt/Heat Tracer Experiments in the BK Site (Phase III)

April 1995

P. Marschall and S. Vomvoris (eds.)

P. Bossart, N. Correa, D. Guyonnet, B. Heinemann-Glutsch
E. Hurtig, R. Johns, T. Kohl, U. Kuhlmann, F. Müri, L. Rybach

Hardstrasse 73, CH-5430 Wettingen/Switzerland, Telephone +41-56-37 11 11

nagra National Cooperative for the Disposal of Radioactive Waste

TECHNICAL REPORT 93-47

Grimsel Test Site

Developments in Hydrotesting, Fluid Logging and Combined Salt/Heat Tracer Experiments in the BK Site (Phase III)

April 1995

P. Marschall[1] and S. Vomvoris[1] (eds.)

P. Bossart[2], N. Correa[1], D. Guyonnet[3], B. Heinemann-Glutsch[4], E. Hurtig[5], R. Johns[3], T. Kohl[6], U. Kuhlmann[7], F. Müri[7], L. Rybach[6]

1) NAGRA, Wettingen
2) Geotechnisches Institut AG, Bern
3) Colenco Power Consulting AG, Baden
4) GTC Kappelmeyer GmbH, Karlsruhe
5) GESO mbH, Jena
6) ETH, Zürich
7) ETH/VAW, Zürich

Hardstrasse 73, CH-5430 Wettingen/Switzerland, Telephone +41-56-37 11 11

"Copyright © 1994 by Nagra, Wettingen (Switzerland) / All rights reserved.
All parts of this work are protected by copyright. Any utilisation outwith the remit of the copyright law is unlawful and liable to prosecution. This applies in particular to translations, storage and processing in electronic systems and programs, microfilms, reproductions, etc. "

FOREWORD

Concepts for the disposal of radioactive waste in geological formations place a significant emphasis on acquiring extensive knowledge of the proposed host rock and the surrounding strata. For this reason, Nagra has, since May 1984, been operating the **Grimsel Test Site (GTS)** which is located at a depth of 450 m in the crystalline rock of the Aare Massif of the Central Swiss Alps. The general objectives of the research being carried out in this underground laboratory include

- the build-up of know-how in planning, performing and interpreting field experiments in various scientific and technical disciplines and

- the acquisition of practical experience in the development of investigation methodologies, measuring techniques and test equipment which will be of use during actual repository site explorations.

The GTS is operated by Nagra and, on the basis of a German-Swiss cooperative agreement, various experiments are carried out by Nagra, the "Bundesanstalt für Geowissenschaften und Rohstoffe, Hannover" (BGR) and the "Forschungszentrum für Umwelt und Gesundheit, München" (GSF). The Grimsel projects of both GSF and BGR are supported by the German Federal Ministry for Research and Technology (BMFT). NTB 85-46 (German version NTB 86-47) provides an overview of the German-Swiss investigation programme. In a special issue of the Nagra Bulletin 1988 (German version "Nagra Informiert 1+2/1988") the status of the programme up to 1988 is described.

This report was produced in accordance with the cooperation agreements mentioned above. The authors have presented their own opinions and conclusions which do not necessarily coincide with those of Nagra or its participating partners.

VORWORT

Bei Konzepten, welche die Endlagerung radioaktiver Abfällen in geologischen Formationen vorsehen, ist die Kenntnis des Wirtgesteins und der angrenzenden Gesteinsschichten von grundlegender Bedeutung. Die Nagra betreibt deshalb seit Mai 1984 das **Felslabor Grimsel (FLG)** in 450 m Tiefe im Kristallin des Aarmassivs. Die generelle Zielsetzung für die Arbeiten in diesem System von Versuchsstollen umfasst

- den Aufbau von Know-how in der Planung, Ausführung und Interpretation von Untergrundversuchen in verschiedenen wissenschaftlichen und technischen Fachgebieten, und

- den Erwerb praktischer Erfahrung in der Entwicklung und der Anwendung von Untersuchungsmethoden, Messverfahren und Messgeräten, die für die Erkundung von potentiellen Endlagerstandorten in Frage kommen.

Im Felslabor der Nagra werden, auf der Basis eines deutsch-schweizerischen Zusammenarbeitsvertrages, verschiedene Versuche von den beiden deutschen Partnern Bundesanstalt für Geowissenschaften und Rohstoffe, Hannover (BGR) und Forschungszentrum für Umwelt und Gesundheit GmbH, München (GSF) durchgeführt. Das Deutsche Bundesministerium für Forschung und Technologie (BMFT) fördert die Arbeiten der BGR und der GSF im FLG. Der NTB 85-47 (englische Version NTB 85-46) enthält eine Übersicht des FLG und die Zusammenfassung der Untersuchungsprogramme mit Status August 1985. In der Ausgabe 1+2/1988 des Heftes "Nagra informiert" bzw. der englischen Spezialausgabe "Nagra Bulletin 1988" ist der Stand der FLG Arbeiten anfangs 1988 beschrieben.

Der vorliegende Bericht wurde im Rahmen der erwähnten Zusammenarbeitsverträge erstellt. Die Autoren haben ihre eigenen Ansichten und Schlussfolgerungen dargelegt. Diese müssen nicht unbedingt mit denjenigen der Nagra oder des beteiligten Partner übereinstimmen.

AVANT-PROPOS

Lors d'etudes de concepts de stockage de déchets radioactifs dans des formations géologiques, on attache une grande importance à l'acquisition d'informations étendues sur la roche d'accueil et les formations rocheuses environnantes. C'est pour cette raison que la Cédra exploite depuis mai 1984 son **laboratoire souterrain du Grimsel (LSG)** situé à 450 m de profondeur dans le cristallin du massif de l'Aar, situé au milieu des alpes centrales. Les principaux objectifs des recherches effectuées dans ce réseau de galeries comprennent:

- l'acquisition de savoir-faire dans diverses disciplines techniques et scientifiques en ce qui concerne la conception, la réalisation et l'interpretation d'expériences in situ, ainsi que

- l'accumulation d'expériences pratiques dans la mise au point et l'application de méthodes d'investigation, de techniques et d'appareillages de mesure, qui pourraient être utilisés lors de l'exploration de sites potentiels de dépots finals.

Le LSG est exploité par la Cédra et diverses expériences y sont réalisées par celle-ci et deux institutions allemandes: la "Bundesanstalt für Geowissenschaften und Rohstoffe, Hannover" (BGR) et le "Forschungszentrum für Umwelt und Gesundheit GmbH, München" (GSF) dans le cadre d'un traité de collaboration germano-suisse. Les projets poursuivis au Grimsel par la BGR et le GSF sont financés par le Ministère fédéral allemand de la recherche et de la technologie (BMFT). Les rapports NTB 85-46 (version anglaise) et NTB 85-47 (version allemande) présentent un aperçu du laboratoire souterrain et un résumé des programmes de recherches avec état au mois d'août 1985. L'état d'avancement de ce programme en 1988 est présenté dans la publication "Cédra informe 1+2/1988" (version française) et "Nagra informiert 1+2/1988" (version allemande), ainsi que dans une édition spéciale en anglais (Nagra Bulletin 1988).

Le présent rapport a été élaboré dans le cadre des accords de collaboration mentionnés. Les auteurs ont présenté leurs vues et conclusions personnelles. Celles-ci ne doivent pas forcément correspondre à celles de Nagra ou ses partenaires participants.

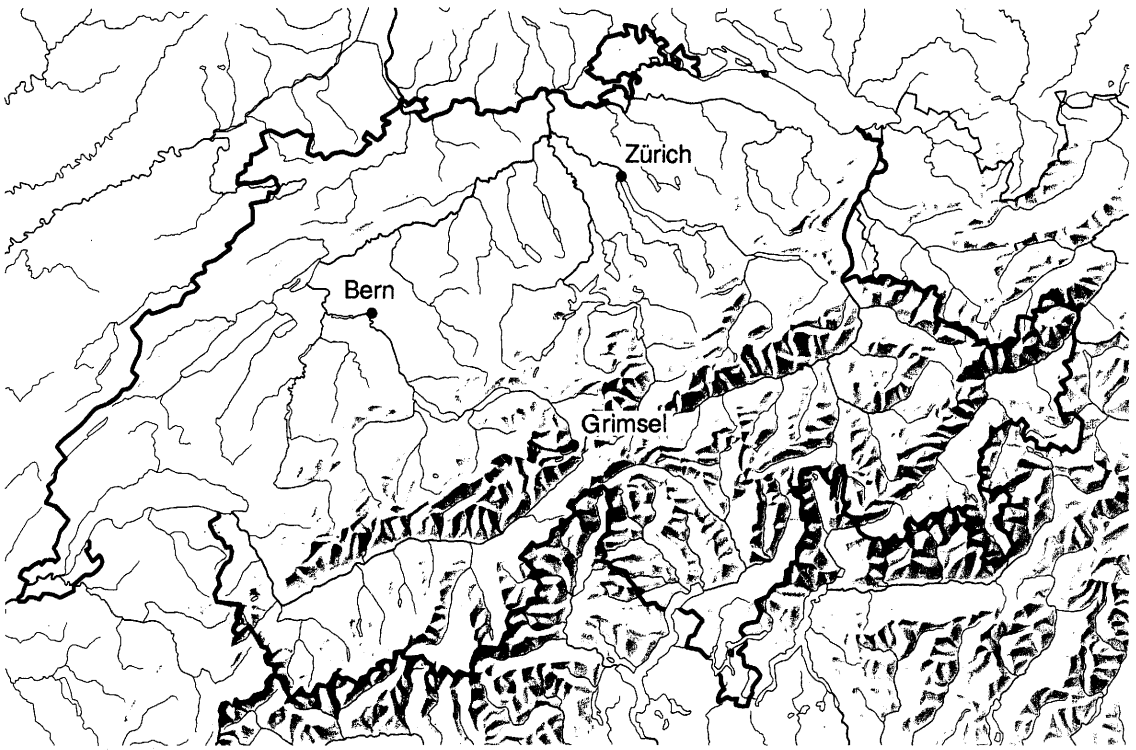

Reproduziert mit Bewilligung des Bundesamtes für Landestopographie vom 19.6.1991

Location of Nagra's underground test facility at the Grimsel Pass in the Central Alps (Bernese Alps) of Switzerland (approximate scale 1 cm = 25 km).

Geographische Lage des Nagra Felslabors am Grimselpass (Berner Oberland) in den schweizerischen Zentralalpen (Massstab: 1 cm = ca. 25 km)

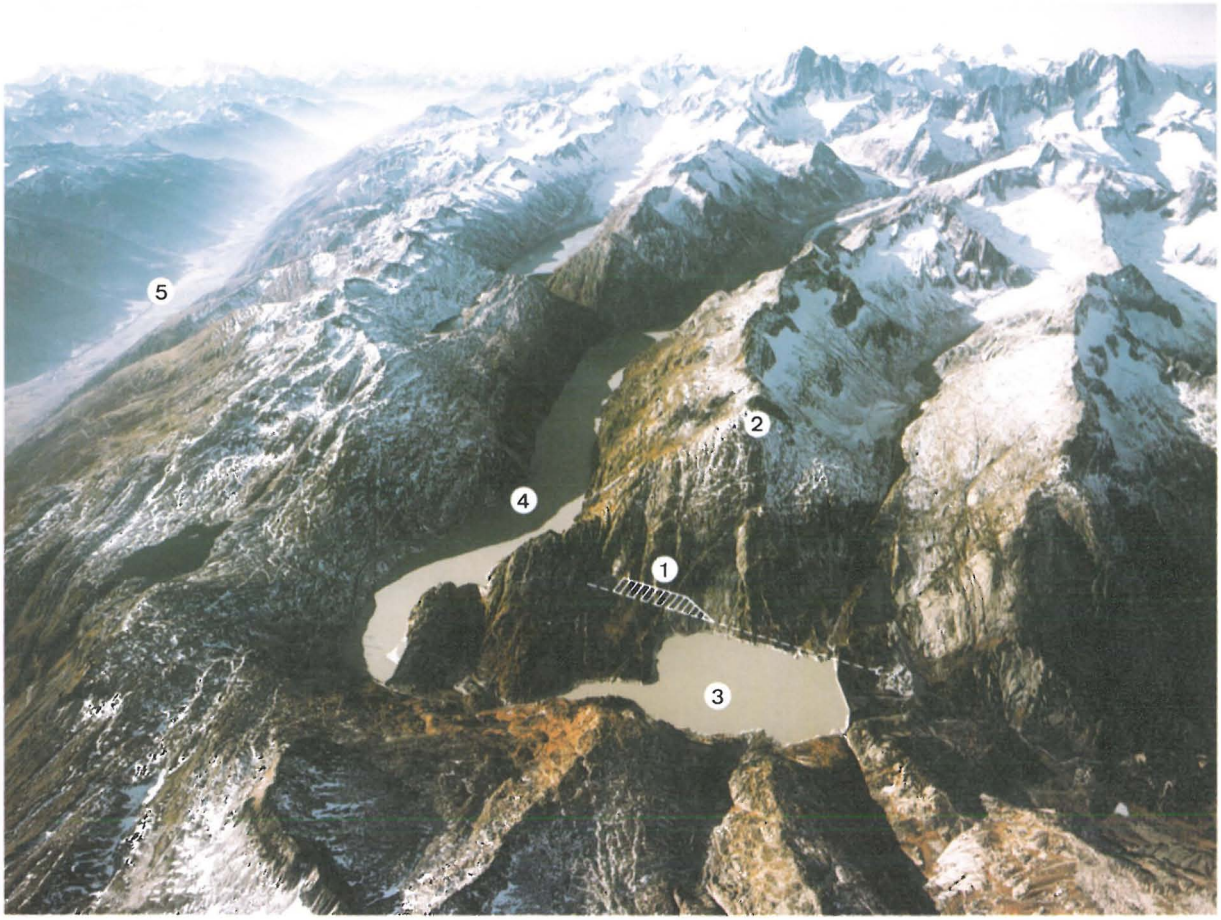

GRIMSEL-GEBIET

Blick nach Westen

1 Felslabor
2 Juchlistock
3 Räterichsbodensee
4 Grimselsee
5 Rhonetal

GRIMSEL AREA

View looking West

1 Test Site
2 Juchlistock
3 Lake Raeterichsboden
4 Lake Grimsel
5 Rhone Valley

FLG FELSLABOR GRIMSEL
GTS *GRIMSEL TEST SITE*

Situation

0 100 m

- Zugangsstollen/*Access tunnel*
- Fräsvortrieb/*by tunnel boring machine*
- Sprengvortrieb/*excavated by blasting*
- Zentraler Aaregranit ZAGR / *Central Aaregranite CAGR*
- Biotitreicher ZAGR / *CAGR with high content of biotite*
- Grimsel-Granodiorit / *Grimsel-Granodiorite*
- Scherzone/*Shear zone*
- Lamprophyr/*Lamprophyre*
- Wasserzutritt/*Water inflow*
- SB Sondierbohrung/*Exploratory borehole*
- US US Bohrung/*US borehole*

ZB	Zentraler Bereich/*Central facilities*
AU	Auflockerung/*Excavation effects*
BK	Bohrlochkranz/*Fracture system flow*
EM	El.magn. HF-Messungen/*-measurements*
FRI	Kluftzone/*Fracture zone investigation*
GS	Gebirgsspannungen/*Rock stresses*
HPA	Hydr. Parameter/*Hydr. parameters*
MI	Migration/*Migration*
MOD	Hydrodyn. Modellierung/*H. modeling*
NM	Neigungsmesser/*Tiltmeters*
UR	Untertageradar/*Underground radar*
US	Seismik/*Underground seismic testing*
VE	Ventilationstest/*Ventilation test*
WT	Wärmeversuch/*Heat test*

A — A Schnitt/*Section*

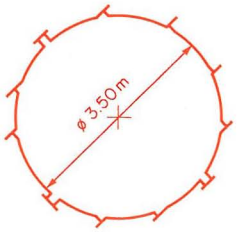

6/88

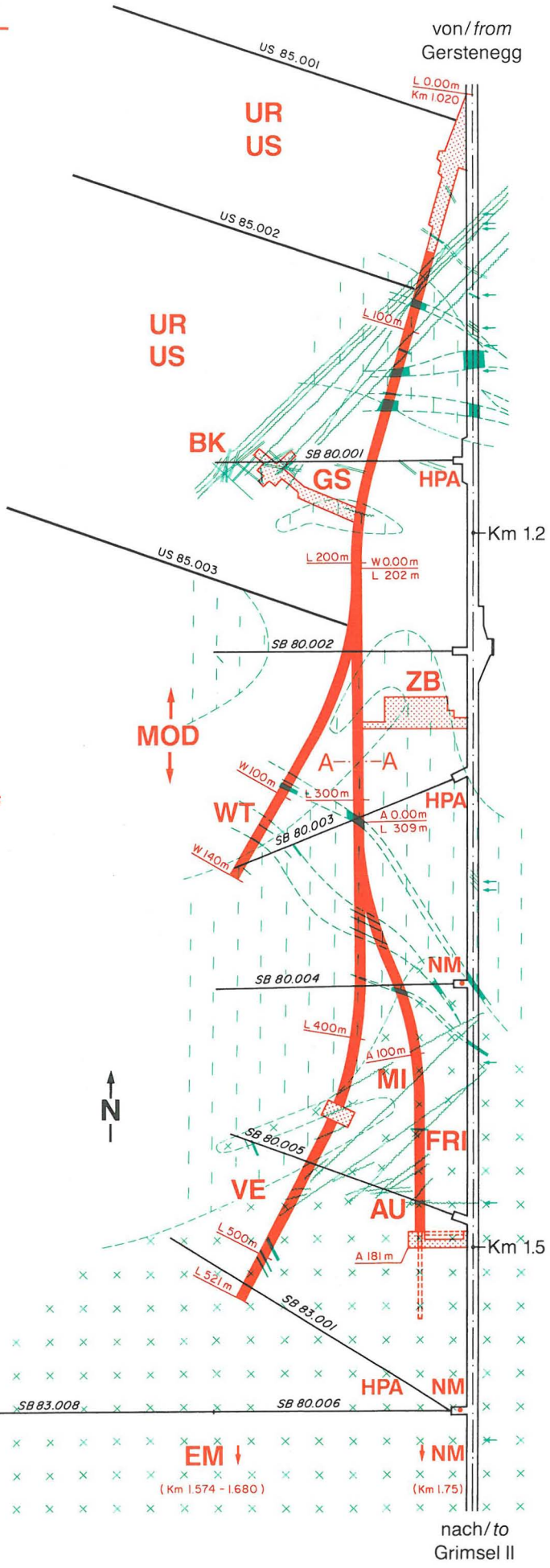

Abstract

This report documents the scientific studies carried out between January 1991 and December 1993 during Phase 3 of the Fracture System Flow Test Project (BK) at the Grimsel Test Site. The work was carried out as part of a joint investigation program between Nagra and the Federal Institute for Geoscience and Natural Resources (BGR), Hannover, and was aimed at developing new methods and concepts for characterizing flow processes in fractured formations. Numerical modeling of fracture flow also formed a focal point of the studies.

In the past, conventional fluid logging techniques (temperature/conductivity logging) in vertical boreholes have been used in Nagra's site investigation programs with considerable success. In the BK subproject "Fluid logging in inclined boreholes", it was shown that these techniques are either inapplicable, or have only restricted application, in inclined boreholes. New methods were therefore developed where the measuring probes are fixed in the boreholes before testing begins (**fluid logging with fixed probes**). Pilot tests showed that, in principle, this approach is also suitable for use in inclined boreholes.

Hydraulic crosshole tests represent the most frequently used method for investigating water-bearing fracture networks. The **Multiple Source Crosshole Test** (MSCT) was developed within the framework of the BK project with the aim of achieving an improved spatial resolution of the structure of such fracture networks. The principle of the MSCT is to carry out numerous short crosshole tests at different locations in the network to be characterized. A spectral interpretation procedure was developed for the MSCT, whereby hydraulic crosshole tests with variable flowrates can be evaluated using a diagnostic type curve procedure. A synthetic experiment was also performed to investigate a possible means of characterizing simple fracture structures deterministically on the basis of spectral hydrotest interpretations.

The focal point of the **Salt/Heat Tracer Test** (SHT) was characterization of the transport properties of fracture systems. The test focused around dipole tracer tests with complementary flow-fields (i.e. inversion of the dipole flow-field) and complementary tracers (NaCl and heat), which were aimed at providing a more detailed description of the complex transport processes in a fracture network. One particular aspect to be investigated was whether any information on the structure of the pore spaces in the fracture system can be derived from the differing transport behavior of salt (advective-dispersive) and heat (diffusion-dominated). Modeling of the field experiments clearly showed the sensitivity, and hence the selectivity, of such a test concept as regards different hypotheses of the fracture structure.

Data on structural geology and the results of hydrogeological tests from earlier phases of the BK project were synthesized to provide a conceptual hydrodynamic model of the BK fracture system. This was done using computer-aided **3D visualization** of the structural and hydrogeological data. Commercial graphics software was used to develop applications which fulfil the specific criteria of a structural geology/hydrogeological interpretation (e.g. spatial correlation of petrography, structural data, fluid logging results, etc.). The conceptual model then serves as a basis for formulating a numerical model which is used to **simulate fracture flow** in the BK fracture system.

The main objective of this work was not to provide a detailed hydraulic model of the flow-field at the test location, but rather to try out inverse modeling methods based on a discrete fracture zone model.

Besides the development of techniques which was achieved in Phase 3 of the Fracture System Flow Test Project, important information was also obtained on the hydrogeological characterization of the test location. For example, it was shown that the two lamprophyres to the north and south of the site almost completely decouple the BK fracture system from the surrounding test locations. The hydraulic system of the BK is therefore restricted and has a free surface which is controlled by drainage into the drift and by boundary influxes. Despite the large number of fractures identified from core logging, the component which is hydraulically active is very small. Hydraulic testing has shown that the significance of the so-called S-fractures in the vicinity of the northern lamprophyre has been underestimated in the past.

The numerical model was used for inverse modeling of a hydraulic crosshole test. Despite the relatively simple structure of the model, which was selected because of restricted timescales, the fit with observed data was surprisingly good. Finally a sensitivity study was carried out; this highlighted possibilities for improving the underlying structural model for application in future modeling studies.

Zusammenfassung

Der vorliegende Bericht dokumentiert die wissenschaftlichen Arbeiten, die im Rahmen des Projekts Bohrlochkranzversuch (BK) - Phase 3 von der Nagra in Auftrag gegeben und zwischen Januar 1991 und Dezember 1993 abgeschlossen wurden. Die Arbeiten sind Teil eines gemeinsamen Untersuchungsprogramms mit der Bundesanstalt für Geowissenschaften und Rohstoffe BGR (Hannover) mit dem Ziel, neue Methoden und Konzepte zur Charakterisierung von Fliessprozessen in geklüfteten Formationen zu entwickeln. Einen weiteren Schwerpunkt bildete die numerische Modellierung von Kluftströmungen.

In der Vergangenheit wurden konventionelle Fluid Logging Verfahren (Temperatur/ Leitfähigkeits-Logging) in den Standorterkundungsprogrammen der Nagra in Vertikalbohrungen mit grossem Erfolg eingesetzt. Im BK-Teilprojekt "Fluid Logging in geneigten Bohrungen" wurde nachgewiesen, dass diese Verfahren in Schrägbohrungen nicht bzw. in sehr beschränktem Umfang anwendbar sind. Es wurden daher neue Methoden entwickelt, bei denen die Messsonden vor Testbeginn stationär ins Bohrloch eingebaut werden (**Fluid Logging mit stationären Sonden**). Im Rahmen von Pilotuntersuchungen konnte die prinzipielle Eignung dieser Verfahren auch in geneigten Bohrungen bestätigt werden.

Hydraulische Crosshole Tests stellen die am häufigsten verwendete Erkundungsmethode in Kluftgrundwasserleitern dar. Der **Multiple Source Crosshole Test** (MSCT) wurde im BK-Projekt entwickelt mit dem Ziel, eine verbesserte räumliche Auflösung der Stuktur von solchen Kluftnetzwerken zu ermöglichen. Die Methode beruht auf der Durchführung einer Vielzahl von kurzen Crosshole Tests an verschiedenen Lokationen des zu charakterisierenden Kluftnetzwerks. Zur Interpretation des MSCT wurde ein spektrales Auswerteverfahren entwickelt, mit dem hydraulische Crosshole Tests mit variablen Fliessraten im Rahmen eines diagnostischen Typkurvenverfahrens ausgewertet werden können. Darüber hinaus wurde in einem synthetischen Experiment eine mögliche Vorgehensweise aufgezeigt, mit der einfache Kluftstrukturen auf der Grundlage von spektralen Hydrotestauswertungen deterministisch charakte risiert werden können.

Beim **Salz/Wärme-Tracertest** (SHT) stand die Charakterisierung der Transporteigenschaften von Kluftsystemen im Mittelpunkt. Den Kern des Versuchskonzepts bildeten Dipol-Tracertests mit komplementären Fliessfeldern (z.B. Umkehren des Dipol-Fliessfeldes) und komplementären Tracern (NaCl und Wärme), um eine umfassendere Beschreibung der komplizierten Transportvorgänge in einem Kluftnetzwerk zu ermöglichen. Insbesondere sollte überprüft werden, ob aus dem unterschiedlichen Transportverhalten von Salz (advektiv-dispersiv) und Wärme (diffusiv dominiert) Aufschlüsse über die Struktur der Porenräume im Kluftsystem gewonnen werden können. Die Modellierungen der Feldexperimente zeigen eindrucksvoll die Sensitivität und damit auch die Selektivität eines solches Versuchskonzepts bezüglich unterschiedlicher Hypothesen zur Kluftstruktur.

Im Sinne einer Synthese wurden die in den vergangenen Projektphasen am BK-Standort erhobenen strukturgeologischen Daten sowie die hydrogeologischen Tests aufgearbeitet und zu einem konzeptuellen hydrodynamischen Modell des BK-Kluftsystems zusammengefügt. Die Konzepterstellung erfolgte auf der Grundlage einer rechnergestützten **3D Visualisierung** der struktur- und hydrogeologischen Daten. Zu

diesem Zweck wurden mit einer kommerziellen Grafik-Software Applikationen entwickelt, die den spezifischen Kriterien einer strukturgeologisch / hydrogeologischen Interpretation genügten (z.B. räumliche Korrelation von Petrographie, Strukturdaten, Fluid Logging Ergebnissen etc.). Das erstellte konzeptuelle Modell diente schliesslich als Basis für ein numerisches Modell zur **Simulation von Kluftströmungen** im BK-Kluftsystem. Vorrangiges Ziel dieser Arbeiten war allerdings nicht eine umfassende hydraulische Modellierung der Fliessverhältnisse am Versuchsstandort, sondern die Erprobung von Methoden zur inversen Modellierung auf der Grundlage einer diskreten Kluftzonen-Modellierung.

In der Phase 3 des Projekts Bohrlochkranzversuch wurden neben den methodischen Entwicklungen wichtige Erkenntnisse zur hydrogeologischen Charakterisierung des Versuchsstandorts gewonnen. So konnte gezeigt werden, dass die beiden Lamprophyre im Norden und Süden des Standorts das BK-Kluftsystem hydraulisch fast vollständig von den umgebenden Versuchsstandorten entkoppeln. Das hydraulische System des BK ist daher beschränkt und besitzt eine freie Oberfläche, die durch die Entwässerung in den Stollen sowie durch die Randzuflüsse kontrolliert wird. Trotz der Vielzahl an Klüften, die anhand der Kernaufnahme erkannt wurden, ist der Anteil an hydraulisch wirksamen Klüften sehr klein. Im Rahmen der hydraulischen Tests konnte gezeigt werden, dass die hydraulische Bedeutung der sogenannten S-Klüfte im Bereich des nordlichen Lamprophyrs in der Vergangenheit unterschätzt wurde.

Mit dem Modell wurden inverse Modellierungen eines hydraulischen Crosshole Tests durchgeführt. Trotz der relativ einfachen Modellstruktur, die aufgrund des begrenzten Zeitrahmens gewählt worden war, gelang eine überraschend gute Anpassung der beobachteten Daten. In einer Sensitivitätsstudie wurde schliesslich aufgezeigt, auf welche Weise das zugrunde liegende Strukturmodell im Rahmen zukünftiger Modellierungen verbessert werden könnte.

Résumé

Ce rapport présente les travaux scientifiques qui ont été réalisés dans le cadre de la phase 3 du projet d'essais dans un faisceau de forages (BK) de janvier 1991 à décembre 1993 sous mandat de la Cédra. Ces travaux font partie d'un programme de recherche commun avec la BGR ("Bundesanstalt für Geowissenschaften und Rohstoffe", Hannovre) ayant pour objectif la mise au point de nouvelles méthodes et concepts pour la caractérisation des phénomènes de circulation d'eau dans des formations rocheuses diaclasées. Un autre point capital consistait à modéliser la circulation de l'eau dans des diaclases.

Des essais classiques de diagraphie de température et de conductivité ont été utilisés avec succès dans le passé par la Cédra dans des forages verticaux. Le projet partiel BK-diagraphies dans des forages inclinés a montré que ce procédé n'était pas applicable aux forages obliques, ou alors seulement de façon limitée. De nouvelles méthodes ont par conséquent été développées, dans lesquelles les sondes de mesure sont installées de manière fixe dans les forages avant le début des essais (**diagraphies avec sondes fixes**). Des essais pilotes ont confirmé, en principe, la validité de cette méthode pour des forages obliques également.

Des essais hydrauliques d'interférence entre plusieurs forages (crosshole) représentent la méthode d'exploration la plus fréquemment utilisée dans les aquifères diaclasés. Une méthode à source multiple, le **multiple source crosshole test** (MSCT), a été développée dans le cadre du projet BK avec pour objectif de permettre l'obtention d'une meilleure résolution spatiale de la structure de réseaux de diaclases. La méthode consiste à réaliser un grand nombre de courts essais de type crosshole en divers points du réseau de diaclases. Pour l'interprétation du MSCT, on a mis au point une méthode d'analyse spectrale par laquelle les essais hydrauliques entre forages peuvent être évalués pour des débits variables à l'aide d'abaques. Par une expérience synthétique on a de plus montré une marche à suivre possible par laquelle des structures simples de diaclases peuvent être caractérisées de façon déterministe sur la base de l'évaluation spectrale d'essais hydrauliques.

Lors des **essais de traçage par sel/chaleur** (SHT), la caractérisation des conditions de transport dans le système de diaclases était l'objectif premier. Des essais de traçage par dipôles (couple injection-soutirage) avec des champs d'écoulement complémentaires (par ex. par inversion du dipôle) ou avec des traceurs complémentaires (NaCl et chaleur) constituaient le coeur du concept des essais, afin de permettre une description plus complète des phénomènes de transport compliqués dans un réseau de diaclases. Il fallait notamment examiner si en raison des comportements de transport différents du sel (advectif-dispersif) et de la chaleur (diffusif dominant) on pouvait tirer des informations concernant la structure des espaces poreux dans le système de diaclases. La modélisation des essais de terrain montre de façon remarquable la sensibilité, et par là également la sélectivité, d'un tel concept d'investigation en ce qui concerne les différentes hypothèses relatives à la structure des diaclases.

Les données géologiques structurales et les résultats des essais hydrogéologiques des phases antérieures du projet BK ont été synthétisées dans un modèle hydrodynamique conceptuel du système de diaclases BK. Ceci a été fait à l'aide d'une **visualisation 3D** par ordinateur des données structurales et hydrogéologiques. On a

dans ce but développé, à partir d'un logiciel graphique du commerce, une application permettant une interprétation tenant compte des critères spécifiques de structures géologiques/hydrogéologiques (par ex. corrélation spatiale de la pétrographie, de données structurales, de résultats de diagraphies, etc). Le modèle conceptuel résultant a finalement servi de base à un modèle numérique de **simulation de la circulation dans les diaclases** pour le système de diaclases BK. Le but essentiel de ces travaux n'était pas la modélisation des conditions d'écoulement sur le site étudié, mais le développement de méthodes de modélisation inverse à partir de la modélisation d'une zone discrète de diaclases.

Au cours de la phase 3 du projet BK on a acquis, en plus des développements méthodologiques, des éléments importants pour la caractérisation hydrogéologique du site d'étude. On a pu monter par exemple que les deux lamprophyres situés au nord et au sud du système de diaclases BK découplent presque entièrement hydrauliquement des sites d'essais voisins. Le système hydraulique du faisceau de forages BK est donc limité et possède une surface libre contrôlée par le drainage dans les galeries et les apports latéraux. Seule une très petite partie des diaclases inventoriées sur les carottes est hydrauliquement active. Les essais hydrauliques ont montré que le rôle des diaclases dans les zones soi-disontes S a été sousestimé dans le passé. Le modèle développé a permis de réaliser des modélisations inverses d'un essai hydraulique de type crosshole. Malgré la structure relativement simple du modèle choisi en raison du temps limité disponible, la correspondance avec les données observées est étonnamment bonne. Une étude de sensibilité a finalement montré de quelle façon le modèle structural utilisé pouvait être amélioré dans le cadre de futures modélisations.

Table of Contents

Page

FOREWORD I

VORWORT II

AVANT-PROPOS III

Abstract IX

Zusammenfassung XI

Résumé XIII

Table of Contents XV

List of Tables XVIII

List of Figures XIX

1 INTRODUCTION 3

1.1 Background and scope 3
1.2 Complementary investigations 5
1.3 Report organisation and persons involved 8

2 FLUID LOGGING WITH A MOVING PROBE 11

2.1 Introduction 11
2.2 Field experiments 11
2.2.1 Equipment and test program 11
2.2.2 Results 12
2.3 Discussion and conclusions 18
2.3.1 Discussion of the results 18
2.3.2 Conclusions 19

3 FLUID LOGGING WITH FIXED PROBE ARRAYS 21

3.1 Introduction 21
3.1.1 Motivation 21
3.1.2 Objectives 21
3.1.3 Methodologies and pilot investigations 22
3.2 Fixed temperature probes: the discrete PT-100 probe array 23
3.2.1 Equipment 23
3.2.2 Field experiments 24
3.3 Fixed temperature probe arrays: The distributed optical temperature-sensing technique 29
3.3.1 Principles and fundamentals 29
3.3.2 Calibration and resolution 31
3.3.3 Equipment 33
3.3.4 Field experiments 33

3.4	Fixed temperature probe arrays: interpretation and discussion	37
3.4.1	Heat exchange in a system with countercurrent flow	37
3.4.2	Quantification of fluid logging	40
3.4.3	Interpretation of the fluid logging experiments with fixed probe arrays	41
3.4.4	Discussion of the results	45
3.5	Pilot investigations with a fixed sal/temp probe array	45
4	ANALYSIS OF SELECTED HYDROTESTS	47
4.1	Introduction and scope	47
4.2	Pressure recovery tests VE 478 and VE 484	48
4.3	Step withdrawal test VE 485	51
4.4	Summary and implications for the BK conceptual flow model	53
5	MULTIPLE SOURCE CROSSHOLE TEST (MSCT)	57
5.1	Introduction	57
5.1.1	Motivation for the MSCT	57
5.1.2	Objectives and outline of the MSCT analysis	58
5.2	The spectral analysis approach	59
5.2.1	Literature review	59
5.2.2	Fourier transform and the transmission function	60
5.2.3	Transmission functions for selected flow models	61
5.2.4	Numerical Fourier transform	66
5.2.5	Verification of spectral approach using GTFM	67
5.3	Modeling of a synthetic fracture zone system	69
5.3.1	A discrete model approach	69
5.3.2	Modeling with CASA	71
5.4	The MSCT field experiment	75
5.4.1	Procedure, equipment and data acquisition	75
5.4.2	Estimates of pressure losses	78
5.4.3	Crosshole test analyses	79
5.4.4	Single-hole analysis	80
5.4.4.1	Diagnostic plots for flow model identification	80
5.4.3.2	Calculation of cross-sectional area of the fracture network	83
5.4.3.3	Estimates of flow parameters using GTFM	83
5.5	Summary and Conclusions	88
6	THE SALT / HEAT TRACER EXPERIMENTS	91
6.1	Introduction and scope	91
6.2	Modeling heat and solute transport	92
6.2.1	Fundamentals	92
6.2.2	Simulator FRACTure	95
6.3	Design calculations for SHT experiment	97
6.3.1	Data basis and general approach	97
6.3.2	Discretization and model parameters	98
6.3.3	Prediction of the thermal response	99
6.4	Overview of the SHT experiments	102
6.4.1	The experimental arrangement and equipment	102

6.4.2 The experimental conditions 102
6.4.3 The experimental results 105
6.5 Model selection 106
6.5.1 Scope of modeling 106
6.5.2 Basic conceptual models and discretization 107
6.5.3 Flow and transport parameters 112
6.6 Simulation of solute and thermal transport 113
6.6.1 Approach 113
6.6.2 Solute transport 115
6.6.3 Thermal transport 119
6.7 Discussion of the results 121

7 VISUALIZATION AND CONCEPTUALIZATION OF HYDROGEOLOGICAL DATA IN FRACTURED ROCK 127

7.1 Introduction and scope 127
7.1.1 Objectives 127
7.1.2 Overview of the 3D visualization program AVS 128
7.2 Spectrum of applications 129
7.2.1 Visualization of major structural objects 129
7.2.2 Visualization of structural data from boreholes 130
7.2.3 Visualization of hydrogeological test data 133
7.3 Derivation of the conceptual model by 3D visualization 136
7.3.1 Basic derivation procedure for a discrete fracture zone model 137
7.3.2 Structural geology 140
7.3.3 Hydrogeological tests 143
7.3.4 The derivation of the deterministic fracture zone model 147
7.5 Summary and conclusions 153

8 FRACTURE ZONE MODELING 155

8.1 Introduction 155
8.1.1 Scope of the investigations 155
8.1.2 Objectives and chapter outlines 155
8.2 Conceptualization and data selection 156
8.2.1 Basic concepts 156
8.2.2 Data selection 159
8.2.3 Data processing 159
8.3 Methodology of inverse modeling 161
8.3.1 Direct Problem 161
8.3.2 Inverse Problem 162
8.4 FE discretization 163
8.4.1 Groundwater flow into small structures 163
8.4.2 Mesh generation procedure 164
8.4.3 Initial and boundary conditions 167
8.4.4 Time stepping scheme 168
8.5 Calibration and sensitivity analysis 169
8.5.1 Model structures 169
8.5.2 Prior information 171

8.5.3 Calibration results 172
8.5.4 Sensitivity analysis 176
8.5.5 Run-time environment 179
8.6 Principal findings and conclusions 180

9 HYDROGEOLOGICAL INVESTIGATIONS AT THE BK SITE 183

9.1 Hydrogeological investigations at the BK site: a retrospective 183
9.2 The current conceptual model of the BK fracture system 185

10 REFERENCES 187

List of Tables

Tab. 2.1: Summary of fluid logging experiments between the 27th and 30th of July 1992 12
Tab. 2.2: Comparison of fracture location by fluid logging and FEL 13
Tab. 3.1: Fluid logging in the boreholes BK 88.015 and BK 85.008 28
Tab. 3.2: Fluid logging experiments in the boreholes BK 85.015 and BK 85.005 ... 36
Tab. 3.3: Localization of fractures and quantification of flowrates 44
Tab. 4.1: List of main tests performed at the BK site since December 1989 48
Tab. 5.1: Analytical transmission functions for selected flow models 63
Tab. 5.2: Geometric parameters and hydraulic properties of the analytical models presented in Fig. 5.3 65
Tab. 5.3: Hydraulic parameters of the CASA model 69
Tab. 5.4: Results of the analysis of the CASA simulated data 73
Tab. 5.5: Summary of test sequence with relevant test parameters 78
Tab. 5.6: Equivalent fracture network cross-sectional areas 83
Tab. 5.7: Summary of results from GTFM analysis of single-hole data 86
Tab. 6.1: Material parameters used in the SHT design study 99
Tab. 6.2: Experimental layout parameters in the design study 100
Tab. 6.3: Summary of activities before and during the SHT experiments 104
Tab. 6.6: Range of material parameters used for the simulation of VE 520 112
Tab. 6.7: Parameters used for double-porosity simulation 118
Tab. 7.1: Petrography of cores, sampled from boreholes at the BK site 133
Tab. 7.2: The deriviation procedure of the conceptual flow model 139
Tab. 7.3: The BK conceptual models (Abbreviations: p = pressure, T = transmissivity, S = storativity, K = Hydraulic conductivity, S_S = Specific storativity) 148
Tab. 7.4: Traced inflows along observation boreholes. Injection borehole is BK 85.004 (6.7 - 107 m). ? = the traced inflow could not be linked with any structure (K, S) 150
Tab. 8.1: Computed intersections between fractures and BK boreholes for Model A 170
Tab. 8.2: Additional intersections between fractures and BK boreholes for Model B 171
Tab. 8.3: Evaluations of the objective function Z (equation 8.5) for the Model A variants 172

Tab. 8.4: Computed parameters, approx. 95 % confidence interval and standard deviations for model A.2 174
Tab. 8.5: Computed model parameters, approx. 95 % confidence intervals and standard deviations for Model B 176

List of Figures

Fig. 1.1: Ground plan of the BK test site 4
Fig. 1.2: Representation of the boreholes in the central BK area 6
Fig. 2.1: Schematic illustration of the conductivity probe traction procedure in the inclined boreholes of the BK site at the GTS 12
Fig. 2.2: Results of the fluid logging and FEL logging with a moving probe in the borehole BK 85.004 at the GTS performed on July 30th, 1992 14
Fig. 2.3: Results of the fluid logging and FEL logging with a moving probe in the borehole BK 88.014 at the GTS performed on July 29th, 1992 15
Fig. 2.4: Results of the fluid logging and FEL logging with a moving probe in the borehole BK 88.016 at the GTS performed on July 29th, 1992 16
Fig. 2.5: Results of the fluid logging and FEL logging with a moving probe in the borehole BK 88.018 at the GTS performed on July 27th, 1992 17
Fig. 2.6: Results of the FEL logging in the borehole BK 85.005 at the GTS performed in July 1992 18
Fig. 2.7: Results of the FEL logging in the borehole BK 88.015 at the GTS performed in July 1992 18
Fig. 3.1: Sketch of fluid logging with fixed probe arrays 23
Fig. 3.2: Fluid logging with fixed probe arrays (PT-100) performed in borehole BK 88.015 on April 20th, 1993. Temperature logs are shown with inter vals of 5 min 25
Fig. 3.3: Fluid logging with fixed probe arrays (PT-100) performed in borehole BK 85.008 on April 21st and 22nd, 1993. Temperature profiles are shown with time steps of a) 5 min and b) 10 min 26
Fig. 3.4: Fluid logging with fixed probe arrays (PT-100) performed in borehole BK 85.008 on April 22nd, 1993. Temperature profiles are shown with time steps of 5 min 27
Fig. 3.5: Principle of distributed fibre optic temperature sensing 29
Fig. 3.6: Spectrum of the backscattered light 30
Fig. 3.7: Equipment for fibre optic temperature measurements 32
Fig. 3.8: Fibre optic temperature-sensing cable consisting of optical fibres inserted in a steel tube and covered by a plastic mantle 32
Fig. 3.9: Fluid logging experiment borehole BK 88.015: the time interval between logs is 10 min (June 23rd, 1993) 34
Fig. 3.10: Fluid logging experiment borehole BK 85.005: the time interval between logs is 10 min (June 24th, 1993) 35
Fig. 3.11: Temperature-time-depth diagram borehole BK 85.005; free outflow; June 24th, 1993 from 14:45 36
Fig. 3.12: Scheme of the fluid logging arrangement comparable to a heat exchanger with countercurrent flow 37
Fig. 3.13: Estimation of relative flowrates in borehole BK 85.005 42
Fig. 3.14: Estimation of relative flowrates in borehole BK 85.008 43
Fig. 3.15: Estimation of relative flowrates in borehole BK 85.015 44
Fig. 4.1: Long duration pressure recovery tests: a) VE 478 and b) VE 484 50

Fig. 4.2: Pressure in BK 85.003 during withdrawal test VE 485 51
Fig. 4.3: Log-log plot of pressure data for test VE 485 after desuperposition 53
Fig. 4.4: Conceptual model of the BK site, derived from long-term hydrotests 54
Fig. 5.1: Schematic sketch of the Multiple Source Crosshole Test (MSCT) 57
Fig. 5.2: Conceptual aquifer models: a) radial composite system and b) radial flow with two linear boundaries 62
Fig. 5.3: Analytical transmission functions for different aquifer models 64
Fig. 5.4: Analysis of synthetic data sets: a) GTFM simulation for a double-porosity system and b) the corresponding transfer function, fitted by the analytical model 68
Fig. 5.5: Simulating crosshole tests with CASA: intersection of a) the S^- zone (#954) and b) the S^+ zone (#902) with the other fractures and borehole intervals of the model shown in Fig. 8.1 70
Fig. 5.6: Spectral analysis of synthetic crosshole data: transmission functions and fitted models 72
Fig. 5.7: Spectral analysis of synthetic crosshole data: transmission functions and fitted models 74
Fig. 5.8: Packer positions in the boreholes of the central BK area 76
Fig. 5.9: Spectral analysis of test VE 508: transmission functions 77
Fig. 5.10: Log-log representation of pressure data in BK 15-I1 during test VE 512. 81
Fig. 5.11: Measured head in BK 8-I2 during test VE 513 82
Fig. 5.12: Measured head in BK 5-I4 during test VE 452 82
Fig. 5.13: GTFM simulations of test VE 513: a) fit of the injection period and b) fit of the recovery 84
Fig. 5.14: GTFM simulation of test VE 503 85
Fig. 5.15: GTFM simulation of test VE 506 86
Fig. 5.16: GTFM simulation of test VE 510 87
Fig. 5.17: GTFM simulation of test VE 511 87
Fig. 6.1: Combining elements with different dimensions: lower dimension elements can be mapped in elements with higher dimension. Only for optical reasons the nodes are plotted separately 96
Fig. 6.2: Dimensions and size of the discretized domain for the design study (in continuous lines). The interpretation of experiment VE 520 required slightly (10 m) larger dimensions to the left and to the back (indicated with dashed lines). In this case the injection and extraction point were not centered around the midpoint of the total domain 98
Fig. 6.3: Solute transport simultations MS05-2, MS05-5 and MS05-10 for pulse injection, with different fracture aperture. C/Co is the ratio of the concentrations measured in the extraction and the injection interval in percent 100
Fig. 6.4: Predictions for the thermal breakthrough. $(T-T_i) / (T_o-T_i)$ is the ratio of the temperature differences in the extraction and the injection interval, where T_i is the initial temperature and T_o the maximum injection temperature. The curves of the models MW2-2, MW2-5, MW2-10 cannot be distinguished visually. The simulation MW1-4 did not show any thermal breakthrough. All curves have been calculated with a constant injection of heated water of except run MW4-10B, which assumes a week-long lasting injection 101
Fig. 6.5: Packer positions and fracture traces for the boreholes in plane B 103
Fig. 6.6: Scheme of the equipment for saline / heated water injection/extraction 103

Fig. 6.7: The experimental results during VE 520 - pressure, flow, concentration and temperature in (a) BK 5-I2 and (b) BK 15-I2 108
Fig. 6.8: Basic conceptual models: (a) single fracture, single porosity model, (b) single fracture model with preferential flow due to variable apertures, (c) single fracture, double-porosity model and (d) dual fracture, single porosity model 109
Fig. 6.9: Discretized model for the simulation of 2D solute transport 110
Fig. 6.10: Perspective view of the discretization of the lower part of rock matrix for simulating the 3D thermal transport. The 2D fracture plane is on the top of the discretized 3D body 111
Fig. 6.11: Comparison of models with different discretization and with variable vs. constant flowrates. The very fine discretized SFSP-models FP1 models FD1, FD2, FD3 are close to the model AM, which was the base model accepted for all following solute transport calculations. The maximum difference between these 4 models which assume constant flowrates is smaller than 5 %. Another interesting comparison contrasts model AM with VR that accounts for the measured variable flowrates 113
Fig. 6.12: Variation of aperture range for fixed dispersivity lengths (α_L = 2.5 m, α_T = 1.4 m) and 100 % porosity. The apertures are indicated in mm on their labels. VE 520: measurement curve 113
Fig. 6.13: Variation of dispersivity lengths with fixed aperture of 70 mm and 100 % porosity. The dispersivities are given on the Fig. table: mid column - α_L, right column - α_T 115
Fig. 6.14: Discretization of the single fracture, preferential flow models PF1 (a) and PF2 (b) with variable apertures in the range between 10 and 70 mm 116
Fig. 6.15: Single fracture, preferential flow model: variation of aperture on the fracture plane. The models are explained in the text 117
Fig. 6.16: Double-porosity approach: variation of fracture aperture, intermediate layer's permeabilities and dispersivity lengths. The models are described in the text 119
Fig. 6.17: Thermal simulation of VE 520: the curves SF1 and SF2 represent single fracture, single porosity models with apertures of 70 and 140 mm, respectively. The models DP3 to DP5 represent double-porosity models as specified in Tab. 6.7. DF1 and DF2 are dual fracture models with apertures of 35 and 70 mm. The shaded part of the thermal breakthrough curve was disturbed by cross coupling effects with the solute breakthrough 121
Fig. 7.1: Plan view of the BK site 131
Fig. 7.2: Compilation of structural information at the BK site, out of previous characterization 132
Fig. 7.3: Examples of AVS visualization in BK plane D
a) petrographic data 134
Fig. 7.3: Examples of AVS visualization in BK plane D
b) inflow locations along boreholes, c) pressure build-up and packer positions 135
Fig. 7.4: The formation of ductile conjugate shear-zones. a) undeformed state, b) deformed state. The matrix (part inbetween the shear-zones) always remains undeformed 141

Fig. 7.5: The structural fracture network 144
Fig. 7.6: S and K fractures of the structural model in plane D; L is the resulting fracture plane, which links the three boreholes 145
Fig. 7.7: AVS visualization in BK plane D .....
a) inflow locations, b) structural model combined with inflow locations .. 150
Fig. 7.8: The minimal fracture network (8 S fractures), many of the densely clustered S fractures are linked to 1 high transmissive S zone (horizontal cut at 1,730 m) 152
Fig. 8.1: Idealized system of fracture zones in the BK area 158
Fig. 8.2: Examples of final observation data processed by 'smoothing interpolation' compared to the original data sets 160
Fig. 8.3: Borehole discretization and corresponding mesh refinement 164
Fig. 8.4: Output of the different mesh generation tools (example of a K fracture, see also Fig. 8.1) 166
Fig. 8.5: Example of FE mesh for K fracture zone (#780), final mesh as output by BHOLE (2) (borehole refinement see Fig. 8.3) 167
Fig. 8.6: Comparison of computed and measured head variation for Model A.2 . 173
Fig. 8.7: Comparison of computed and measured head variation for Model B 175
Fig. 8.8: Sums of computed residuals (equation 8.9) for the individual test sections (run A.2) 178
Fig. 8.9: Gradient contributions (equation 8.10) for the individual test sections (run A.2) 178
Fig. 8.10: Sums (over time) of sensitivities (equation 8.11) and gradient contributions (equation 8.12) for individual test sections (run A.2) 179

PART I

INTRODUCTION

1 INTRODUCTION

P. Marschall and S. Vomvoris (Nagra)

1.1 Background and scope

For the performance assessment of radioactive waste repositories, special emphasis is placed on the evaluation of possible migration of nuclides from an underground repository through the geosphere. In the past, various processes have been identified, which may substantially affect subsurface transport of radionuclides. Since 1984, Nagra has been operating the Grimsel Test Site (GTS) to perform specific experiments, which aim to verify and further develop recent concepts of radionuclide transport in granitic rock. An overview of the GTS experiments can be found in LIEB (1988).

Within the scope of the **Fracture System Flow Test** (Bohrlochkranzversuch - BK) emphasis was placed on improving characterization techniques and the understanding of flow and non-reactive transport in complex fracture networks. This included the development of equipment and methodologies for the estimation of hydraulic and transport parameters in fractured rock, as well as numerical codes for simulation of fracture flow.

In **Phase 1 and Phase 2** of the research activities at the GTS (1985-1990), the Federal Institute for Geoscience and Natural Resources (BGR), the Hannover, Federal Republic of Germany was the principal investigator at the BK site. Numerous boreholes were drilled and detailed structural description was performed by fracture mapping and core analysis (BRÄUER et al. 1989, KEUSEN et al. 1989). Hydrotests and systematic tracer experiments were also conducted. A summary of these investigations can be found in PAHL et al. (1992).

Towards the **end of Phase 2**, Nagra strengthened its participation, focusing on the development of new techniques in fluid logging and hydraulic crosshole testing (VOMVORIS & FRIEG 1992).

In **Phase 3** (1991-1993), Nagra's investigation program within the joint project encompassed research activities predominantly aimed at solving pertinent methodological and equipment questions which have emerged during Nagra's current exploration programs for low-level as well as for high and intermediate level waste (LLW and HLW/ILW). The main topics and accomplishments during Phase 3 can be summarized as:

- **Fluid logging in inclined boreholes**

  Fixed probe arrays have been developed and tested, allowing for fluid logging in inclined boreholes and even in boreholes which are oriented upwards.

- **Hydraulic crosshole testing**

  Improved hydrotest arrangements and test procedures were tested and new methods for hydrotest analysis have been developed, providing a better spatial resolution of hydraulic parameters in fracture networks.

- **Salt/Heat Tracer Test**

  A combined Salt/Heat Tracer Experiment was performed to investigate the applicability of heat as a non-reactive, easy-to-detect tracer, which potentially could help to identify conceptual models for transport in fractured networks where hydrochemistry should not be disturbed.

- **Visualization and simulation of fracture flow**

  A 3D visualization software package was adopted to develop a strategy for the conceptualization of the multitude of field data, collected during previous investigation phases. The resulting conceptual model was used to develop a numerical model for fracture flow simulations in the BK.

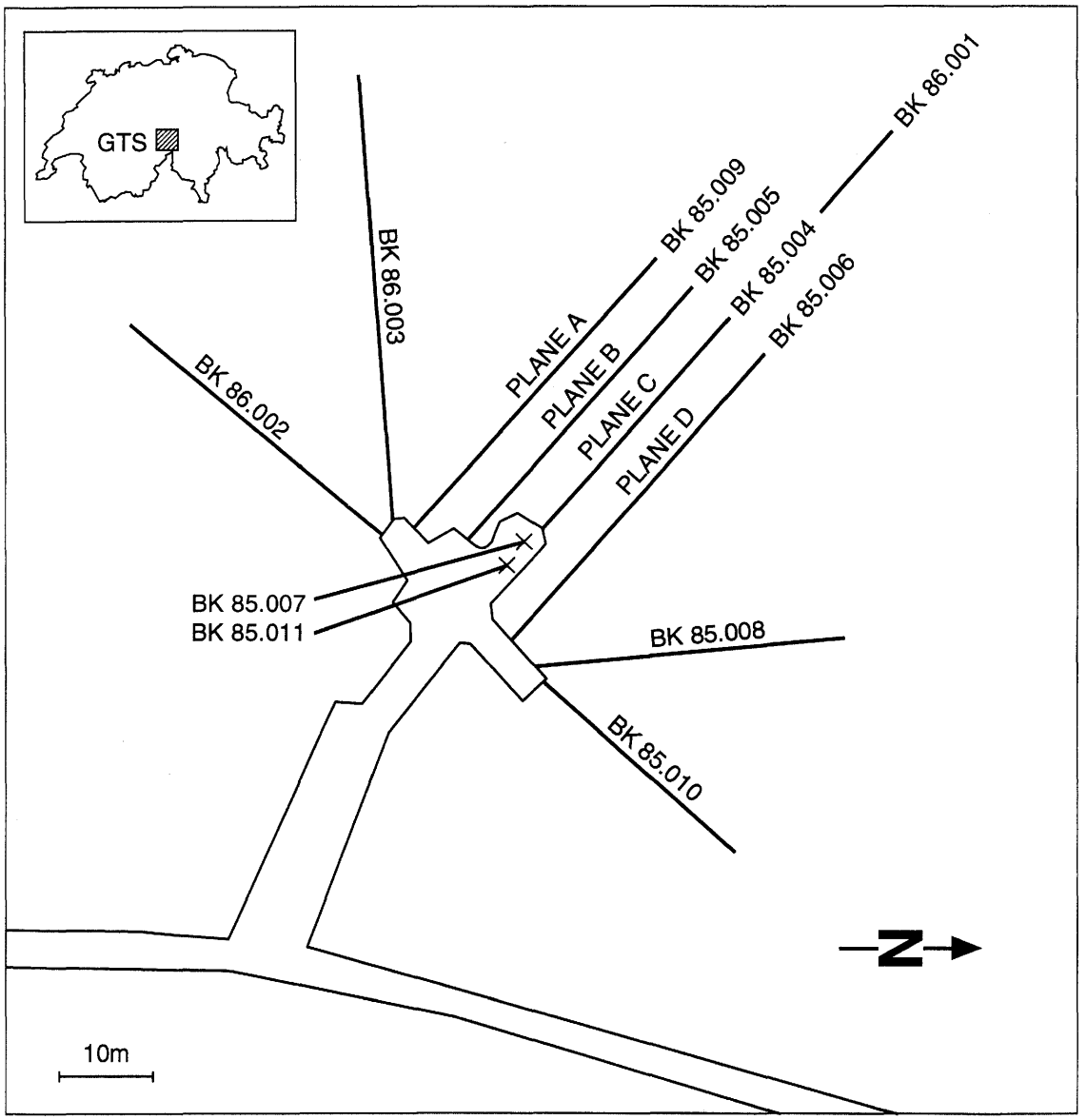

Fig. 1.1: Ground plan of the BK test site

About 20 boreholes have been drilled to investigate the highly permeable fracture zone in the vicinity of the BK site. Fig. 1.1 shows a schematic representation of the test site with a ground plan of the BK cavern.

The central part of the area under investigation was explored by four fan-like arrangements of boreholes (plane A - D). Cross-sections of these planes are given in Fig. 1.2, including total depth and inclination of the boreholes.

1.2 Complementary investigations

As part of the joint research project, the BGR carried out its own investigation programme at the BK site. In addition to the main objectives outlined above, this programme, which was approved by Nagra, also included specific studies on developing methods and equipment for measuring fracture flow and on the possibility of simulating material transport processes in fractured rock zones.

Development of equipment for determining fracture flow

The reliability of the packer and probe systems was further increased by replacing interference-prone components. The system for compressed air supply and distribution to the packers was completely renewed. An increased element of redundancy in the data acquisition system reduces data losses which may occur if there are perturbations during testing. A new pumping assembly was developed for the long-term injection tests.

The recently developed multipacker-combiprobe system was tested for the first time in water-saturated boreholes. The system consists of a bottom probe, several probe-packer combinations (injection probes) and a top probe with connecting socket. The measurement intervals are connected to the injection line, which runs along the probe string, by computer-controlled shut-off units. All intervals can be opened and closed at will, which results in a wide range of injection and extraction possibilities.

The measured signals are digitized by the probe computer and transferred to the data logger in the cavern. The multipacker-combiprobe system is controlled with the program PC_MULI, which can be run on DOS computers. The necessary data (test configuration, calibration data, channel assignment) are input by the user via interactive communication and then stored in files. The process conditions and the measured values are shown on-line on the screen. All probe functions ("open interval", "close interval", "shut-in") can be menu-triggered during the measurement phase.

Software development - program system DURST/Rockflow

The modular program system DURST/Rockflow was systematically extended and tested to meet the requirements of the in-situ tests. In the actual computational model, the transport module was extended to allow free selection of an initial boundary condition; this provides a better fit with complex structures in the domain to be modeled. The program system also contains a new version of the gas model. This subroutine allows simulation of gas flow processes in a fracture network.

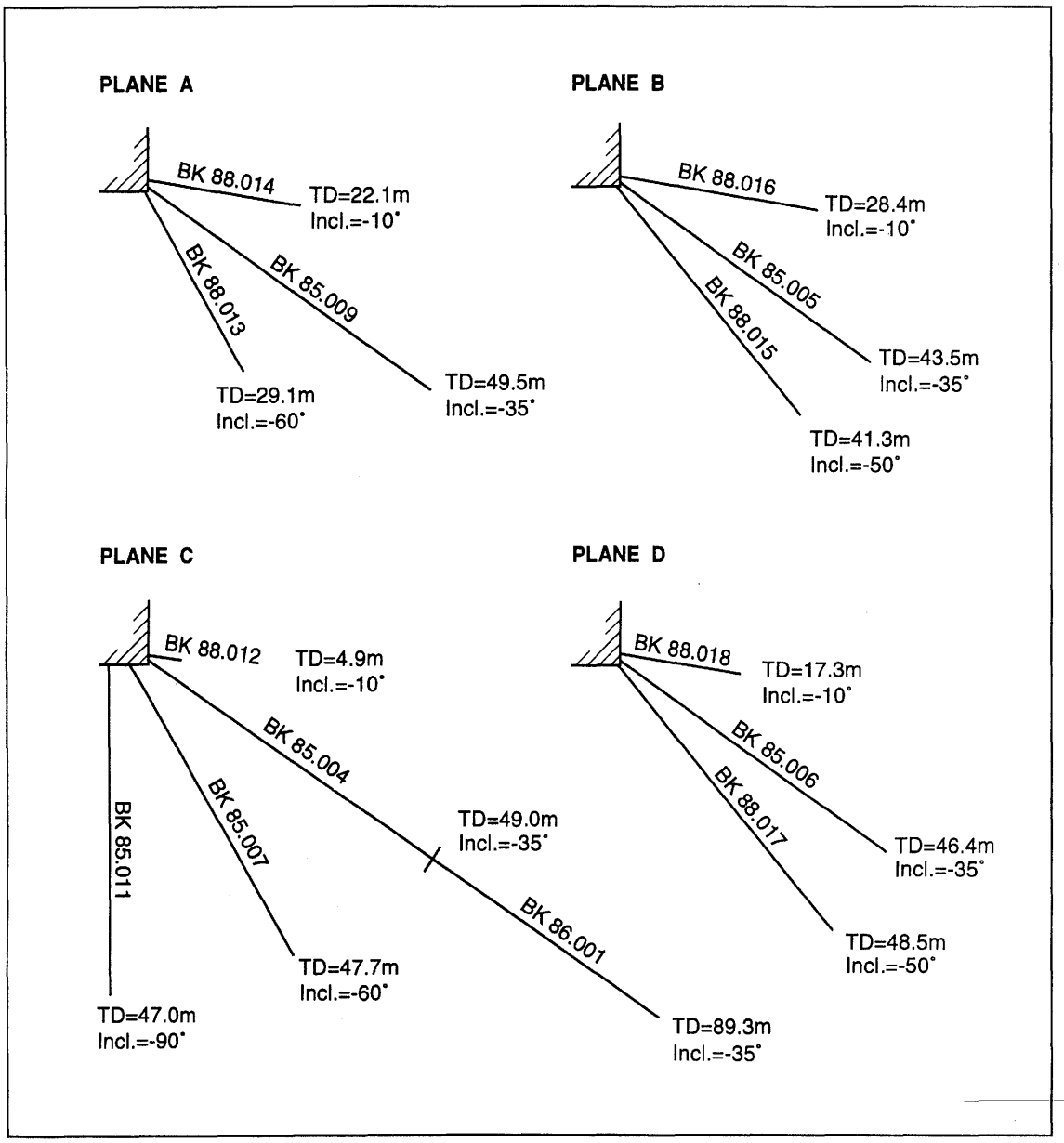

Fig. 1.2: Representation of the boreholes in the central BK area

Multiphase flow

The simulation of multiphase flow with the numerical model DURST represents a new aspect of the work being carried out in the BK project. In order to approximate such multiphase processes in a fractured-porous medium, it is necessary to represent the fluid phases themselves, but also their mutual interaction as determined by the site geology. Possible approaches from the relevant literature were processed theoretically and then integrated into a mathematical formulation. For fracture flow systems, this mathematical formulation gives the relationships between capillary pressure and saturation on the one hand and relative permeability and saturation on the other. The result of this study was the "gas model" finite-element program.

Hydraulic testing at the BK site

As in previous phases, the in-situ hydraulic tests carried out at the BK site also formed the focal point of the work in Phase III of the fracture system flow test project. These tests can basically be divided into two categories: the tests investigating the **stress-dependent permeability** of the fractured rock were carried out in the peripheral zone (BK 86.003 and 85.003) and gave no indication of any significant stress-dependence of this parameter. The **tracer experiments** (see below) and pre-tests for the tracer experiments were carried out in the central area of the BK cavern. These also included interference tests and fluid logging tests aimed at identifying inflow points and detecting potential flow paths. The objective of these tests was to determine the transport rate of (toxic) materials in fractured rock.

Tracer tests and their simulation

The development of the tracer tests moved towards longer duration experiments over greater distances, with the aim of simulating the flow and transport characteristics of such tests in a numerical model. Great importance was therefore attached to defining all the boundary conditions as accurately as possible, including drip points and their tracer concentrations.

In tracer test VE 483, a salt solution with 1,000 µS/cm was injected over a period of 13 days and a distance of approx. 25 m. In tracer test VE 493, over a distance of approx. 70 m, the flow path crossed three intersecting fracture systems. In this case, the brine tracer with a conductivity of 10,000 µS/cm was injected over a period of 24 hours. In tracer test VE 520 (see Chapter 6), salt and heat were used as tracers for the first time; analytical solutions were used for evaluating heat transport in a fracture-matrix system (2D-advective, 1D-conductive).

All three tests were calculated with the program system DURST/Rockflow in simulation runs with systematic parameter variations. A mass balance was set up for verifying the flow paths in the rock.

As was already assumed from previous experience, the measurement and calculation results show that, even over greater distances, flow paths can be identified in a fracture system. The spatial distribution of the tracers indicates a hydraulic link between fracture systems.

Desk study

A desk study was initiated in the second half of Phase III of the fracture system flow test. This provides an overview and a comparative evaluation of the in-situ tests being carried out at the Grimsel Test Site, the supporting laboratory experiments, the data which have been collected and the numerical techniques and models used to simulate the in-situ tests. The study focuses on the fracture system flow test, the ventilation test and the migration experiments, since these all relate to the question of hydraulic material transport.

1.3 Report organisation and persons involved

The research activities during Phase 3 of the investigation program at the BK site is summarized in the form of an edited report. As described in Section 1.1, the investigations consist of major subtasks, which are presented in Parts II - V.

Part II summarizes the present experiences with fluid logging in inclined boreholes. In Chapter 2 (B. Heinemann-Glutsch), the results of a fluid logging experiment with conventional methodology are presented. The field tests were carried out by GEOTEST (Zollikofen). Chapter 3 (B. Heinemann-Glutsch, E. Hurtig, P. Marschall) describes the investigations of fluid logging with stationary temperature probe arrays. Fluid logging experiments with stationary temperature probes were performed by GTC (Karlsruhe) and by GESO (Jena).

Part III focuses on the analysis of hydrotests. Chapter 4 (D. Guyonnet) summarizes the new analysis of previous hydrotests performed by BGR. The main objective is to characterize the general description of the hydraulic behavior of the BK site, which includes outer boundaries and recharge conditions. Chapter 5 (D. Guyonnet, P. Marschall, R. Johns) deals with the Multiple Source Crosshole Test (MSCT). The field experiments are described and a spectral method for the analysis of crosshole tests is presented.

Part IV, Chapter 6 (Th. Kohl, P. Marschall, N. Correa, L. Rybach) documents the field experiments and the modeling activities during the Salt/Heat Tracer Test. The field experiments were carried out by BGR under the supervision of S. Mohr (University of Heidelberg). Numerical simulations of both solute and heat transport were done by Th. Kohl (ETH Zürich).

Part V is concerned with the development of conceptual models of fracture flow in the BK area. In Chapter 7 (F. Müri, N. Correa, P. Bossart); a 3D visualization tool is presented, which is used to develop a reasonable model of fracture flow at the BK site. This concept forms the basis for the fracture flow simulations, described in Chapter 8 (U. Kuhlmann, N. Correa).

Acknowledgements

The authors gratefully acknowledge the efforts of a large number of individuals who have contributed to the Grimsel Fracture Flow Experiment. Particularly appreciated is the extensive work of L. Liedtke, A. Götschenberg, M. Jobmann and W. Siemering from BGR, who were responsible for the test equipment.

The technical staff and local administration at the GTS (T. Baer, H. Abplanalp and W. Kickmaier) provided helpful assistance during the field experiments.

The manuscript benefited from critical reviews by R. Johns (Colenco), W. Kinzelbach (University of Heidelberg), H. Wilhelm (University of Karlsruhe) and U. Spring (Simultec).

Finally we would like to acknowledge B. Frieg, who was responsible for the planning of the experimental phase BK-III.

PART II

FLUID LOGGING IN INCLINED BOREHOLES

2 FLUID LOGGING WITH A MOVING PROBE

B. Heinemann-Glutsch (GTC Kappelmeyer GmbH, Karlsruhe)

2.1 Introduction

Between the 27th and the 30th of July 1992, conductivity / temperature logging (sal/temp logging) was performed in four inclined boreholes (BK 85.004, BK 88.014, BK 88.016 and BK 88.018) of the BK site at the Grimsel Test Site. In addition, Focused Electro Logs (FEL) were run in these boreholes as well as in BK 85.005 and BK 88.015. The tests were performed by GEOTEST (Zollikofen) and the data analysis was done by COLENCO PC (GUYONNET 1992).

The objectives of the field investigations were:

- to identify the main inflow zones with a view to the determination of packer positions required for the MSCT (Multiple Source Crosshole Hydraulic Test, see Chapter 5)
- to test the performance of conventional fluid logging in subhorizontal boreholes (inclination about 10°)
- to evaluate FEL for the detection of inflow zones.

2.2 Field experiments

2.2.1 Equipment and test program

The fluid logging with a moving probe consists of continuous conductivity and temperature (sal/temp) logging inspace i.e. during the movement of the measuring probe into the borehole at constant speed. In inclined boreholes the conductivity probe drags along the borehole wall, not allowing a smooth logging procedure. To ensure a relatively constant movement of the tool, it was connected with a cable to a pulley fixed at the bottom of the borehole (Fig. 2.1). The procedure was especially required in the subhorizontal boreholes, where irregularities at the borehole wall would impede progress. The measuring tool velocity was relatively constant during logging with approximately 5.8 m/min.

Between the 27th and the 30th of July 1992, sal/temp logging was performed in four boreholes of the BK area, namely 85.004, 88.014, 88.016 and 88.018 (Fig. 1.2). In borehole BK 85.004, with a total depth of 138.3 m, flushing was possible only to 70 m depth. To obtain satisfactory results from this borehole, the fluid logging was run twice. In BK 88.014 and BK 88.018 the probe dragged along the borehole wall and got "stuck" in the boreholes several times. Considerable force had to be applied to free the probes, which influenced the quality of the corresponding data. For all experiments the flushing fluid conductivity was 1790-1800 µS/cm. The detailed information relative to test conditions and performances is documented in GUYONNET (1992). An overview of the performed tests is given in Tab. 2.1:

Tab. 2.1: Summary of fluid logging experiments between the 27th and 30th of July 1992

Borehole id. number	Date	Flushing time	Logging time	Number of runs	Total depth (m)	Logging depth (m)
BK 88.018	27.07.92	14:04-14:19	11:24-14:52	7	17.3	15.7
BK 84.004	28.07.92	09:21-11.24	11:26-14.25	7	138.5	69.9
BK 88.014	29.07.92	07:28-07.48	07:56-10:04	7	22.12	20.6
BK 88.016	29.07.92	12:49-13:11	13:15-14:51	6	28.4	26.6
BK 85.004	30.07.92	08:03-09:59	07:35-14:20	7	138.3	70.6

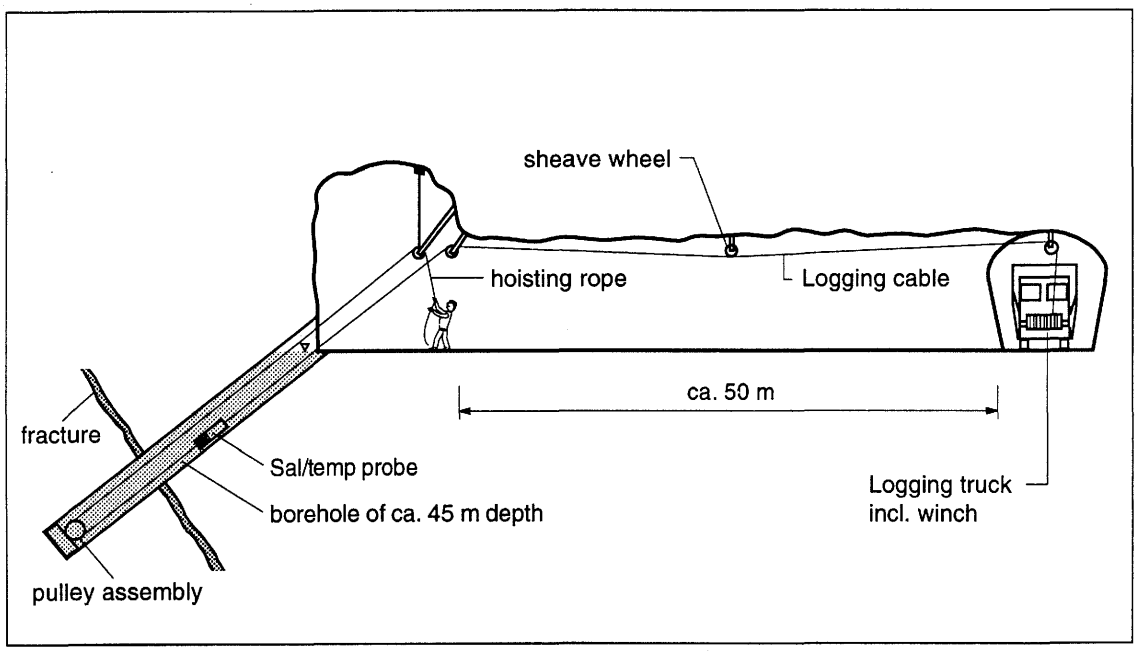

Fig. 2.1: Schematic illustration of the conductivity probe traction procedure in the inclined boreholes of the BK site at the GTS

2.2.2 Results

To illustrate the results of the fluid logging the salinity and temperature logs were plotted versus depth. In addition, FEL logs were run for each borehole. Figs. 2.2 to 2.5 show the three plots of conductivities (a), temperatures (b) and FEL (c) for the boreholes BK 85.004, BK 88.014, BK 88.016 and BK 88.018; Figs. 2.6 and 2.7 represent the FEL logs for the two additional boreholes BK 85.005 and BK 88.015 respectively. In general, indications of inflow points are clearly seen in the conductivity logs as well as in the temperature logs. Some of the anomalies identified in the FEL log coincide with major inflow zones.

Due to density differences between the flushing water and the formation water, density-driven separation of freshwater and saltwater occurred within each borehole, resulting in noise effects influencing the records. Nevertheless, the detection of inflow zones was successful and a summary of the fracture locations for each borehole identified from fluid logging with a moving probe and from FEL logs is given in Tab. 2.2.

BK 85.004 (Fig. 2.2):

The fluid logging was run twice in BK 85.004. On July 28th a major inflow zone was detected in the conductivity log to be at 8 m depth. Due to technical problems during the first runs, BK 85.004 was logged again on July 30th (Fig. 2.2). The first log of this second phase was measured before flushing and is particularly useful for the identification of inflow zones as it shows the evolution since the last log measured on July 28th at 14:25. Minor inflow locations were identified at 32 m, 34 m, 39 m, 44 m, 49.2 m, and possible inflows at 57 m and 69 m depth. However, there is no development of these inflow points seen, as expected but the salinity decreases more or less uniquely along the logged section between 15 and 70 m. This behaviour is explained by flow separation due to density differences between the flushing water and formation water. In addition to the fracture depths detected in sal/temp logs, the FEL log shows some more zones with low resistivity values, indicating locations of fractures. These are illustrated in Fig. 2.2c.

BK 88.014 (Fig. 2.3):

The conductivity log reveals evidence of one major inflow zone located between 17.5 m and 18.5 m depth. Minor inflow locations were detected at 9.5 m and 11.8 m depth. The small conductivity anomaly at 20.4 m depth as well as the zone at 17.5-18.5 m depth correspond eventually with the anomalies identified in the FEL log.

BK 88.016 (Fig. 2.4):

Major inflow locations were detected in the conductivity as well as in the temperature logs at 19.3 m and 22.1 m depth. Minor inflow locations are at 24.1 m and 25.2 m depth. The latter zone coincides with the anomaly in the FEL log at 25.5 m depth, indicating an inflow zone, whereas all others are not shown.

BK 88.018 (Fig. 2.5):

One major inflow zone was observed between 14.5 m and 16 m depth in the conductivity and temperature log. This inflow zone is confirmed by the FEL log showing anomalies at 15.9 m and 16.1 m depth. It is remarkable that the salinity logs are rather noisy, which can be attributed to an incomplete cross-sectional mixing in the borehole due to density effects.

Tab. 2.2: Comparison of fracture location by fluid logging and FEL

Borehole id. number	Fracture locations from fluid logging (in m along hole)	Fracture locations from FEL logs (in m along hole)
BK 85.004	8, 32, 34, 39, 44, 49.2, 57(?), 69(?)	
BK 88.014	9.5, 11.8, 17.5-18.5	17, 20
BK 88.016	19.3, 22.1, 24.1, 25.2	25.5
BK 88.018	14.5-16	15.9, 16.1

a) Conductivity logging

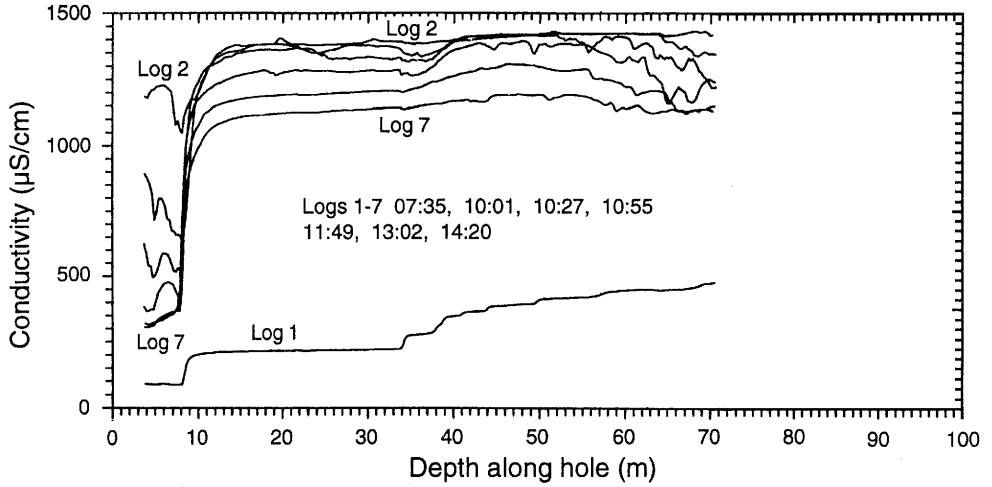

b) Temperature logging

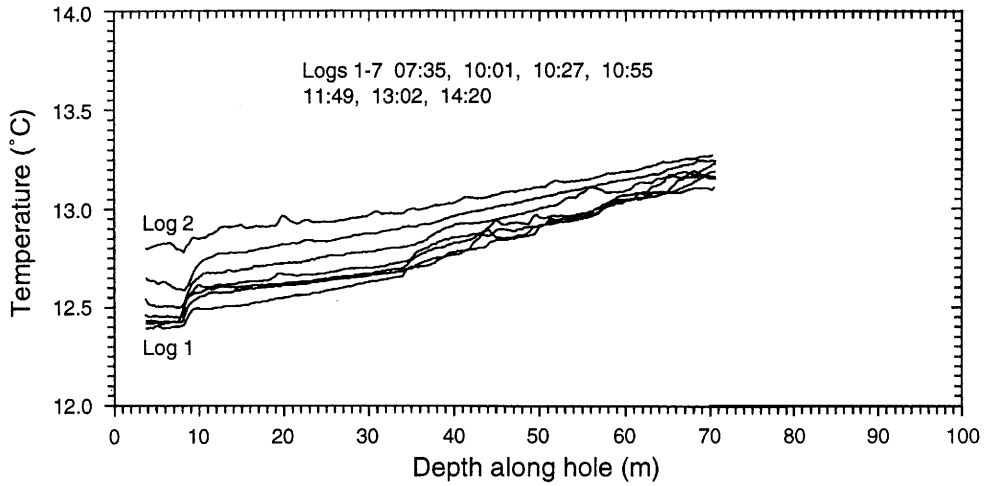

c) FEL log

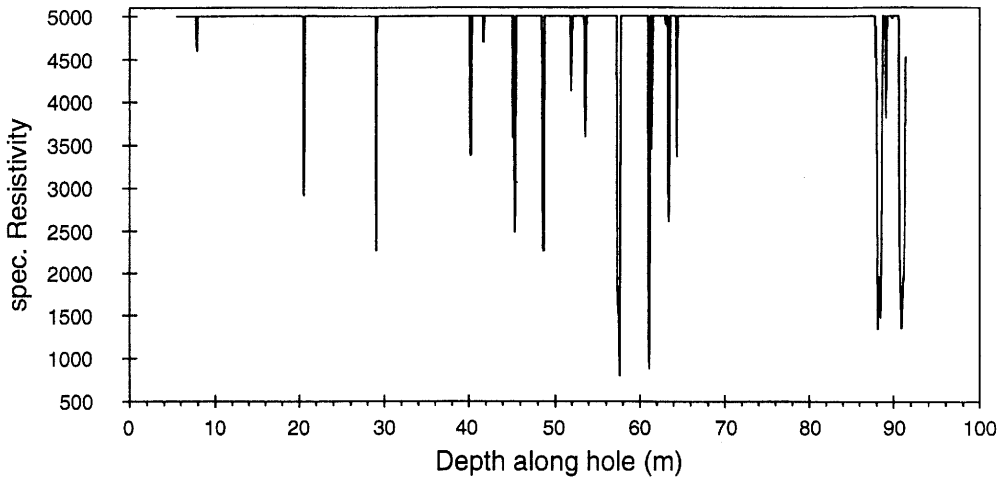

Fig. 2.2: Results of the fluid logging and FEL logging with a moving probe in the borehole BK 85.004 at the GTS performed on July 30th, 1992

a) Conductivity logging

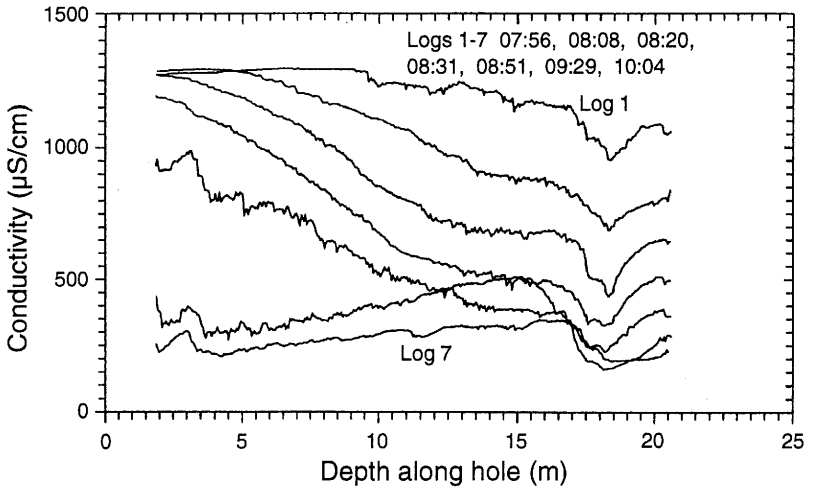

b) Temperature logging

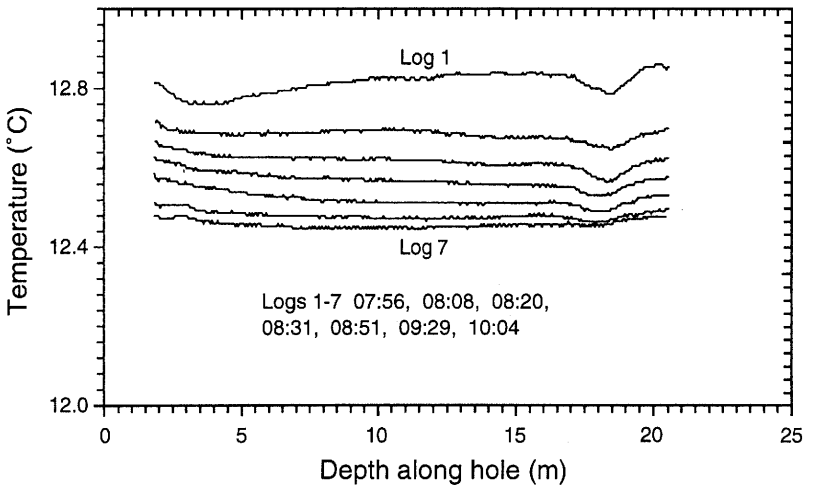

c) FEL log

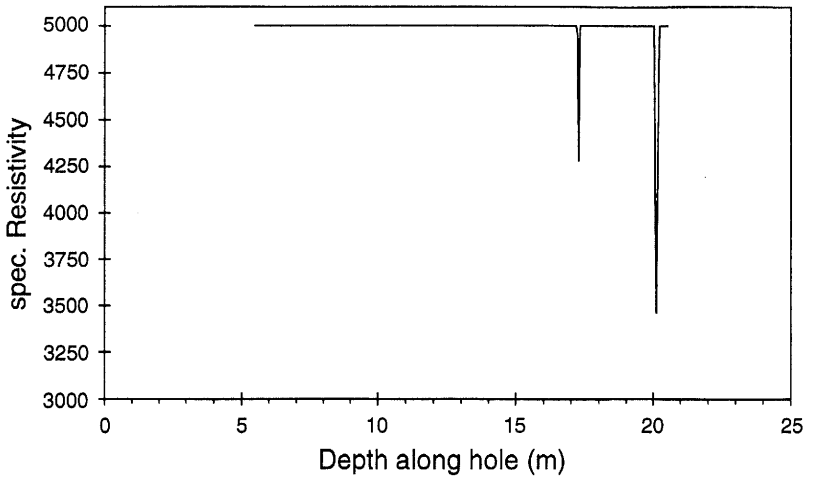

Fig. 2.3: Results of the fluid logging and FEL logging with a moving probe in the borehole BK 88.014 at the GTS performed on July 29th, 1992

a) Conductivity logging

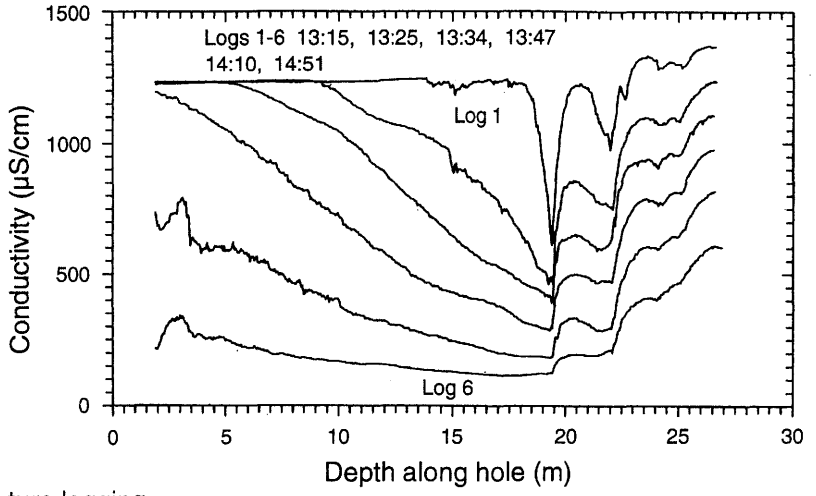

b) Temperature logging

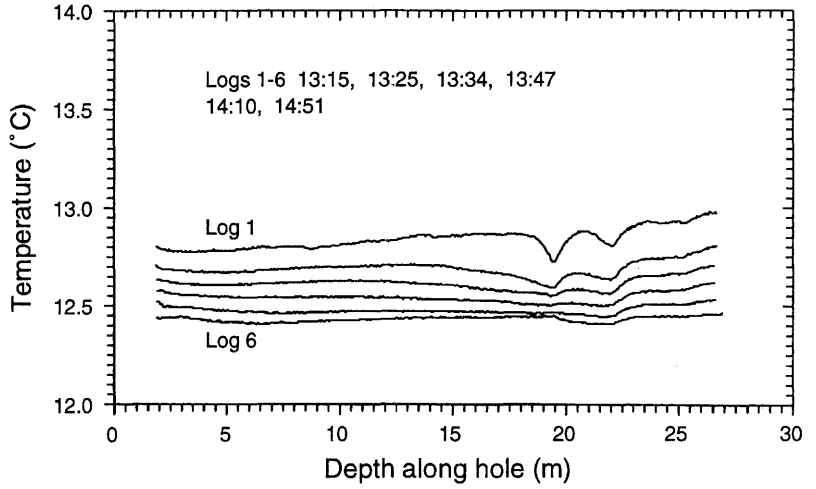

c) FEL log

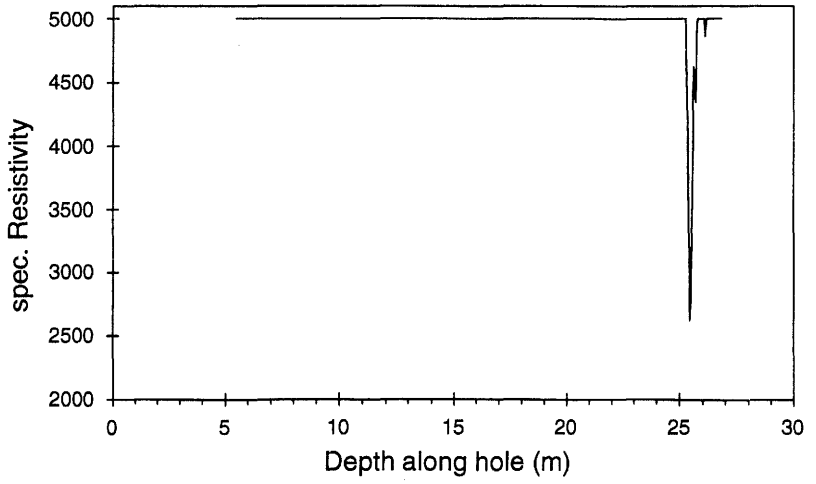

Fig. 2.4: Results of the fluid logging and FEL logging with a moving probe in the borehole BK 88.016 at the GTS performed on July 29th, 1992

a) Conductivity logging

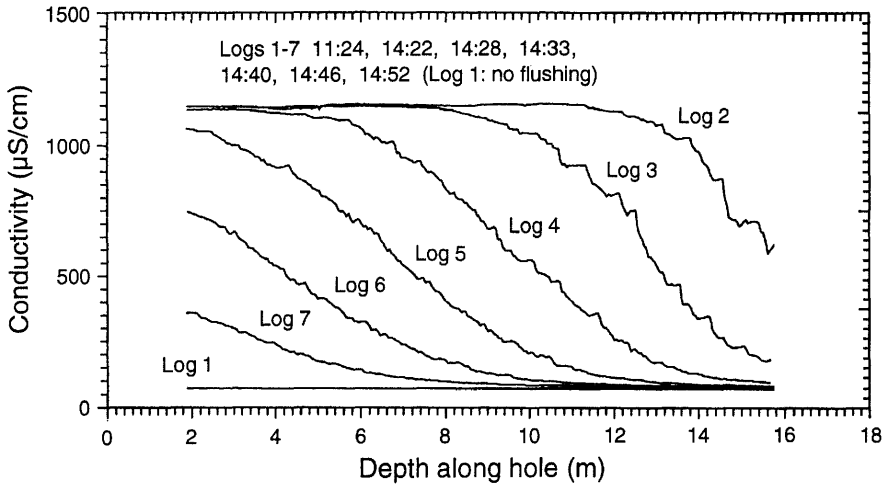

b) Temperature logging

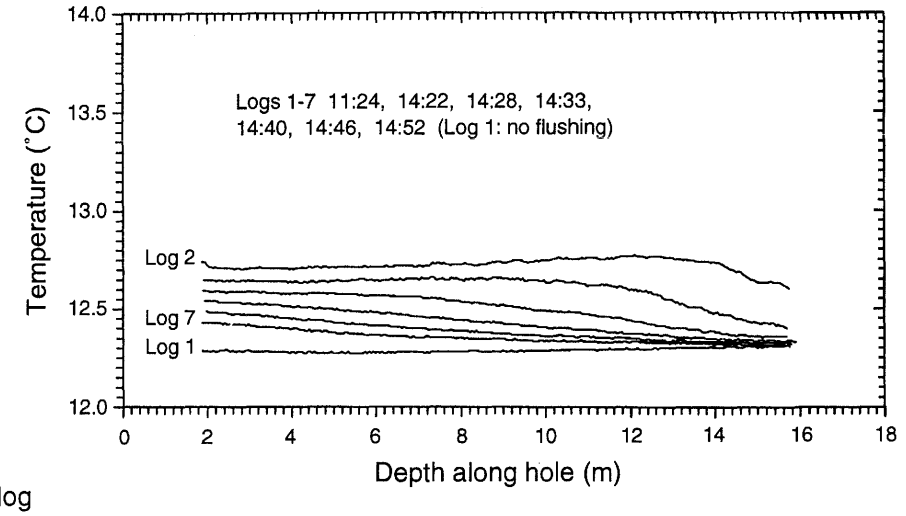

c) FEL log

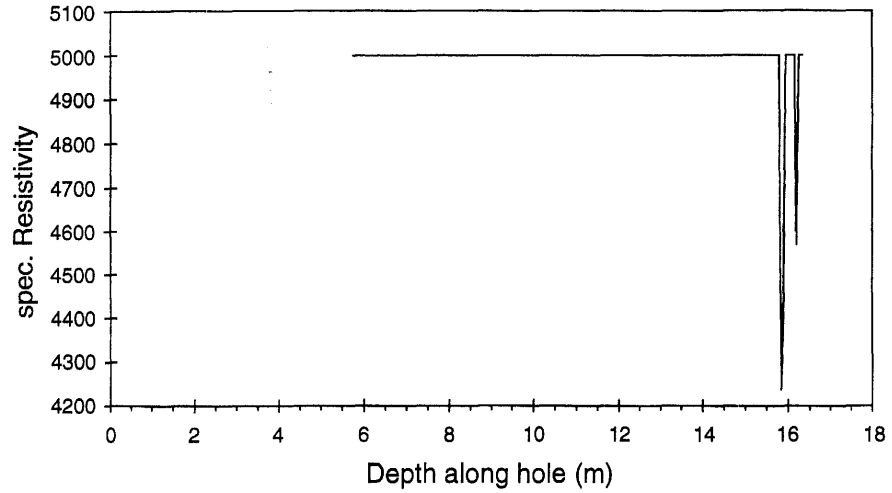

Fig. 2.5: Results of the fluid logging and FEL logging with a moving probe in the borehole BK 88.018 at the GTS performed on July 27th, 1992

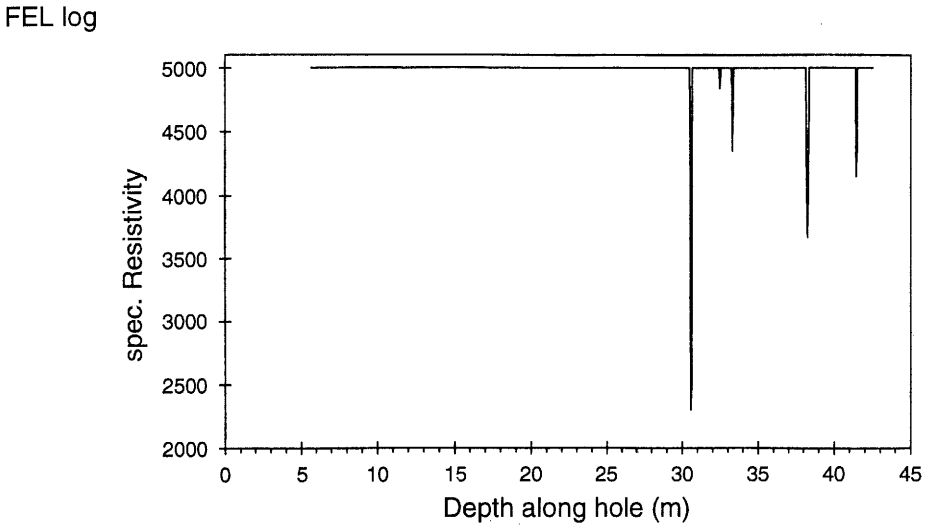

Fig. 2.6: Results of the FEL logging in the borehole BK 85.005 at the GTS performed in July 1992

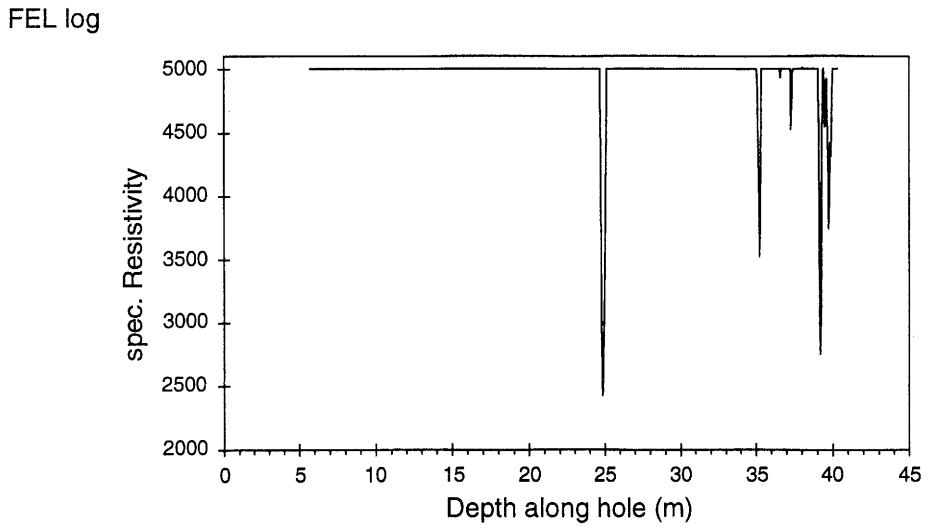

Fig. 2.7: Results of the FEL logging in the borehole BK 88.015 at the GTS performed in July 1992

2.3 Discussion and conclusions

2.3.1 Discussion of the results

The main purpose of the fluid logging campaign of July 1992 was to identify inflow zones in the boreholes BK 85.004, BK 88.014, BK 88.016 and BK 88.018. This objective was successfully accomplished and, later on, the resulting inflow locations were used to determine the packer positions for the test arrangement of the MSCT (see Chapter 5).

Furthermore, the performance of the conventional fluid logging techniques had to be checked for subhorizontal boreholes. It has been shown that even in BK 85.004, with an inclination of 35°, density effects strongly affect the quantification of formation flowrates. In the subhorizontal boreholes (inclination 10°) the test performance was complicated by 'hangers' when moving the probe along the borehole wall, although the borehole wall was extremely smooth. These experiences resulted in the conclusion that conventional fluid logging is not applicable in long subhorizontal boreholes (inclination $\leq 10°$, length ≥ 100 m). In particular, under worse conditions of borehole stability, as expected for the marl formations at the Wellenberg, this method can at best be applied in short inclined boreholes.

Finally, the FEL probe used for the detection of inflow zones was compared to fluid logging. The depths of inflow zones can be more accurately localized in FEL logs than in fluid logs. Even when fluid logging fails for inclined boreholes, FEL logging is still applicable using the coiled tubing technology. However, the FEL does not allow even a rough quantification of inflows and the deduction of an unequivocal relation between low resistivity peaks and amounts of inflows is impossible. About 50 % of the resistivity peaks did not correspond to the results of fluid logging. FEL logging is recommended as a screening method in addition to fluid logging for precise localization of inflow zones. When fluid logging is not suitable from technical reasons (e.g. in subhorizontal boreholes), FEL logs may indicate potential inflow zones.

2.3.2 Conclusions

In vertical boreholes accurate registration during constant movement of the probe causes no difficulties. It is also possible to perform fluid logging for different hydraulic heads and to deduce transmissivities and steady state heads for individual inflow zones. However, for subhorizontal boreholes such as most of the ones at the BK site, the technical performance of fluid logging is governed by several restrictions:

- The probe, when lowered down into the borehole, drags along the borehole wall and the data may be disturbed by the "rubbing" probe or, even worse, the probe may be damaged or get stuck in the borehole. In long boreholes it is laborious work to pull down the probe (see Section 2.2.1).
- Highly permeable fractures near the top of the borehole are difficult to detect because the flushing water is replenished by formation water before the probe is inserted into the borehole.
- In inclined boreholes, a density-driven separation between flushing water and formation water tends to be much more pronounced than for vertical boreholes. Such density effects cannot be accounted for by standard procedures for fluid logging analysis.
- Fluid logging in subhorizontal boreholes can be run at only one head level (atmospheric pressure, open hole). Usually the pressure and flow history of the borehole (i.e. the transient flowrate prior to the logging) are not well known. For this reason, heads and transmissivities of individual inflow zones cannot be accurately estimated by conventional fluid logging.

Thus, in subhorizontal boreholes the use of fluid logging with a moving probe is restricted to the localization of inflow zones, which is, however, important information.

3 FLUID LOGGING WITH FIXED PROBE ARRAYS

B. Heinemann-Glutsch (GTC Kappelmeyer GmbH, Karlsruhe),
E. Hurtig (GESO mbH, Jena), P. Marschall (Nagra)

3.1 Introduction

3.1.1 Motivation

In recent years, fluid logging by combined conductivity/temperature logging (sal/temp logging) has advanced to become a standard method in Nagra's hydraulic investigation programs (TSANG & HUFSCHMIED 1988, TSANG et al. 1990 and KELLEY et al. 1991). In particular, when applied in deep vertical boreholes and in tight formations, fluid logging has proved to be an efficient complement to conventional hydrotests. At the BK site, fluid logging was used to locate permeable fractures in inclined boreholes (see Chapter 2). Further logging methods such as heat pulse or thermal flow have been tested successfully by other investigators (PAILLET et al. 1990 and SCHELLSCHMIDT & HAENEL 1987).

All logging methods mentioned above require a moving probe to be lowered into the borehole during the test period. Consequently, some experimental restrictions are associated with these methods:

- in inclined boreholes from underground tunnels, fracture locations can be detected, but not the head and, hence, the transmissivity of individual fractures. Moreover in long, inclined boreholes or in boreholes which are directed upwards, conventional methods are not applicable for technical reasons (see Section 2.2.1).

- the spatial resolution of conventional fluid logging data is excellent; however, for a given depth, the resolution in time may be poor, in particular for long test intervals.

- the viscous mud (e.g. bentonite, polymers) has to be exchanged with de-ionized or saline water before fluid logging; when the borehole is in unstable sections of a formation, an exchange of mud involves a considerable risk for the entire borehole.

In the current Nagra exploration concepts for high and low level waste disposal sites, inclined boreholes in underground investigation facilities, but also inclined deep boreholes from the surface, are of particular importance for site characterization. Up to now, there are no appropriate fluid logging methods available which can be applied for a quantitative analysis in such boreholes.

3.1.2 Objectives

The difficulties arising with conventional fluid logging can be removed by the use of multiple probe arrays, which are installed in the borehole prior to the fluid logging experiment. The investigations presented in this section were aimed at the develop-

ment of appropriate methodologies and equipment for fluid logging with such fixed probe arrays. The main objectives were:

- to study mixing of flushing and formation water in the test interval, when fluid logging is conducted with fixed probes.
- to test and compare two different technical devices for fluid logging with fixed temperature probes, namely a PT-100-probe array and an optical fibre temperature-sensing system
- to perform an interpretation and quantitative analysis of temperature logs obtained by fluid logging with fixed temperature probes.
- to develop a novel probe array with combined sal/temp sensors.

A further objective was to evaluate simple temperature logs with respect to their "sufficiency" for quantifying the flow conditions in the tested interval. For a multiple probe array, it would involve a considerable simplification of the equipment and test execution to substitute sal/temp measurements by temperature measurements for certain borehole sections.

3.1.3 Methodologies and pilot investigations

Fluid logging with fixed probe arrays shows significant differences to conventional fluid logging with regard to the equipment and test performance. Prior to the experiment, the probe array is lowered down into the borehole along an injection line, as shown in Fig. 3.1. The borehole is then shut in by a packer. After this, fluid logging experiments can be performed by injecting tracer-marked water through the injection line and by controlling the flowrate into the test interval and the interval pressure. The propagation of the tracer along the borehole is measured by continuous concentration and temperature measurements along the multiple probe array.

When conducting conventional fluid logging, the moving probe acts as a mixing device, which minimizes a density-induced separation of formation water and flushing water during the test. For fluid logging with fixed probes, the mixing of formation water and flushing water has to be induced by special mixing facilities such as flow contractions, which are placed near the individual sensors. To ensure that proper mixing is feasible, in principle, with a fixed probe array, a pilot experiment was initiated in a laboratory set-up (BARCZEWSKI & SCHMID 1992). It was shown that sufficient cross-sectional mixing can be achieved with fixed probe arrays using simple centralizers, which act hydraulically as flow constrictions.

For injection, a solute (e.g. NaCl) or heat may be added as a tracer to the water. If heat is used, the equipment required is a simple temperature probe array, which can be handled much more easily than combined sal/temp probes. In particular, when stability problems are expected in inclined boreholes, temperature probes are recommended, because the risk of getting "stuck" is lower than with fixed sal/temp probes due to their smaller diameter.

In this chapter two types of temperature probe array are presented, which were applied for temperature logging at the BK site. The first system consists of an array of equispaced PT-100 temperature sensors, providing local temperature values along the borehole. On the other hand, a novel device was tested, the so-called distributed optical fibre sensing technique (HURTIG et al. 1993). With this method, temperature profiles are determined continuously along an optical fibre, by measuring the intensity of the Raman backscattering light (see Section 3.3.1).

Besides this, pilot investigations were conducted with a prototype system of fixed sal/temp probes. The experiments included calibration tests and a series of basic studies on density effects initiated at Lawrence Berkeley Laboratory in a borehole simulator.

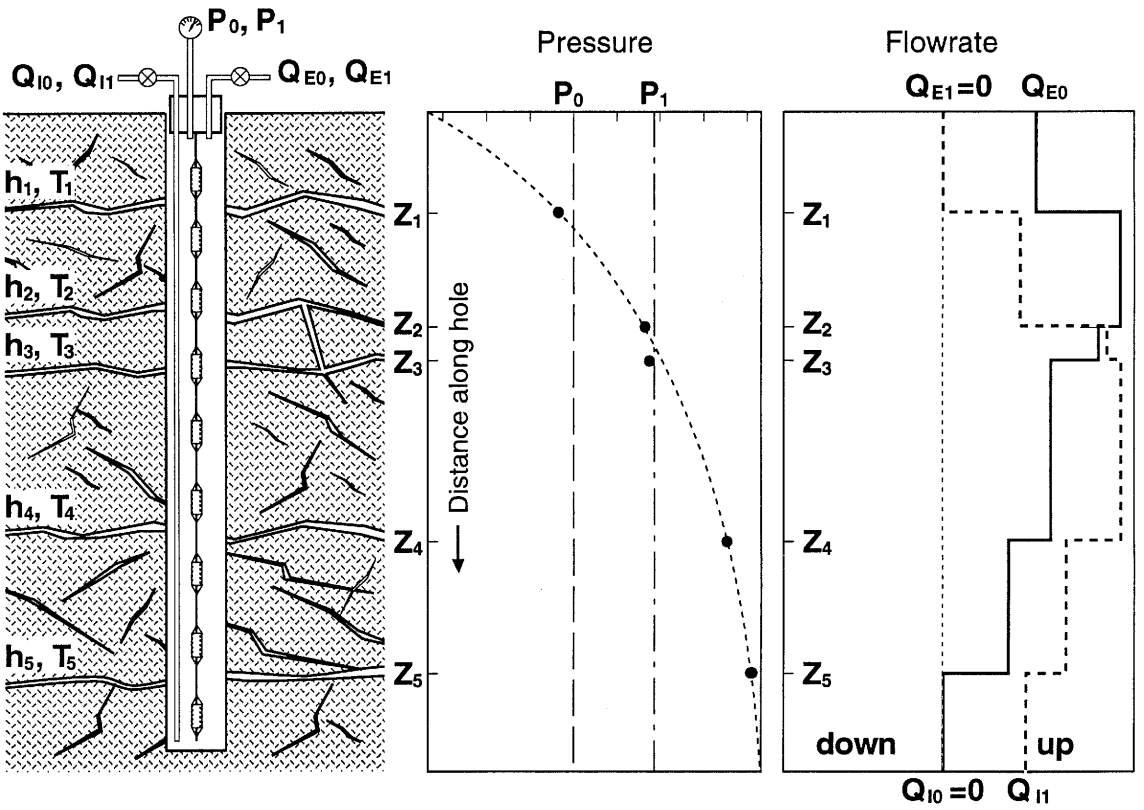

Fig. 3.1: Sketch of fluid logging with fixed probe arrays

3.2 Fixed temperature probes: the discrete PT-100 probe array

3.2.1 Equipment

The "PT-100" temperature sensor is known as an extremely precise device for temperature measurements. Based on the principle of temperature-dependent resistivities, the resolution of the temperature measurement is as low as 0.01 °C. This high resolution results from the 4-wire technique which provides the accurate resistivity of the PT-100 probe which is converted into temperature.

The PT-100 probe array used for the fluid logging with fixed probe arrays at the Grimsel Test Site consisted of a multi-core cable including up to 10 PT-100 units spaced at 1 m intervals. The array was fixed onto the injection tubing and then lowered down to the bottom of the borehole. To record fluid logging data in a 50 m deep borehole, five of the arrays were installed in the borehole to ensure local temperature measurement with a spatial resolution of one meter. A direct connection of the cables to the computer station via a recording unit ensured a rapid and reliable recording of fluid logs with fixed probes.

3.2.2 Field experiments

Different fluid logging experiments with a fixed probe array (PT-100 sensors) were recorded by GTC (Karlsruhe) at the BK site in the boreholes BK 85.008 and BK 88.015 (see Fig. 1.1) from April 19th to 23rd, 1993. The installation of the array (fixed on a PVC injection tube) between the injection tube and the borehole wall (annulus) presented no problems. While fluid injection took place at different injection rates and temperatures, with opened or shut outlet, local temperatures at 1 m intervals were monitored every 30 seconds. The injection and extraction flowrates were recorded by BGR's data acquisition system (see Chapter 5). The interval pressure at the inlet was monitored by SOLEXPERTS AG. A brief description of the experiments performed in BK 85.008 and BK 88.015 follows. Further details can be found in DORNSTÄDTER et al. (1993).

BK 88.015:

The first test series was initiated on April 20th, 1993 in BK 88.015. The fluid logging started at 09:40 with the injection of warm water (20 °C) at the opened outlet. The injection rate was measured to be 5.4 l/min and the extraction rate was 2.88 l/min. The interval pressure increased from 8.5 bar and stabilized at 8.65 bar. The temperature logs monitored for this experiment are illustrated in Fig. 3.2a.

Injection of cold water (15 °C) started at 11:40 with a rate of 5.3 l/min. At the opened outlet the extraction rate was monitored to be 2.85 l/min. During this test, the interval pressure increased from 8.65 bar to 8.75 bar. The fluid log recorded for this experiment is illustrated in Fig. 3.2b.

Finally an injection test was performed at the closed outlet. The injection temperature was 20 °C and the injection rate 5.1 l/min. Pressure built up in the borehole; it increased from 12.25 bar to 13.8 bar and was not yet stable at the end of the test. The test ended at 15:40. The corresponding fluid logging data are illustrated in Fig. 3.2c.

At the end of these first test series of April 20th, 1993, the borehole BK 88.015 was closed by a single packer.

BK 85.008:

The first test series in BK 85.008 started on April 21st, 1993, at 14:00. For half an hour cold water (12 °C) was injected into the borehole, followed by the injection of warm water (20 °C) between 14:30 and 16:00. For this test, the injection rate at the opened outlet was 4.8 l/min and the extraction rate was 2.7 l/min. While injecting

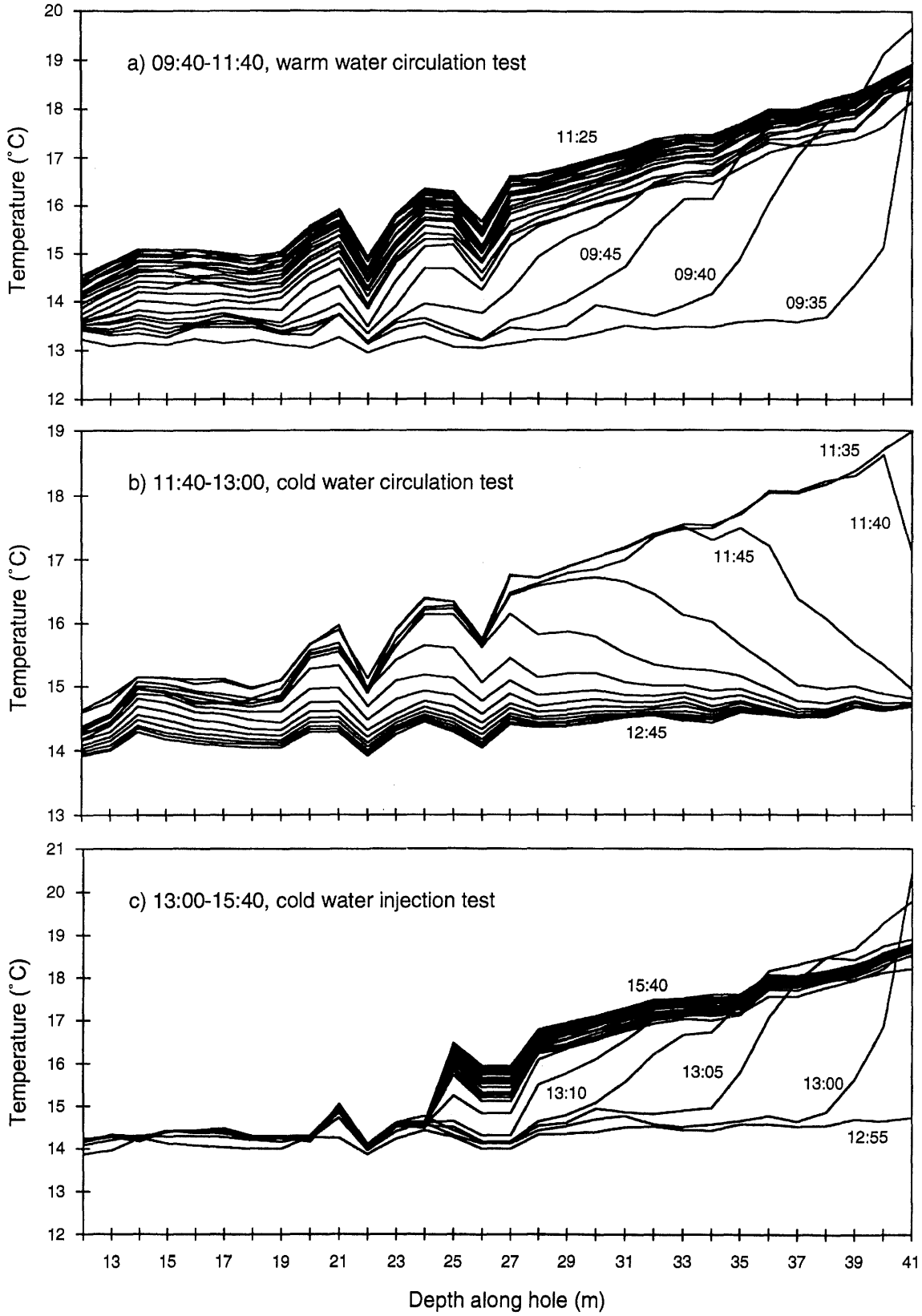

Fig. 3.2: Fluid logging with fixed probe arrays (PT-100) performed in borehole BK 88.015 on April 20th, 1993. Temperature logs are shown with intervals of 5 min

warm water the interval pressure stabilized at about 5.68 bar. The fluid logging data for the injection with cold and warm water are illustrated in Fig. 3.3a.

The final test on April 21st was a constant outflow test in BK 85.008, which started at 16:00. During this test, the interval pressure continuously decreased from 4.6 bar down to 3.4 bar at 01:00 on April 22nd. The pressure then built up again and stabilized at about 4.1 bar between 03:00 and 07:30 (April 22nd). The fluid log monitored for the constant outflow test is illustrated in Fig. 3.3b.

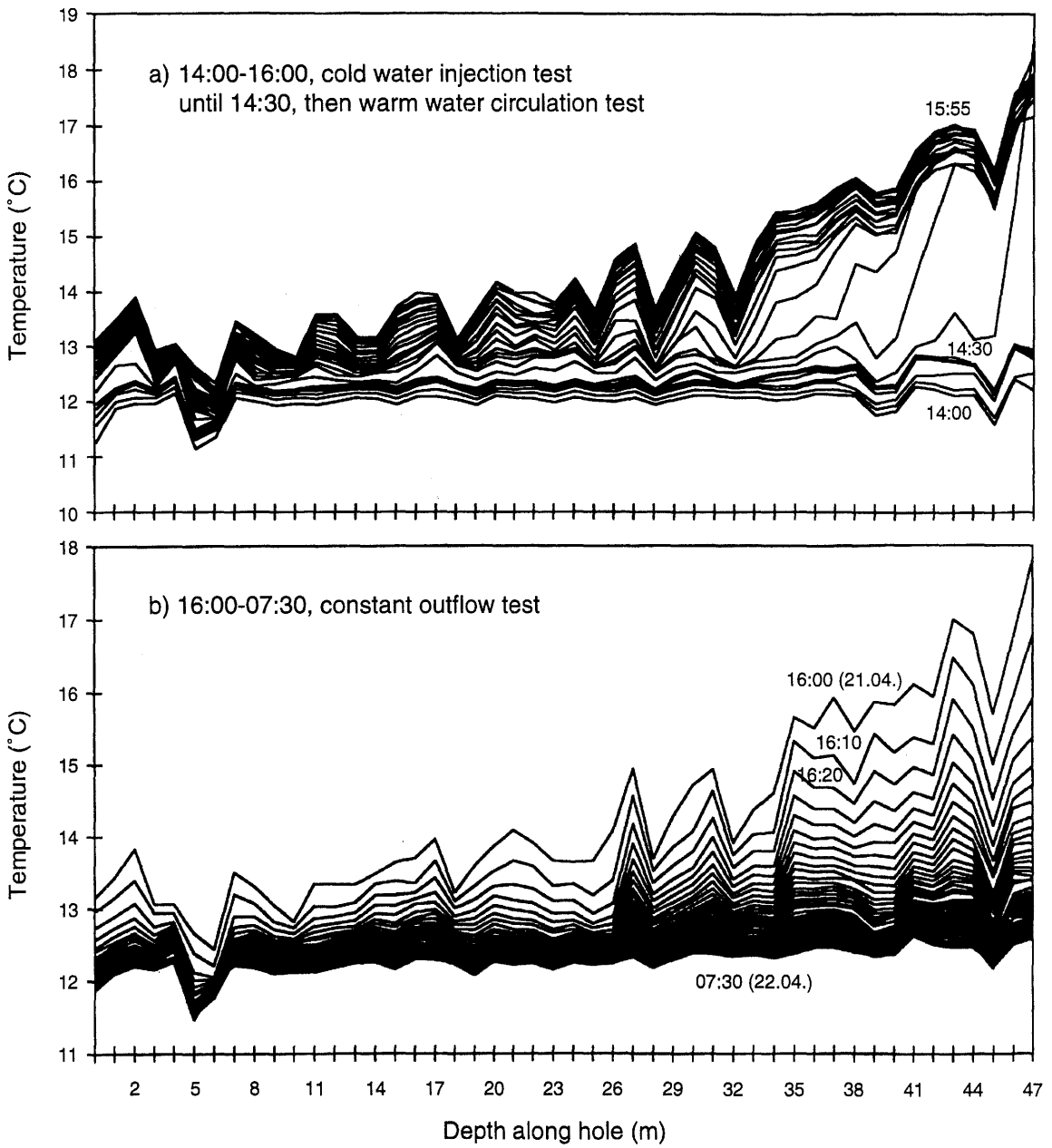

Fig. 3.3: Fluid logging with fixed probe arrays (PT-100) performed in borehole BK 85.008 on April 21st and 22nd, 1993. Temperature profiles are shown with time steps of a) 5 min and b) 10 min

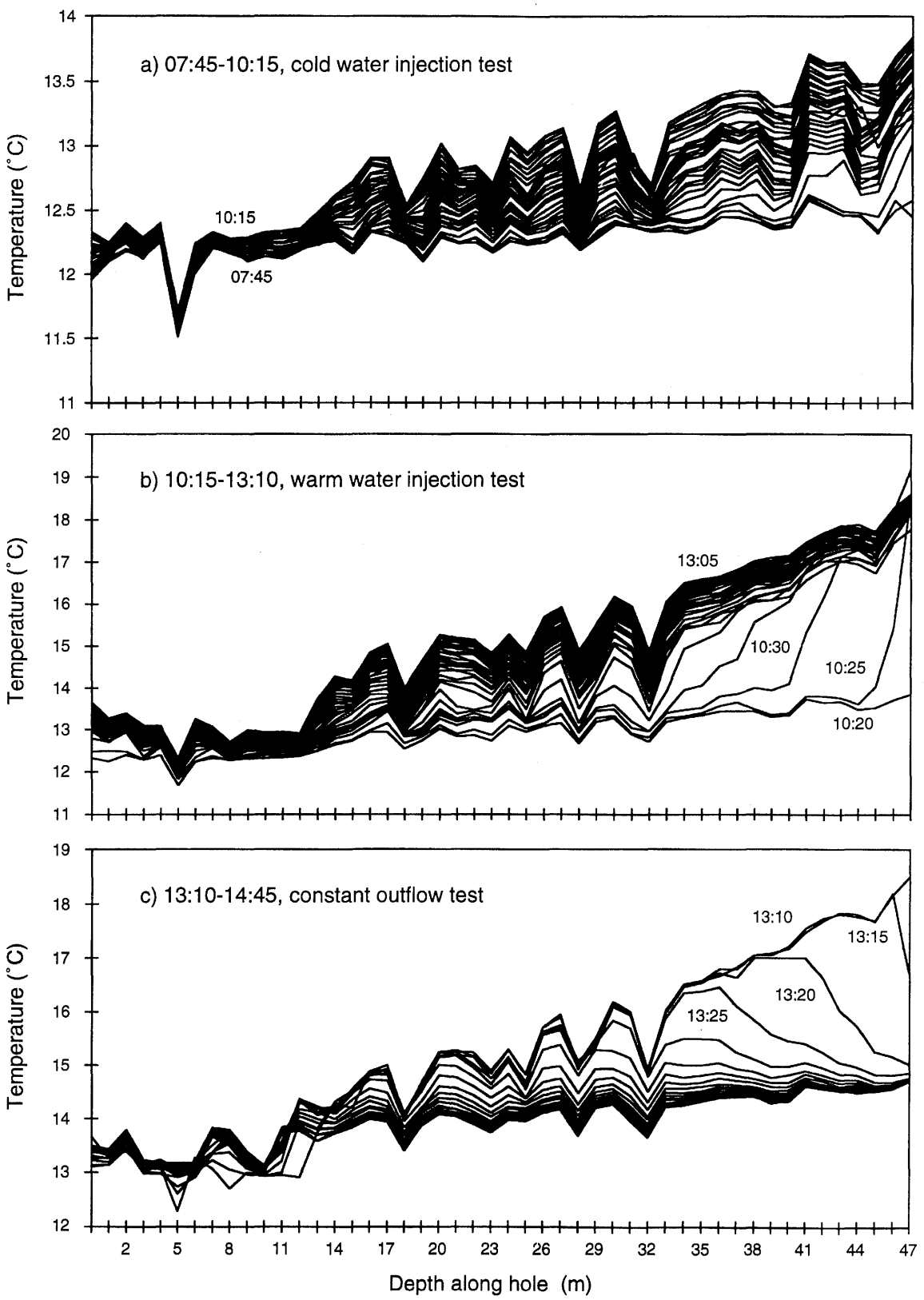

Fig. 3.4: Fluid logging with fixed probe arrays (PT-100) performed in borehole BK 85.008 on April 22nd, 1993. Temperature profiles are shown with time steps of 5 min

A second test series with closed outlet started on April 22nd, 1993, in BK 85.008. From 07:45 to 10:15, fluid logging while injecting cold water (12.5 °C) into the borehole was performed at three different injection rates of 3.5 l/min (07:45-08:35), 4.2 l/min (08:35-09:23) and 5.8 l/min (09:23-10:15). For the different injection rates, mean interval pressures were 6.1 bar, 6.8 bar and 8-9 bar respectively. The corresponding records of the logs with a fixed probe array are illustrated in Fig. 3.4a.

Still with a closed outlet, injection of warm water (20 °C) followed the injection of cold water from 10:15 to 13:10. A mean injection rate of 5.75 l/min was observed, while the interval pressure continuously increased from 9.2 bar to 10.25 bar. The fluid logs for this test are illustrated in Fig. 3.4b.

Finally, the test series in BK 85.008 ended with a venting test between 13:10 and 14:45 on April 22nd. An extraction rate of 3.45 l/min was observed during this test period. The interval pressure was constant at 7.3 bar. The measurements from this fluid logging phase are illustrated in Fig. 3.4c.

A summary of all experimental events is listed in the Table below:

Tab. 3.1: Fluid logging in the boreholes BK 88.015 and BK 85.008

Borehole BK 88.015						
No.	Date/time	Inj. rate (l/min)	Extr. rate (l/min)	Interval pressure (bar)	Inj. temp. (°C)	Test spec.
1	20.04.93 09:40-11:40	5.4	2.88	8.5-8.65	20	open outlet
2	11:40-13:00	5.3	2.85	8.65-8.75	15	open outlet
3	13:00-15:40	5.1	0	12.25-13.8	20	closed outlet
4	15:00- ...	-	1.9			open outlet

Borehole BK 85.008						
No.	Date/time	Inj. rate (l/min)	Extr. rate (l/min)	Interval pressure (bar)	Inj. temp. (°C)	Remarks
5	21.04.93 14:00-14:30	4.8	2.7	5.9-5.7	12	cold water circulation
6	14:30-16:00	4.8	2.7	5.68	20	warm water circulation
7	16:00-07:30 on 22.04.93	-	2.3	4.6-3.4-4.1		free outflow
8	07:45-10:15	3.5, 4.2, 5.8	0	6.1, 6.8, 8-9	12.5	cold water injection
9	10:15-13:10	5.75	0	9.2-10.25	20	warm water injection
10	13:10-14:45	-	3.45			free outflow

3.3 Fixed temperature probe arrays: The distributed optical temperature-sensing technique

3.3.1 Principles and fundamentals

The distributed optical fibre temperature sensing method was developed at the beginning of the 1980s at Southampton University in England. It is based on optical time domain reflectrometry OTDR (HARTOG & GAMBLE 1991 and SCHICKETANZ 1981). A pulsed laser is coupled to an optical fibre which is the sensing element (Fig. 3.5). The light is backscattered as the pulse propagates through the fibre owing to changes in density and composition as well as to molecular and bulk vibrations.

The intensity and spectral composition of the backscattered light are determined by the molecules in the optical fibre. In a homogeneous fibre the intensity of the back-scattered light is decays exponentially with time. As the velocity of light propagation in the optical fibre is well known, the distance can be determined from the attenuation of the intensity of the backscattered light. Therefore, the temperature can be allocated exactly to the distance along cable.

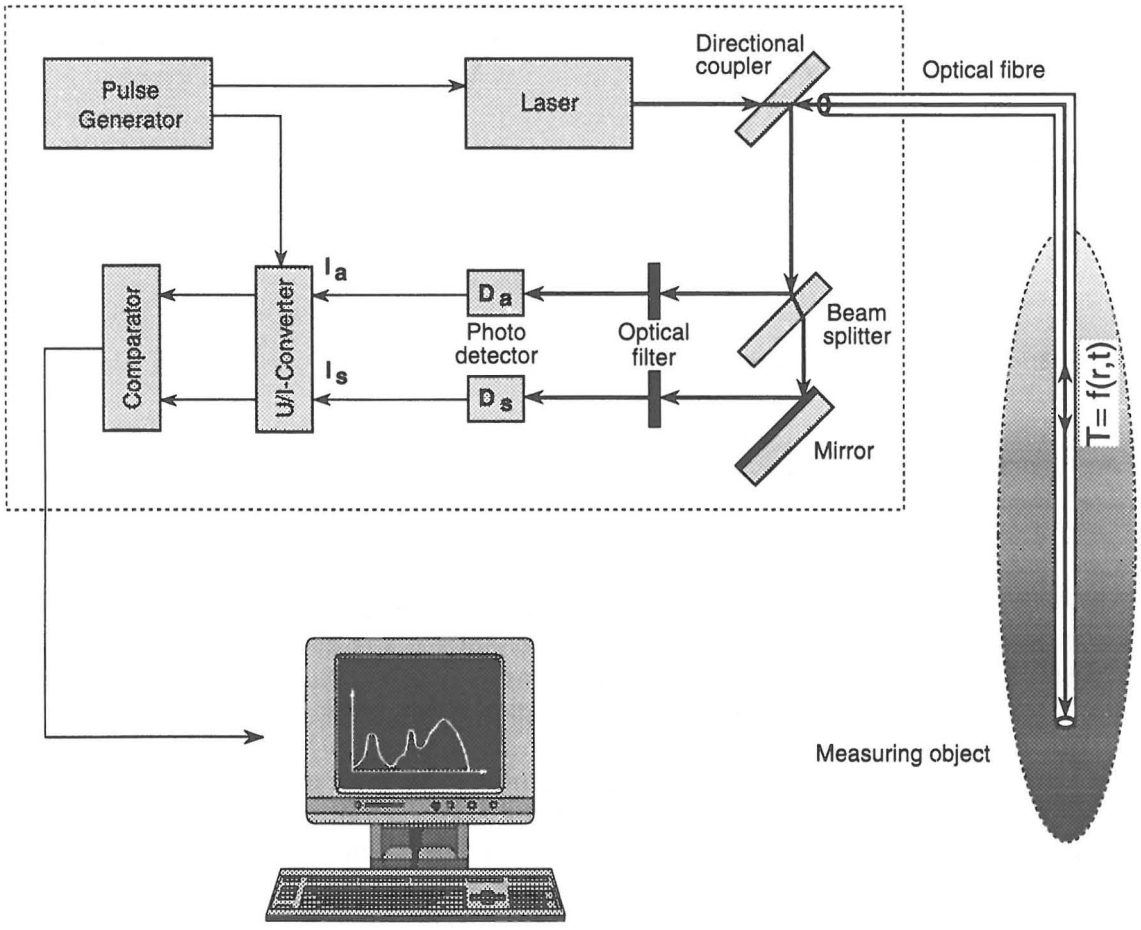

Fig. 3.5: Principle of distributed fibre optic temperature sensing

The backscattered light includes different spectral components (Fig. 3.6) which are caused by differing interaction mechanisms between the propagating light pulse and the optical fibre. The Rayleigh backscattering component is the strongest and has the same wavelength as the primary laser pulse. This Rayleigh component controls the main slope of the intensity decay curve and is commonly used for identifying breaks and inhomogeneities along the fibre line which cause an increase in the absorption. Thus, this component is a main tool for quality surveillance of optical fibres. The Rayleigh component is practically independent of temperature.

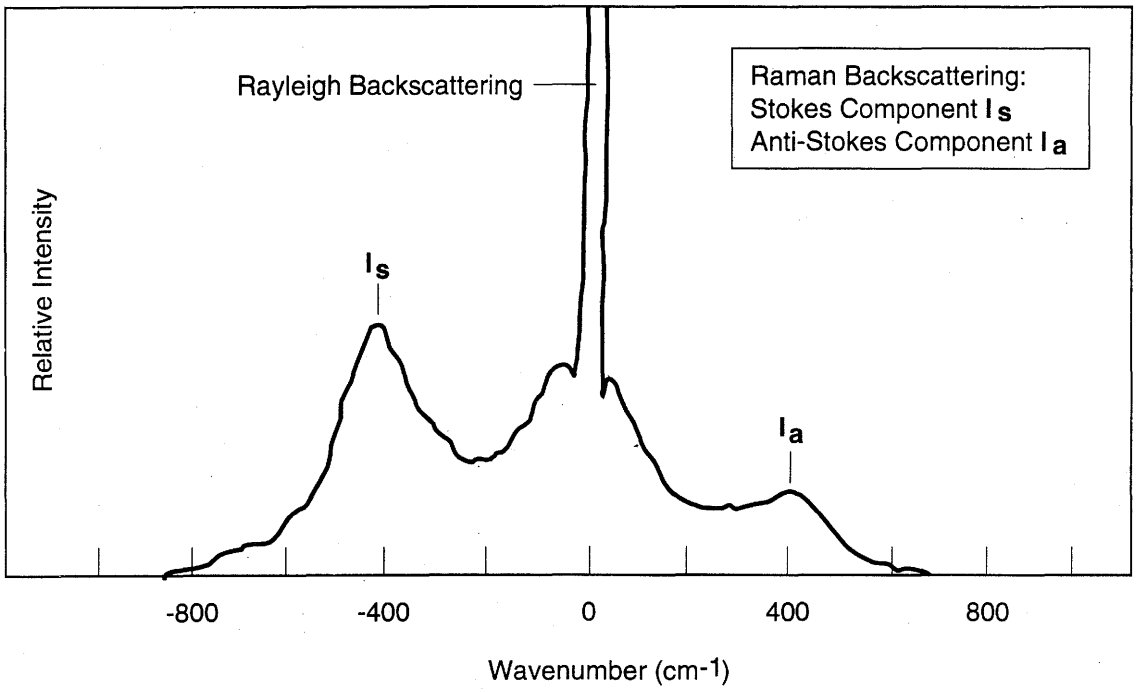

Fig. 3.6: Spectrum of the backscattered light

The Raman backscattering component is caused by thermally influenced molecular vibrations. Thus, its intensity depends on temperature. This effect is of a fundamental nature and is observed in glass as well as in fluids, gases and solids.

The Raman backscattered light has two components which lie symmetrically to the Rayleigh line; namely the Stokes line and the Anti-Stokes line which have different intensities. While the intensity of the Stokes line is only slightly dependent on temperature, the Anti-Stokes line shows a strong relation to temperature.

The basic principle of fibre optic temperature measurements thus consists of filtering the Stokes and the Anti-Stokes lines out of the backscattered light. This is possible due to their differences in wavelength with regard to the Rayleigh backscattered light. Taking the ratio of the intensities of the Stokes and the Anti-Stokes lines, external influences such as changes of the light source or of the optical fibre can be eliminated.

The following relationship holds:

$$\frac{I_a}{I_s} = \left[\frac{\nu_o + \nu_k}{\nu_o - \nu_k}\right]^4 \exp\left(\frac{-hc\nu_k}{kT}\right) \qquad (3.1)$$

I_a - intensity of the Anti-Stokes line (W/m^2)
I_s - intensity of the Stokes line (W/m^2)
ν_o - wavenumber of the incident light (1/m)
ν_k - shift amount of wavenumber (1/m)
T - temperature (K)
k - Boltzman´s constant (J/K)
h - Planck´s constant (Js)
c - velocity of light (m/s)

The relationship between temperature and the intensity ratio I_a/I_s can be treated as linear at least up to 150 °C.

3.3.2 Calibration and resolution

Similarly to the radar principle, the laser light is coupled into the optical fibre as a short light pulse (several nanoseconds). The intensities of both Raman lines are recorded with a time resolving power in the order of 10 ns. The temperature is determined as an integral value for a short section of the optical fibre (e.g. 1 m) and the space coordinate is determined precisely from the travel time of the propagating light pulse. Thus, it is possible to measure the temperature simultaneously along the entire length of the fibre. The space resolution is basically 1 m. This resolution can be increased to 0.5 or 0.25 m, respectively, by a two- or four-fold oversampling.

As the temperature values and their location along the optical fibre are determined simultaneously, an independent recording of the fibre length or distance (depth) using a conventional borehole winch technique is not required.

The system is internally calibrated. In the measuring device, a given length of the optical fibre is kept at a constant temperature level. In addition, the calibration function of the fibre can be determined experimentally. The temperature resolution is 0.1 K, but depends on the properties of the optical fibre type used.

The fibre optic temperature-sensing system operates without any electronic circuits along the fibre and the temperature is determined from the ratio of the two intensities of the Stokes and Anti-Stokes lines. Thus, long-term stability of the system is guaranteed.

The fibre optic temperature-sensing technique is based on the determination of the Raman backscattering component. Backscattering of light is a stochastic process. Therefore, it is necessary to integrate the backscattering intensity over a given time interval. For a spatial resolution of 1 m, an integration time of 1 min is sufficient. As there is a correlation between space and time resolution, the integration time must be

increased by a factor of 2 or 4 if the space resolution is increased to 0.5 or 0.25 m, respectively. For a long fibre length (> 8 km) the optical absorption in the fibre decreases the available space and time resolution.

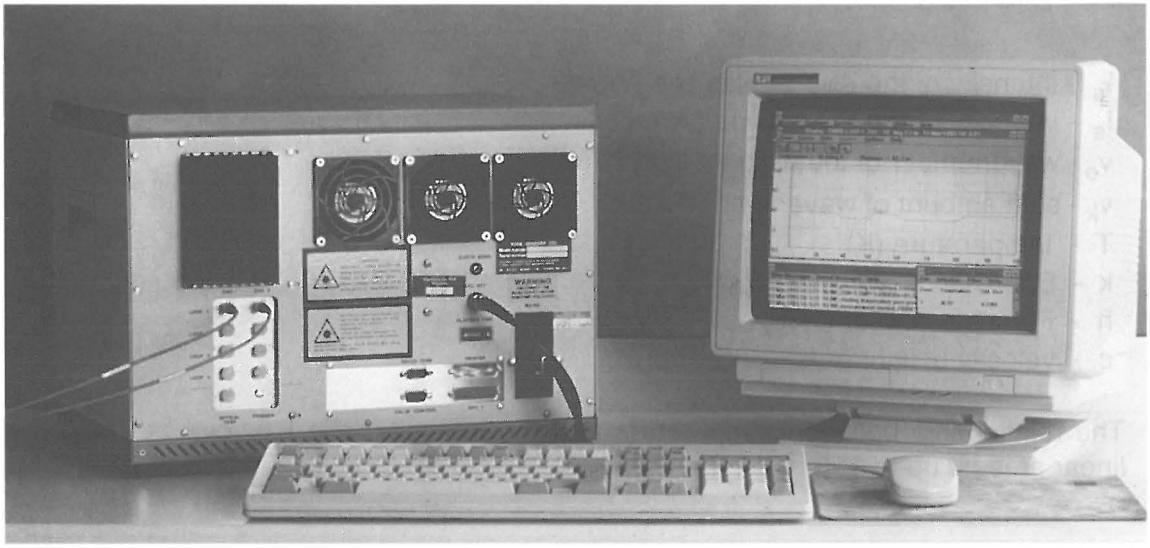

Fig. 3.7: Equipment for fibre optic temperature measurements

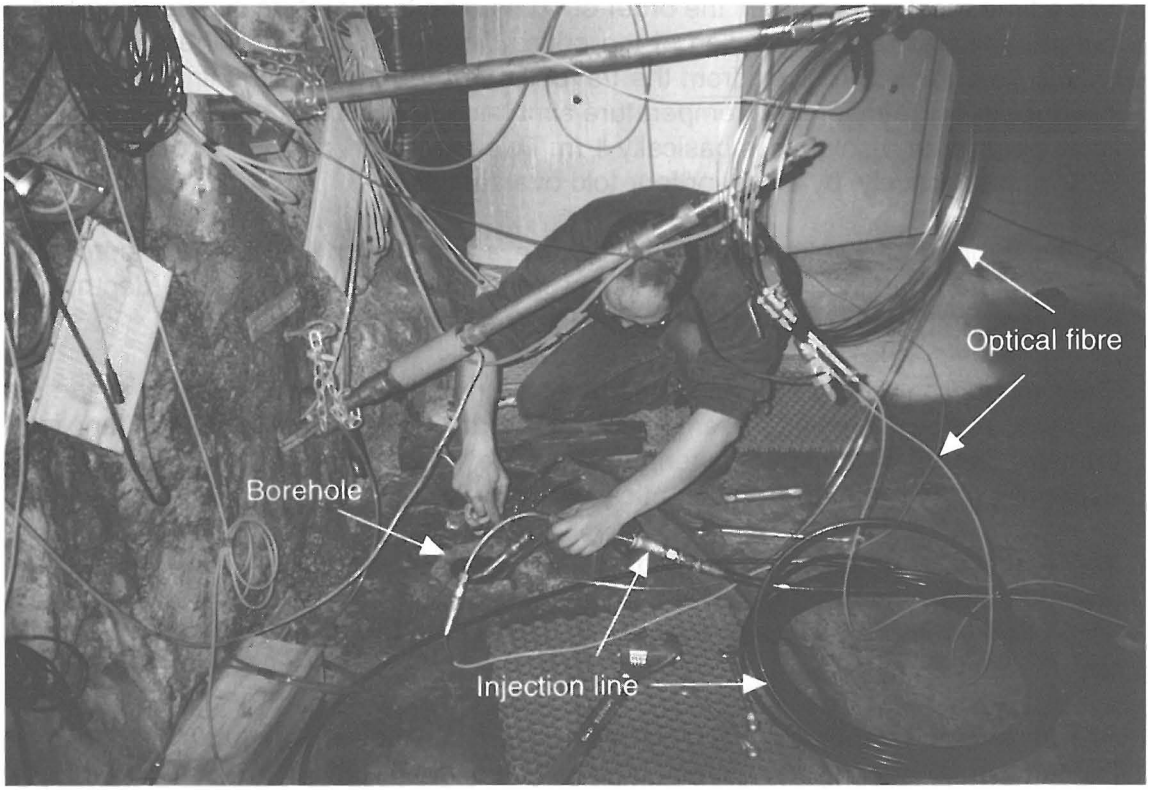

Fig. 3.8: Fibre optic temperature-sensing cable consisting of optical fibres inserted in a steel tube and covered by a plastic mantle

3.3.3 Equipment

The device for fibre optic temperature measurements (GROSSWIG et al. 1993) includes the transmitting and recording unit, a portable computer for control and data analysis and the optical fibre cable (Fig. 3.6, 3.7 and 3.8). The optical fibre laser is neodymium-doped and has a wavelength of 1064 nm; the pulse duration is 10 ns. The directional coupler separates the backscattered light from the incident light pulse. By means of a beam splitter, optical filter and photo-receiver, the two Raman bands (Stokes (s) and Anti-Stokes (a) lines) are separated and their intensities are determined. Finally, the ratio of the two intensities is calculated and transferred into temperature values using both the internal calibration of the equipment and an externally determined calibration function for the particular fibre type. The dimensions of the equipment are 450 x 320 x 340 mm and the total weight is 20 kg.

The fibre optic cable used for the field experiment at the Grimsel Test Site consisted of a high-grade steel tube with a diameter of 2 mm and 5 optical fibres. The weight of the cable was about 2.5 kg per 100 m.

3.3.4 Field experiments

The field experiments were performed in the boreholes BK 88.015 and BK 88.005 (see Fig. 1.1). As described in Section 3.2.2, plastic tubing was used for the fluid injection. The optical fibre cable was clamped to the tubing by the spacers and was passed through openings of the packer (12 mm diameter). The installation of the measurement system caused no problems. After finishing the fluid logging experiment in the borehole BK 88.015, the complete unit of plastic tubing and attached fibre optic cable was removed from the hole and moved into borehole BK 85.005.

The flowrates for injection and extraction, as well as the pressure in the borehole, were monitored using a BGR data logger. In Tab. 3.2 the sequences of the fluid logging experiments in both boreholes are summarized.

BK 88.015

The fluid logging experiment was performed in three phases: warm water injection, cold water injection and free outflow.

For the first phase, the temperature of the injected water was initially 25 °C. In order to obtain clear temperature effects, the water temperature was increased 18 min after starting the fluid logging experiment by 3 °C up to 28 °C. An average pressure of 8.5 bar was obtained for a mean flowrate of 7.7 l/min (injection) and 2.8 l/min (extraction).

Fig. 3.9 shows that quasi-stationary conditions were already reached after about 1 h. For the second phase, the injection and extraction rates were reduced to 5.2 l/min. At a pressure level of 2.1 bar, cold water was injected (Fig. 3.9) until the normal geothermal gradient within the borehole was reached. In the third phase, at first warm water was injected again. When the quasi-stationary condition was reached, the injection was stopped and free outflow of water was adjusted.

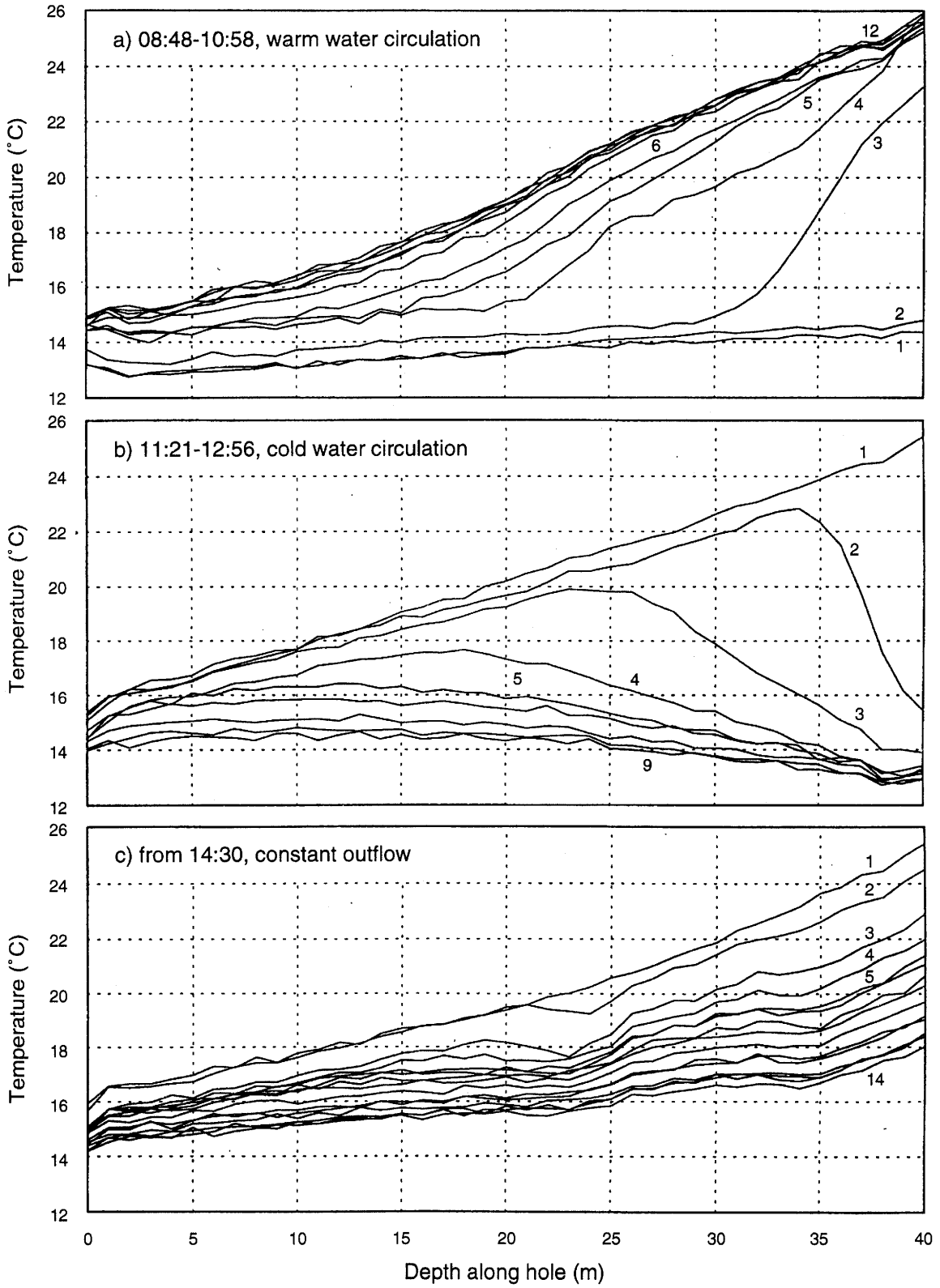

Fig. 3.9: Fluid logging experiment borehole BK 88.015: the time interval between logs is 10 min (June 23rd, 1993)

BK 85.005

In borehole BK 85.005 the fluid logging experiment included the phases of warm water injection and free outflow. A pressure level of 2.95 bar was obtained for a mean flowrate of 8.5 l/min (injection) and 1.5 l/min (extraction). At this pressure level, warm water (28 °C) was injected (Fig. 3.10). Due to pump failure the injection had to be stopped. For free outflow of the water the temperature was recorded until the equilibrium temperature was reached (Fig. 3.11).

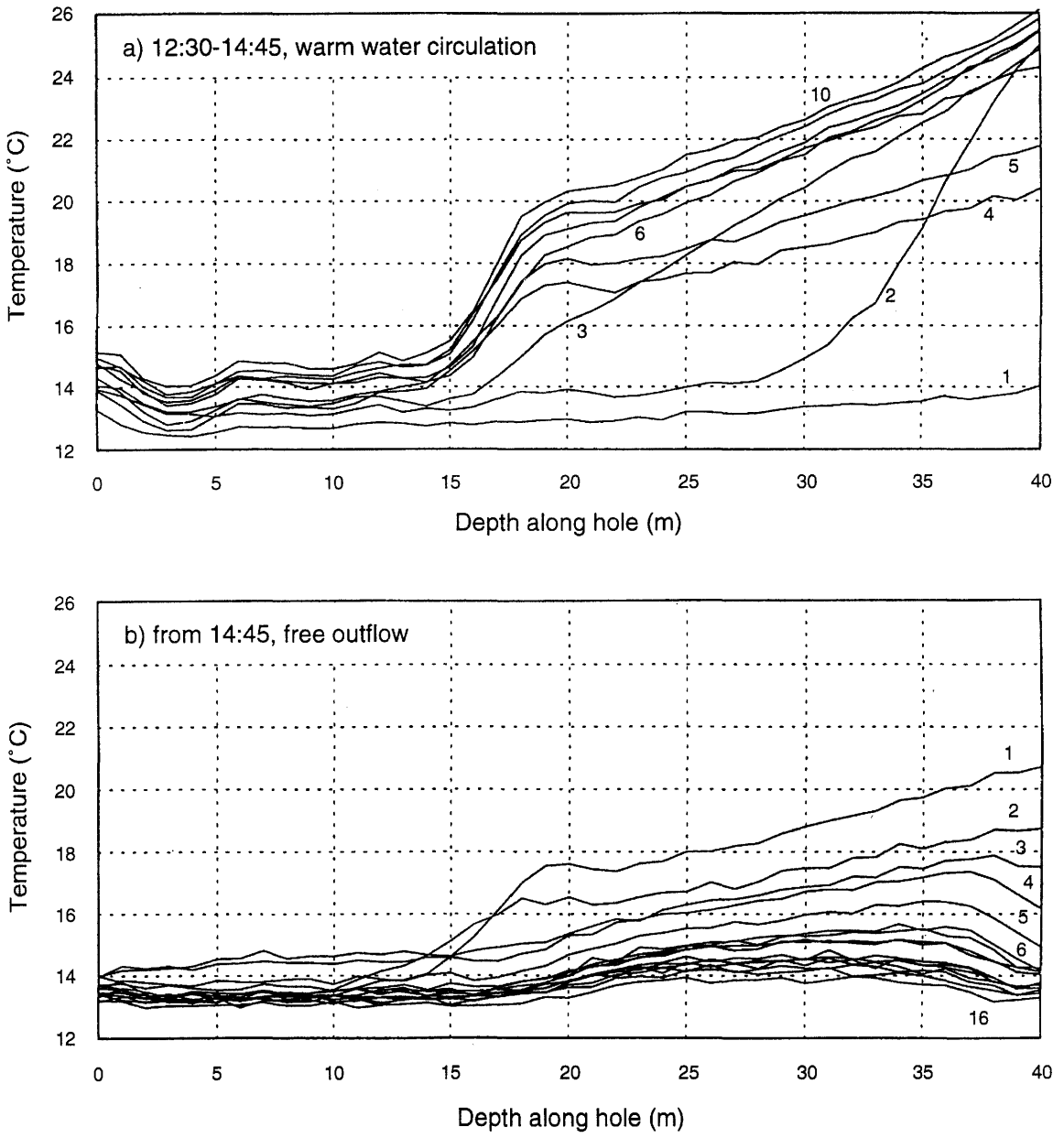

Fig. 3.10: Fluid logging experiment borehole BK 85.005: the time interval between logs is 10 min (June 24th, 1993)

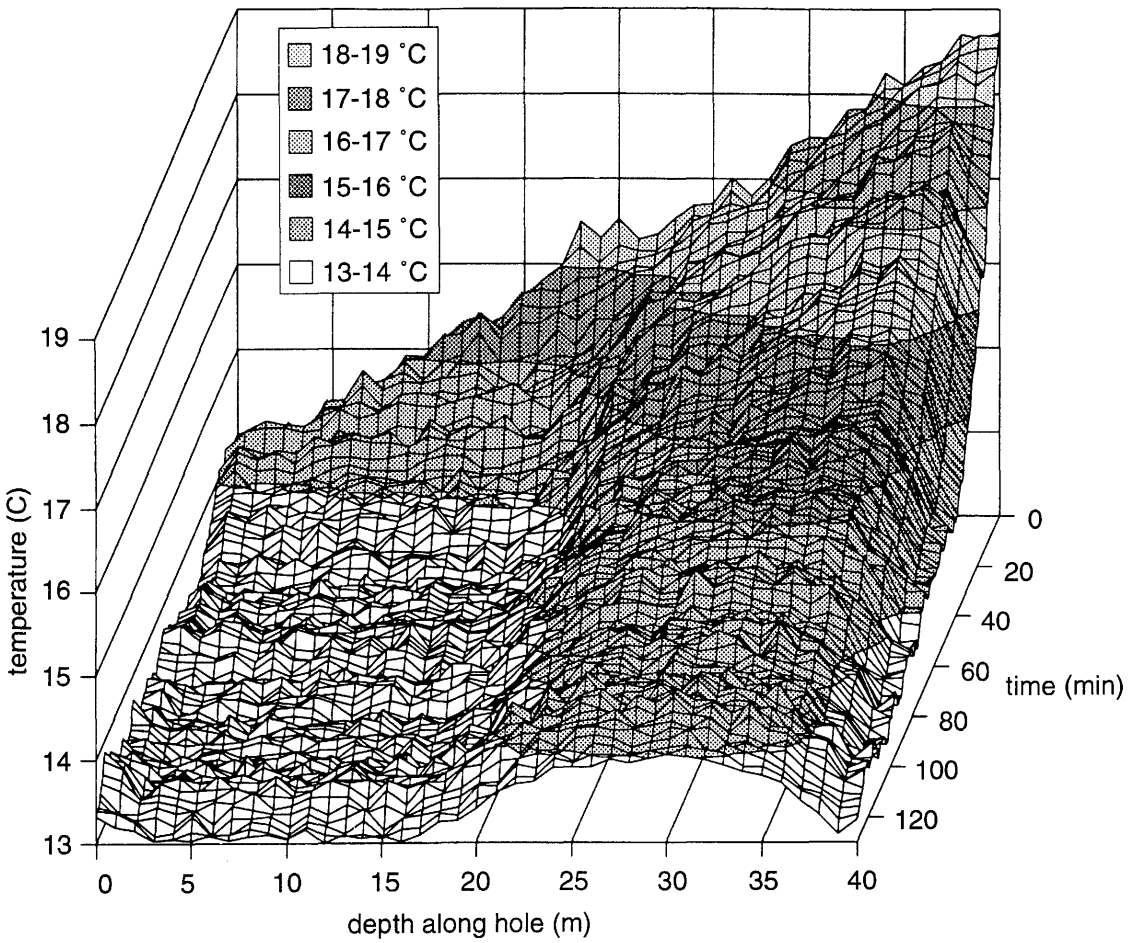

Fig. 3.11: Temperature-time-depth diagram borehole BK 85.005; free outflow; June 24th, 1993 from 14:45

Tab. 3.2: Fluid logging experiments in the boreholes BK 85.015 and BK 85.005

Borehole BK 88.015: 23.6.1993					
No.	Measuring time	Injection (l/min)	Extraction (l/min)	Pressure (bar)	Remarks
1	08:48-10:58	7.7	2.8	8.5	warm water circulation
2	10:58-11:21	5.2	5.2	2.1	warm water circulation
3	11:21-12:56	5.2	5.2	2.1	cold water circulation
4	12:57-14:30	5.2	5.2	2.1	warm water circulation
	from 14:30				free outflow

Borehole BK 85.005: 24.6.1993					
No.	Measuring time	Injection (l/min)	Extraction (l/min)	Pressure (bar)	Remarks
5	12:30-14:45	8.5	1.5	2.95	warm water circulation
6	from 14:45				free outflow

3.4 Fixed temperature probe arrays: interpretation and discussion

3.4.1 Heat exchange in a system with countercurrent flow

The fluid logging arrangement used at the BK site consisted of the injection of water of defined temperature through an injection tube which had been inserted down to the bottom of the borehole. Downhole the injected water flow turned round into the annulus (between injection tubing and borehole wall) and flowed back to the wellhead countercurrently to the injection direction. Fig. 3.12 illustrates schematically the described fluid logging arrangement, which is comparable to a heat exchanger with countercurrent flow. Such systems are well known in mechanical engineering, and simulations exist for calculating the temperature distributions in (heat exchangers). In combination with interpretations of temperature surveys made during injection or production (MURPHY 1977 and 1982), DORNSTÄDTER (1987) transferred the heat exchanger system to borehole geophysical problems for the interpretation and evaluation of temperature profiles.

Considering an element of the borehole volume the heat exchange within that element can be studied by taking into account the different contributions to the heat balance.

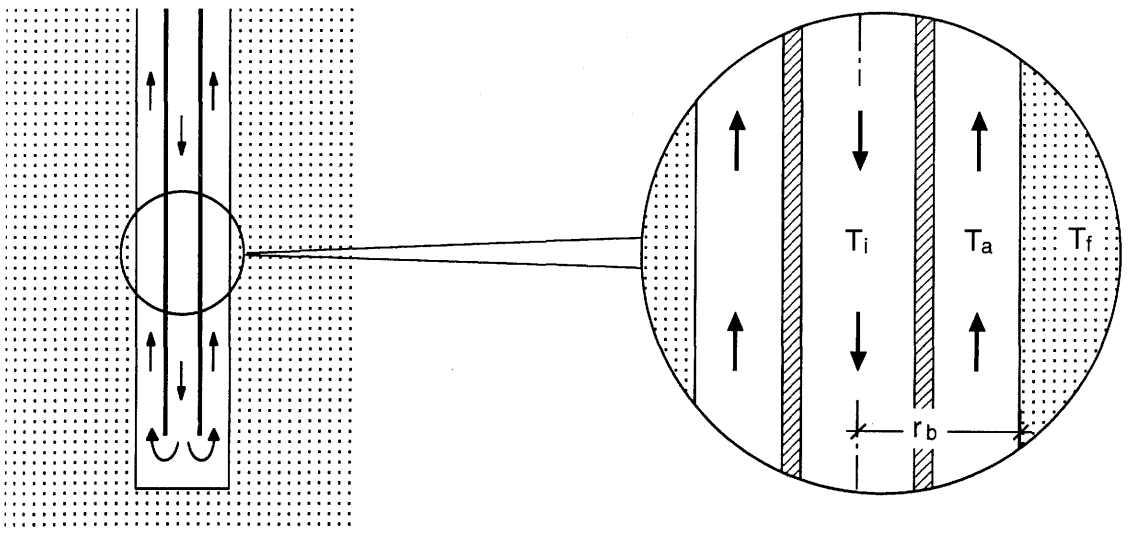

T_i Temperature inside tubing

T_a Temperature between tubing and borehole wall

T_f Temperature of formation at thermal equilibrium

r_b Borehole radius

Fig. 3.12: Scheme of the fluid logging arrangement comparable to a heat exchanger with countercurrent flow

Assumptions:

Except in the case of low flowrates, the flow of water is turbulent (Pe > 2000) and, because wellbore radii are small, the water temperature is expected to be uniform in cross-section. For typical flowrates the Peclet number is extremely large, so that axial conduction of heat in the fluid is negligible compared to axial convection. In additional geothermal gradients in the depth direction are small compared to the radial gradients induced by injection, so axial conduction of heat in the formation can also be ignored.

Borehole-formation heat exchange:

The heat exchange within an element of the borehole volume can be evaluated by taking into account the different contributions to the heat conservation equation. The heat conservation equation considers the conductive as well as the convective heat exchange within the borehole and takes into account the heat conduction from the formation into the borehole and from the injection tubing into the borehole.

Considering the heat exchange between formation and borehole, CARSLAW & JAEGER (1959) deduced the analytical solution for the temperature difference between borehole temperature and formation temperature:

$$T_a - T_f = \frac{q}{K} G_o(t) \tag{3.2}$$

where

$$G_o(t) = \frac{8}{\pi^3}\left[\frac{\rho c}{\rho_w C_w}\right]^2 \int_0^\infty \frac{\left[1 - \exp(-\kappa t \frac{u^2}{r_b^2})\right]}{\left[u^3 \Delta u\right]} du \tag{3.3}$$

with

$\Delta u = P^2 + R^2$

and

$P = u\ J_0(u) + K\ [u^2/(r_b H) - 2/(\kappa \rho_w C_w)]\ J_1(u)$
$R = u\ Y_0(u) + K\ [u^2/(r_b H) - 2/(\kappa \rho_w C_w)]\ Y_1(u)$
J_0, J_1, Y_0, Y_1 : Bessel's functions

and

T_f: formation temperature at thermal equilibrium (K)
T_a: temperature in annulus (K)
q: heat efficiency (W/m)
K: formation thermal conductivity (W/(mK))
H: contact resistivity borehole-formation
ρ: density of formation (kg/m^3)
c: specific heat capacity of formation (J(kgK))
ρ_w: density of injected fluid (kg/m^3)
C_w: specific heat capacity of injected fluid (J/(kgK))

r_b: borehole radius (m)
κ: thermal diffusivity of formation (m^2/s)

In practice, the heat efficiency supplied to the formation results from fluid circulation in the borehole. A heat exchange takes place between formation and borehole fluid as well as between the fluid in the injection line and the fluid in the annulus. This results in a heat exchanger with countercurrent flow and with heat losses. The heat losses are given by the heat exchange between annulus and formation and are equal to the heat efficiency. As the heat efficiency is expected to be constant, the case considered corresponds to a quasi-stationary case (CARSLAW & JAEGER 1959).

From the above equation the heat exchange between borehole and formation is computed using the function H_f defining the heat transfer coefficient from formation to annulus:

$$H_f = \frac{K}{G_o(t)} \tag{3.4}$$

H_f: coefficient of heat transition from formation to annulus (W/(mK))

Injection line-borehole heat exchange:

In a similar way, heat exchange between the injection line and the annulus can be expressed by an exchange coefficient. The radial heat conduction from injection line to annulus is defined by the coefficient C which involves geometrical and thermal parameters of the tubing (GIECK 1979):

$$C = \frac{1}{\frac{1}{\alpha_i d_i} + \frac{1}{2\pi K'} \ln\frac{d_a}{d_i} + \frac{1}{\alpha_a d_a}} \tag{3.5}$$

where
C: coefficient of heat transition from injection line to annulus (W/(mK))
α_i: coefficient of heat transition on tubing surface at tubing inside ($W/(m^2K)$)
α_a: coefficient of heat transition on tubing surface at tubing outside ($W/(m^2K)$)
d_i: inside diameter of tubing (m)
d_a: outside diameter of tubing (m)
K': thermal conductivity of tubing material (W/(mK))

Heat balance:

Finally, the consideration of all contributions to the heat balance in the annulus of the heat exchanger with countercurrent flow results in the following differential equation:

$$\rho_w C_w Q \frac{\partial T}{\partial z} + \pi(r_b^2 - r_a^2)\rho_w C_w \frac{\partial T}{\partial t} - H_f(T_a - T_f) - C(T_a - T_f) = 0 \tag{3.6}$$

T_f: formation temperature at thermal equilibrium (K)

T_a: temperature in annulus (K)
T_i: temperature in injection tubing (K)
Q: axial flowrate in borehole (m^3/s)
H_f: coefficient of heat exchange from formation to annulus (W/(mK))
C: coefficient of heat exchange from injection line to annulus (W/mK)
ρ_w: density of injected fluid (kg/m^3)
C_w: specific heat capacity of injected fluid (J/(kgK))
r_b: borehole radius (m)
r_a: outside radius of tubing (m)

The first term of equation 3.6 takes into account the convective heat exchange, dependent on the axial flowrate in the borehole. The second term considers the time-dependent change in heat within an element of volume. Finally, the third and fourth terms stand for the heat exchange between formation and annulus and between injection line and annulus, respectively.

The complete differential equation 3.6 constitutes the basis for the evaluation of the fluid logging.

3.4.2 Quantification of fluid logging

For the fluid logging experiments run at the BK site, the temperature distribution T_a (array with temperature sensors at 1 m intervals) was measured within the annulus. With the recorded injection temperatures and the downhole temperatures, the temperature distribution T_i within the injection tube could be approximated.

Considering an element of the borehole annulus volume where temperature has been monitored, the different contributions to the heat conservation equation may again be studied according to Section 3.4.1. Following MURPHY (1977), as a final simplification the depth interval in which water is actually leaving the borehole has not been rigorously analysed. The convective cooling of the formation by the water leaving the well is not accounted for in the heat conservation equations. Thus, the existence of these intervals will be established by solving the equation above and below these intervals for the injection rates. Changes in injection rate indicate their existence and the change represents the amount of fluid being lost at that depth interval. The evaluation of fluid logging data in terms of flowrates will thus reveal inflow zones of the corresponding borehole.

To evaluate equation 3.6, the function H_f has to be solved. For this purpose the finite difference code developed by DORNSTÄDTER (1987) to simulate a heat exchanger with countercurrent flow for the quasi-stationary case (Section 3.4.1) has been applied. The monitored fluid logs illustrated in Section 3.3 were thus evaluated according to flowrates by solving equation 3.6 for the flowrate Q:

$$Q(z,t) = -\frac{[\pi(r_b^2 - r_a^2)\frac{\partial T}{\partial t} - H_f\frac{T_a - T_f}{\rho_w C_w} - \frac{C(T_a - T_i)}{\rho_w \cdot C_w}]}{\frac{\partial T}{\partial z}} \qquad (3.7)$$

Usually, the initial temperature T_f is measured after closing the borehole for a time sufficient to approach thermal equilibrium (MURPHY 1977). If the borehole has been producing or injecting for some time, the time period for thermal equilibration can be shortened by invoking the Duhamel superposition principle. In this situation the borehole is simply shut in for a period several times that required to run the subsequent fluid logging during injection. For the evaluation of the successive fluid logging runs under different conditions at the BK site, the first temperature survey of each test series has been defined to represent T_f although it was not measured during quasi-thermal equilibrium. In any case, the fluid logging could be successfully analysed and - as mentioned above - changes in axial flowrates indicated the existence of permeable (fracture) zones and the amount of fluid being lost at that depth interval.

3.4.3 Interpretation of the fluid logging experiments with fixed probe arrays

The interpretation of the fluid logging data obtained from both the PT-100 sensor array and the fibre optic method resulted in the determination of the depths of joint and fracture zones as well as flowrate profiles along hole (HEINEMANN-GLUTSCH & DORNSTÄDTER 1993).

The depths of inflow zones could be identified in the successive temperature logs (raw data) presented in Section 3.3.

(a) Localization of joint and fracture zones

Borehole BK 85.005:

The fracture at a depth of 17-18 m is dominant (see Figs. 3.10 and 3.11). The warm water front breaks down sharply, indicating a high transmissivity of this fracture zone. Further open fracture zones can be identified at depths of 5 m, 23 m and, finally, 32-33 m.

Borehole BK 85.008:

In the circulation test several negative anomalies developed after injection of water (20 °C) at depths of 5-6 m, 9-10 m, 13-14 m, 18 m, 25 m, 28 m, 32 m, 39-40 m and 45 m (Fig. 3.3a); these correlate with water bearing zones identified in earlier fluid logging experiments (KELLEY & LOEW 1992). Temperature profiles taken during injection tests also indicate dominant water bearing zones.

Fig. 3.4a illustrates the fluid logging run for the injection of cold water with shut outlet. Fracture zones were identified at 5 m, 12 m, 18 m, 23 m, 28 m, 32 m, 39-40 m and 45 m depth and they are more clearly detectable than in the circulation test. The interval pressure of 6-9 bar might be the reason that the water bearing zones in the depth range 0-15 m differ from those identified in the circulation test.

Borehole BK 88.015:

In the circulation test negative anomalies developed after injection of warm water (20 °C) at depths of 22 and 26 m (Fig. 3.2a). These zones correlate with depths of water bearing zones identified in earlier fluid logging experiments (KELLEY & LOEW 1992). Temperature profiles taken during injection tests revealed a dominant fracture

zone at a depth of about 24 m (Fig. 3.2c). Very smooth temperature curves are obtained from the optical fibre measurements. There are only weak indications of fracture zones. For the phases of cold water injection and free outflow, clear indications of open fracture zones are obtained at depths of 22-23 m and about 35 m. There are also weak indications of open fracture zones at depths of 7 m and 27-28 m.

From the temperature-time relation there is some evidence that the behavior of the two main fracture zones at 23 and 33 m might change with time.

In general, the localization of fracture zones was quite successful, although the spatial resolution is not as high as for the conventional fluid logging with a moving probe. The indications of a time-dependence of individual fracture zones on the temperature distribution is interesting. Most probably, this is controlled by the flowrates and the pressure regime in the boreholes during the fluid logging experiment; but changes in the transmissivity with time cannot be excluded. Further detailed studies including modeling of the hydraulic regime are necessary.

(b) Quantification of flowrates

Normalized axial flowrates along the boreholes were calculated from the temperature profiles applying equation 3.7. The results of the fluid logging experiments performed in the boreholes BK 85.005, BK 85.008, and BK 88.015 are shown in Figs. 3.13 to 3.15.

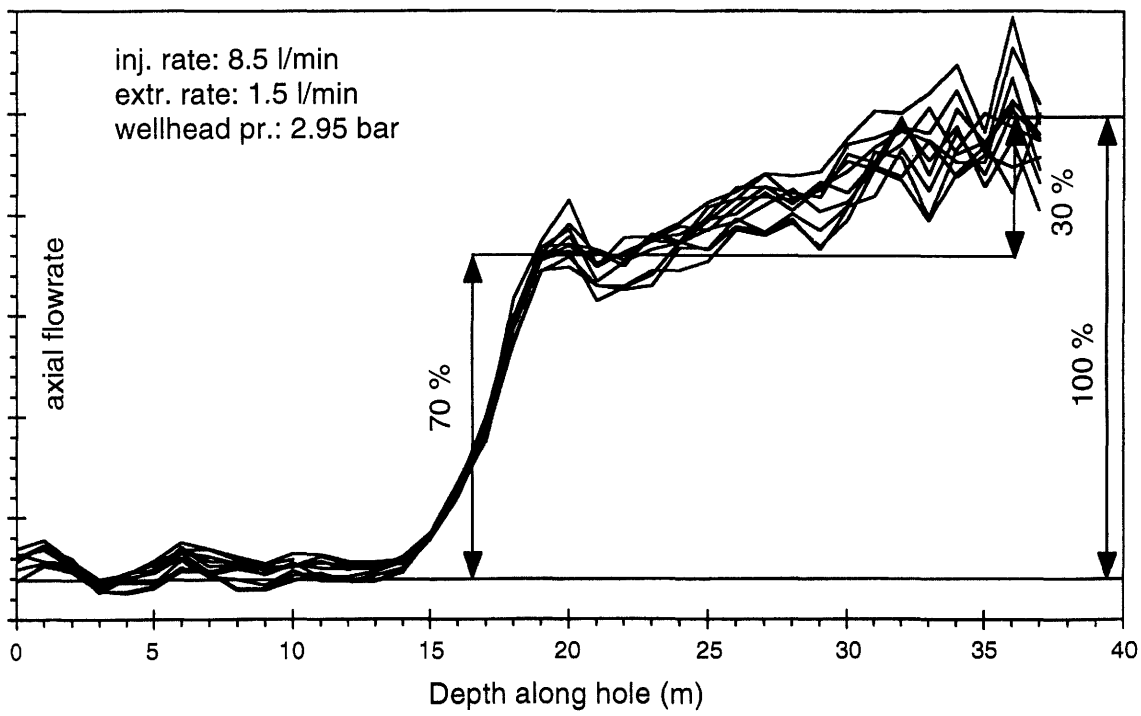

Fig. 3.13: Estimation of relative flowrates in borehole BK 85.005

Borehole BK 85.005:

The flowrate was determined using the fibre optic temperature measurements. The injection temperature was 28 °C, the injection rate 8.5 l/min and the extraction rate 1.5 l/min. During the injection test a wellhead pressure of 2.95 bar was monitored. A clear drop in flowrate is observed between 15 and 18 m depth where most (70 %) of the injected fluid permeates into the formation (Fig. 3.13). The continuous decrease in flowrate from 36 to 20 m depth indicates small water losses within this depth interval.

Borehole BK 85.008:

This borehole intersects numerous fractures. The most significant amounts of water loss were observed at depths of about 13-15 m and 33 m. The results of flowrate determination are given in Fig. 3.14.

The injection temperature was 20 °C. The injection and extraction rates were 5.75 l/min and 0 l/min (closed outlet), respectively. A wellhead pressure of 10.2 bar built up during the experiment. Between the major drops in axial flowrates at depths of 13-15 m and 33 m the flowrate oscillates, indicating several fracture zones of inflowing and outflowing fluid. The flowrate variations between 40 and 45 m depth could be due to initial conditions and the effect of the water flow turning round downhole.

Compared with earlier fluid logging the drop in flowrate at 40 m could also indicate a fluid loss into the formation at that depth. A detailed analysis of the data could reveal additional less important water bearing zones in the depth range between 15 and 33 m.

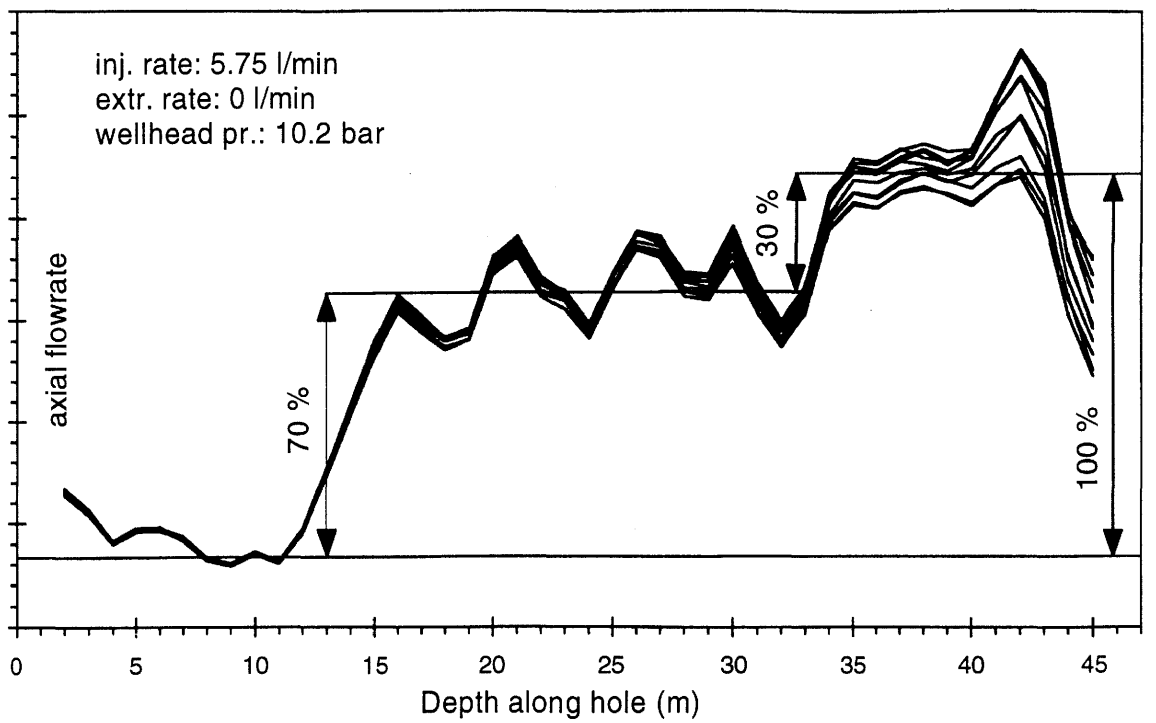

Fig. 3.14: Estimation of relative flowrates in borehole BK 85.008

Borehole BK 88.015:

The flowrate was evaluated from the fluid logging during injection of warm water (20 °C). The injection rate was 5.1 l/min with closed outlet. The interval pressure was 13.8 bar. The only significant drop in flowrate is observed at a depth of 25 m and correlates with a fracture at that depth detected in the FEL log (Fig. 3.15, see also Section 2.2). It seems that, at the interval pressure of 13.8 bar, the injected fluid is completely lost between 23 and 26 m depth.

Finally, the complete results obtained after evaluation of fluid logging experiments with a fixed probe array are summarized in Tab. 3.3:

Tab. 3.3: Localization of fractures and quantification of flowrates

Borehole	Fracture depths from temp.logs in m along hole	Fracture depths from flowrate quantification in m along hole (and losses)
BK 85.005	not analysed	15-18 (70 %) > 18 (30 %)
BK 85.008	5-6, 9-10, 13-14 18, 25, 28, 32, 39-40, 45	13-15 (70 %) 33 (30 %)
BK 88.015	19, 22, 26	23-26 (100 %)

The results reveal the successful feasibility of fluid logging with fixed probe arrays from the technical as well as from the interpretational point of view. The interpretation of fluid logging data with the presented method for the evaluation of fluid losses (approach for heat exchange in the borehole annulus) shows to be valid for logs run at times $\geq$ 1 h after starting injection. The interpretation methods reveals not to be valid for early-time (< 1h) data.

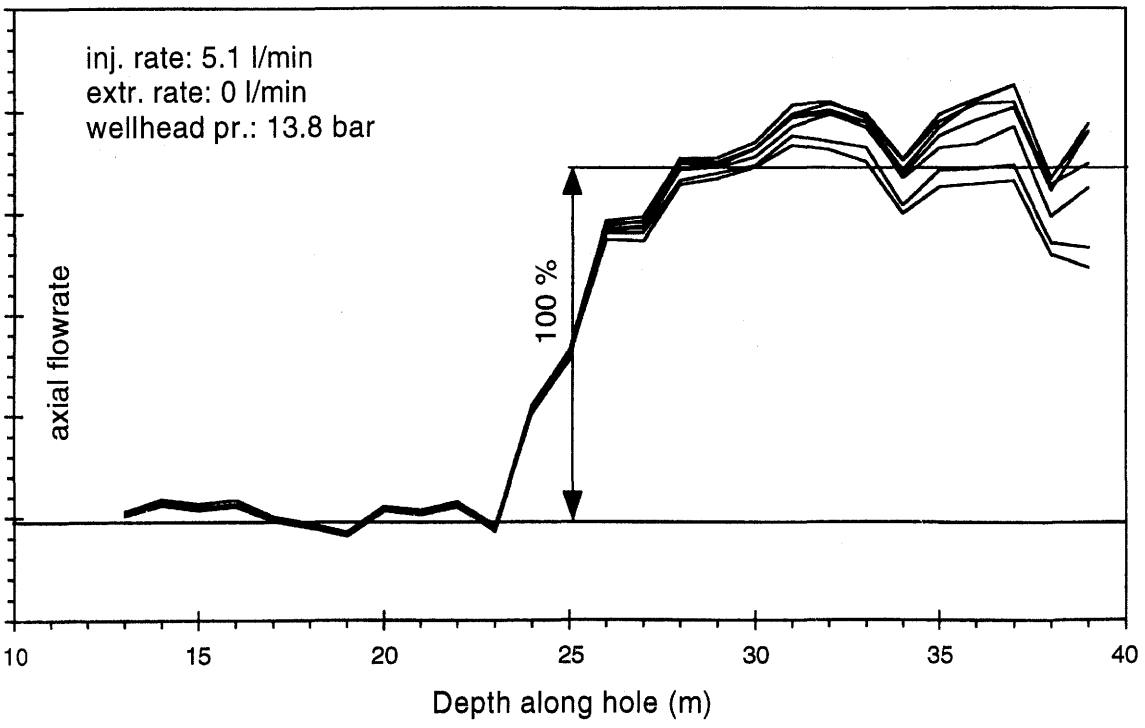

Fig. 3.15: Estimation of relative flowrates in borehole BK 85.015

3.4.4 Discussion of the results

Both fluid logging measurements with fixed probe arrays turned out to be successful. The temperature measurement method with the "distributed fibre optic temperature-sensing technique" yielded as good results as the temperature monitoring with discrete "PT-100" probes. The fluid logging performed with the optical fibre happened to be easier to handle but the temperature measurement with the PT-100 probe had a higher accuracy.

Although fluid logging experiments with a moving probe provide better spatial resolution, fluid logging data with fixed probe arrays could satisfactorily be analysed in terms of depths of inflow zones. The deduced fracture depths coincide with fracture depths resulting from earlier conventional fluid logging experiments (KELLEY & LOEW 1992).

Although the fluid logging evaluation was not valid for the interpretation of temperature logs run < 1h after the start of injection, the application of the method presented for the evaluation according to flowrates proved to be successful when considering the temperature logs run ≥ 1h after the start of injection. The evaluation of fluid logging data for flowrates resulted in the identification of depths of permeable zones and the corresponding amounts of in/outflowing fluid. The amounts of fluid losses are consistent with transmissivities deduced from earlier hydrotests. This emphasizes the validity of the method presented for evaluating axial flowrates in the borehole.

3.5 Pilot investigations with a fixed sal/temp probe array

Within the scope of the current investigations, a new sal/temp probe array was developed by SOLEXPERTS (Schwertzenbach). The device consists of multiple sal/temp probes, which are connected to each other by rigid tubing of variable length. With this tool, pilot investigations were conducted in a borehole simulator at Lawrence Berkeley Laboratory (RATZ 1993). The experiments at LBL's borehole simulator showed that fluid logging in inclined boreholes may be strongly disturbed by density effects. The quantification of flowrates along the borehole proved to be impossible using conventional fluid logging techniques. This fact is confirmed by the field experiments described in Chapter 2.

PART III

HYDROTEST ANALYSIS

4 ANALYSIS OF SELECTED HYDROTESTS

D. Guyonnet (Colenco)

4.1 Introduction and scope

The primary objectives of hydraulic testing at the BK site (Grimsel Test Site) are:

- to develop methodologies and equipment for the characterization of fractured media
- to increase the current conceptual understanding of flow and non-reactive transport in the BK site's fracture network
- to provide estimates of parameters which control flow and non-reactive transport in the BK site's fracture network

The BK tests described herein were all performed after the crosshole constant-head tests VE 451 to VE 457 (PAHL et al. 1992 and GUYONNET & LAVANCHY 1992). Although the analysis of the single and crosshole data from the constant-head tests yielded important results with respect to the BK conceptual flow model, many aspects remained unresolved. The main results of the analysis were to demonstrate evidence of:

- boundaries which acted as a resistance to flow (suspected to be the lamprophyre dykes)
- complex flow geometries (homogeneous 1D radial flow could not always be assumed)
- preferential pathways for flow between boreholes

Hydraulic parameters (transmissivities, storativities) were derived, although these values are strongly dependent on the assumed conceptual flow model (confined, 1D radial homogeneous or composite). Transmissivities estimated from the analysis of the single-hole data range between 8E-07 and 2E-05 m^2/s. Hydraulic diffusivities estimated from the crosshole analysis range between 0.01 and 5 m^2/s.

A significant drawback of these crosshole constant-head tests was that, for all tests, the source borehole was the same (BK 85.004). Such a testing procedure is unable to resolve the fracture network's complex heterogeneity. To address this problem, the Multiple Source Crosshole Test (MSCT) was performed between the 26th of November and the 3rd of December 1992 (VE 499 to VE 513). The analysis of MSCT data is presented in Chapter 5.

Tab. 4.1 lists hydraulic tests which have been performed at the BK site since the constant-head tests. The Table also indicates at which level of documentation the analyses were reported. Some of these tests provide valuable insight into the conceptual flow model at the BK site and are therefore examined in this chapter. We selected the pressure build-up tests VE 478 and VE 484, and the step withdrawal test VE 485. Although test VE 485 was performed in borehole BK 86.003 (Fig. 1.1), which intersects fractures located primarily on the other side of the western lamprophyre relative to the central BK area, it is particularly interesting due to its long duration, compared to active tests commonly performed at the BK site.

Tab. 4.1: List of main tests performed at the BK site since December 1989

Test Designation	Event	Start Date	Documen-tation
450	Pressure Recovery in all Boreholes	14.12.89	NTB 91-09
451-457	Constant-Head Injection Tests in BK 85.004	18.1.90	NTB 91-09
458-464	Crosshole Fluid Logging	30.1090	NTB 91-09
465	Pressure Recovery in all Boreholes	8.2.90	NIB
466	Constant-Rate Withdrawal Test in BK 85.004	7.3.90	NIB
475	Constant-Head Withdrawal Test in BK 86.003	10.12.90	BGR
476	Constant-Head Withdrawal Test in BK 85.008	29.1.91	BGR
478	Pressure Recovery in all Boreholes	7.2.91	BGR
479	Constant-Head Withdrawal Test in BK 88.014	26.2.91	BGR
481	Constant Rate Injection and Recovery in BK 88.014	4.3.91	QLR
482	Constant Rate Injection Test in 88.014	5.3.91	BGR, QLR
483	Salt Injection in BK 88.014	6.3.91	BGR, QLR
484	Pressure Recovery in all Boreholes	19.4.91	BGR
485	Step-Withdrawal Test in BK 86.003	26.6.91	QLR
486	Pressure Recovery in BK 86.003	18.7.91	QLR
487	Step-Drawdown Test in BK 86.003	25.8.91	QLR
488-489	Pressure Recovery in 85.010	1.92	BGR
490	Fluid Logging in BK 85.010	14.1.92	BGR
493	Tracer injection in BK 85.014, Extraction in BK 85.010	19.3.92	BGR
BK_FL 92	Fluid Logging in BK 85.004, 88.014, 88.016, 88.018	27.7.92	QLR
499-513	Multiple Source Crosshole Test (MSCT)	26.11.92	NIB
516-521	Salt Heat Tracer Test	1.3.93	QLR
522	Fluid Logging in BK 85.005, BK 85.008, BK 88.015 with PT 100 - probe array	19.4.93	QLR, NIB
523-526	Fluid Logging in BK 85.005 and BK 88.015 with fibre optical temperature sensing system	21.4.93	NIB

Notes: NTB: Nagra Technical Report, NIB: Nagra Internal Report, QLR: Quick Look Report, BGR: BGR Handouts.

4.2 Pressure recovery tests VE 478 and VE 484

Pressure recovery tests are useful for several reasons:

- it is recommended to perform a pressure recovery test prior to active hydraulic testing because standard hydraulic test analysis methodologies assume steady-state pre-test conditions

- knowledge of the stabilized pressure distribution is required to evaluate the drift's effect on the flow system
- steady-state pressures are required for flow and transport simulations
- the stabilized pressure distribution provides indications of short-circuiting by highly permeable fractures

An important characteristic of the recovery tests at the BK site is that they must last very long before pseudo-stabilized conditions are reached because the drift has affected the flow system since it was constructed in the early eighties and also due to the system's large storativity (see below). Long duration tests are difficult due to equipment constraints, i.e. the potential for packer leakage and failure. For this reason relatively few long duration pressure recovery tests were performed at the BK site. Exceptions are tests VE 478 and VE 484. Details concerning packer positions during these tests can be found in BGR handouts / Tischvorlage (1991a and 1991b).

Test VE 478 was started on the 7th of February 1991 and lasted 19 days. The head data (in m above drift elevation i.e. 1730 m asl) measured in the boreholes located in plane A of Fig. 1.2 (see Chapter 1) are presented in Fig. 4.1a. The data exhibit two very remarkable characteristics. First they show a nearly perfect linear trend, and next, this trend persists for nearly 19 days - no indication of pressure stabilization is seen at the end of the test. A unit slope on a linear plot is usually indicative of data dominated by storage in the borehole. However, it is impossible that the borehole storage period should last so long. For a packed-off interval this period lasts typically in the order of a few to tens of seconds.

A possible explanation for the observed behavior is that the fracture network in the vicinity of the drift is bounded laterally by boundaries which inhibit lateral flow and that the network is connected to the surface (if the system were confined, a linear pressure increase over 19 days would not be possible). The measured pressure build-up therefore corresponds to an increase in a free-surface water level within the fractures. Further evidence for this conceptual model is presented below and the model is illustrated schematically in Fig. 4.4.

Lateral confinement is interpreted in Fig. 4.4 as limited lateral fracture connectivity. However, another possible explanation is that the lamprophyres at the BK site act as lateral impermeable boundaries (BRÄUER et al. 1989). This hypothesis is suggested in particular from pressure recovery test VE 484, which began in April 1991 and lasted nearly 90 days (the first 70 days of data are shown in Fig. 4.1b). During this test, the lower interval in borehole BK 85.008 (30.0-48.9 m depth) stabilized at a head of about 33 m above drift, whereas the upper two intervals in borehole BK 85.008 (9.4-18.7, 19.7-29.0 m depth) stabilized around 90 m above drift, as did most intervals in the central BK area. Examination of the cores from borehole BK 85.008 shows that the lower interval was located on the other side of the northern lamprophyre relative to the central BK area. Also, heads measured in borehole BK 86.003 stabilized around 387 m above drift. The data are not shown in Fig. 4.1b because they are not available in digital format. As mentioned previously, this borehole intersects fractures which are primarily located on the other side of the western lamprophyre relative to the central BK area. The data clearly indicate a decoupling of the flow systems on either side of the lamprophyres.

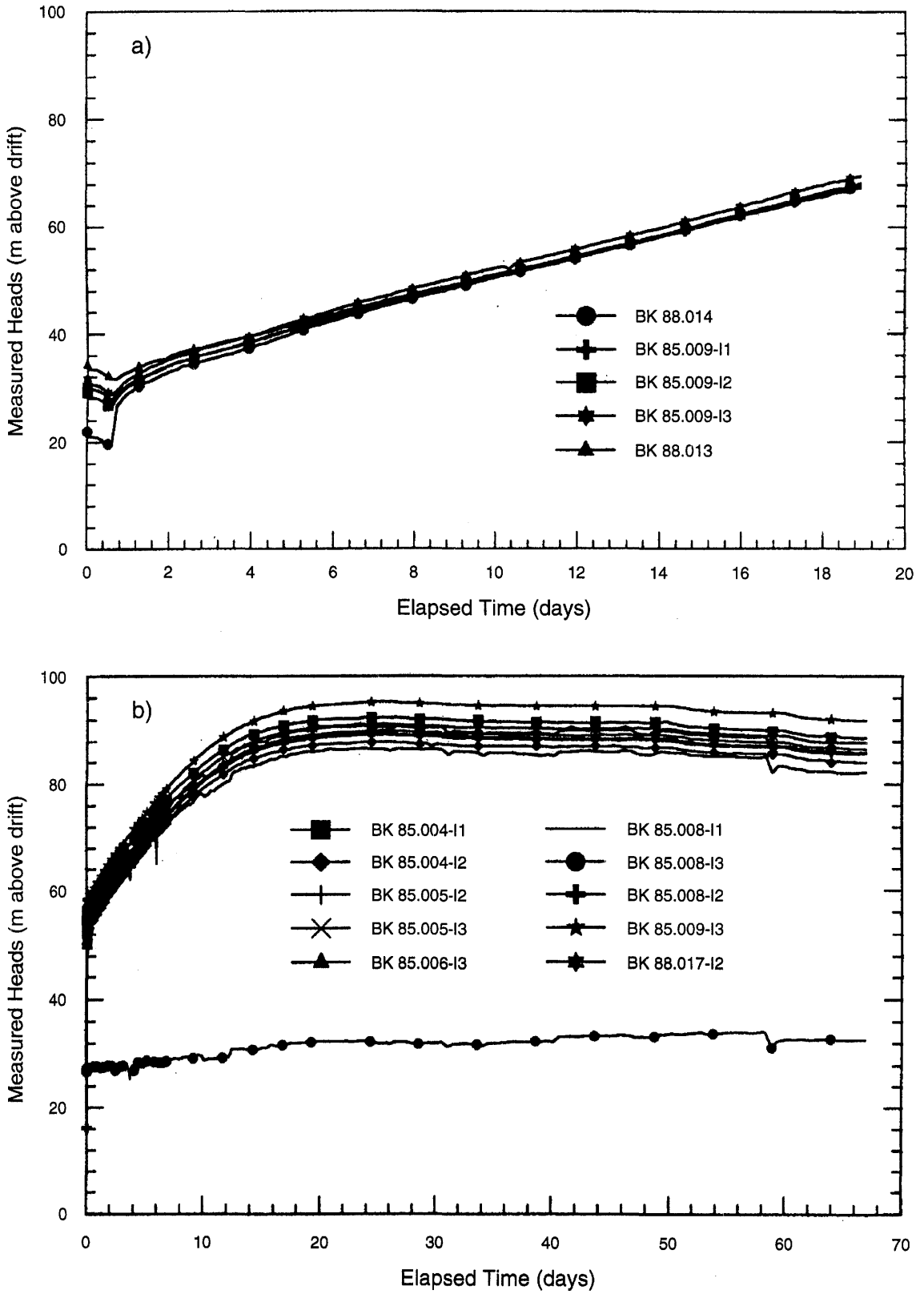

Fig. 4.1: Long duration pressure recovery tests: a) VE 478 and b) VE 484

A comparison of Fig. 4.1a and 4.1b reveals that unlike test VE 478, which showed a linear increase of pressure over a 19 day period, the measurements during test VE 484 showed a stabilization after approximately the same time. This is due to the fact that test VE 484 started at a higher pressure (≈ 55 m above drift) than test VE 478 (≈ 30 m above drift) and therefore less time was required to reach stabilization. The data collected during the first 8 to 10 days of test VE 484 also show a linear trend. Although the hypotheses of packer malfunction (leakage) or trapped air, for example, cannot be ruled out, the late-time heads measured during test VE 484 appear to reflect true stabilized heads in the central BK area.

4.3 Step withdrawal test VE 485

The concept of unconfined flow at the BK site is suggested by other tests and in particular by test VE 485 which started on June 26th, 1991. Seven constant-rate withdrawal tests were performed in sequence, at rates ranging from 0.8 to 6 l/min. The raw data are shown in Fig. 4.2.

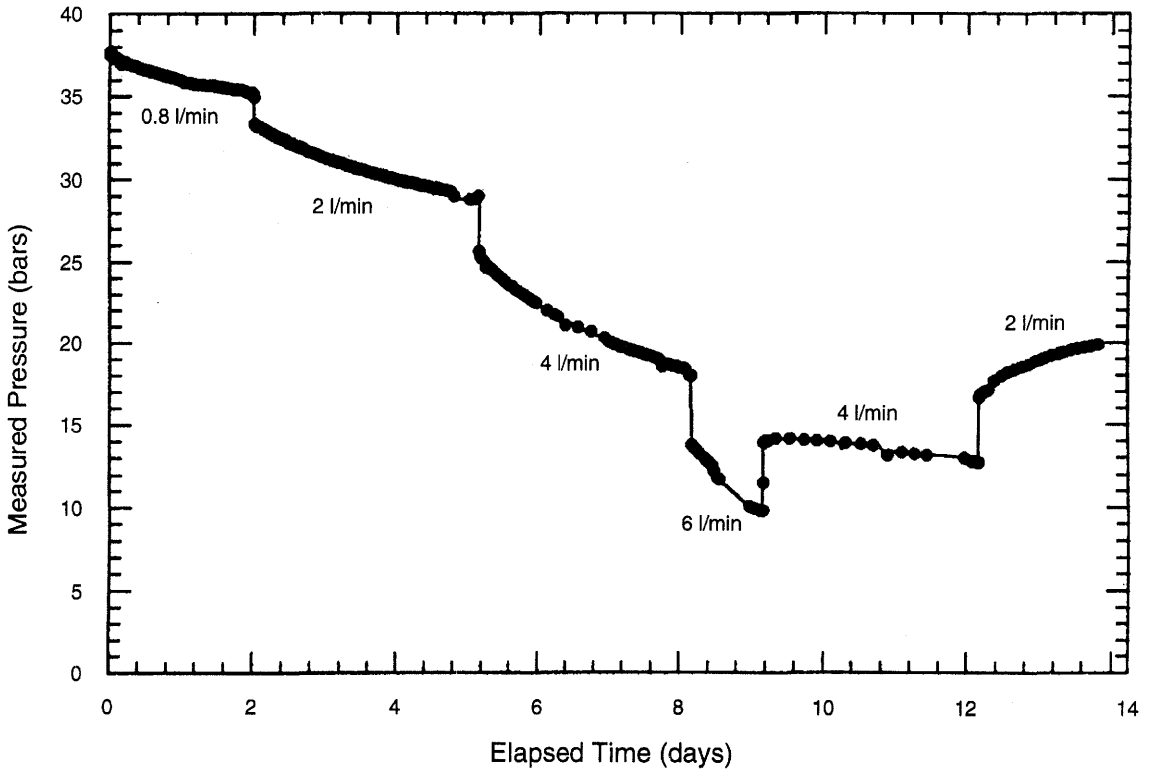

Fig. 4.2: Pressure in BK 85.003 during withdrawal test VE 485

In order to perform a diagnostic plot analysis on data from individual steps, the data were detrended using the principle of superposition (EARLOUGHER 1977). After detrending, the data from each step showed similar characteristics when plotted in log-log coordinates. These characteristics suggest unconfined flow conditions.

During pumping in an unconfined aquifer three distinct phases are observed (NEUMAN 1972):

- an early-time phase during which water comes only from elastic storage and the measured response resembles classical Theis-type behavior

- an intermediate-time response during which water comes from elastic storage and from dewatering of the pore-space by gravity drainage

- a late-time response which again exhibits Theis-type behavior

In NEUMAN (1975), type curves are tabulated which relate dimensionless drawdown to dimensionless time. Type curve matching in the case of unconfined flow is performed in two steps. First the early-time data (if available) are fitted to the early portion of the type curve (Type A curves in NEUMAN 1975). The match along the Y-axis yields the transmissivity (T) while the match along the X-axis yields the specific storage (S). Then the late-time data are fitted to the late portion of the type curve (Type B curves in NEUMAN 1975). The Y-axis match again yields T and the X-axis match yields specific yield (S_y). Both the early-time and late-time data should fit onto the same type curve.

The type curves were plotted and the data from test VE 485 (Step 2, flowrate = 2 l/min) were fitted visually. From the best-fits, the following hydraulic parameters were estimated: T_r = 0.6-1.0E-07 m^2/s, S = 1.0E-03, Sy ≈ 0.4. The measured data were then plotted in terms of dimensionless parameters (equation 4.1) so that the match could be visualized on one plot (Fig. 4.3). The match between theoretical and measured data in Fig. 4.3 is seen to be excellent.

$$\beta = \frac{T_z}{T_r}\left[\frac{r}{b}\right]^2 \quad t_s = \frac{T_r t}{Sr^2} \quad t_y = \frac{T_r t}{S_y r^2} \quad S_D = \frac{4\pi T_r \Delta h}{Q} \tag{4.1}$$

where:

t_s and t_y are dimensionless time
S_D is dimensionless drawdown
T_r is transmissivity in the radial direction (m^2/s)
T_z is transmissivity in the vertical direction (m^2/s)
S is specific storage
S_y is specific yield
Q is flowrate (m^3/s)
Δ h is drawdown (m)
r is radial distance to the well (in this case the borehole diameter r_w) (m)
b is the thickness of the producing zone (m)
t is time (s)

that the most important pressure variations occur. A match in log-log coordinates is therefore far more convincing.

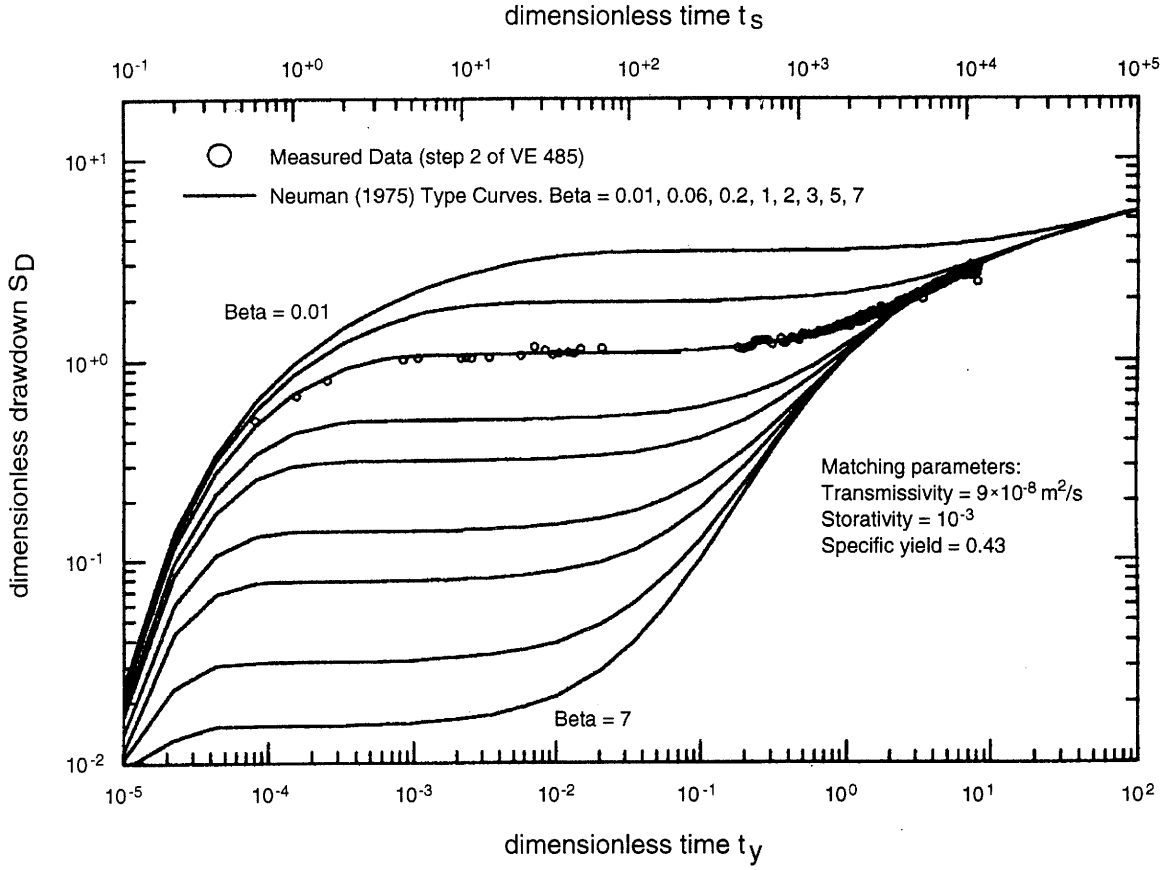

Fig. 4.3: Log-log plot of pressure data for test VE 485 after desuperposition

4.4 Summary and implications for the BK conceptual flow model

Linear plots of pressure recovery data measured during test VE 478 show a linear increase over a period of 19 days. Such behavior implies a response dominated by storage in a bounded system to persist for so long. Moreover, the system must be unconfined for a linear trend.

Lateral confinement is confirmed by data measured during pressure recovery test VE 484 which shows a decoupling of the flow systems on either side of the lamprophyre dykes. These dykes act as boundaries which inhibit flow in the perpendicular direction. Test VE 484 lasted long enough to reach stabilized heads in the central BK area. These heads range between 86 to 92 m above the elevation of the drift. As there are no indications of packer malfunction (leakage) during VE 484, and unless there is a considerable volume of trapped air above the central BK site, this test appears to have reached true stabilized heads. If this were the case, it would imply the existence of a thick unsaturated zone above the central BK area in the many fracture zones, extending from approximately 1830 m asl to ground surface at 2180 m asl.

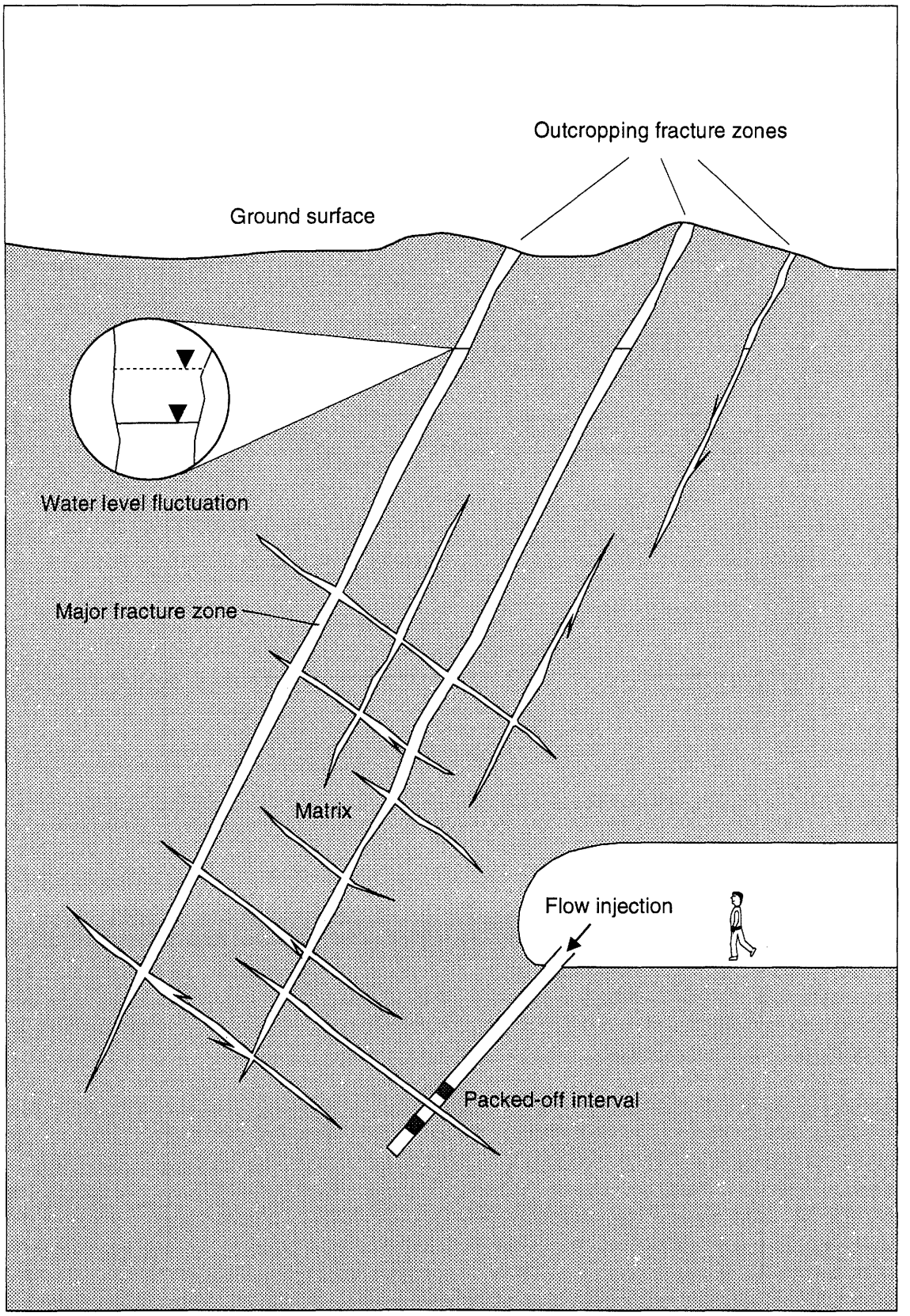

Fig. 4.4: Conceptual model of the BK site, derived from long-term hydrotests

Step withdrawal test VE 485 also suggests unconfined flow in the vicinity of the BK site. This test was however performed in BK 86.003 which is decoupled from the central BK area as it intersects fractures on the other side of the western lamprophyre. When plotted in log-log coordinates, data from this test show a nearly perfect match to type curves for unconfined flow. Data from test VE 487, a step-withdrawal test performed in August 1991 in the same borehole, show similar geometric characteristics when plotted in log-log and can be matched to the same type curve as the data from VE 485. The stabilized head measured in BK 86.003 during test VE 484 lies around 390 m above drift elevation, which is very close to the surface.

The concept of unconfined flow at the BK site is also consistent with numerical simulations of previous tests using the borehole simulator GTFM (PICKENS et al. 1987), which assumes 1D radial confined flow. It was often noted that very large storativity values were required to obtain an approximate match between measured and simulated data. Water released from storage in an unconfined system is much larger than in a confined system because, in addition to water and medium compressibility, it reflects dewatering of void space.

The evidence presented above leads to the conceptual model schematically illustrated in Fig. 4.4. This model is consistent with hydraulic but also geological evidence collected at the BK site. In KEUSEN et al. (1989) it is seen that the major shear-zone (S Zone) observed in cores from the central BK boreholes also appears in surface outcrops at ≈270 m above the elevation of the drift.

In the model illustrated in Fig. 4.4, as water is injected into the fracture network it diffuses rapidly and causes a water level fluctuation in the free-surface water level within major fractures. If the system is bounded laterally, one would expect the water level change to persist after injection has ceased and the borehole is closed. This phenomenon was truly observed during the constant-head tests (VE 451 to 457) and also during the MSCT tests, as shown in the next chapter. Assuming the injected water fills up a bounded system, the measured permanent water level change at the end of injection is used in Chapter 5 to estimate an equivalent fracture network cross-sectional area. This area is then combined with the rates of pressure increase measured during recovery test VE 478 to determine a flux to the BK site.

The proposed model assumes that the granitic matrix does not participate in the flow during active testing. It should be noted, however, that a flow model which leads to similar geometric characteristics in log-log diagnostic plots is the double-porosity model (GRINGARTEN 1984). However, the double-porosity model does not explain the linear trend observed for 19 days during recovery test VE 478, nor the persistence of the water level change observed after water injection. This particular model is investigated further in the analysis of the MSCT data presented in Chapter 5.

5 MULTIPLE SOURCE CROSSHOLE TEST (MSCT)

D. Guyonnet (Colenco), P. Marschall (Nagra), R. Johns (Colenco)

5.1 Introduction

5.1.1 Motivation for the MSCT

Crosshole hydraulic tests are motivated by the desire to adequately characterize flow and transport within a complex geological environment, such as the heterogeneous fracture network at the BK site. The degree of difficulty in adequately describing the physical processes in heterogeneous systems is strongly related to the scale at which the investigation is performed. Studies at the GTS have focused on flow and transport on the scale of a single fracture (FRICK et al. 1992), and on a scale so large that the fracture network could be treated as an equivalent porous medium (VOBORNY et al. 1991). The major difficulty in understanding flow and transport at the BK site results from the investigation scale which is the same as the fracture lengths and interconnections between fractures. On this scale, an equivalent porous medium approach is not applicable (SHAPIRO & BEAR 1985); hence, it is extremely difficult to describe in detail the network's geometry and its hydrogeological properties.

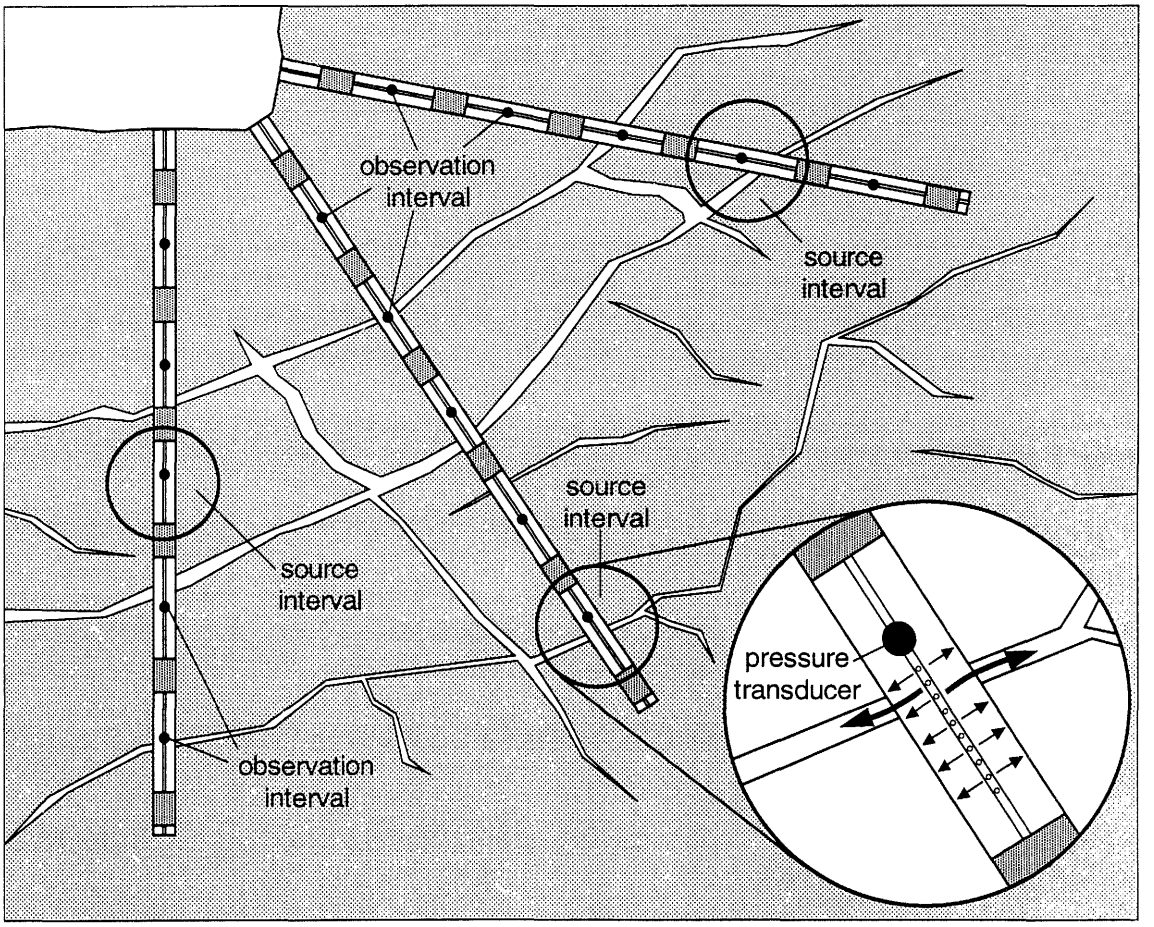

Fig. 5.1: Schematic sketch of the Multiple Source Crosshole Test (MSCT)

An important characteristic of fracture networks is the existence of preferential pathways for flow and transport. Such pathways are of fundamental significance when evaluating the safety of waste repositories because they may provide short-cuts for contaminant migration, and also affect transport phenomena such as dispersion and sorption. A realistic assessment of a waste disposal site's safety would require that all major preferential pathways in the vicinity of the site be known and characterized, or that they can be adequately represented by probability density functions. Such a result may be achieved by performing tests in two boreholes that investigate the region between them (i.e. crosshole hydraulic and tracer tests). Crosshole tests are particularly useful because a significantly larger volume of rock is investigated than during single-hole tests, thereby increasing the scale on which to resolve the medium's heterogeneity. Single-hole tests only provide information about the "localized" heterogeneities around the borehole.

One limitation of the crosshole tests VE 451 to VE 457, described in PAHL et al. (1992) and GUYONNET & LAVANCHY (1992), is that for all these tests the active borehole was the same (BK 85.004). This significantly limits the investigator's ability to describe the fracture network heterogeneity and to detect/characterize all of the main hydraulic features. The Multiple Source Crosshole Test (MSCT) described here was designed to circumvent this limitation and thereby address the problem of fracture network heterogeneity and complexity more adequately. Resolution capability can be enhanced by increasing the number of source and observation intervals as shown in Fig. 5.1.

5.1.2 Objectives and outline of the MSCT analysis

The primary objective of the MSCT analysis is to improve the current understanding of the heterogeneous nature of flow at the BK site and to determine hydraulic parameters which govern this flow. Due to the lack of reliable data and equipment, however, this objective is only partially realized. Nevertheless, other important specific objectives are satisfactorily completed using both single-hole and crosshole data obtained during the MSCT. As discussed in this chapter, the specific objectives of the MSCT analysis are:

- to develop a new methodology to analyse and interpret multiple source crosshole tests using the spectral analysis approach;
- to demonstrate the advantage of using a multiple source technique over that of a single source;
- to test the applicability of the spectral approach for analysing crosshole pressure data;
- to identify possible flow models for BK and estimate diffusivities (T/S) from the analysis of crosshole data;
- to identify possible flow models and estimate transmissivities and storativities on a local scale from the analysis of all available single-hole data.

The first section (Section 5.2) presents the spectral approach for analysing crosshole tests. The basics of the Fourier transform and its attributes are discussed. In addition, new analytical transmission functions for crosshole testing in formations of various geometries and boundaries are developed that can be used to determine the flow model and estimate the diffusivity. A brief discussion of the method used to transform the actual field data to a transmission function is also presented. An example crosshole test using synthetic data is analysed to verify the spectral approach.

Section 5.3 uses a finite-element simulator (KUHLMANN 1992) to generate synthetic crosshole data for a complex fracture zone system. The crosshole data are analysed using the spectral approach for a variety of fracture geometries. It is shown that, depending on the geometry, simple models can be used to adequately characterize fractures within the region between the source-observation borehole pair. Multiple crosshole tests, however, are shown to be necessary to characterize the entire fracture zone system.

The next section (Section 5.4) presents the analysis of the MSCT field data using the spectral and classical time-domain approach. The equipment and test procedures used are described as well as the acquistion problems that occurred. The simple models presented in Section 5.2 are used to attempt to match the observed transmission functions derived from the crosshole data. The transmission functions, however, are strongly influenced by problems related to the test equipment and further extensive analysis using the spectral approach is not done. Subsequently, an analysis of all available single-hole data is presented using a time-domain approach. Just as for the spectral method, however, it is shown that the applicability of using standard time-domain log-log diagnostic plots to identify the flow model is limited due to the noisy data. Instead, linear plots of the pressure data are used to provide additional evidence for the possible flow model identified in Chapter 4 (i.e. unconfined flow with lateral no-flow boundaries). This flow model is used to calculate the fracture network cross-sectional area and estimate the recharge rate to the central BK area. In addition, the numerical simulator GTFM (a 1D radial simulator developed by PICKENS et al. 1987) is used to estimate the hydraulic parameters by matching each individual injection and production cycle. It is shown that the parameter estimates for each cycle do not yield similar values and that the entire observed pressure response (i.e. both the injection and production cycle) cannot be matched using standard simple flow models. This provides further justification for the unconfined flow model hypothesized in Chapter 4.

The last section, Section 5.5, provides a summary of the results and conclusions with respect to the objectives defined above.

5.2 The spectral analysis approach

5.2.1 Literature review

In communication science (which deals with the transmission of signals), it is known that a spectral representation of linear processes provides better opportunities for model identification, parameter estimation and uncertainty analysis than time-domain analysis (e.g. JENKINS & WATTS 1968). DUFFY & GELHAR (1985) reviewed the

application of spectral methods to hydrogeological problems. They showed that both pressure propagation and solute transport in a porous medium can be described in terms of linear filter theory. In both cases, the formation acts as a low-pass filter, which gives rise to frequency-dependent attenuation and phase shift for any harmonic perturbation. These filter characteristics are described by the so-called frequency response function and can be used to identify the hydraulic properties of the formation. RITZI et al. (1991) outlined the advantages of spectral methods for parameter estimation and error analysis. The spectral approach to crosshole hydraulic test analysis is promising in particular because analytical solutions in the frequency domain are applicable for any rate/pressure function in the source borehole. Classical methodologies for hydraulic crosshole test analysis in the time domain require that either the rate or the pressure in the test borehole is constant during testing.

There are two different ways of deriving the frequency response function of a linear system. With a sinusoidal input perturbation, attenuation and phase shift of the output signal can be observed directly and the system's response to a specified frequency is characterized. To obtain the entire frequency response function, the experiment must be repeated for different frequencies. Hence, it would be faster to use an arbitrary input signal that consists of a continuous band of frequencies. The arbitrary input signal can be decomposed into harmonic components using the Fourier transform. Knowing the time-domain response of the system, the frequency response function can then be calculated for the entire frequency range.

Several authors have proposed and successfully implemented sinusoidal hydrotests (BLACK & KIPP 1983 and JOUANA 1992). However, this method is time-consuming and requires sophisticated equipment. Therefore, the approach selected here and described below is based on the derivation of the frequency response function by numerical transformation of input and output signals into the frequency-domain.

5.2.2 Fourier transform and the transmission function

This section briefly describes the approach underlying the spectral analysis of hydraulic crosshole test data. A more detailed description is found in MARSCHALL & JOHNS (1993).

During crosshole pressure testing, an arbitrary pressure signal h(t) induced at the source interval passes through the geological medium and causes a perturbation g(t) measured at an observation interval. The spectrum of the signal h(t) can be estimated using the Fourier transform:

$$F[h(t)] \equiv H(\nu) = \int_{-\infty}^{\infty} h(t) e^{-j2\pi\nu t}\, dt \qquad (5.1)$$

where ν is the frequency and $j = \sqrt{-1}$.

If the hydraulic properties of the geological medium are time-invariant then superposition applies and the output response g(t) is a convolution of the input signal h(t) with a weighting function t(t) (or impulse response function). That is:

$$g(t) = \int_{-\infty}^{\infty} t(\lambda)\, h(t-\lambda)d\lambda \qquad (5.2)$$

where λ is an integration variable.

For crosshole testing, a transmission function can be defined as the ratio of the input and output function spectra:

$$T(\nu) = \frac{G(\nu)}{H(\nu)} = A(\nu)\, e^{j2\pi\nu\varphi(\nu)} \qquad (5.3)$$

where $H(\nu)$ and $G(\nu)$ are the Fourier transforms of $h(t)$ and $g(t)$, respectively. Expressed in terms of the modulus $A(\nu)$ and the phase $\varphi(\nu)$, the transmission function can be thought of as a measure of the medium's ability to transfer a pressure signal. The modulus represents a frequency-dependent damping factor of the transmitted signal and $\varphi(\nu)$ is the phase shift (i.e. delay) of the response with respect to the input signal.

The transmission function is dependent on the medium's diffusivity but also on the flow geometry and boundary conditions. As the formation diffusivity is increased, the efficiency of the transmission is increased and higher frequency components travel further through the formation. For a given flow model, matching a theoretical transmission function to the transmission function of the measured data yields an estimate of the diffusivity.

5.2.3 Transmission functions for selected flow models

Transmission functions were derived analytically by MARSCHALL & JOHNS (1993) for six conceptual models which were thought to be applicable to flow at the BK site. The solutions are presented in terms of Bessel Functions K_0, K_1, I_0 and I_1 (see e.g. ABRAMOWITZ & STEGUN 1972) for the following models:

- radial flow in a homogeneous aquifer of infinite lateral extent (RFH);
- linear flow in a homogeneous aquifer of infinite lateral extent (LFH);
- radial flow with infinitesimal skin in an aquifer of infinite lateral extent (RFSH);
- radial flow in a composite aquifer of infinite lateral extent (RFC, Fig. 5.2a);
- radial flow in a double-porosity aquifer of infinite lateral extent (RFDP);
- radial flow with one or two parallel linear constant-head or no-flow boundaries (RFLB, Fig. 5.2b).

The transmission functions for the six flow models are presented in Tab. 5.1. The wellbore storage and skin are assumed to be "zero" in the observation well. Furthermore, the transmission functions are independent of the wellbore storage in the source well (but not the skin). In Tab. 5.1, S_d is the wellbore skin (s/m^2), r_w is the radius of the source well (m) and r_o is the distance to the observation well (m). Subscripts 1 and 2 are for the inner and outer zones respectively and R is the radial distance from the source well to the discontinuity (m) as indicated in Fig. 5.2a. The

parameter η is the diffusivity (T/S) of the formation (m^2/s). For the double-porosity model (RFDP), λ is the interporosity flow coefficient (m^2) and ϖ is the dimensionless storativity ratio of the fractures to the matrix (WARREN & ROOT 1963). The interporosity coefficient is related to a geometric term, α, and the fracture and matrix conductivities (i.e. K_m and K_f), whereas the storativity ratio is related to the specific storativity of the matrix and fractures (S_f and S_m). Subscripts f and m are for the fractures and the matrix respectively. For the RFLB model, A and B are the distances from the source well to the linear boundaries and θ is the angle between the observation and source wells as indicated in Fig. 5.2b. The distance r_{no} is the distance from the observation well to the source well and image wells (m), while r_{ns} is the distance from the source well to the image wells (m). The + sign indicates a no flow boundary, while the - sign indicates a constant pressure boundary.

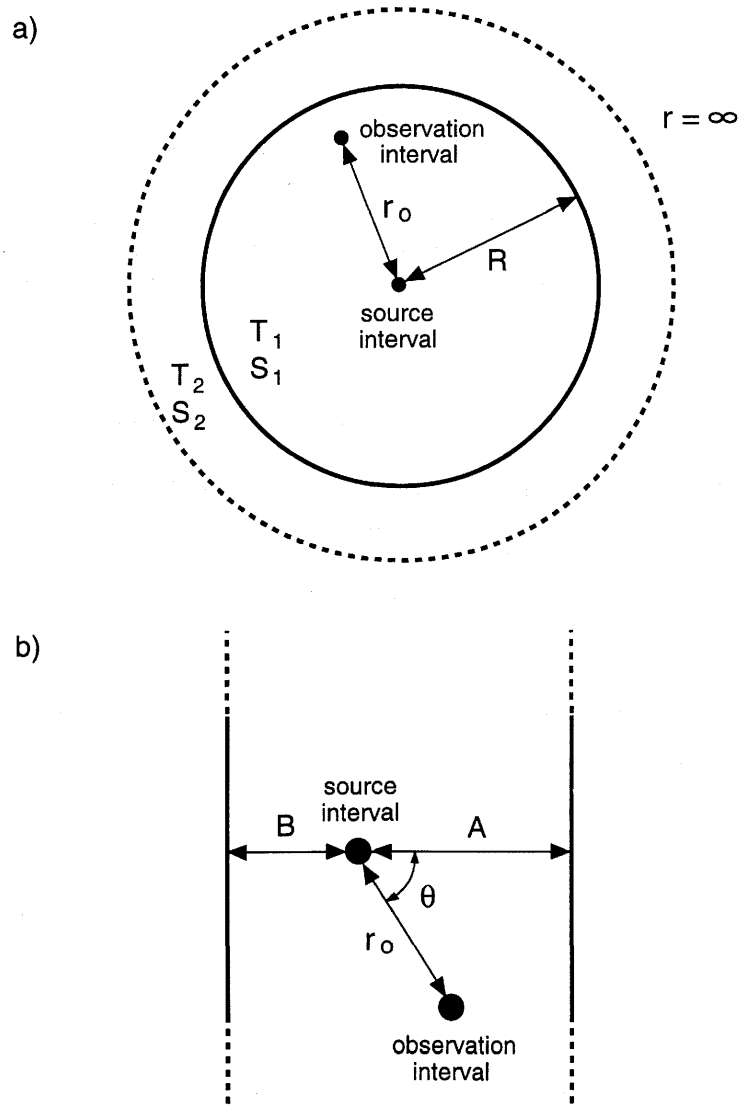

Fig. 5.2: Conceptual aquifer models: a) radial composite system and b) radial flow with two linear boundaries

Tab. 5.1: Analytical transmission functions for selected flow models

Model	Transmission function	Coefficients	Eq. No.
RFH	$T(\nu) = \frac{K_o(\mu r_o\sqrt{j})}{K_o(\mu r_w\sqrt{j})}$	$\mu = \sqrt{2\pi\nu D}$	(5.4)
LFH	$T(\nu) = \exp\left[-(j+1)\mu(X_o - X_w)/\sqrt{2}\right]$		(5.5)
RFSH	$T(\nu) = \frac{K_o(\mu r_o\sqrt{j})}{K_o(\mu r_w\sqrt{j}) + S_d\mu r_w\sqrt{j}\,K_1(\mu r_w\sqrt{j})}$		(5.6)
RFC	$T(\nu) = \frac{\alpha I_o(\mu r_o\sqrt{j}) + K_o(\mu r_o\sqrt{j})}{\alpha I_o(\mu r_w\sqrt{j}) + K_o(\mu r_w\sqrt{j})}$	$\alpha = \frac{F_T\left[K_1(\mu R\sqrt{j})\,K_o(\mu R\sqrt{jF})\right] - \sqrt{F}\left[K_o(\mu R\sqrt{j})\,K_1(\mu R\sqrt{jF})\right]}{\sqrt{F}\left[I_o(\mu R\sqrt{j})\,K_1(\mu R\sqrt{jF})\right] + F_T\left[I_1(\mu R\sqrt{j})\,K_o(\mu R\sqrt{jF})\right]}$ with: $F_T = \frac{T_1}{T_2}$ and $F = \frac{D_2}{D_1}$	(5.7)
RFDP	$T(\nu) = \frac{K_o(\mu r_o\sqrt{jf(\nu)})}{K_o(\mu r_w\sqrt{jf(\nu)})}$	$f(\nu) = \frac{\omega(1-\omega)(\mu^2 r_w^2 j) + \lambda}{(1-\omega)(\mu^2 r_w^2 j) + \lambda}$ with: $\lambda = \frac{\alpha r_w^2 K_m}{K_f}$ and $\omega = \frac{S_f}{S_f + S_m}$	(5.8)
RFLB	$T(\nu) = \frac{\sum_{n=-\infty}^{\infty}(\pm 1)^n K_o(\mu r_{no}\sqrt{j})}{\sum_{n=-\infty}^{\infty}(\pm 1)^n K_c(\mu r_{ns}\sqrt{j})}$	$r_{no} = \sqrt{r_o^2\sin^2\theta + (r_{ns} - r_o\cos\theta)^2}$ $r_{ns} = 2\left[\sum_{\text{odd } n=1}^{\infty} A + \sum_{\text{even } n=2}^{\infty} B\right]$ } for $n > 0$ $r_{no} = \sqrt{r_o^2\sin^2\theta + (r_{ns} + r_o\cos\theta)^2}$ $r_{ns} = 2\left[\sum_{\text{odd } n=1}^{\infty} B + \sum_{\text{even } n=2}^{\infty} A\right]$ } for $n < 0$ $r_{no} = r_o$ and $r_{ns} = r_w$ } for $n = 0$	(5.9)

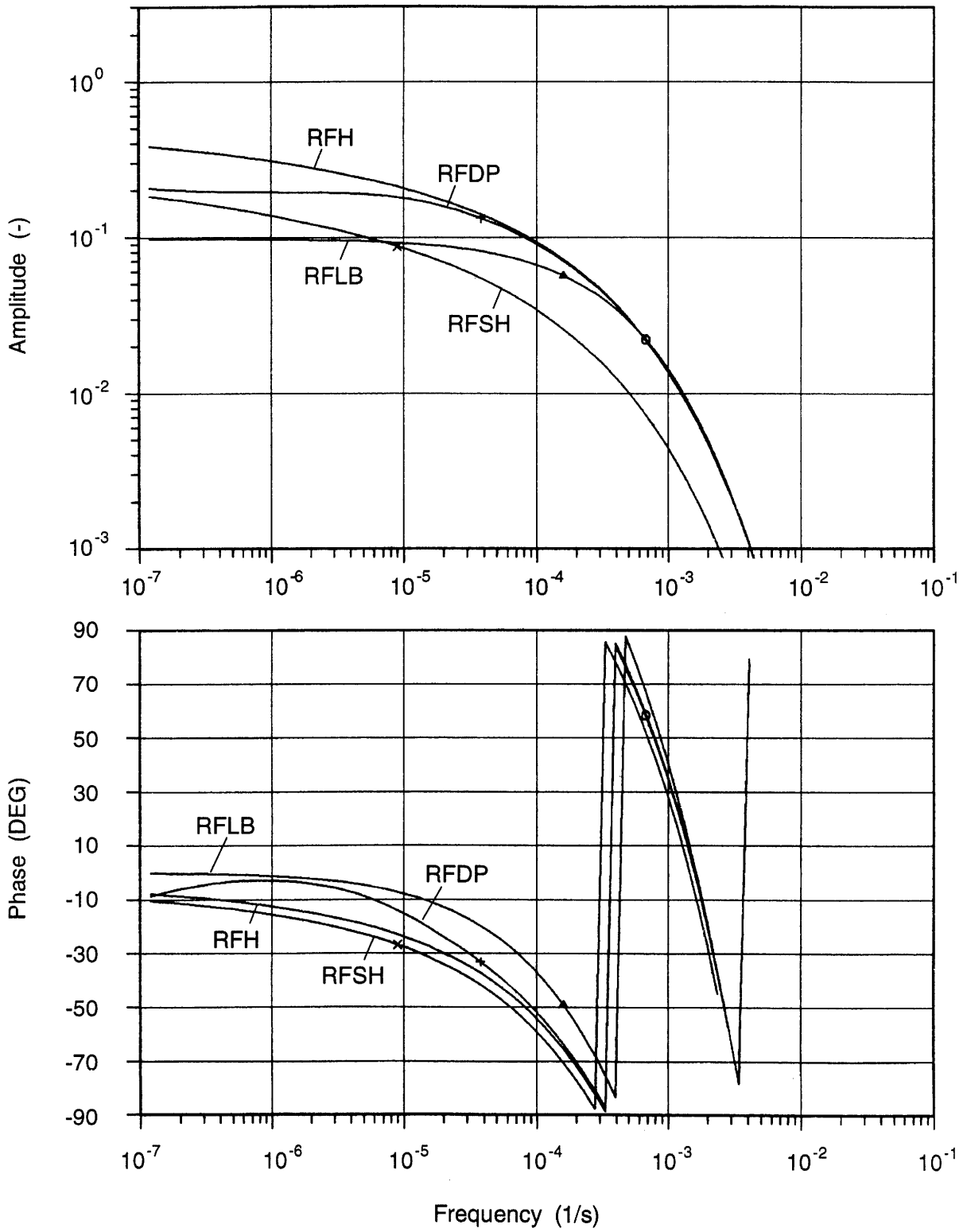

Fig. 5.3: Analytical transmission functions for different aquifer models

Analytical transmission functions for the RFH, RFSH, RFDP and RFLB models are plotted in Fig. 5.3 for the aquifer parameters given in Tab. 5.2. In the high frequency range (i.e. fast periodic time variations), the amplitude is damped rapidly as these frequencies have a very shallow depth of investigation, whereas the phase spectrum changes discontinuously between $-\pi/2$ and $+\pi/2$. The reason for the abrupt phase change is that the lag of the response to the input signal becomes a multiple of 2π, i.e. the arc-tangent function given in equation 5.3 only calculates the primary branch between $-\pi 2$ and $+\pi/2$. In the low frequency range (i.e. long periodic time variations), the amplitude of the transmission function approaches "one", whereas the phase approaches "zero".

A comparison of the four flow models in Fig. 5.3 shows that the amplitude is more useful for identifying the flow model than the phase. The phase and amplitude, however, are useful for determining the formation diffusivity. The amplitudes for the RFH, RFDP and RFLB models merge into one curve in the high frequency range because the short-lived high frequency components are only transmitted in the near-wellbore region and by the fractures. The effects of the linear boundary and matrix flow, however, are significant in the low frequency range. This is because these frequencies, which have a greater depth of investigation, are influenced by the constant pressure boundary and the slow influx from the matrix. The amplitude spectrum of the RFSH model is shifted along the entire vertical axis because all of the frequency components have been dampened at the wellbore wall. Detailed description of the flow models as well as type curves for each flow model can be found in MARSCHALL & JOHNS (1993).

Tab. 5.2: Geometric parameters and hydraulic properties of the analytical models presented in Fig. 5.3

Model	Hydraulic Parameters	
Radial homogeneous (RFH model)	Diffusivity: $\eta = 1\ m^2/s$	
Infinitesimal skin (RFSH model)	Diffusivity: $\eta = 1\ m^2/s$ Skin coefficient: S = 10	Radius of the source well $r_w = 0.044$ m
Double-porosity (RFDP model)	Fracture diffusivity: $\eta = 1 \times 10^{-2}\ m^2/s$ Interporosity flow: $\lambda = 1 \times 10^{-5}$ $1/m^2$ Storativity ratio: $\varpi = 1 \times 10^{-2}$	Distance to the observation well $r_o = 3.2$ m
Linear boundary (RFLB model)	Diffusivity: $\eta = 1\ m^2/s$ Distance: A = 10.0 m Angle: $\varphi = 90$ Constant head boundary	

It can be difficult to distinguish between various flow models if only a part of the frequency spectrum is available. For example, in Fig. 5.3 the linear boundary and double-porosity models would be difficult to differentiate, if only the low frequency or high frequency components are known. Hence, to distinguish between various flow

models, the transmission function is needed over both the low and high frequency components. The next section presents a robust technique to reliably calculate the transmission function over the full frequency range of the available field data.

5.2.4 Numerical Fourier transform

To calculate the transmission function (equation 5.3) of real field data, both the source signal h(t) and the response g(t) are decomposed into spectral components. The decomposition is done by a numerical Fourier transform (FT). For application to real field data, the numerical code should satisfy two specific requirements:

- it must work with non-equidistant sampling intervals in time;
- the spectrum should be calculated on a logarithmic frequency scale.

For this work, the FT was developed using a numerical integration method which makes use of piecewise analytical transformations of the discrete time series. Consider a finite time series f(t), which is continuous in time:

$$f(t) = \begin{cases} 0 \text{ when } t < t_o \\ \text{differentiable when } t_o < t < t_n \\ 0 \text{ when } t > t_n \end{cases} \qquad (5.10)$$

The function f(t), digitized into non-equispaced time data (i.e. as typically recorded in the field) is:

$$f_k = f(t_k) \text{ where } t_k = t_o + \sum_{k=1}^{N} \Delta t_k \text{ and } k = 0,\ldots,N \qquad (5.11)$$

The continuous time series f(t) can be approximated by f^* using a linear interpolation:

$$f^*(t) = f_k + \frac{f_{k+1} - f_k}{\Delta t_k}(t - t_k) \quad \text{where } t_k \le t \le t_{k+1} \qquad (5.12)$$

The function $f^*(t)$ can then be transformed to the frequency domain by piecewise analytical transformation:

$$F^*(\nu) = \sum_{k=0}^{N} \int_{t_k}^{t_{k+1}} f^*(t) e^{-j2\pi\nu t} dt \qquad (5.13)$$

which finally results in:

$$F^*(\nu) = \frac{1}{2\pi\nu}\sum_{k=0}^{N-1}\left[e^{-j2\pi\nu t_{k+1}}\left(jf_{k+1}+\frac{1}{2\pi\nu}\frac{f_{k+1}-f_k}{\Delta t_k}\right)-e^{-j2\pi\nu t_k}\left(jf_k+\frac{1}{2\pi\nu}\frac{f_{k+1}-f_k}{\Delta t_k}\right)\right] \qquad (5.14)$$

For practical use, the FT is calculated on a log-equidistant frequency scale using:

$$\nu_l = \nu_{min}\exp\left[\frac{1}{M}(\ln\nu_{max} - \ln\nu_{min})\right] \text{ where } l = 1,\ldots,M \qquad (5.15)$$

where the limits of this finite frequency scale ν_{min} and ν_{max} are determined by the discretization function t_k given in equation 5.11. That is, the reliable frequency range obtained is increased as the sampling rate is increased. The limits of the reliable frequency range are given by:

$$\nu_{min} = \frac{1}{t_N - t_o} \text{ and } \nu_{max} = \frac{1}{2\max\{\Delta t_k\}} \qquad (5.16)$$

As derived by equation 5.14, $F^*(\nu)$ approximates the true FT $F(\nu)$ by a first order interpolation scheme. A higher accuracy of the numerical procedure could be obtained (i.e. improved high frequency resolution) if the continuous function f(t) was approximated by cubic splines (e.g. AVDEYENKO & MALYUKOV 1989). However, the use of splines is not robust because it can generate significant noise when the data undergoing transformation are noisy. For this reason, the more robust FT given in equation 5.14 was chosen to analyse the BK data.

5.2.5 Verification of spectral approach using GTFM

In this section, the well test simulator GTFM (PICKENS et al. 1987) is used to verify the analytical transmission functions and the numerical FT procedure. GTFM can generate synthetic data sets for all the conceptual models listed in Section 5.2.2. Because MARSCHALL & JOHNS (1993) have verified all the flow models, however, only one model, the double-porosity model (RFDP), is verified here.

Fig. 5.4a shows the simulated crosshole pressure data for a constant flow injection test in a double-porosity formation. The geometric parameters and hydraulic properties correspond to those given in Tab. 5.2. The GTFM pressure data were recorded every 10 seconds. The transmission functions of the synthetic data were calculated using the FT as given in Section 5.2.4. Fig. 5.4b gives the calculated numerical transmission function (shown by dots) as well as the RFDP analytical solution (shown by solid lines). The fit is excellent in the entire frequency range, which demonstrates the accuracy of the numerical FT procedure for almost zero-noise data.

MARSCHALL & JOHNS (1993) further verified that the shape of the transmission function does not depend on the type of hydraulic perturbation. In particular, the effect of alternating flow conditions on the results of the spectral analysis was investigated.

This showed that the spectral resolution in the high frequency part of the transmission function can be improved by using variable flow or alternating flow conditions.

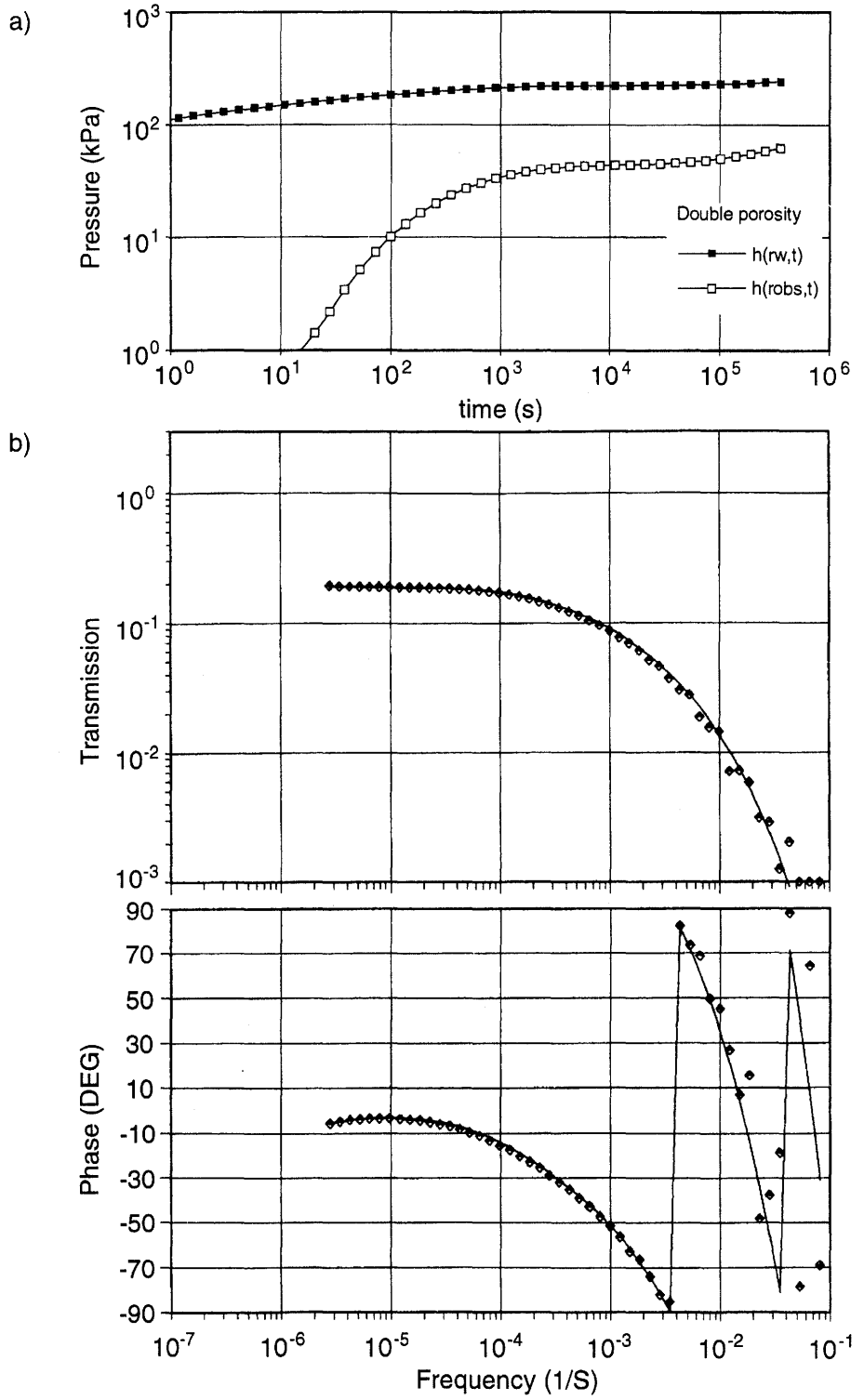

Fig. 5.4: Analysis of synthetic data sets: a) GTFM simulation for a double-porosity system and b) the corresponding transfer function, fitted by the analytical model

5.3 Modeling of a synthetic fracture zone system

This section uses a finite-element simulator to generate synthetic crosshole data for a complex fracture zone system. The crosshole data are analysed using the spectral approach for a variety of fracture geometries. The objective of the section is to show the utility of the spectral approach in characterizing a fracture network, especially for MSCT testing and also to gain a better understanding of flow in a fractured formation.

5.3.1 A discrete model approach

Continuum approaches are frequently applied to simulate flow in highly fractured rock. The heterogeneity of the fracture network is modeled by introducing variations in the hydraulic parameters, which can be determined by analysing fracture apertures and fracture densities with geostatistical methods. Double-porosity approaches are used when the network consists of a large number of intersecting fractures. These continuum or double-porosity models, however, are not suitable for interpreting hydrotests in sparsely fractured formations. Instead, numerical simulations using discontinuous models with discrete fractures are more useful (ELSWORTH 1986) if the locations and orientation of those fractures which represent the main hydraulic components of the flow system are known. This approach is called fracture zone modeling.

Although it is known from core inspection and trace mapping that the BK site is intensely fractured, geological and long-term observations of hydraulic heads suggest that only a few major fractures significantly contribute to flow in this fracture system (see Section 4.4). These major fracture zones are well connected to each other and may be intersected by various classes of minor fractures.

The finite-element simulator CASA (KUHLMANN 1992) was used to model these highly transmissive fractures. Details of the CASA simulator and the model used can be found in Chapter 8. As shown in Fig. 8.1, the model consists of five fractures: two lamprophyre dykes, one so-called K zone and two S zones. The location of the source and observation intervals were the same as those used during the MSCT hydrotests. The transmissivities, storage coefficients and diffusivities of the individual layers were arbitrarily assumed and are given in Tab. 5.3. The matrix was assumed to be impermeable.

Tab. 5.3: Hydraulic parameters of the CASA model

Fracture ID	Transmissivity T	Storage coefficient S	Diffusivity $\eta = T/S$
	[m^2 /s]	[-]	[m^2 /s]
#801 (LamN)	3.66E-08	1.20E-06	3.1E-2
#802 (LamS)	0	-	0
#780 (K^+)	1.05E-06	1.03E-06	1.0E0
#902 (S^+)	4.33E-07	7.70E-06	5.6E-1
#954 (S^-)	7.92E-07	2.38E-06	3.3E-1

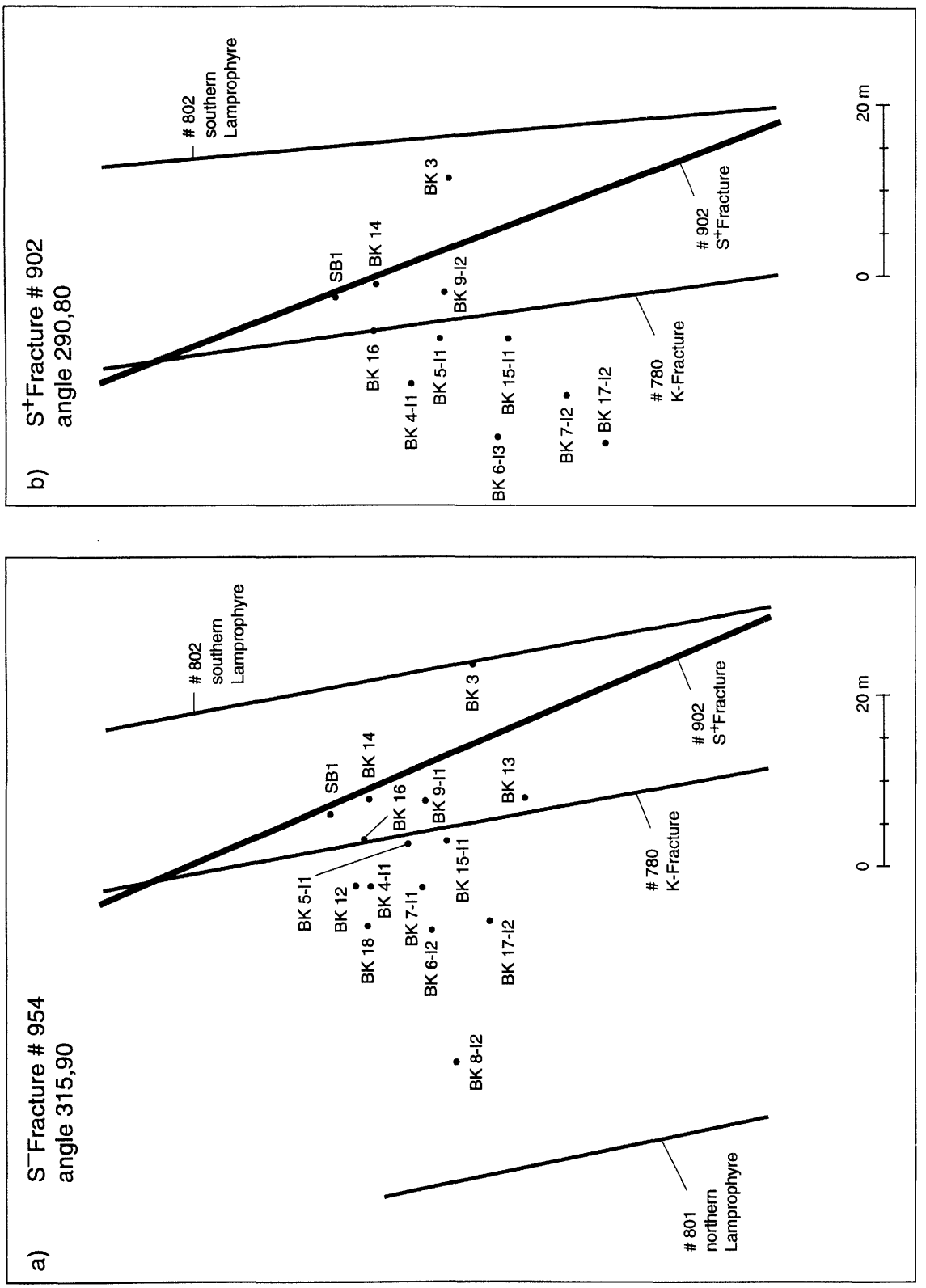

Fig. 5.5: Simulating crosshole tests with CASA: intersection of a) the S^- zone (#954) and b) the S^+ zone (#902) with the other fractures and borehole intervals of the model shown in Fig. 8.1

Figs. 5.5a and b show a planar view of the intersection of the S^- zone (#954) and S^+ zone (#902), respectively, with the other fractures and borehole intervals. It becomes evident that, even in such a simple fracture network, the geometric grouping of the intervals with respect to the fracture intersections are complicated. This is because some of the intervals are close together within the same fracture, whereas others are separated by one or two intersecting fractures. Several intervals do not even intersect the fracture. It will be shown below that each of these different arrangements produces a characteristic transmission spectrum, which may help to identify the location and the orientation of the individual fracture intersections.

5.3.2 Modeling with CASA

When analysing hydraulic crosshole tests performed in fracture networks, it is often difficult to interpret the observed pressure response. Depending on the connectivity of the fracture system, observation intervals with a short distance to the source borehole may not respond at all, whereas other intervals which are far away are strongly affected. Hence, the CASA simulations focused on the development of a strategy for using crosshole tests as a diagnostic tool to characterize sparsely fractured rock. The strategy and specific objectives were:

a) to identify "localized" flow models and to estimate local hydraulic parameters by the analysis of the synthetic data from selected source-observation pairs. The analysis is based on the analytical models given in Section 5.2.3;

b) to assemble these localized flow models into a consistent global model;

c) to investigate the positioning of multiple source-observation pairs for determining the locations and orientations of the fractures.

Synthetic data sets of the transient pressure response in all intervals were generated using the intervals BK 5-I1 and BK 4-I1 (Figs. 5.5a, b), respectively, as source boreholes during a finite duration constant-rate test. The simulated data were analysed by the spectral approach and then fitted with the appropriate analytical solution to estimate the hydraulic parameters. The known geometric properties, such as the linear distance between the source and observation intervals and the distance of the source interval to a fracture intersection, were assumed in the inverse modeling. The inverse modeling program is described by MARSCHALL & JOHNS (1993). Although not done here, future work is planned to fit both the distance to the fracture intersection and the fracture diffusivity using multiple sets of transmission functions.

The approach is based on the philosophy that the best flow model is the simplest one that can produce the observed response. For the synthetic source test in BK 4-I1, transmission spectra corresponding to observation intervals BK 12, BK 7-I1 and BK 14 are plotted in Fig. 5.6 (shown as dots). The transmission functions of BK 12 and BK 7-I1 were satisfactorily fitted with a constant-pressure linear boundary model (RFLB), whereas interval BK 14 could only be fitted with an infinitesimal skin model (RFSH). Amazingly, these simple analytical models were able to fit the (synthetic) data well even though the synthetic fracture network is much more complicated. The estimated parameters from each of the observation intervals are given in Tab. 5.4.

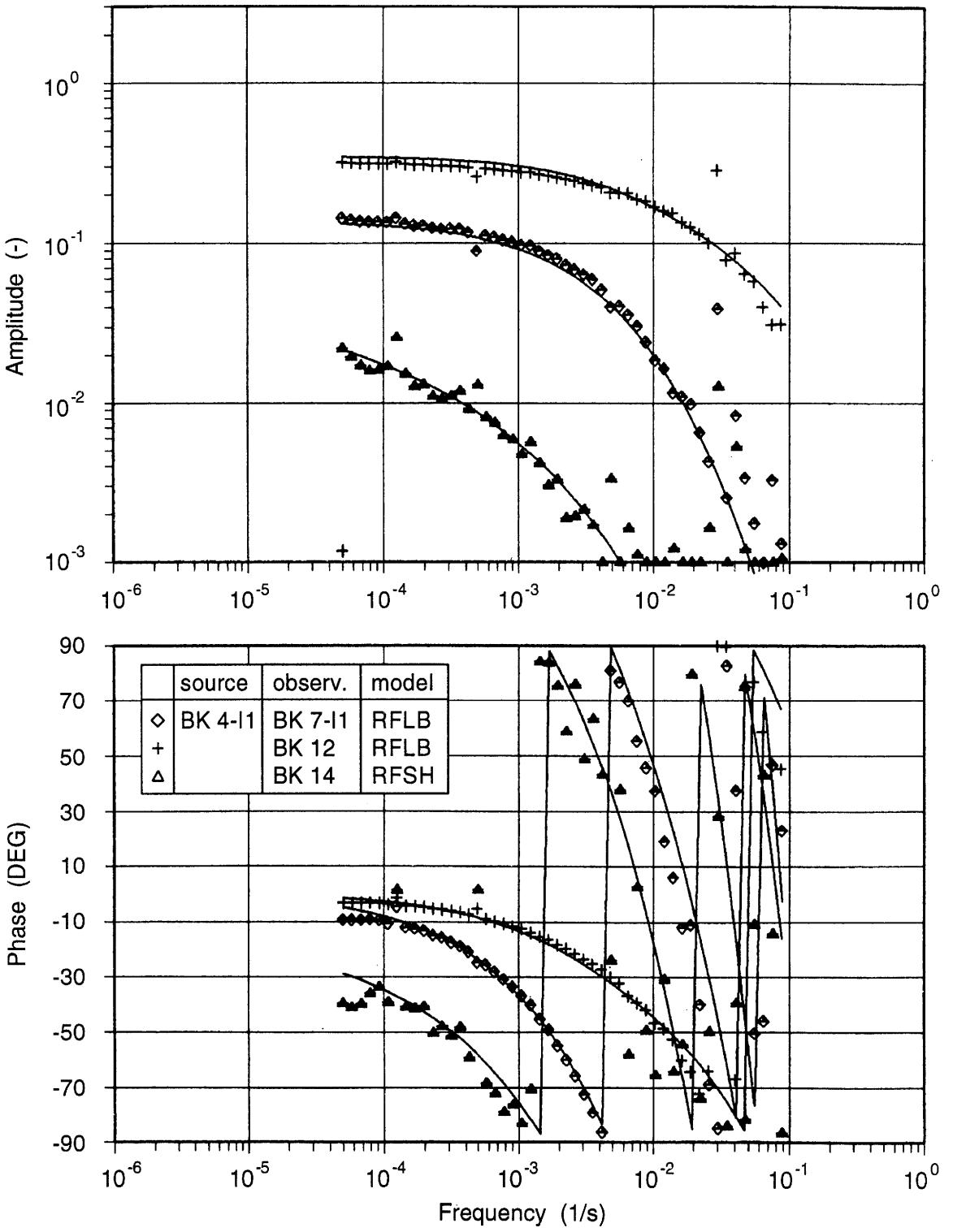

△ + ◇ CASA results based on model presented in Chapter 8.

——— synthetic data (see Chapter 5.2.5)

Fig. 5.6: Spectral analysis of synthetic crosshole data: transmission functions and fitted models

The spectra of BK 12 and BK 7-I1 show linear constant-pressure boundary responses because these observation intervals are located in fracture #954 and on the same side of the #780 - #954 fracture intersection as the source interval (BK 4-I1). The intersection acts as a constant-head source because the transmissivity of fracture #780 is larger than fracture #954. The estimate of the diffusivity of fracture #954 from the analysis of these observation intervals compares well with the true diffusivity used in the simulation (Tab. 5.4).

The BK 14 observation interval, however, could not be fitted with a linear constant-pressure boundary because it is located on the other side of the #780 - #954 fracture intersection. Instead, an infinitesimal skin response (RFSH) gave a good fit as shown in Fig. 5.6. The reason for this is that the fracture intersection caused an instantaneous drop in the amplitude of the frequencies transmitted to the BK 14 interval, but the phase was nearly unaffected. The fitting was satisfactory even though the transmission function contained significant noise (i.e. due to the amplitude reduction). Again, the estimated diffusivity agreed well with the true diffusivity of the #954 fracture (see Tab. 5.3).

Tab. 5.4: Results of the analysis of the CASA simulated data

Source int.	Observ.int.	Parameters	Model
BK 4-I1 r_w = 0.044 m	BK 5-I1 r_{obs} = 6.7 m	η_{est} = 0.27 m^2/s φ = 55°	Linear boundary (constant head) r_d = 5.0 m
	BK 7-I1 r_{obs} = 6.2 m	η_{est} = 0.25 m^2/s φ = 105°	
	BK 12 r_{obs} = 1.5 m	η_{est} =0.17 m^2/s φ = 80°	
	BK 14 r_{obs} = 10.5 m	η_{est} = 0.36 m^2/s Skin = 62.8	Inf. Skin
	BK 15-I1 r_{obs} = 10.5 m	-	-
BK 5-I1 r_w = 0.044 m	BK 4-I1 r_{obs} = 6.7 m	η_{est} = 0.40 m^2/s φ = 125°	Linear boundary (const. head), r_d = 5.0 m

In Fig. 5.7, three additional transmission functions using the source interval BK 4-I1 are presented for the observation intervals BK 15-I1, BK 5-I1, and BK 4-I1. Although the linear distance between BK 15-I1 and the source interval BK 4-I1 is not more than several meters, the response of BK 15-I1 is very small. This is because BK 15-I1 does not intersect fracture #954 and the pressure wave has to join fracture #902, before it is transferred to BK 15-I1. Consequently, the amplitude spectrum of BK 15-I1 is strongly damped. For parameter estimation with one of the analytical models given in Tab. 5.1 an apparent travel distance had to be fixed, which is difficult due to the complex pattern of pressure propagation.

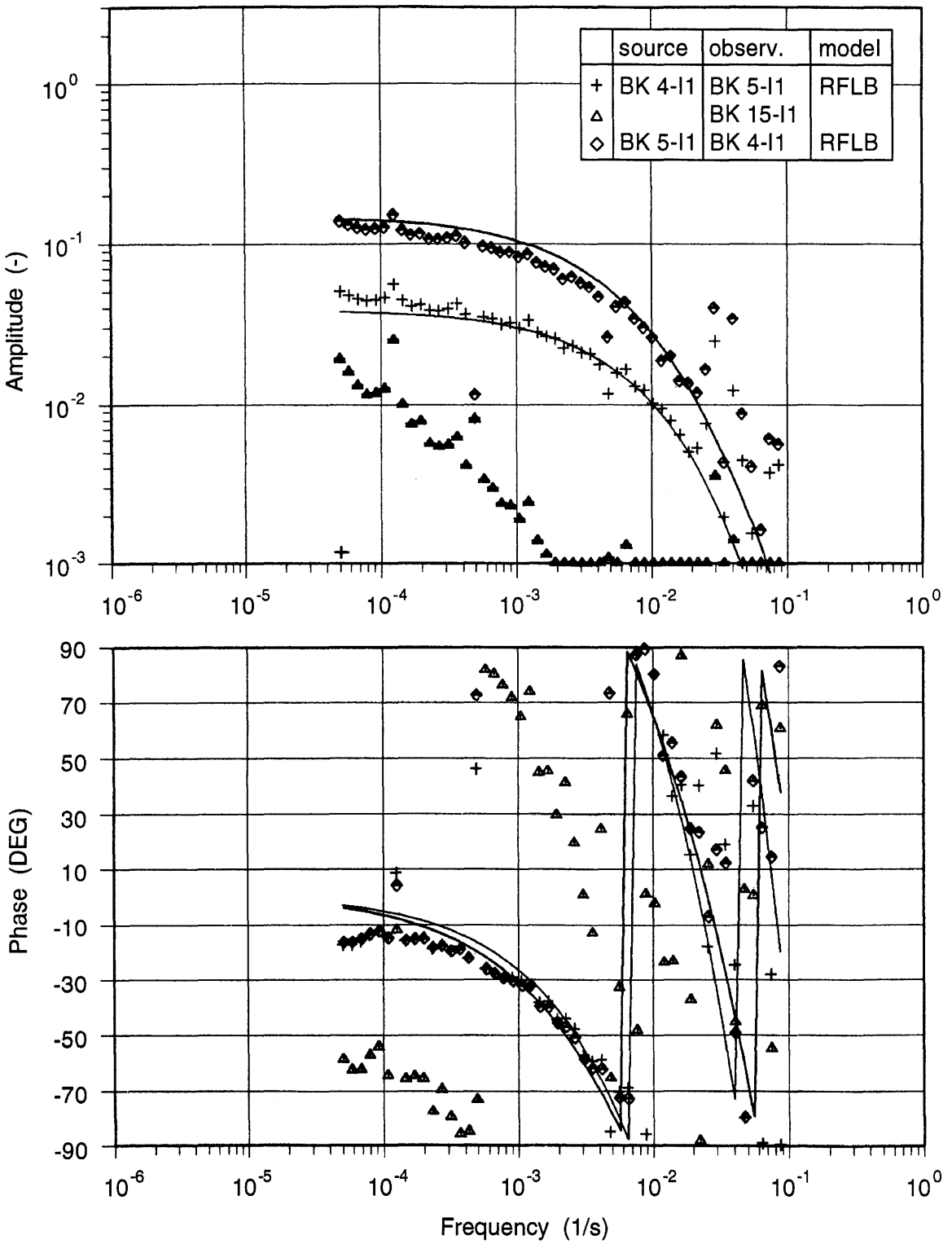

△ + ◇ CASA results based on model presented in Chapter 8.

——— synthetic data (see Chapter 5.2.5)

Fig. 5.7: Spectral analysis of synthetic crosshole data: transmission functions and fitted models

The two other transmission spectra shown in Fig. 5.7 correspond to the source-observation pair BK 5-I1 and BK 4-I1. The first transmission function is when BK 5-I1 is the observation interval and BK 4-I1 is the source interval, whereas the second is when they are interchanged. As shown, the transmission functions are not the same when the source and observation intervals are reversed. Hence, this is an indication that heterogeneities exist in the formation. For both transmission functions, the constant-pressure linear boundary model gives the best fit. The estimated diffusivities for each configuration are within a factor of 2 as shown in Tab. 5.4.

Although only a few crosshole tests were analysed, the above analysis demonstrates the utility and potential of obtaining Multiple Source Crosshole Test data in characterizing the fracture network. Two simple analytical models were successfully used to match the transmission functions for crosshole tests in the complex fracture zone system. The next section uses the lessons learned from the CASA simulations to attempt to obtain a global model for the BK site.

5.4 The MSCT field experiment

5.4.1 Procedure, equipment and data acquisition

The MSCT experiment was performed between the 26th of November and the 3rd of December 1993 at the BK site, and consisted of fifteen hydraulic crosshole tests (VE 499 to VE 513). The BK site (as shown in Figs. 1.1 and 1.2) is extensively drilled with 17 boreholes that originate from the BK drift. Data collection and packer installation in these boreholes were done by BGR. Fig. 5.8 shows the packer positions in the boreholes of the central BK area during the MSCT. Ideally, all hydraulically active fractures should have been isolated by packers during testing, but this was not possible due to the limited number of packers available. A total of 29 intervals were monitored during the test. The distances between the source and observation intervals ranged from 4 to 60 meters. Four intervals located in borehole BK 85.007 could not be monitored due to technical problems (i.e. data acquisition failed). For further details of the test configuration and design, the reader is referred to GUYONNET & DOMSKI (1993).

All intervals were monitored using BGR's TORBEN acquisition system which runs on an HP 9836 computer system. The TORBEN system samples pressure data at a sampling rate of 40 seconds per data point. As pointed out in Section 5.2, a large sampling rate creates noise in the high frequency range that can obscure flow model identification using the spectral analysis approach. This is also true of the classical time-domain methods that use log-log diagnostic plots for flow model identification. For example, the timescale of the fracture pressure response in a double-porosity model may be in the order of tens of seconds and, hence, the fracture response would not be detected by such a large sampling rate.

In addition to the large sampling rate, data from the TORBEN system showed spikes caused by an electronic problem related to the transfer of the signal from the transducers to the acquisition system. These spikes are usually positive peaks and hence are biased to one side. The TORBEN data are affected by these spikes because each

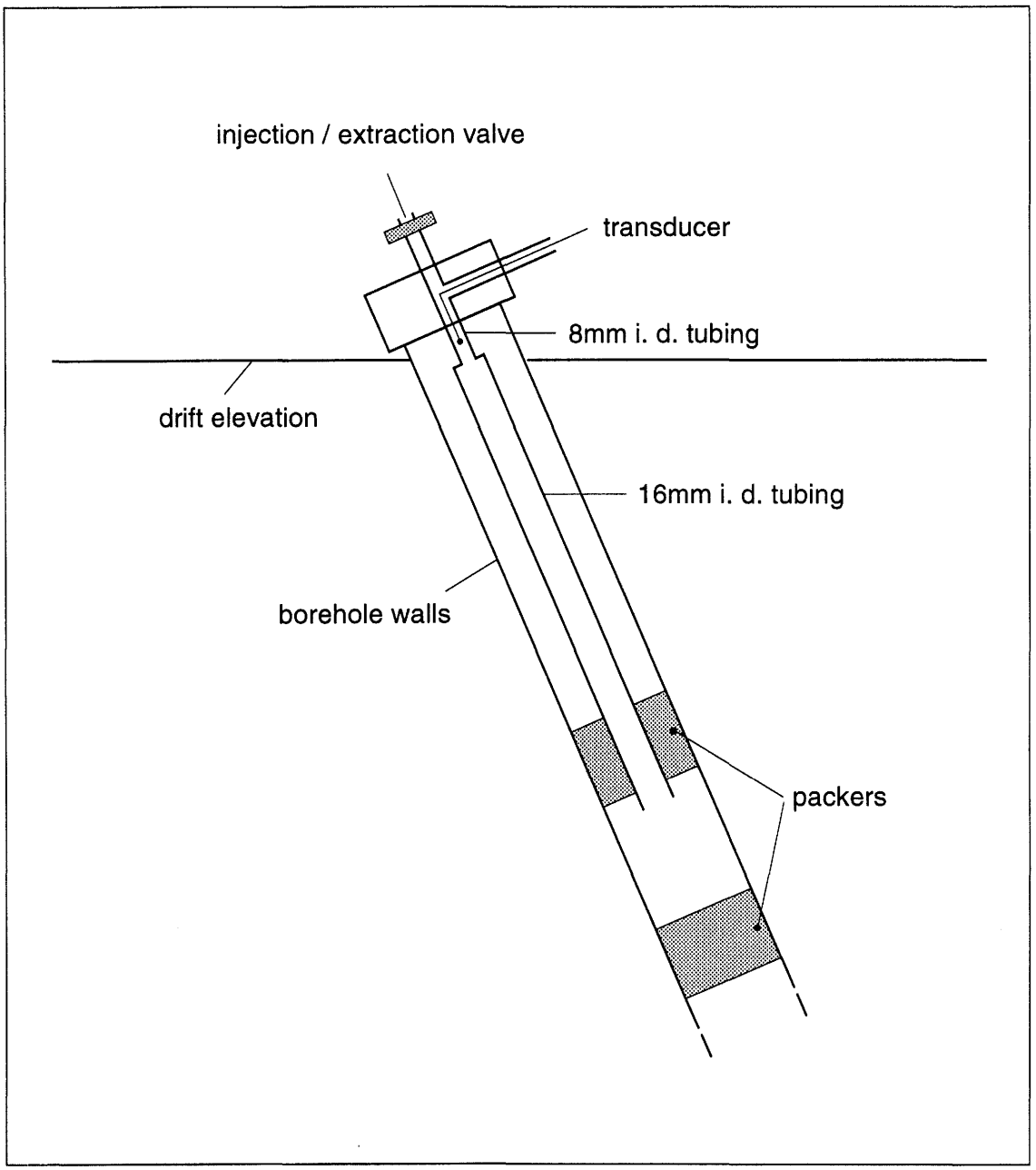

Fig. 5.8: Packer positions in the boreholes of the central BK area

recorded value is a moving average over 40 to 60 samples, i.e. the averaging process is biased to positive pressures by the spikes. Tab. 5.5 summarizes which intervals were used as source intervals and gives details concerning the test events. The tests began with a constant-rate injection into a given source interval until a stabilization of the injection pressure was observed. Next, the tubing connected to the source interval was opened and the interval was allowed to flow until an equivalent volume was produced as that which had been previously injected (i.e. zero net recharge). Once this condition was met, the tubing was closed and the recovery of pressure measured.

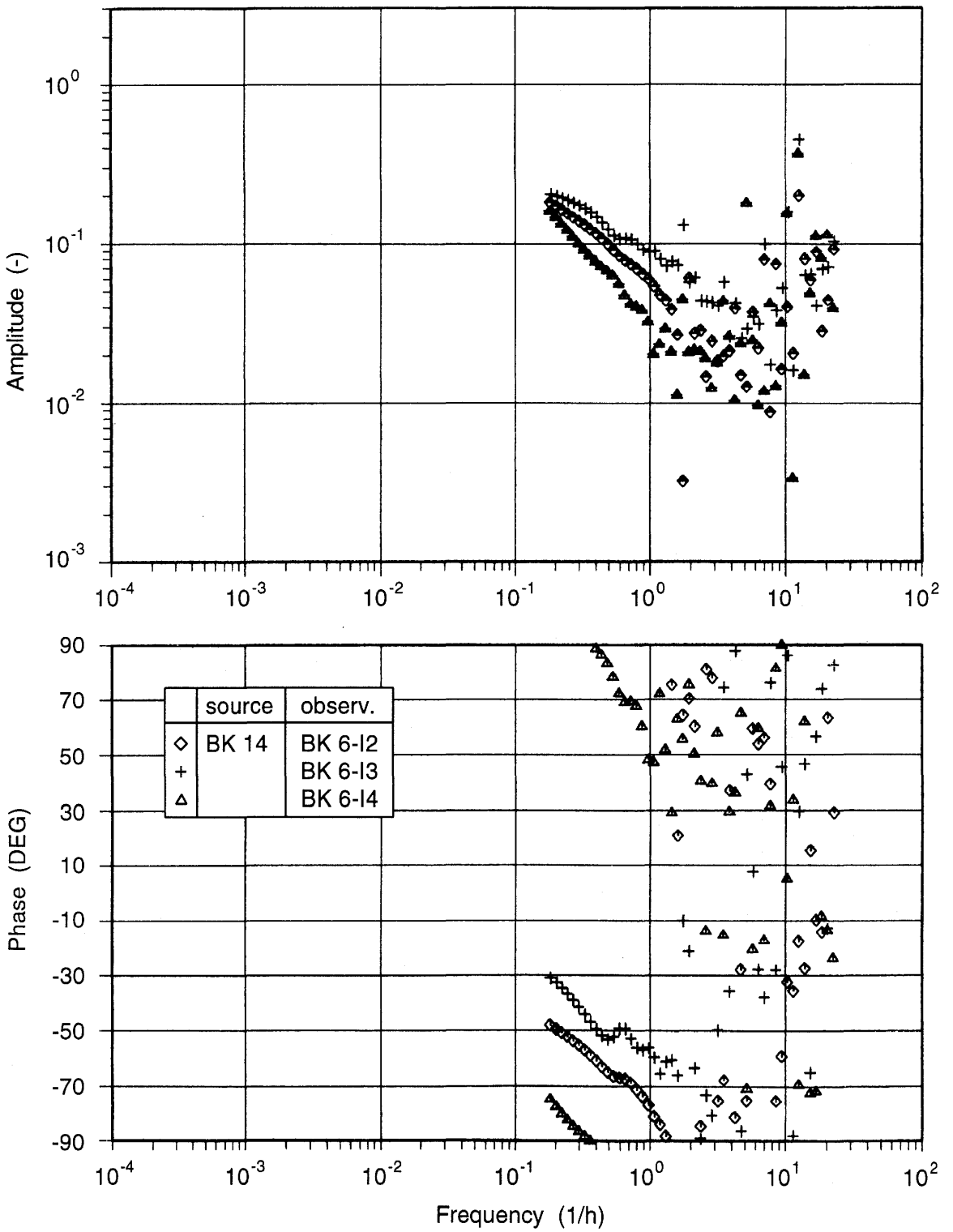

△ + ◇ CASA results based on model presented in Chapter 8.

——— synthetic data (see Chapter 5.2.5)

Fig. 5.9: Spectral analysis of test VE 508: transmission functions

The advantage of this procedure is that the time required for recovery of the pre-test pressure in the source interval is minimized and, therefore, the overall test duration is optimized. For five of the source intervals, however, it was not possible to conduct the head withdrawal test (see Tab. 5.5). In addition, test VE 501 gave unreliable pressure values because the pressure losses in the tubing were extremely large (2 mm tubing was used). The next section describes the pressure losses that occurred during the tests.

Tab. 5.5: Summary of test sequence with relevant test parameters

Date	Test	Interval	Constant Rate Injection			Constant Head Withdrawal	
			Duration (hrs)	Rate (l/min)	dP (bars)	Duration (hrs)	Rate (l/min)
26.11.93	VE 499	BK 015-I1	0.2	? 4	13	0	--
	VE 500	BK 015-I2	0.25	0.5	9.5	0.2	3
	VE 501	BK 005-I2	?	?	?	?	?
27.11.93	VE 502	BK 005-I1	0.8	11.5	7.5-9.5	1.4	5
	VE 503	BK 004-I2	0.9	16	1.4-2.4	0	--
30.11.93	VE 504	BK 004-I1	0.4	14	3	0.8	5
	VE 505	BK 012	0.5	13	3	0.8	5
	VE 506	BK 011	0.42	3-10	15	0	--
01.12.93	VE 507	BK 013	0.34	2.5	7.5	0.15	3
	VE 508	BK 014	0.6	15	1.1	1.7	5
	VE 509	BK 017-I1	0.4	10	? 9	1.3	3
02.12.93	VE 510	BK 010	1	? 3.4	11	2	? 1.6
	VE 511	BK 002	0	--	--	0.2	2
03.12.93	VE 512	BK 015-I1	1.1	? 1.3	9.5	2.9	5
	VE 513	BK 005-I1	2.4	11.5	9.5	0	--

Note: I1 = Interval 1

5.4.2 Estimates of pressure losses

Six boreholes were equipped with downhole transducers connected to digital channels. The other boreholes were equipped with uphole transducers (i.e. at the drift elevation) connected to analog channels of the multiprogrammer system (see PAHL et al. 1992 for details). Because the pressure was measured uphole in these boreholes, some pressure loss occurred from the transducer to the source interval. We calculate here the typical pressure losses expected during the MSCT experiment for boreholes with uphole transducers. These losses would have been negligible if a downhole transducer or a separate piezometer line had been used.

A schematic illustration of the test equipment for intervals linked to the analog channels is shown in Fig. 5.8. Flow injection and pressure measurements were done near the drift floor in the same tubing. There are three components of the total head loss which should be taken into account: the head loss due to friction in the 8 mm inner diameter (i.d.) tubing, the head loss due to friction in the 16 mm i.d. tubing and the head loss due to the constriction from 16 to 8 mm i.d. tubing. Methods for estimating these head losses can be found in standard hydraulics text books (for example DRISCOLL 1986).

Consider test VE 513 (interval 85.005-I1) for which the injection rate was high compared to most other MSCT tests (12 l/min). With a 16 mm i.d. tubing and the measured flowrate of 12 l/min, the calculated Reynolds number is approximately 16000. A Reynolds number greater than 2000 is indicative of turbulent flow. Using the Reynolds number and a pipe roughness of 0.02, the head drop for a tubing length of 10 meters is approximately 1.0 m. A similar calculation for the 8 mm tubing of length 10 cm yields a pressure drop near 0.4 m. The head drop due to the constriction is dependent upon the direction of flow relative to the constriction. If flow occurs down the borehole (injection) the pressure drop is estimated to be approximately 0.5 m, whereas if flow is in the other direction the calculation yields 0.2 m. The summation of these individual head drops show that a maximum drop of 2 m is expected. Considering the magnitude of the overpressure measured at the transducer (150 m) during the injection period of test VE 513, this drop is not significant (1.3 %). Repeating this calculation for the other tests (except for VE 501) gave similar results; hence, the pressure at the source intervals was assumed to be equal to that measured at the surface.

5.4.3 Crosshole test analyses

Prior to the analysis of the tests, a selection of the MSCT data was done to exclude those tests which had less than 10 % pressure recovery or were strongly contaminated by noise. Crosshole tests were also not analysed when the data acquisition system failed, producing gaps in the time series. Of the 15 tests performed, only tests VE 503, VE 504, VE 509, VE 510 and VE 513 were considered to be suitable for the numerical analysis by the spectral crosshole approach.

After calculating the transmission spectra from the selected tests, however, additional problems became apparent. First, the range of the frequency spectrum was less than two decades for all the crosshole tests. Second, the high frequency part of that range was primarily noise due to the poor time resolution of the recording device (i.e. $\Delta t = 40$ seconds). Because of these problems, an extensive quantitative interpretation of the crosshole tests could not be done with reasonable accuracy. Nevertheless, a few typical examples of the calculated transmission spectra and a short summary of the qualitative conclusions are given here.

Fig. 5.9 shows the transmission spectra from the source interval VE 508 to the observation intervals BK 85.006-I1, -I3 and -I4. The poor quality of the high frequency data is easily seen by the scattered amplitude and phase spectra. Because of the poor frequency spectrum, it was not possible to discriminate between the simple models of Section 5.2. Only the radial homogeneous model (RFH) could be excluded

because of the low frequency response. Similar results were obtained when analysing the response from the other source intervals.

For the VE 503 tests, the transmission functions calculated for the observation intervals BK 85.009-I2, 85.005-I1, 88.015-I2, 88.015-I3, 85.004-I1 85.004-I2, 88.018, 85.006-I1, 85.006-I3, 88.017-I1 and 88.017-I2 were practically identical within the uncertainty of the data. A weak but clear response was seen in BK 85.008-I1, 85.008-I2, 85.009-I1, SB1 and 85.006-I2. No data were recorded in BK 85.007. The observation intervals BK 86.002, 86.003, 85.011, 88.013 and 88.014 did not have an observable response. Similar results were observed from the source tests VE 504, VE 509 and VE 513.

A conclusion from the crosshole data is that the transmission functions may be strongly dominated by outer boundary effects. This would explain why many of the hydrotests in the central BK area show nearly the same transmission spectra, independent of the linear distance from the source to the observation intervals (as suggested by VOMVORIS & FRIEG 1992). It is possible, however, that if the transmission spectra had contained sufficiently high frequency components (at least up to frequencies of about 0.01 h^{-1}), the transmission functions would have differed depending on the local flow geometry.

The crosshole tests also showed that both lamprophyre dykes are nearly impermeable (in all principle directions). This is evidenced by the tests performed in the southern lamprophyre of the boreholes BK 86.002 and 86.003, which did not cause any pressure disturbance in the central BK area. Furthermore, the borehole BK 85.008 in the northern lamprophyre showed a very weak response during the source test VE 510.

5.4.4 Single-hole analysis

5.4.4.1 Diagnostic plots for flow model identification

Because of the poor quality of the crosshole data, the pressure response recorded in the source intervals were analysed using a time-domain approach. The spectral approach was not used due to the time constraints of the project and the poor quality of the data.

The classical time-domain analysis uses specialized plots to identify the relevant flow model prior to parameter estimation (VOMVORIS & FRIEG 1992). Typical diagnostic plots are log-log plots of the measured delta pressures and their pressure derivatives. For example, a unit slope in the delta pressure and derivative is indicative of data dominated by wellbore storage effects, while a stabilized pressure derivative may indicate infinite-acting flow.

For BK data, however, the applicability of diagnostic plots was found to be limited due to the absence of early-time data and noise in the data. Fig. 5.10 shows a typical log-log plot for test VE 512 in the source interval 85.015-I1. Due to the noise in the

pressure derivative and the uncertainty in the early-time data, it is difficult to conclusively state what the flow model may be.

Besides log-log diagnostic plots, simple linear plots of the pressure data were examined as shown in Figs. 5.11 and 5.12. Fig. 5.11 shows the pressure response measured in borehole 85.008 interval I2 during test VE 513. During this test, water was injected into borehole 85.005 interval I1 for approximately 2.3 hours at a rate of 11.5 l/min. After this time, the interval was closed and the pressure was allowed to recover. A remarkable characteristic of the response in Fig. 5.11 is evidenced by the fact that the pressure does not recover to its pre-test steady-state level. Similar behavior was observed not only in all intervals of the central BK area during the MSCT injection tests, but also during previous tests at the BK site. Fig. 5.12 shows another example of this behavior for borehole 85.005 (interval I4) during test VE 452. The pressure shift is smaller than for VE 513, probably because the injected volume of water was smaller in VE 452. The anomalous response, however, did not occur for those injection tests that were immediately followed by the production of the same volume of water as had been injected. For these tests, the pressures recovered to their pre-test level.

These observations imply that, as water is injected, the fracture network, which is bounded laterally by no-flow dykes or poor lateral connectivity, is filled vertically. For the water level to rise, the top of the BK site must be unconfined. This conceptual model is consistent with the model hypothesized in Chapter 4.

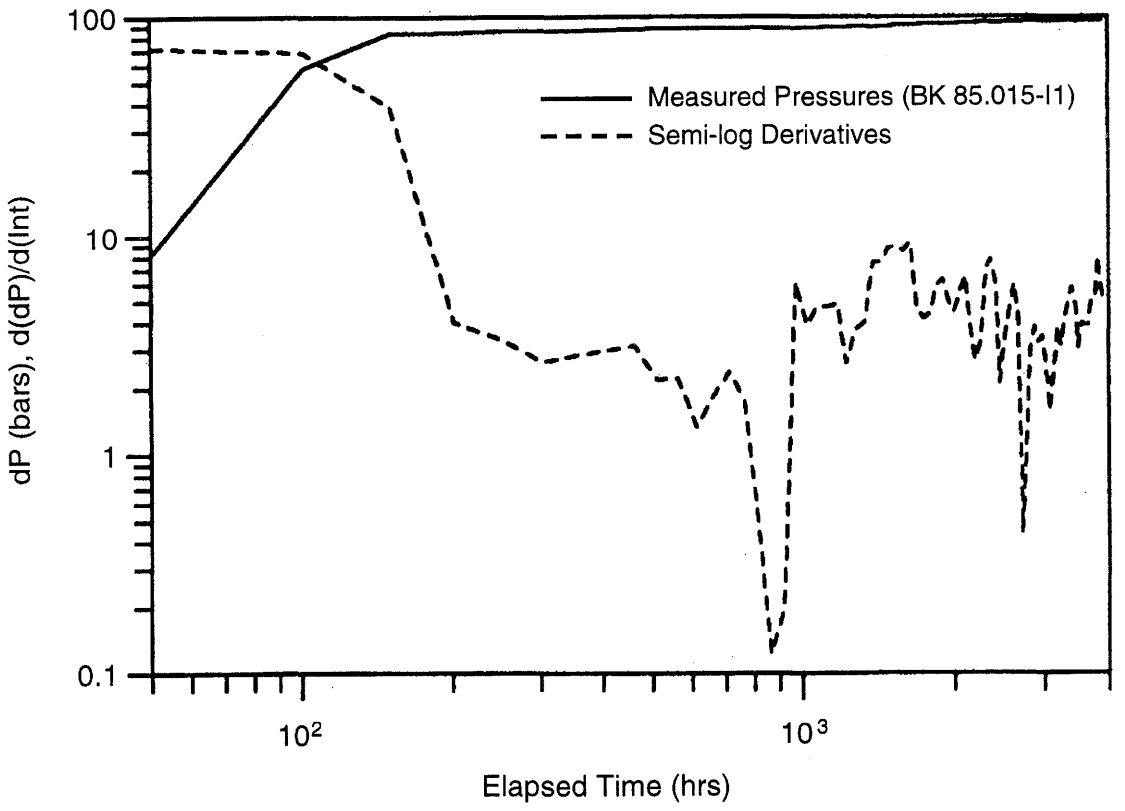

Fig. 5.10: Log-log representation of pressure data in BK 15-I1 during test VE 512

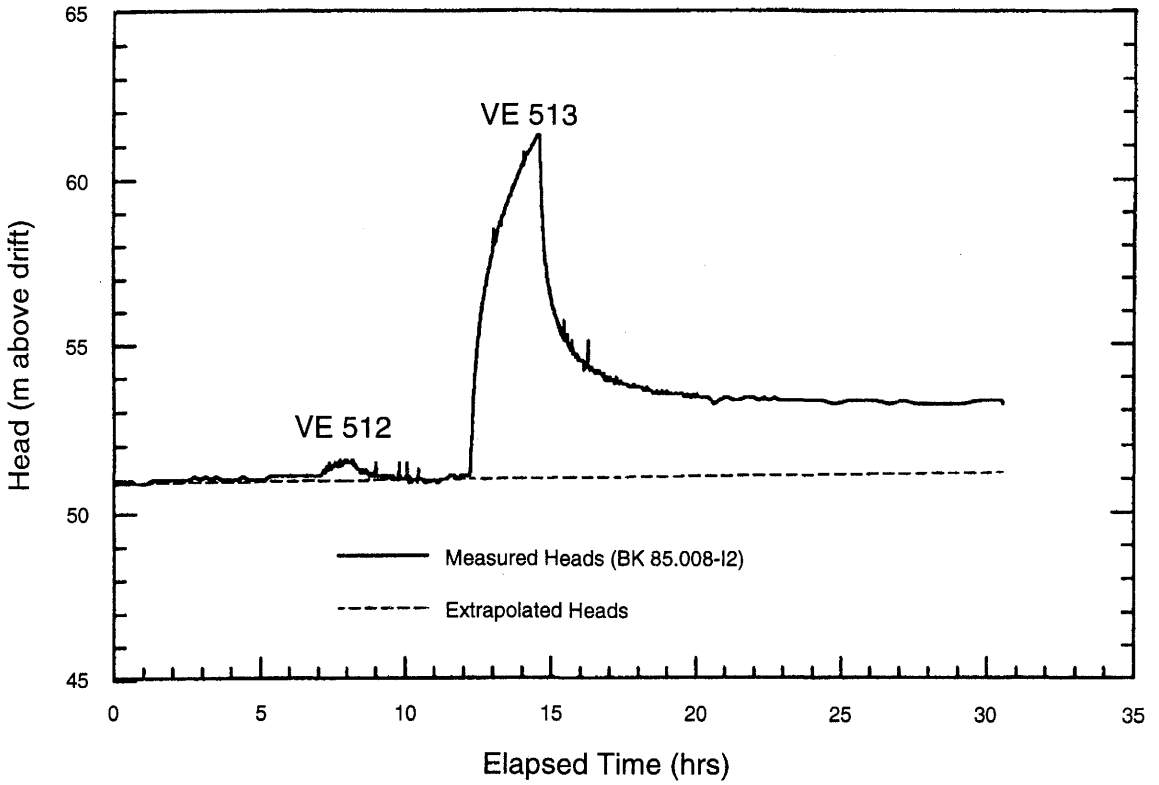

Fig. 5.11: Measured head in BK 8-I2 during test VE 513

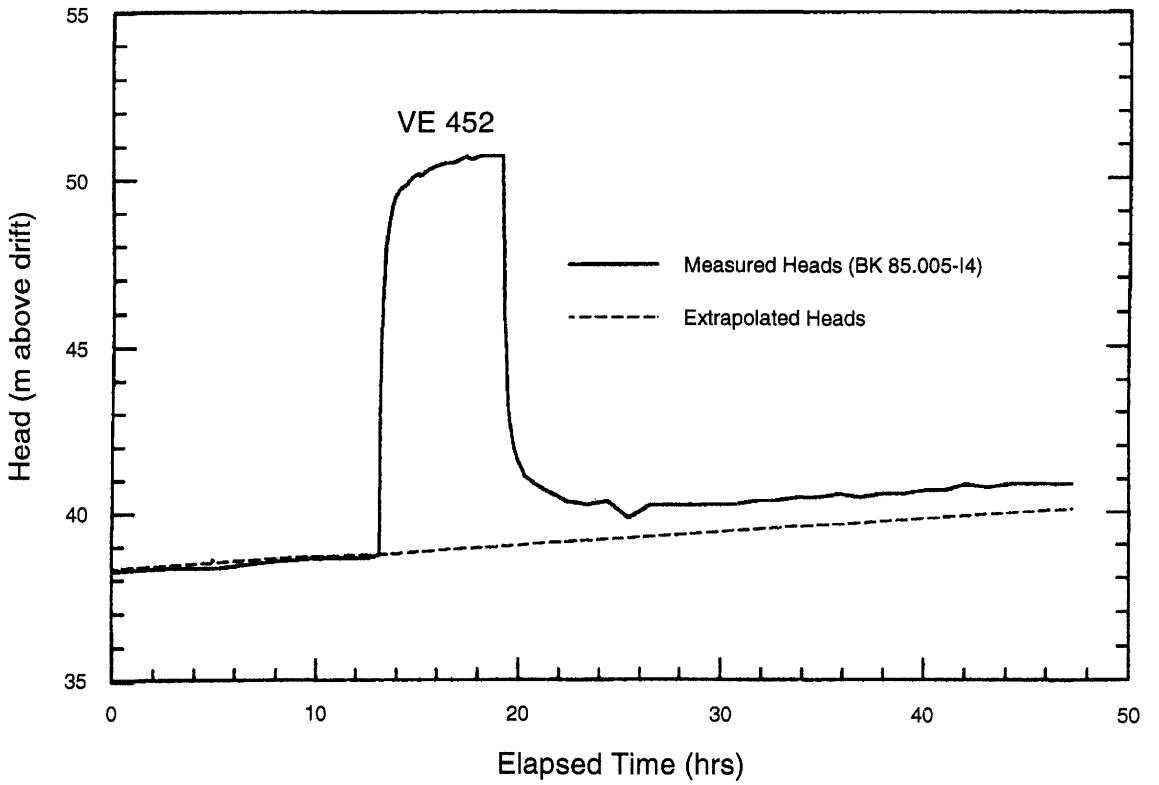

Fig. 5.12: Measured head in BK 5-I4 during test VE 452

5.4.3.2 Calculation of cross-sectional area of the fracture network

Assuming the unconfined model is correct, the observed pressure shift during the test and the injected water volume can be used to estimate an equivalent fracture network cross-sectional area from:

$$\Delta h = \frac{Q}{C} \qquad (5.17)$$

where Δh (m) is the difference in head measured over time Δt (s), Q is the volume of water injection (m^3), and C is the equivalent cross-sectional area (m^2). Taking Δt as the total duration of the test and Q as the cumulative injected water volume yields the estimates for the cross-sectional areas given in Tab. 5.5. The cross-sectional areas are only calculated for those tests that had accurate flowrate and head measurements. The average cross-sectional area is approximately 0.9 m^2.

Tab. 5.6: Equivalent fracture network cross-sectional areas

TEST	Injected Volume (m^3)	Interval	Δh (m)	C (m^2)
VE 452	1.076	85.005-I4	0.9	1.2
VE 454	4.395	85.006-I4	5.0	0.9
		85.004-I2	5.6	0.8
VE 503	0.864	85.008-I2	1.1	0.8
VE 513	1.656	85.008-I2	2.1	0.8

The results in Tab. 5.6 can be combined with the head gradients measured during the pressure recovery phase of a test to estimate the recharge rate (Q) to the fracture network. For example, the pressure recovery of 0.082 m/h for test VE 478 (Fig. 4.1a) gives an estimated recharge rate of approximately 1.2 l/min. Other tests were not considered to be of good enough quality to calculate the recharge rate.

5.4.3.3 Estimates of flow parameters using GTFM

The numerical borehole simulator GTFM (PICKENS et al. 1987) was also used to provide a rough estimate of the hydraulic parameters and possibly identify the flow model by fitting the entire test sequence. GTFM can simulate radial confined flow to a borehole for a variety of flow models (radial infinite-acting, radial composite and radial with double-porosity), but cannot model the unconfined flow system as suggested by the field measurements. Nevertheless, GTFM was used to explore whether these other flow models could produce the anomalous pressure responses (i.e. shifted steady-state pressures).

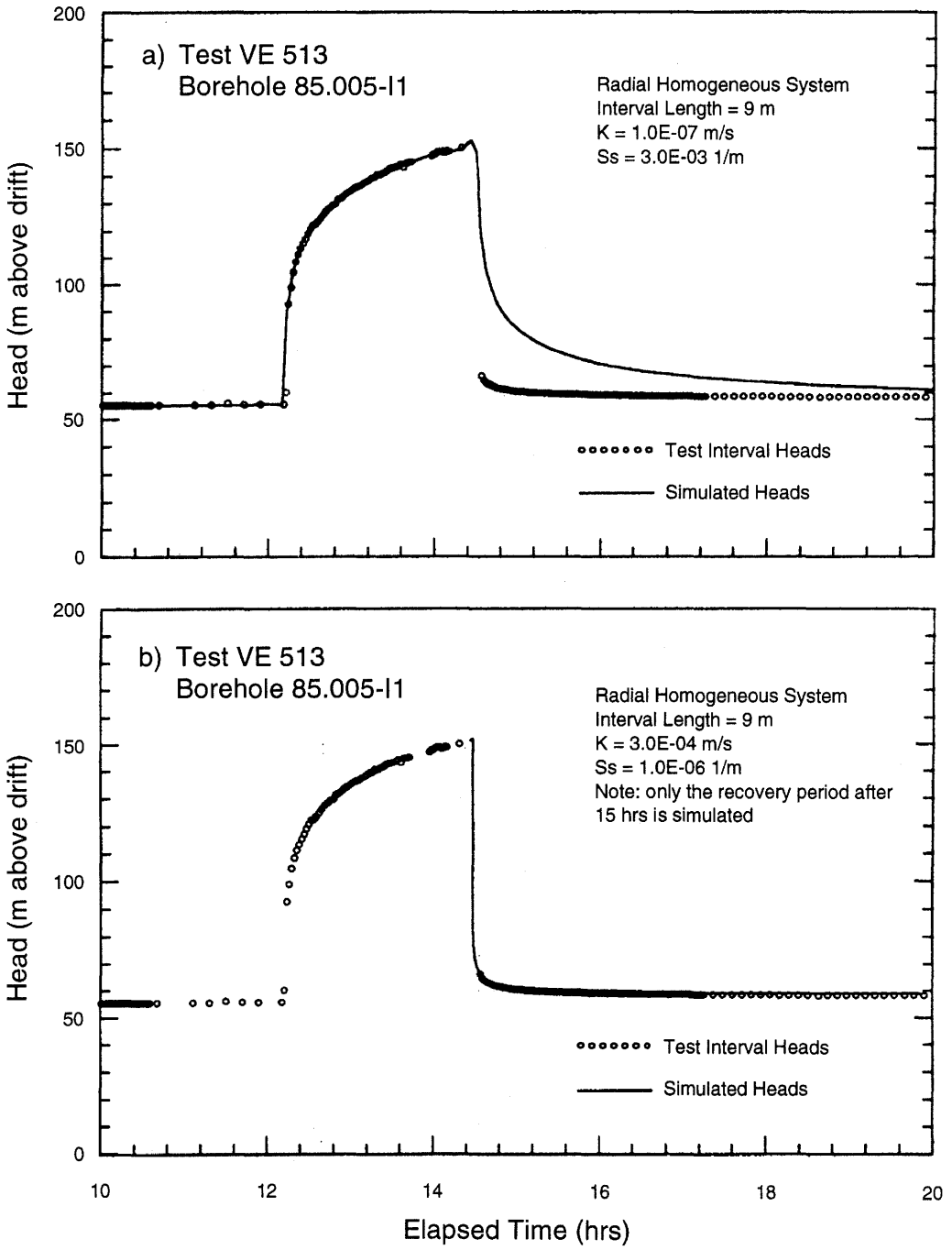

Fig. 5.13: GTFM simulations of test VE 513: a) fit of the injection period and b) fit of the recovery

Fig. 5.13a shows a typical fit of GTFM to the observed pressures during VE 513. The injection period can be matched very well but the subsequent recovery cannot. As shown in Fig. 5.13b, an excellent match to the recovery can be obtained by adjusting the parameters, but then the injection period is not matched well (for the simulation in

Fig. 5.13b the injection period was treated as a pressure history, hence the apparent perfect match). A GTFM match to the injection pressures would require a large specific storage coefficient (3E-03 m^{-1}). As mentioned previously (see Section 4.4), the fact that large storage coefficients are required has been repeatedly observed and is consistent with the proposed unconfined flow model. In addition, the inability of GTFM to match both test events (i.e. the injection and production period) with simple models gives further support for the unconfined model.

The "best-fit" GTFM simulations for tests VE 503, 506, 510 and 511 are shown in Figs. 5.14 to 5.17. Formation parameter estimates were determined by iteratively varying the parameters until a satisfactory visual match to the observed pressures was obtained. The parameters derived from this subjective analysis are summarized in

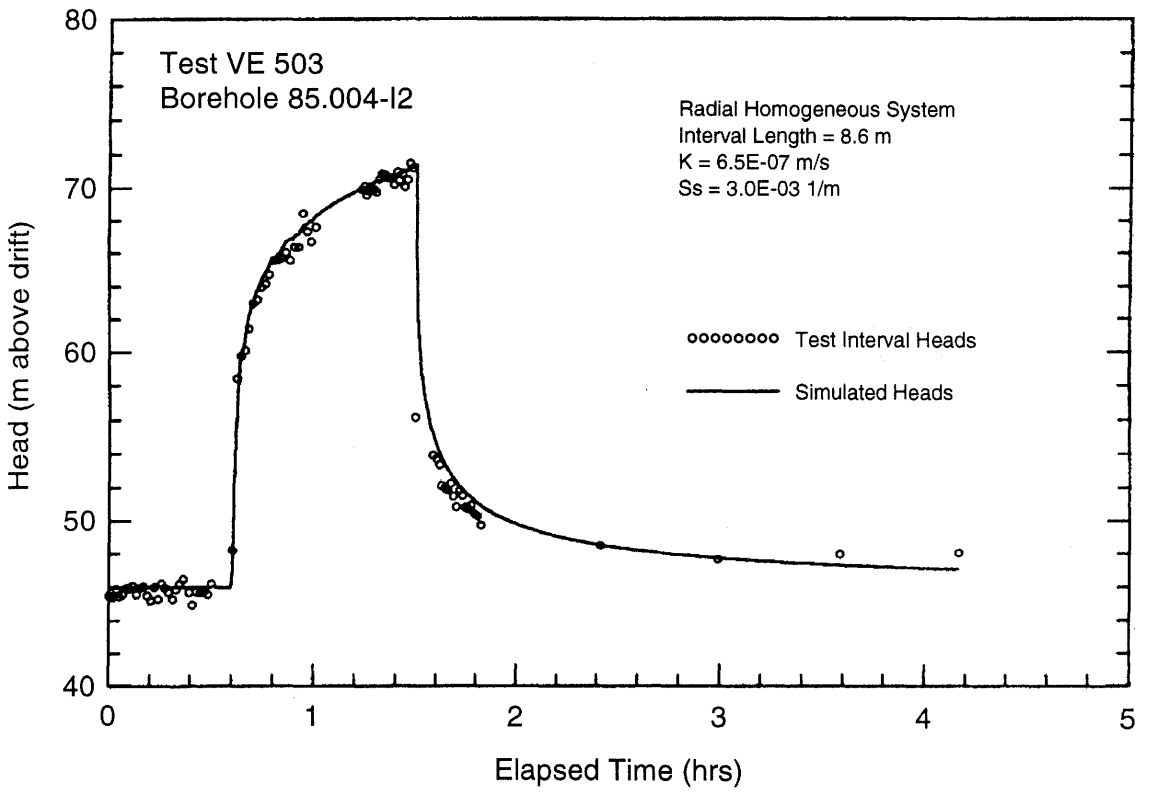

Fig. 5.14: GTFM simulation of test VE 503

Tab. 5.7. As illustrated, the parameters derived from each event within the same test sequence can be extremely different (in particular for VE 513 in which the results differ by over four orders of magnitude). The large differences are probably a result of using a flow model which is not consistent with field observations. Hence, these parameters should be considered as very qualitative and used only as a means of comparing one test interval to another.

Tab. 5.7: Summary of results from GTFM analysis of single-hole data

TEST	T (m^2/s) derived from:		S (-) derived from:	
	Injection period	Recovery period	Injection period	Recovery period
VE 502	8.6E-07	9.0E-06	9.0E-03	9.0E-06
VE 503	5.6E-06	-	2.6E-02	-
VE 506	-	4.6E-11	-	4.6E-05
VE 507	1.8E-08	-	4.6E-04	-
VE 508	2.0E-05	2.0E-04	2.0E-02	2.0E-02
VE 510	3.0E-07	-	4.0E-04	-
VE 511	-	5.6E-10	-	4.7E-05
VE 512	1.2E-07	7.2E-05	1.2E-03	2.4E-07
VE 513	9E-07	2.7E-03	2.7E-02	9.0E-06

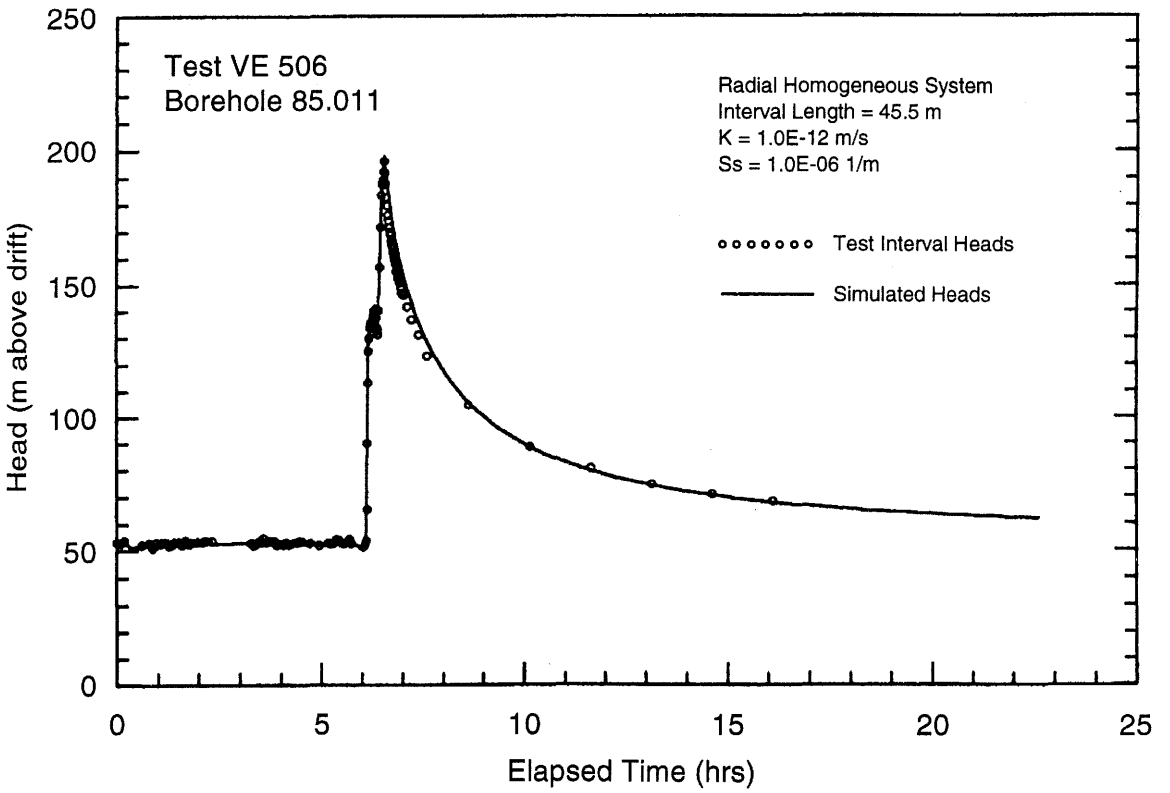

Fig. 5.15: GTFM simulation of test VE 506

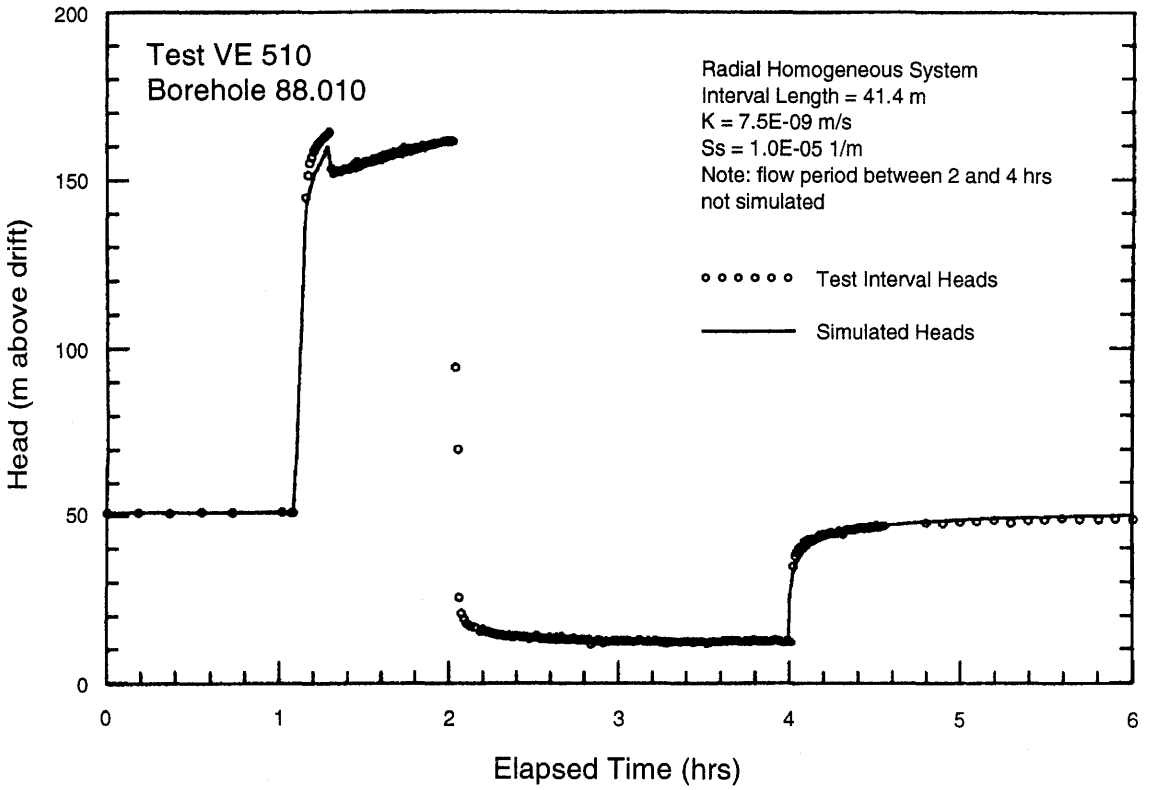

Fig. 5.16: GTFM simulation of test VE 510

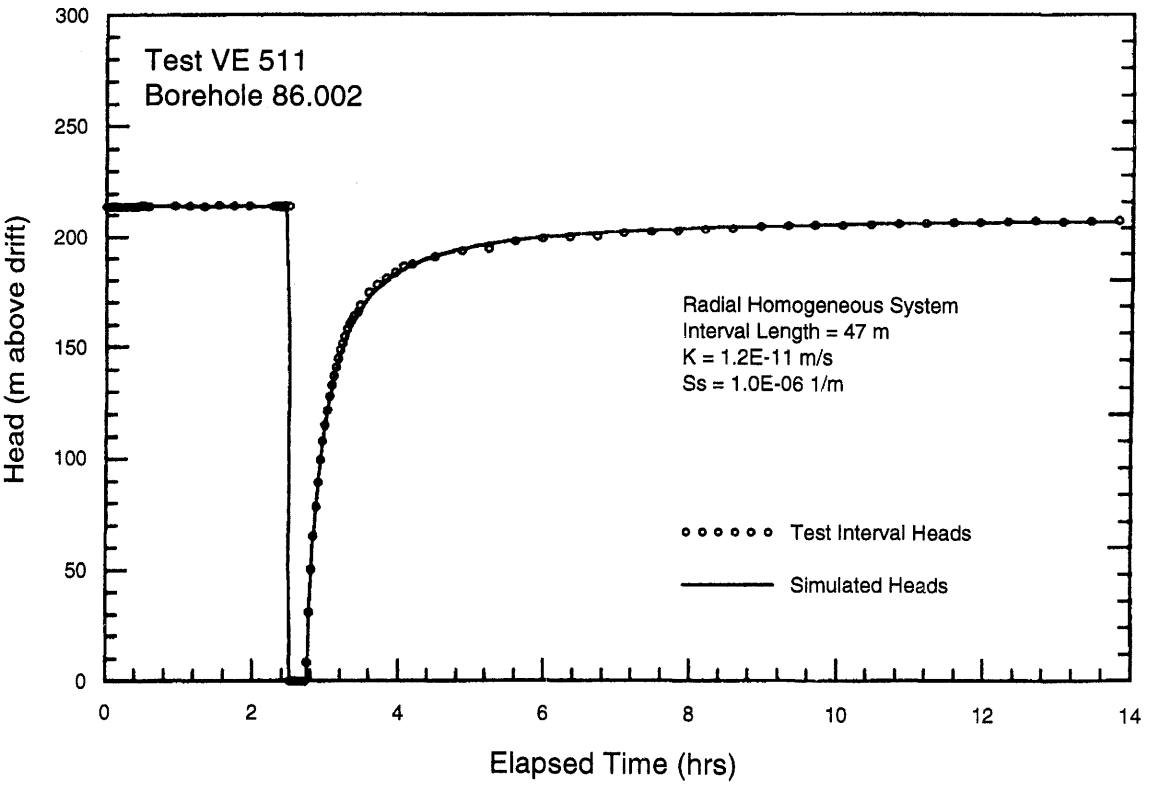

Fig. 5.17: GTFM simulation of test VE 511

5.5 Summary and Conclusions

In this chapter, we developed and applied a novel methodology to perform and interpret hydraulic tests in a highly complex environment in which the scale of investigation is in the same order as the characteristic length of the main hydraulic features. The approach used is summarized as follows:

- Multiple Source Crosshole Tests (MSCT) were performed at the BK site by coupling multiple source intervals with as many observation intervals as possible. The MSCT experiment consisted of 15 individual tests with 12 different source intervals and 30 observation intervals.

- The fundamentals of spectral crosshole analysis were presented. Transmission functions for six simple analytical models were discussed. A procedure for the numerical Fourier transform was developed and verified by simulated hydrotest data.

- Synthetic data were generated with the fracture flow hydrotest simulator CASA to develop an efficient strategy for crosshole data interpretation. The effect of intersecting fractures was examined for different source-observation pairs. Simple analytical models were shown to be successful in matching the observed pressure response on a local scale. Furthermore, it was shown that the capability to resolve a complex fracture zone system on a global scale is very limited when using only one source borehole. This is only because observation intervals show a significant response, which are directly connected to the source borehole in the same fracture zone without multiple intersections.

- The MSCT data were analysed by standard single-hole time-domain methods as well as by a spectral crosshole approach. Specialized plots (for the single-hole analysis) and transmission spectra (for the crosshole analysis) were made to attempt to identify the conceptual flow model and estimate hydraulic parameters. The interpretation of selected crosshole tests provided the identification of "localized" flow models, which when assembled were consistent with the global model.

The main objective of the MSCT test, namely a detailed characterization of fracture flow at the BK site, was not fully achieved due to the complex nature of the formation and also the problems associated with the data acquisition and test equipment. Nevertheless, some conclusions and characteristics of the BK fracture network were obtained. These are:

- The southern and northern lamprophyre act as no-flow boundaries.

- The BK system is probably unconfined. When injecting water in any of the boreholes, the steady-state pressure in the entire BK system increased linearly with the volume of water injected. An equivalent fracture network cross-sectional area was calculated for different tests and test conditions. These cross-sectional areas were consistent for all tests.

PART IV

The Salt/Heat Tracer Test

6 THE SALT / HEAT TRACER EXPERIMENTS

T. Kohl (ETH, Zürich), P. Marschall, N. Correa (both Nagra), L. Rybach (ETH, Zürich)

6.1 Introduction and scope

The migration of radionuclides in fracture networks is determined by the interplay of three concurrent transport processes, namely *advection* and *dispersion* in the fractures as well as *diffusion* into the porespaces of the solid rock matrix. Hereby, advective transport is controlled by the mean fluid velocity along the streamlines of the flow-field. Due to the discontinuous distribution of the fractures in the rock matrix and the heterogeneity within the fractures, advection occurs along preferential pathways (i.e. flow is channelized) and, therefore, represents a potential mechanism for a fast transport of radionuclides from an underground repository to the biosphere. Dispersion, however, is controlled by the spatial variability of the flow-field and gives rise to a spreading of the solute's concentration along the preferential pathways. Matrix diffusion is essentially governed by the area of rock matrix accessible to advective flow and results also to a spreading and a retardation of the transported solute. Both, dispersion and matrix diffusion are therefore favorable processes within the scope of performance assessment.

When performing small scale and short-term tracer tests in fracture networks with non-reactive tracers, the effect of matrix diffusion is masked by the predominant advective-dispersive transport. This is because the process of molecular diffusion in fluids and solids is extremely slow. For this reason a measurable mass transfer by molecular diffusion becomes evident only for scales in time and space, which are quite large. Heat transport, however, is dominated by thermal diffusion from the fluid in the fractures into the matrix; because the thermal diffussivity of rock is about five magnitudes higher than molecular diffusion of non-reactive tracers (i.e. 10^{-6} m/s and 10^{-11} m/s respectively) the required time scales are much smaller for the heat diffusion to occur. Tracer tests with heat may be therefore an adequate method to investigate the role of diffusive transport in fracture networks.

One-dimensional scoping calculations have been performed by STIESS (1990) to estimate the retardation of thermal transport when compared with non-reactive solute transport. STIESS (1990) pointed out, that even under linear flow conditions, the matrix diffusion will strongly slow down the propagation of heat through a single fracture, the retardation increasing with the travel time. The simulations were performed with travel distances in the order of 10 m.

Between the 22nd of February and the 24th of March 1993 a combined Salt and Heat Tracer Test (SHT) was performed at the BK site of the Grimsel rock laboratory. The experiment took place in a well recognizable fracture zone and was designed as a dipole flow-field consisting of the injection borehole BK 85.005 and the extraction borehole BK 88.015 (Fig. 1.1 and 1.2). The SHT experiment was motivated by the need to understand the role of diffusive transport in fracture networks. The underlying philosophy was to use simultaneously two different tracers which characterize complementary transport properties of the fracture network in the same spatial domain. Specific objectives of the investigations were:

- to test heat as a non-reactive tracer, which does not disturb the chemical equilibrium of the aqueous phase in the fracture network
- to develop and test the equipment and methodology for a combined SHT experiment
- to investigate the capabilities of the finite element code FRACTure for modeling combined solute and heat transport
- to study the relevance of matrix diffusion at the BK fracture network.

An additional purpose of the experiment was to investigate the benefit dipole tracer experiments with a reversed flow-field. For this reason another tracer test was performed by simply exchanging the injection and extraction borehole and using solely salt to trace the water. The results and the interpretation of the reversed tracer test are not presented in this report. LI & KINZELBACH (1993) and KUNSTMANN (1994) pointed out, that the use of complementary flow-fields (e.g. by exchanging the injection and extraction borehole) is extremely valuable to determine the impact of a natural baseflow on the test results and to characterize large scale heterogeneities.

In Section 6.2, fundamentals of solute and heat transport in fractured rock masses are outlined and the FE-simulator FRACTure is described. Prior to the field experiment design calculations were carried out to get a first estimate of the arrival time and the magnitude of the thermal response. Principle findings of these studies are presented in Section 6.3. Before performing the actual SHT experiment, a series of pre-tests were performed to determine the extraction flowrates achievable and to stabilize the flow-field. An overview of the experimental set up, the pre-tests and the field experiment is given in Section 6.4, leading into a discussion of the experimental results. In Section 6.5, the scope of the modeling activities is outlined and the basic conceptual models considered for the test interpretation are described. Selected models for solute and heat transport are used to perform a sensitivity analysis for special transport parameters such as fracture aperture, dispersivity and matrix conductivity. Finally, in Section 6.7, a discussion of the numerical investigations is presented and concluding remarks are given.

6.2 Modeling heat and solute transport

6.2.1 Fundamentals

Modeling flow and transport processes in fractured rock masses has been the topic of many investigations in the past decades. Most of these studies are based on the assumption, that the fractures behave as a porous medium. The principles of the porous medium approach are described in textbooks (see for example BEAR & VERRUIJT 1987). In the following section, we present a summary of fundamentals concerning the numerical simulation of mass flow, solute transport and thermal transport in porous media, as used in the code FRACTure.

Mass flow

The laminar mass flow in a porous or fractured medium is basically described by Darcy's law:

$$\vec{q} = - \underline{\underline{K}}_f \vec{\nabla} h \qquad (6.1)$$

K_f = hydraulic conductivity [m/s]
q = Darcy velocity [m/s]
h = piezometric head [m]

where $\vec{q}$ is a vector and $\underline{\underline{K}}_f$ is a tensor in the general 3D formulation. When considering flow in a single fracture, a 2D representation provides an adequate description of the effective mass flow. In the present work, K_f is used as a scalar quantity. For flow in fracture zones it is common practice to replace the hydraulic conductivity by the transmissivity, which is defined as the product of the aperture and the hydraulic conductivity K_f :

$$T = a\, K_f \qquad (6.2)$$

T = transmissivity [m^2/s]
a = aperture [m]

The transmissivity is estimated from hydrotests; it can also be assessed directly from the fracture aperture, provided that this quantity is known (e.g. cubic law). Except for the injection and extraction point, the flow-field of a dipole tracer test is divergence free in the entire model domain when steady-state flow conditions are realized (conservation of mass):

$$\nabla q = 0 \qquad (6.3)$$

The hydraulic conductivity is a generalized parameter that depends upon rock and fluid properties:

$$K_f = \rho g\, k/\mu \qquad (6.4)$$

ρ = fluid density [kg/m^3]
g = gravity acceleration [m/s^2]
k = rock permeability [m^2]
μ = dynamic fluid viscosity [Pa s]

Due to the temperature dependence of the fluid density and viscosity, the hydraulic conductivity can no longer be considered as a constant property of the rock, when modeling thermal transport. The maximum temperature difference of $\Delta T = (T_o - T_i) \approx$ 17 °C, which was achieved during the SHT experiment VE 520, produces a reduction of the density of water and rise of the viscosity, which finally causes a deviation in the hydraulic conductivity in the order of 35 %. Despite those effects, the thermally induced drop of the hydraulic conductivity was neglected in the present numerical investigations, because the variability of the hydraulic conductivity is expected to be much higher. Furthermore, the occurence of such high temperature differences is restricted to the immediate vicinity of the injection interval and the consequences on

the actual flow-field are rather local. This was supported by design calculations (KOHL 1993). The change of the fracture's hydraulic conductivity can therefore be treated as a skin effect, which does not change the scope of the flow-field.

Solute transport

The transient solute transport in a porous medium is described by Fick's law, containing advective and dispersive terms:

$$\frac{\partial c}{\partial t} + \vec{v}_a \vec{\nabla} c - \vec{\nabla}(\underline{\underline{D}} + D_m)\vec{\nabla} c = 0 \qquad (6.5)$$

c = concentration
v_a = fluid velocity [m/s]
D = hydrodynamic dispersion [m^2/s]
D_m= molecular diffusivity [m^2/s]

The mean particle velocity v_a as used in equation 6.5 is given by the Darcy velocity q, divided by the porosity Φ. Generally the effects of microscopic variations of the velocity in the vicinity of a considered point are expressed by means of a dispersion tensor. If it is assumed that in an isotropic porous medium the dispersion tensor is simply a function of the longitudinal and transverse dispersivity lengths (α_L and α_T, respectively) and the fluid velocity (BEAR & VERRUIJT 1987), the components of the dispersive tensor D_{ij} are obtained by:

$$D_{ij} = \alpha_T v_f \delta_{ij} + (\alpha_L - \alpha_T)\frac{v_{if} v_{jf}}{v_f} \qquad (6.6)$$

δ_{ij} - Kronnecker delta with i, j = 1, 2, 3

Thermal transport

A transient thermal field in a porous medium is considered to depend upon advective and diffusive transport. If it is assumed that the fluid is in close contact with the solid rock the same temperature is taken for both phases. Therefore the parameters describing thermal transport are averaged over the solid and the fluid phase. The governing equation for thermal transport in a porous medium is given by:

$$\overline{\rho c_p}\,\frac{\partial T}{\partial t} + \vec{q}\left[\rho c_p\right]_f \vec{\nabla} T - \vec{\nabla}\bar{\lambda}\vec{\nabla} T = 0 \qquad (6.7)$$

T = temperature [K]
q = Darcy velocity [m/s]
λ = thermal conductivity [W/m K]
ρc_p = heat capacity [W s / K m^3]

The bar above the heat capacity and the thermal capacity indicates the weighted average over the fluid and the solid phase.

Peclet and Courant number analysis

The non-dimensional Peclet number describes the ratio between the advective and the dispersive transport. For the solute and the thermal transport in a finite discretized volume with characteristic iength ΔL the Peclet numbers are defined as follows:

$$Pe_{st} = \frac{v_a \Delta L}{(D + D_m)} \tag{6.8a}$$

$$Pe_{tt} = \left[\rho c_p\right]_f \frac{q \Delta L}{\bar{\lambda}} \tag{6.8b}$$

When simulating transport processes with the finite element method, the Peclet number of the elements has to be restricted to avoid numerical dispersion. In the present work, $Pe \leq 2$ is considered sufficient for linear elements and $Pe \leq 10$ for elements with quadratic shape functions.

The non-dimensional Courant number, that describes the distance of an advectively transported "information" during one timestep, is for solute and thermal transport respectively:

$$Co_{st} = \frac{v_a \Delta t}{\Delta L} \tag{6.9a}$$

$$Co_{tt} = \left[\rho c_p\right]_f \frac{q \Delta t}{\overline{\rho c_p} \Delta L} \tag{6.9b}$$

In the scope of FE-modeling Courant numbers $Co > 1$ may lead to instability problems (i.e. oscillations) when solving the linear equations by explicit time integration schemes. Such instabilities are avoided by using implicit weighted time integration, as implemented in the code FRACTure (see next section). Nevertheless, care has to be taken in turn of time discretization, because implicit schemes may also fail, when violating the Courant criterion $Co \leq 1$.

Using typical values for the transport parameters and assuming a fluid velocity $v_a \approx 10^{-2}$ m/s the thermal Peclet number is about two orders of magnitude higher than the solute Peclet number. Consequently, the numerical simulation of thermal transport needs a considerably finer spatial discretization than solute transport. The Courant numbers as given in equation 6.9a+b are in the same range.

6.2.2 Simulator FRACTure

FRACTure is a versatile, 3D finite element program for the simulation of various processes in geoscience. It was designed with the specific aim of studying the coupling of different physical processes in the subsurface such as thermal, rock mechanical and hydraulic interactions. Its flexible modular structure facilitates the addition of further processes and elements to the existing library and the handling of linear and non-linear constitutive laws and the calculation of their interactions.

Successful runs of this code have been performed on PC, Macintosh Computers, HP, SUN and VAX workstations (KOHL 1992).

In the current stage of development FRACTure can simulate individual hydraulic, transport (thermal, non-reactive solute, radioactive solutes) and elastic processes as well as special coupled interactions between these processes. The name FRACTure is an acronym for its functional capabilities (**F**low, **R**ock **A**nd **C**oupled **T**emperature effects) while at the same time emphasizing the fracture as the dominant hydraulic structure in crystalline rock.

Any of the physical processes mentioned above can be simulated using 1D, 2D or 3D elements that may have linear or quadratic (both lagrangian or serendipity type) shape functions. There exist triangular and quadrilateral elements in 2D. In 3D, pyramids or tetrahedral elements can be chosen as well as hexahedral and pinched prism elements with a triangular cross-section. Another feature allows elements with different dimensionality to be combined. Since this option was proven to be very useful in hydraulic or transport models for the study of fracture-matrix effects it has been used for all 3D simulations presented in this report. Fig. 6.1 illustrates this option with mixed 2D/3D elements. For the studies presented in this report 2D and 3D hydraulic elements and 2D and 3D transport elements were activated.

Since the original purpose for the development of FRACTure was to model hydraulic dipole systems in crystalline rock, special mesh generation tools were also developed. These tools together with other features were condensed into the mesh generator code FRAM (KOHL 1992). This program can build up the special discretizations being required for dipole flow systems. A strong refinement of the mesh centered at the borehole is needed to account for the high hydraulic gradient around a borehole. Another requirement in mesh generation of fracture flow problems is the option of refinement of the matrix towards the fracture plane. This is necessary because of the strong hydraulic conductivity change between the lower dimensional fracture elements and the 3D matrix elements.

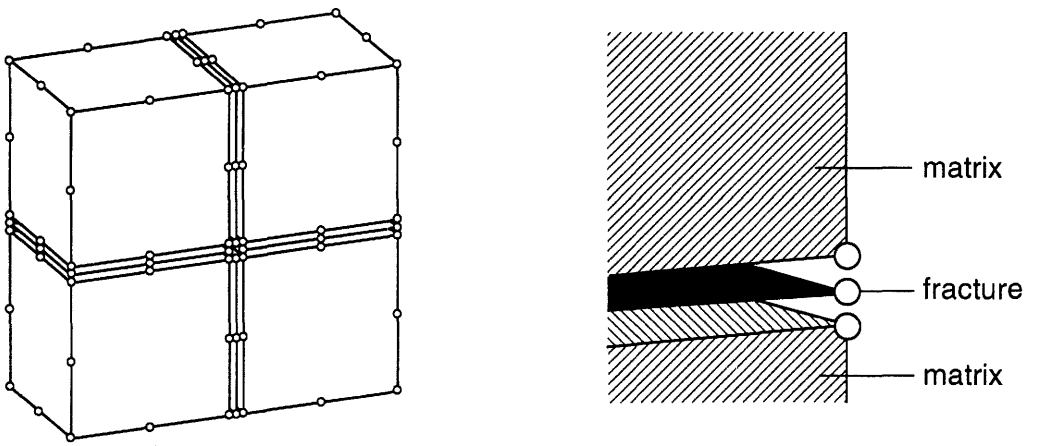

Fig. 6.1: Combining elements with different dimensions: lower dimension elements can be mapped in elements with higher dimension. Only for optical reasons the nodes are plotted separately

6.3 Design calculations for SHT experiment

In a previous study, performed by STIESS (1990), it was outlined that a Combined Salt/Heat Tracer Test may have a good chance of success, when it is carried out as a small scale experiment with travel distances in the order of ten meters. For this reason the SHT experiment was planned to take place as a dipole tracer test between the intervals BK 85.005, interval 2 and BK 88.015, interval 2 (BK 5-I2 and BK 15-I2, respectively; see Fig. 1.1 and 1.2). These two intervals are well connected to each other on the basis of core inspection and hydrotest analysis.The straight line distance between the mid points of the two intervals is less than 10 m. The extraction to injection flowrate ratio was chosen as $Q_{ext}/Q_{inj} = 2$ to ensure a recovery of 100 % (referring to infinite test duration) of the mass of the injected tracer.

With these specifications, an additional design study was initiated to prove the feasibility of such a test and to identify the key parameters, which would control a measurable thermal response at the extraction borehole. The range of possible results was also investigated in order to provide a basis for the design of the field activities. A detailed description of this design study is found in KOHL (1993).

6.3.1 Data basis and general approach

A review of previous tracer tests, which have been performed by BGR at the BK site showed that the design of test VE 449 was to some extent comparable to the SHT experiment planned (LIEDTKE et al. 1989). Consequently the results of this test were used to "calibrate" the parameters of the solute transport in the design calculations. The calibrations consisted basically of fitting the peak arrival time of the breakthrough curve from VE 449, measured in the extraction borehole. Subsequently, the transport parameters derived were used to predict solute and thermal transport for the actual SHT test design.

During the test VE 449 test brine water was injected in BK 85.005 for 5 h at a rate of 0.5 l/min and extracted in BK 85.006 at a rate of 2.0 l/min at a distance of approximately 10 m. After the injection of salt had stopped, steady-state hydraulic conditions were maintained. A maximum salt concentration of 1.2 % of the injected concentration was measured at the extraction well after 76000 s. For further details see LIEDTKE et al. (1989).

It should be re-iterated that the results of these scoping calculations served only as a basis for the design of the SHT experiment. A number of essential differences between VE 449 and the SHT experiment do not allow for a direct comparison. The flow-field in the two tests, for example, was completely different, because the extraction occured over the whole length of the borehole during test VE 449 and not, as in the SHT test, in a small packed off borehole section. Furthermore, it is not clear, whether transport took place on the same hydraulic feature in both tests.

6.3.2 Discretization and model parameters

For the design studies a two-dimensional fracture zone area with a size of 40 x 40 m was considered. It was determined by different model runs, that a distance of 20 m from the boreholes is sufficient to allow for constant pressure conditions at the outer boundaries. The thermal model was discretized in three dimensions to account for the thermal matrix diffusion. The thickness of the matrix was chosen to be 8 m. The model, including the 2D fracture and the matrix is presented in Fig 6.2. The mesh around the injection and extraction points was refined in order to keep the thermal Peclet numbers below the Peclet criterion, defined in Section 6.2.1. The solute transport was calculated using 540 Lagrangian elements with a total of 2215 nodes, whereas the thermal transport needed 903 Lagrangian elements with totally 6467 nodes. An implicit weighted time discretization scheme was applied.

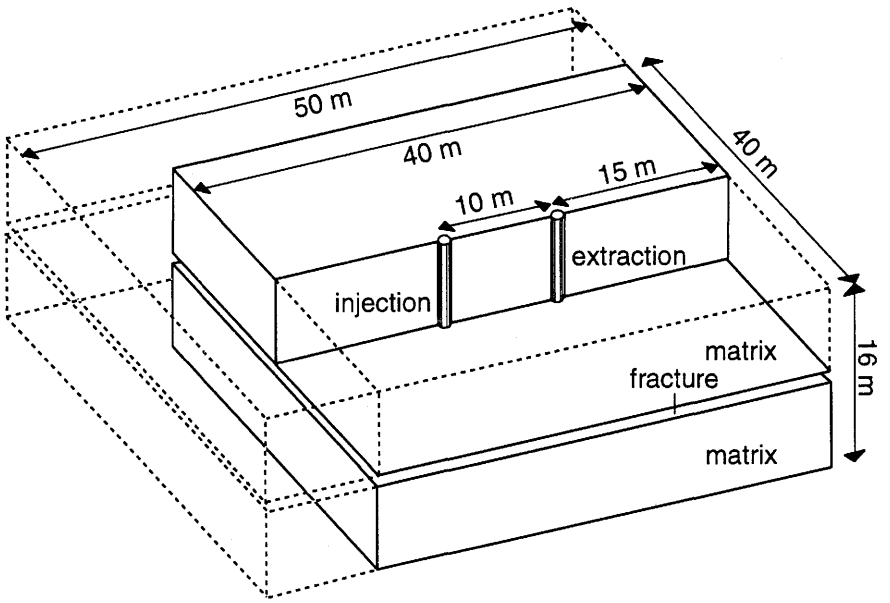

Fig. 6.2: Dimensions and size of the discretized domain for the design study (in continuous lines). The interpretation of experiment VE 520 required slightly (10 m) larger dimensions to the left and to the back (indicated with dashed lines). In this case the injection and extraction point were not centered around the midpoint of the total domain

In order to avoid numerical oscillations near the injection borehole due to the high flow velocities in its neighborhood the following approach was used: it was assumed that in an area with 20 cm radius around the injection point the concentration or temperature is instantaneously the same as in the injection point itself. This allows the use of constant concentration/temperature boundary conditions for this small radial area throughout the whole calculation. Furthermore, a Gaussian concentration or temperature distribution was assumed as initial condition to prevent steep concentration and thermal gradients, respectively. This initial Gaussian distribution dropped very fast with distance and reached only a radius of 0.5 m.

The fracture aperture was varied in a range between 2 mm and 10 mm and the porosity in the fracture was assumed to be 100 % (i.e. fully open). A sensitivity

analysis by KOHL et al. (1994) has shown, that solute transport is not seriously affected by the absolute value of the porosity, provided that the effective cross-sectional area (i.e. total cross-sectional area times porosity) of the fracture is kept constant. Consequently, assuming a smaller fracture porosity implies an increased fracture aperture. For this reason, a fracture porosity of 100 % was applied for simplicity, although such a value is not expected at the BK site. The estimates for the fracture transmissivity were derived from previous hydrotests (see VOMVORIS & FRIEG 1992). Tab. 6.1 summarizes the hydraulic parameters as well as solute and thermal properties of the fluid, the fracture and the matrix, used for the design calculations.

Tab. 6.1: Material parameters used in the SHT design study

Fluid	ρc_p [J / Km^3]	4.0E+06
	λ [W / K m]	0.60
Fracture	T [m^2 / s]	2E-06
	ϕ [%]	100
	α_L [m]	0.10
	α_T [m]	0.01
Matrix	ρc_p [J / Km^3]	2.2E+06
	λ[W / K m]	2.50
	K_f [m / s]	0.00

6.3.3 Prediction of the thermal response

Fig. 6.3 shows the breakthrough curves for the three 2D solute simulations MS05-2, MS05-5 and MS05-10. The simulations vary by their aperture of 2 mm, 5 mm and 10 mm respectively. The flowrates and the distance between injection and extraction interval were used according to the experimental layout of test VE 449. The influence of the fracture aperture on the breakthrough curve can be recognized clearly. Small apertures cause a faster flow in the fracture and therefore a shorter peak arrival time. Furthermore, the peak concentration is higher and the dispersion is smaller. When compared with the peak arrival and peak concentration of test VE 449 (see Section 6.3.1), the simulations indicate that rather large apertures have to be expected.

Using the solute model with an aperture of 10 mm the thermal breakthrough was also predicted for various inflow and outflowrates. Thereby, the ratio between extraction and injection rate was fixed to a value of 2:1 to ensure a recovery rate of 100 %. The 3D simulations MW1-4, MW2-2, MW2-5, MW2-10 and MW4-10 are based on the parameters, given in Tab. 6.2.

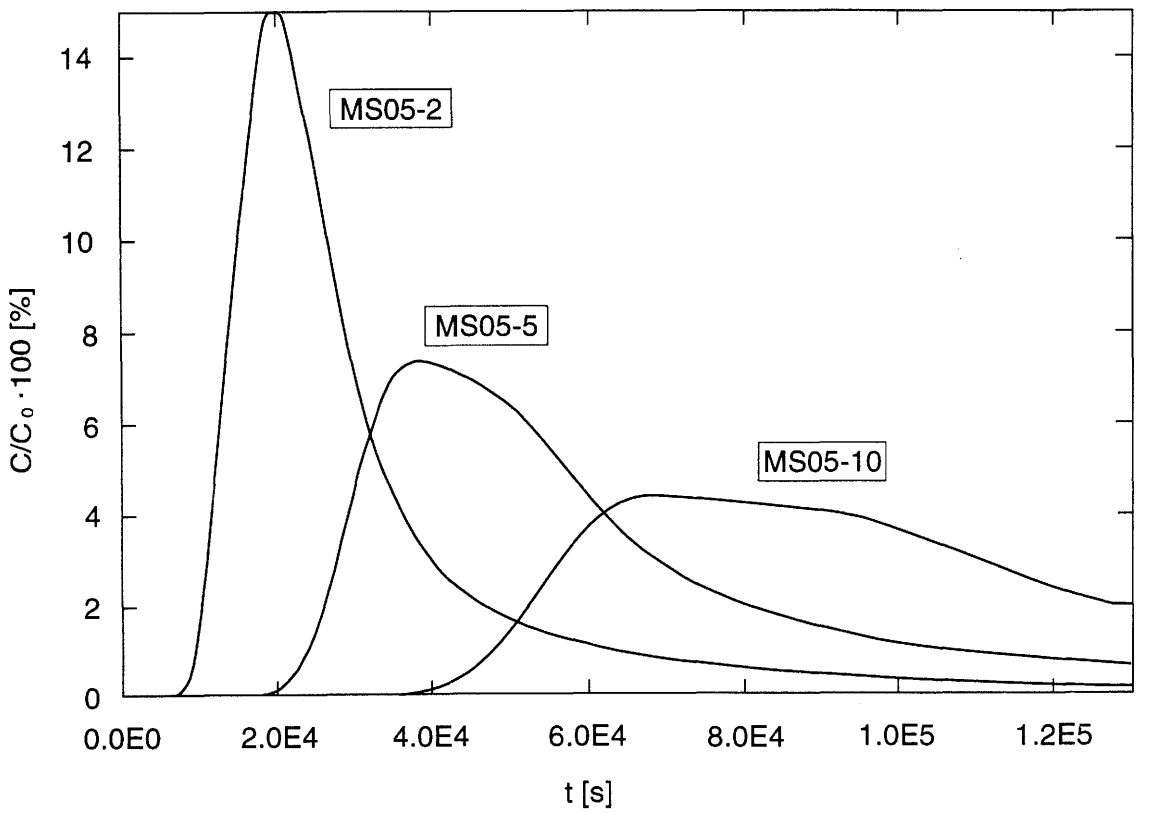

Fig. 6.3: Solute transport simultations MS05-2, MS05-5 and MS05-10 for pulse injection, with different fracture aperture. C/Co is the ratio of the concentrations measured in the extraction and the injection interval in percent

Tab. 6.2: Experimental layout parameters in the design study

	MW1-4	MW2-2	MW2-5	MW2-10	MW4-10
injection [l / min]	1.00	2.00	2.00	2.00	4.00
aperture [mm]	4.00	2.00	5.00	10.00	10.00

Fig. 6.4 shows clearly that the models MW2-2, MW2-5, MW2-10 do produce only a weak thermal breakthrough. Their arrival is preceeded by MW1-4 and succeeded by MW4-10. The results can be explained as follows: due to the dominating influence of the thermal matrix diffusion, the rate of injected fluid will strongly determine the thermal response at the extraction interval. Increasing the rate of hot water injected gives rise to a more pronounced thermal breakthrough at the extraction interval, because the increased flow velocities along the fracture reduce the losses of heat into the rock matrix by thermal diffusion. If instead of the injection rate the temperature difference is increased, the advective component of the thermal transport is not affected, provided that the effects of free convection and the temperature dependence of the hydraulic parameters are negligible. Hence, in the best case the response in the extraction interval increases linearily with the temperature of the injected water.

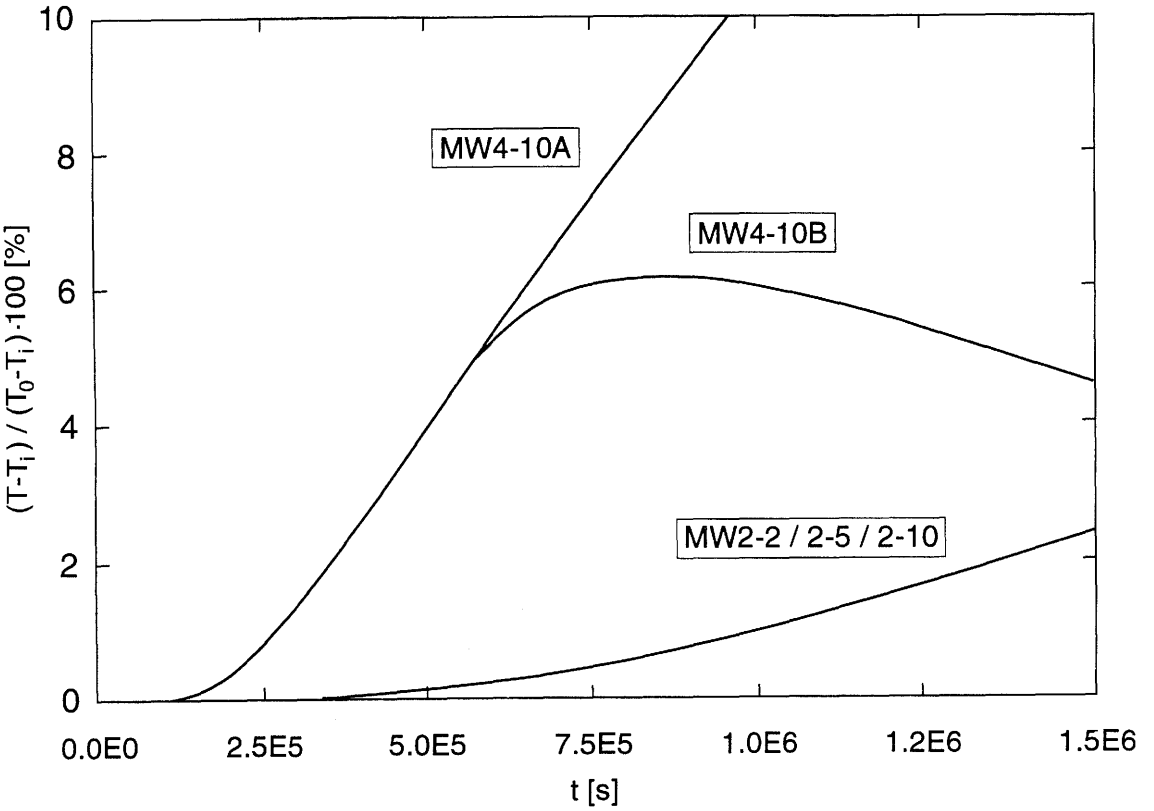

Fig. 6.4: Predictions for the thermal breakthrough. $(T-T_i) / (T_o-T_i)$ is the ratio of the temperature differences in the extraction and the injection interval, where T_i is the initial temperature and T_o the maximum injection temperature. The curves of the models MW2-2, MW2-5, MW2-10 cannot be distinguished visually. The simulation MW1-4 did not show any thermal breakthrough. All curves have been calculated with a constant injection of heated water except run MW4-10B, which assumes a week-long lasting injection

In conclusion, the design study pointed out the relevance of the injection rate on the thermal breakthrough at the extraction point. For a model of that simple geometry, the thermal breakthrough is a linear function of the injection temperature but strongly non-linear with the injection rate. In order to improve the chance of success of a heat tracer experiment, the injection rate should be set as high as possible. For the well known transmissivities at the intervals BK 5-I2 and BK 15-I2 and for a steady state pressure of about 8 bars expected at the BK site prior to the SHT experiment, the recommended injection and extraction rate were 4 l/min and 8 l/min, respectively. This experimental layout was expected to give a thermal response at the extraction interval within 2 or 3 days of injection. Care has to be taken, when the injection temperature is increased to improve the thermal response, because high temperature differences may cause non-linearities in the flow field.

6.4 Overview of the SHT experiments

6.4.1 The experimental arrangement and equipment

Including pre-tests, the SHT experiments consisted of a sequence of 7 single experiments (VE 515 to VE 521, see Tab. 6.3). Almost all boreholes in the BK area were equipped with single- or multi-packers. The packer positions were selected after the extensive evaluations of previous experiments, including core analysis, fluid logging [see e.g. BRÄUER et al. 1989 and VOMVORIS & FRIEG (eds.) 1992] and crosshole hydrotests (see Chapter 5). In Fig. 6.5 the packer positions are shown for the boreholes in plane B, including the injection and extraction intervals BK 5-I2 (Interval 2: 19.8-24.8 m along hole) and BK 15-I2 (Interval 2: 23.7-26.7 m along hole). The straight line distance between the mid points of the injection and extraction interval is approximately 8 m.

The water temperature in the injection and extraction borehole was recorded using high performance PT-100 downhole probes with a resolution better than 0.01 °C. The flowrates to the injection and from the extraction interval were measured using inductive flowmeters. The water salinity, the interval pressure and the flowrate were recorded at the borehole mouth. Furthermore, the flowrates and salinity of 7 dripping positions were monitored at the BK cavern. Experiments and equipment were described by MOHR (1993). Further details concerning the equipment and probes are given in PAHL et al. (1992).

The warm water injection equipment consists of a water heater with an input power of 20 kW (Fig. 6.6), heating the water in a primary circuit. By means of a heat-exchanger, heat is transferred from a primary circuit to a secondary system used for pumping the heated, brine water in the injection borehole. This arrangement enabled a low-pressure circulation in the primary system and a continuous high-pressure injection of the hot, brine water in the boreholes. The adjustment of the water temperature in the secondary system occurs by means of a proportional-integral-differential (PID) control device, which takes a corrective action for a deviation from the target value greater than 2 %.

6.4.2 The experimental conditions

Initial conditions

Prior to the SHT experiment, a pressure recovery phase was implemented in the BK area to provide stable hydraulic conditions (**VE 515**, see Tab. 6.3). The formation's mean temperature in the vicinity of the injection/extraction interval was 12.42 °C and the salinity of the formation water was 83 µS/cm. The water used to establish the dipole flow-field had a temperature of about 13 to 14 °C and a salinity of 80 to 85 µS/cm.

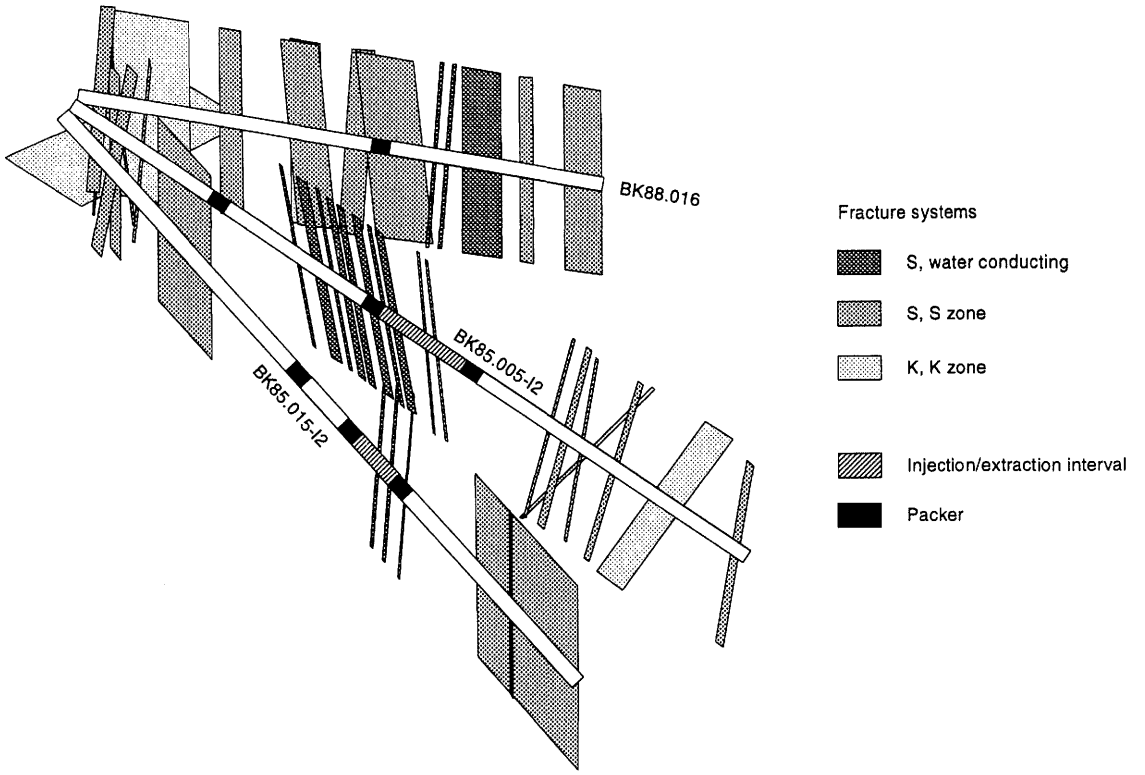

Fig. 6.5: Packer positions and fracture traces for the boreholes in plane B

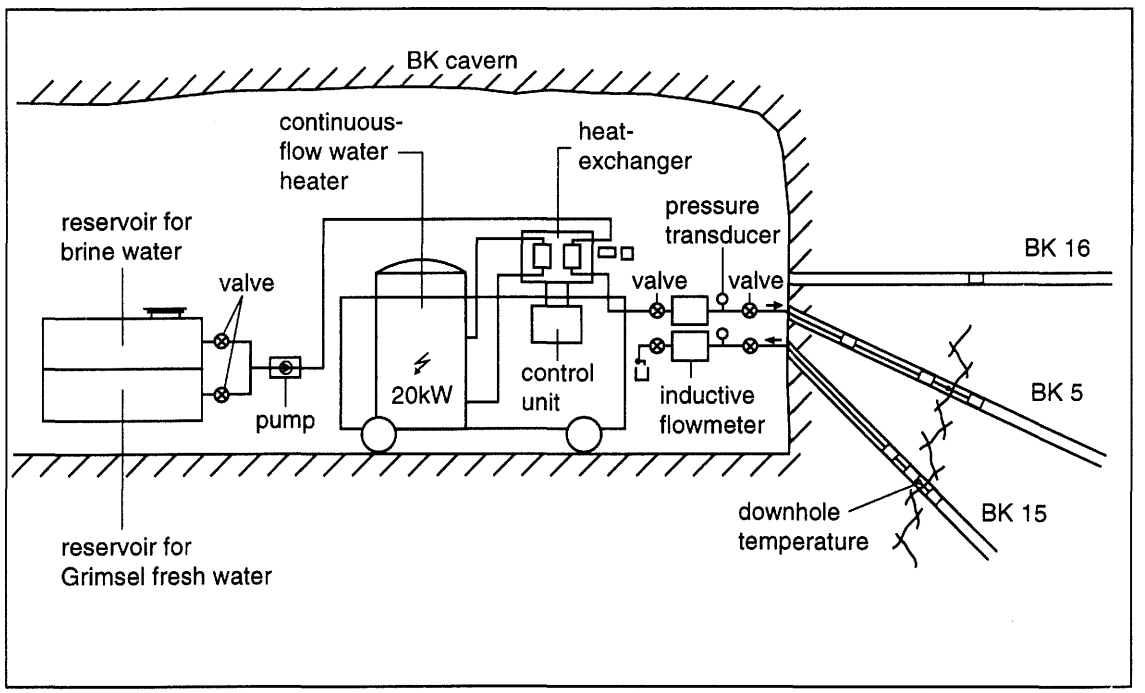

Fig. 6.6: Scheme of the equipment for saline / heated water injection / extraction

Pre-tests

Based on the SHT design calculations, a stable dipole flow-field with an extraction / injection ratio of 2:1 (i.e., 8 l/min: 4 l/min) was aimed at for the SHT experiments. The flowrates and the hydraulic heads observed during **VE 516** and **VE 517** showed that these optimal design values could not be achieved, because the stabilized pressures recorded at the packed borehole intervals ranged between 4.0 and 6.5 bar for the central BK area instead of the expected 8 to 9 bar. The extraction flowrate at BK 15-I2 during the VE 516 experiment decreased from 6.8 l/min in the beginning to 5.1 l/min. The injection flowrate at BK 5-I2 during the VE 517 experiment oscillated between 3.0 l/min and 3.25 l/min. Therefore, the extraction rate (natural flowrate) had to be limited to a maximum of 3 to 4 l/min to avoid water pressures in the extraction borehole to become lower than 0.5 bar, which might cause degassing from the extracted water.

During the test **VE 518** a stable dipole flow-field with an extraction to injection ratio of 2:1 was established by stepwise adjusting the flowrates. After 23:50 the injection rate was set to approximately 2 l/min. Subsequently, the pilot tracer experiment **VE 519** was initiated, aiming at the estimation of the salt tracer breakthrough time and the checking of the equipment and the data acquisition. During this test an one hour pulse of hot and brine water was injected retaining the flowrates for the stabilized dipole flow-field.

Tab. 6.3: Summary of activities before and during the SHT experiments

Test Designation	Date	Time	Event	Remarks
VE 515	03.02.93-23.02.93		Pretest	pressure recovery phase (all intervals closed)
VE 516	23.02.93	09:08-09:38	Pretest	flowrate measurement in BK 88.015-I2 (free outflow)
VE 517	23.02.93	11:08-11:50	Pretest	flowrate measurement in BK 88.005-I2 (free outflow)
VE 518	23.02.93-25.02.93	13:08-08:30	Pretest	stabilization of dipole flow-field: extraction from BK 88.015-I2; injection in BK 85.005-I2
VE 519	25.02.93-01.03.93	09:42-08:00	Pilot tracer test	pulse test with brine water injection for 1 h
VE 520	01.03.93-24.03.93	08:00-08:30	Salt/Heat Tracer Test (SHT)	BK 85.005-I2: brine water injection for 72 h, heat injection for 300 h
VE521	26.03.93-14.04.93	16:00-10:20	Reverse SHT Test	inversion of flow-field: extraction in BK 85.005-I2; injection in BK 88.015-I2

The SHT experiment (VE 520)

The experiment **VE 520** was the actual SHT experiment. Injection of heated (60 °C at surface), brine water (1800 µS/cm) was carried out without changing the flow-field. The average input power of the water heater was about 12 kW. Due to large heat lossed in the injection tubing, the effective downhole water temperature at the injection interval was 30 °C as shown in Fig. 6.7. The injection of brine water was stopped after 3 days and 2 hours, because the brine water breakthrough curve in the

extraction interval was well developed and the principal interest for the analysis was set on the tailing and the recovery. The experiment continued with injection of heated freshwater (60 °C and 83 µS/cm).

Due to the lower injection flowrates, the thermal response in the extraction borehole, as expected from the design calculations (see Section 6.3) could not be achieved during the entire experiment. For this reason, it was decided to prolong the heated water injection to enable the observation of a temperature reaction at the extraction borehole interval at all. The injection of heated water was stopped after 16 days and 4 hours. The dipole flow-field was further retained for a few days using freshwater (13 to 14 °C and 83 µS/cm).

The Reverse SHT experiment

The experiment **VE 521** aimed at checking the downhole temperature probe in the extraction interval of VE 520 (BK 15-I2) and at detecting a possible natural base flow or preferential flow paths in the network structure. For this purpose the injection and extraction intervals were exchanged and a stable flow-field was established with an extraction/injection ratio of 2:1 (i.e. 2.0 l/min: 1.0 l/min). Heated, brine water was injected during more than 1 day into BK 15-I2. When starting the tracer injection, the salinity in the extraction borehole was still about 5 to 10 µS/cm above the expected value of 83 µS/cm for formation water, originating from the previous test VE 520. The flow-field was kept constant for several weeks, and the tracer breakthrough in BK 5-I2 was recorded. It could be assessed that the downhole temperature probe in BK 15-I2 had worked properly during VE 520.

6.4.3 The experimental results

During the SHT experiment, interval pressures, temperature and concentration breakthrough curves as well as flowrates were measured continuously for a time period of 23 days. Fig. 6.7 summarizes the principal experimental results during test VE 520: plots of the pressures, water temperatures, salinity and flowrates are shown for the injection and extraction interval. The results can be summarized as follows:

- the flowrates are decreasing simultaneously during the test. This fact coincides with a pressure reduction in all observation intervals of the central BK area and can be explained by the net drainage of the BK fracture system by the established dipole flow-field. The flowrate ratio of 2:1 remains more or less constant.
- the pressure in the extraction interval was kept constant at a value of about 1 bar. The injection pressure, however, increases from about 6.1 bar up to 6.9 bar.
- the brine water breakthrough at the extraction interval exhibits distinct dispersion effects. The first arrival is observed after 20000 s and the peak arrival after 300000 s. The peak salinity is 460 µS/cm and the salinity at the end of the test is about 110 µS/cm, which is less than 2 % of the salinity of the injected brine water.
- about 70 % of the injected brine water is recovered at the end of the test. An extrapolation of the recovery shows, that about 90 % of the salt would be retrieved

for an infinite test duration. At the dripping points in the BK cavern, considerable salinity values up to 400 µS/cm were measured (see MOHR 1993); however, due to the low flowrates, these losses do not strongly affect the mass balance.

- the temperature breakthrough curve at BK 15-I2 shows an extreme delay and is still weak at the end of the test. The absolute temperature rise since the beginning of the test is 0.02 °C. An early 'apparent' thermal response, which is strongly correlated with the solute's breakthrough, is attributed to an unintentional cross-coupling between temperature and salinity measurements and, therefore, will not be considered in terms of the interpretation.

As stated before, the mass balance for the brine water extracted at the dripping points and at BK 15-I2 shows a total recovery of 70 % up to the end of experiment VE 520 and the extrapolation of the salt breakthrough curves leads to a 90 % recovery. This means that almost 30 % of the injected brine water remained in the central BK area when the reverse test VE 521 started. Consequently, the calculated recovery of 25 % at the end of the experiment VE 521 is rather uncertain and, therefore, those data are considered less suitable for further quantitative analysis.

6.5 Model selection

6.5.1 Scope of modeling

Fully 3D inverse modeling of transport in complex fracture networks leads inevitably to non-uniqueness problems, which means that multiple numerical models exist, fitting the data equally good within a given range of uncertainty. Increasing the complexity of the numerical model does not necessarily improve its predictive capability. The emphasis of the present investigations was, to find simplified conceptual models, which should help to better understand the relevant transport processes in the BK fracture network. This was done by jointly fitting solute and thermal transport during test VE 520 with a single fracture model. Thereby, the evaluation of the solute breakthrough curves focused in characterizing the advective-dispersive flow in the BK area. By analysing thermal transport, additional information was expected concerning the relevance of matrix diffusion in fracture networks.

In the present report, we have not included the data of the VE 521 test, which was a tracer test with a reversed flow-field (injection in BK15-I2, extraction from BK5-I2). A joint interpretation of the salinity breakthrough curves of the tests VE 520 and VE 521 was carried out by LI & KINZELBACH (1993) and KUNSTMANN (1994) using a single fracture, double-porosity model. The emphasis of jointly modeling two tracer tests with complementary flow-fields was to determine whether a natural base flow might be superimposed. KUNSTMANN (1994) has shown, that there is strong evidence for the prescence of a natural base flow at the BK site. By systematically changing the magnitude and the direction of the natural base flow-field, he pointed out by inverse modeling, that a unique set of transport parameters exists for a joint simulation of the two tests VE520 and VE521. In the present report, we have not accounted for such a superimposed flow-field, because our simulations led to transport parameters, which are very close to the results of Kunstmann. It should be mentioned, however, that the assumption of a natural base flow provided a much better fit of the breakthrough curves.

6.5.2 Basic conceptual models and discretization

Planar single and dual fracture models bounded by an impermeable matrix were considered. As shown in Figure 6.8, the basic structural models are a single fracture, single porosity model (SFSP), a single fracture model with preferential flow paths (SFPF), a single fracture, double-porosity model (SFDP) and a dual fracture, single porosity model (DFSP). The fracture behaves as a porous medium, assuming that flow is described by Darcy's law. Steady-state hydraulic conditions were assumed for all transport models. To account for the gently decreasing injection/extraction rates during the SHT experiment, the flowrate data were sampled with a time increment of 10 h and the corresponding steady-state dipole flow-field was repeatedly calculated to update the advective term of the transport model. For the SFSP conceptual model the results were compared with transport simulations, which assumed constant flowrates during the entire experiment. For the peak level of the breakthrough curve, differences on the order of 10 % do arise (see Fig. 6.11).

SFSP model - solute transport

The single fracture, single porosity model (SFSP) assumes flow in a homogeneous fracture with an impermeable matrix. The structural model is determined simply by the fracture aperture. Flow and transport properties of the fracture are expressed by the permeability and the porosity. The discretized flow area has a size of 50 x 50 m (Fig. 6.9). The distance between the two wells is 10 m. Accounting for the non-symmetric 2:1 dipole flow-field, the wells are not arranged symmetrically to the center of the model. The injection point is shifted along the dipole axis and has a distance of 25 m from the left boundary and the extraction point is placed 15 m from the right boundary of the model domain.

The model was discretized in space with 915 nodes having a minimum distance of 15 cm to each other in the neighbourhood of the boreholes and a maximum distance of 1.5 m at the other boundaries. Elements with quadratic shape functions were assumed, the triangle elements in the main flow area have Serendipity type shape functions and the outer quadrilateral elements have Lagrangian type shape functions. The discretized domain is shown in Fig. 6.9. Each discretization has to be fine enough, not to violate numerical accuracy. For the trade-off between numerical accuracy and the practical consideration of "simulation" time a difference of 5 % between the concentration values of the finest discretized test models in time and space and the accepted model was considered to be sufficient. An example of the deviations tolerated can be seen in Fig. 6.11. The largest timestep applied in this optimized model was 400 s.

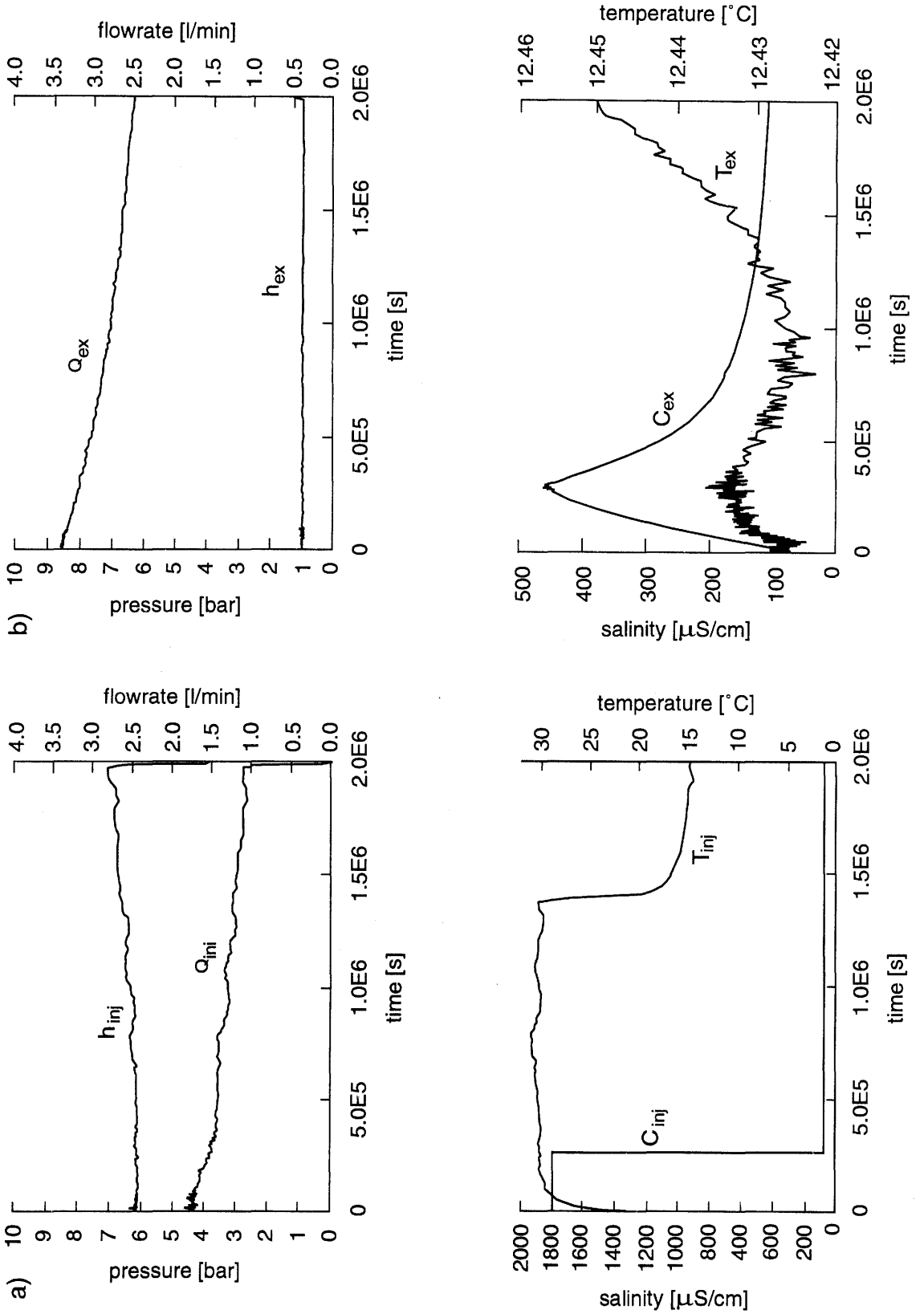

Fig. 6.7: The experimental results during VE 520 - pressure, flow, concentration and temperature in (a) BK 5-I2 and (b) BK 15-I2

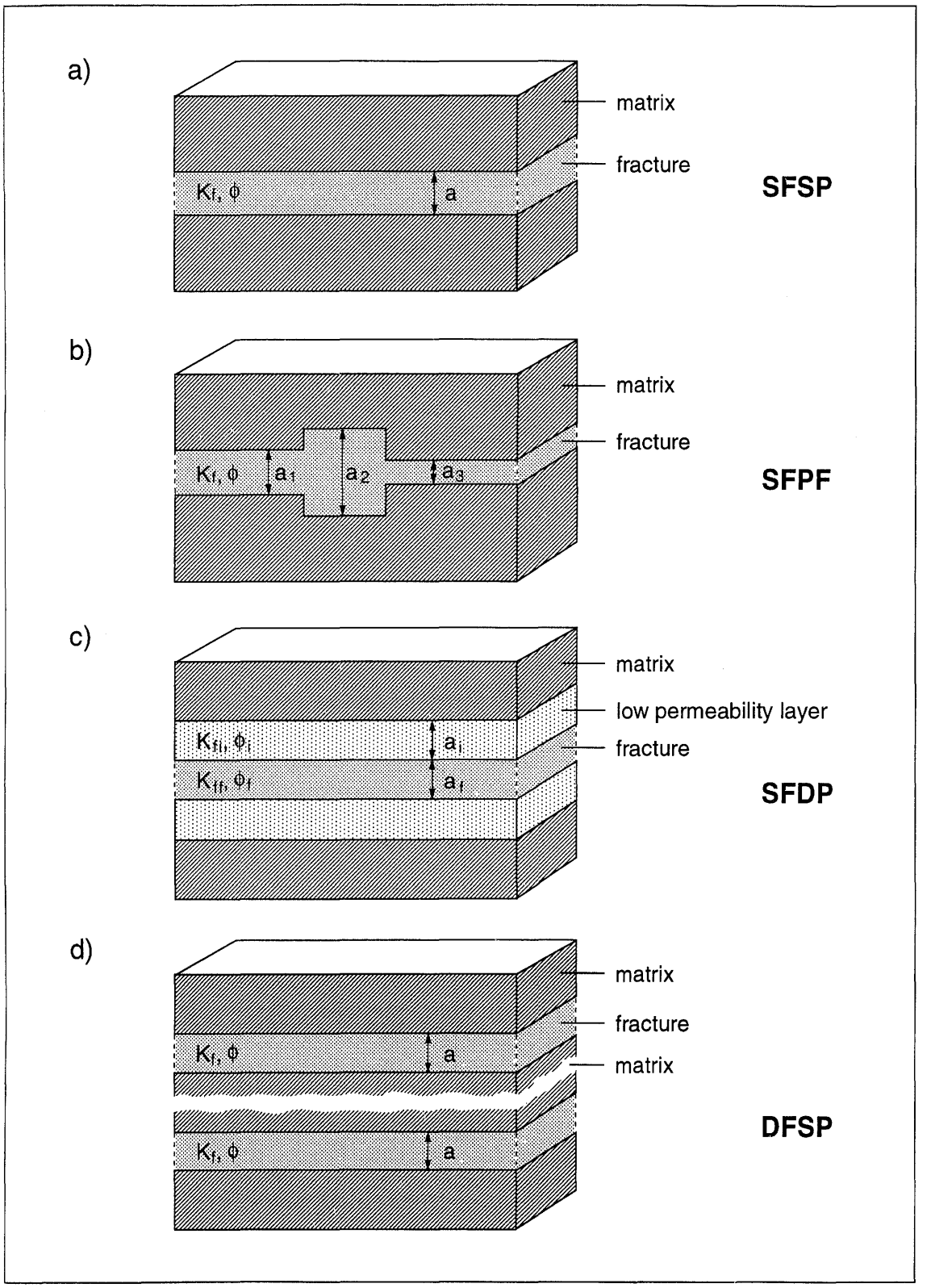

Fig. 6.8: Basic conceptual models: (a) single fracture, single porosity model, (b) single fracture model with preferential flow due to variable apertures, (c) single fracture, double-porosity model and (d) dual fracture, single porosity model

SFPF model - solute transport

The single fracture, preferential flow path model (SFPF) is very similar to the SFSP model, except that the fracture aperture is not constant. The discretization remains unchanged.

SFDP model - solute transport

The single fracture, double-porosity model (SFDP) is a full 3D model and takes into account additionally the interporosity flow between fracture and matrix. The structural model is determined by the fracture aperture and the thickness of the intermediate layer between fracture and impermeable matrix. Flow and transport properties are given by the permeabilities and porosities of the fracture and the intermediate layer, respectively. The discretization scheme from the single fracture model was adopted to discretize the fracture. The 2D elements of the fracture were mapped upon 3D matrix elements (see Section 6.2.2). The matrix was discretized into two domains: a permeable domain close to the fracture, representing the rock volume where double-porosity flow occurs with a thickness of 40 cm to both sides of the fracture and an adjacent impermeable domain with a thickness of 7.6 m. The permeable domain is represented by a row consisting of 3D elements, that is obtained by expanding the 2D element distribution of the fracture into the third dimension. The impermeable domain gets continuously coarser into the third dimension. The discretization could take advantage of this geometry, since it has symmetry planes through the fracture (x-y plane) and a symmetry plane along the fracture (x-z plane). The discretization is shown in Fig. 6.10. Lagrangian shape functions were taken for both domains, which contain about 6900 nodes and 1200 elements.

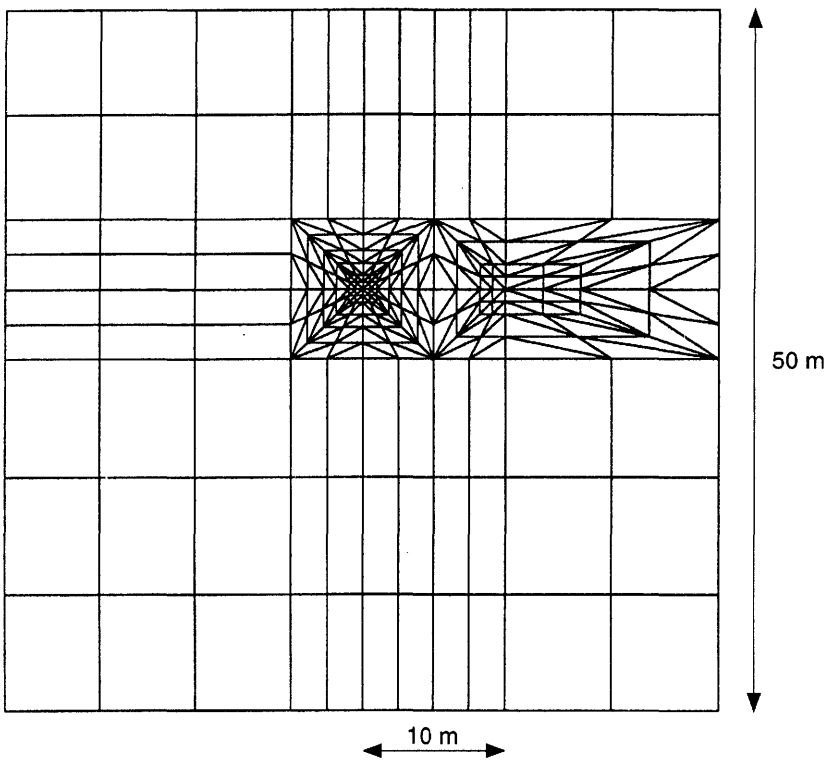

Fig. 6.9: Discretized model for the simulation of 2D solute transport

At the lateral boundaries, fixed head boundary conditions were assumed and at the upper boundaries, Neumann conditions (no-flow boundary) were used for the flow-field. A fixed concentration was assigned to the outer boundaries.

DFSP model - solute transport

The dual fracture, single porosity model (DFSP) consists of two uniform, parallel fractures, which are completely decoupled from each other. The structural model is determined simply by the fracture aperture. Flow and transport properties are given by the fracture permeability and the porosity. When modeling solute transport, the DFSP model can be represented by the SFSP model, where the injection and extraction rates are divided into equal halves. The discretization and the boundary conditions remain unchanged.

Thermal transport

SFSP models, DFSP models and SFDP models were considered for the thermal transport. Uniform thermal properties were assumed for the fracture and the matrix, respectively. The same discretization as for the SFDP model was applied for the thermal transport models. Furthermore, identical hydraulic boundary conditions were assumed. For the thermal boundary conditions a fixed temperature was applied. In the case of the DFSP model, the large thickness of the matrix ensured, that thermal transport in the two fractures was completely decoupled. Since the largest timestep that could be used was 1000 s, each model run required at least 15 h on a HP 720 workstation.

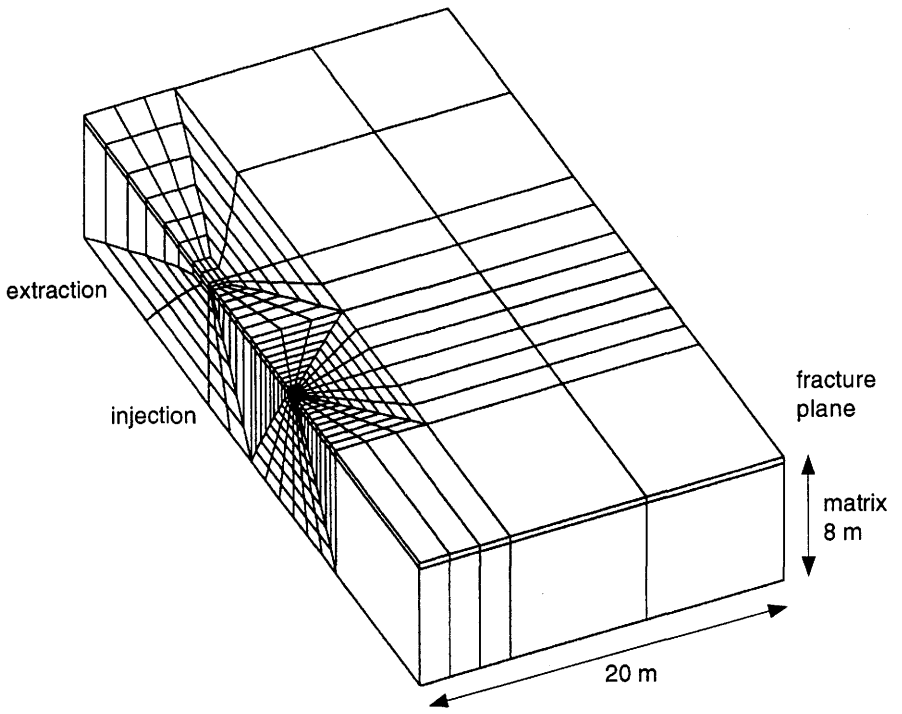

Fig. 6.10: Perspective view of the discretization of the lower part of rock matrix for simulating the 3D thermal transport. The 2D fracture plane is on the top of the discretized 3D body

6.5.3 Flow and transport parameters

In the scope of the present simulations, the transmissivity of the SFSP and the DFSP model is presumed to be constant. Hence the flow model was calibrated by varying the fracture transmissivity until a good fit of the pressure in the injection and extraction intervals was obtained with the given flowrates. The transmissivities used for flow modeling are in the range between 3.6E-6 and 7.5E-5 m^2/s (Tab. 6.6). These values correspond to the results of previous hydrotests, which have been done in the central BK area [VOMVORIS & FRIEG (eds.) 1992, see also Chapter 5]. For the SFPF and the SFDP model, the choice of the transmissivity and hydraulic conductivity values was somewhat arbitrary, because no direct measurements were available.

A fracture porosity of 80-100 % was adopted. As mentioned in Section 6.3, this high fracture porosity was introduced to reduce the number of unknown parameters, although such values were actually not observed at the BK. Consequently, the fracture aperture has to be increased, whereas the porosity is reduced by the same factor to get reasonable porosity estimates according to the definition of the effective cross-sectional area of the fracture, which is proportional to the product of the aperture times the porosity. It was shown by KOHL et al. (1994) that this conversion does not essentially affect the solute transport.

The values for the thermal conductivity of the Grimsel rock were measured in a laboratory program by BGR and at the ETH Zürich. They were summarized by KOHL et al. (1994) and LIEDTKE et al. (1993). The other thermal properties were extracted from literature (LANDOLT-BÖRNSTEIN 1982). The thermal parameters were kept basically unchanged during the simulation of thermal transport. The material parameters used are given in Tab. 6.6.

Tab. 6.6: Range of material parameters used for the simulation of VE 520

Material	Parameter	min. value	max. value
Fluid	ρc_D [J / Km^3]	4.0E+06	same as min. value
	λ [J / K s m]	0.60	same as min. value
Fracture	T [m^2 / s]	7.5E-05	3.6E-06
	ϕ [%]	80	100
	α_L [m]	1.00	5.00
	α_T [m]	0.10	2.00
Intermediate layer (double-porosity)	ρc_D [J / Km^3]	2.2E+06	2.2E+06
	λ [J / K s m]	2.50	3.80
	K_f [m / s]	1.0E-10	1.0E-07
	ϕ [%]	5	same as min. value
	α_L [m]	0.10	same as min. value
	α_T [m]	0.01	same as min. value
Matrix, impermeable	ρc_D [J / Km^3]	2.2E+06	same as min. value
	λ [J / K s m]	3.50	3.80
	K_f [m / s]	1.0E-13	same as min. value
	ϕ [%]	1	same as min. value
	α_L [m]	0.00	same as min. value
	α_T [m]	0.00	same as min. value

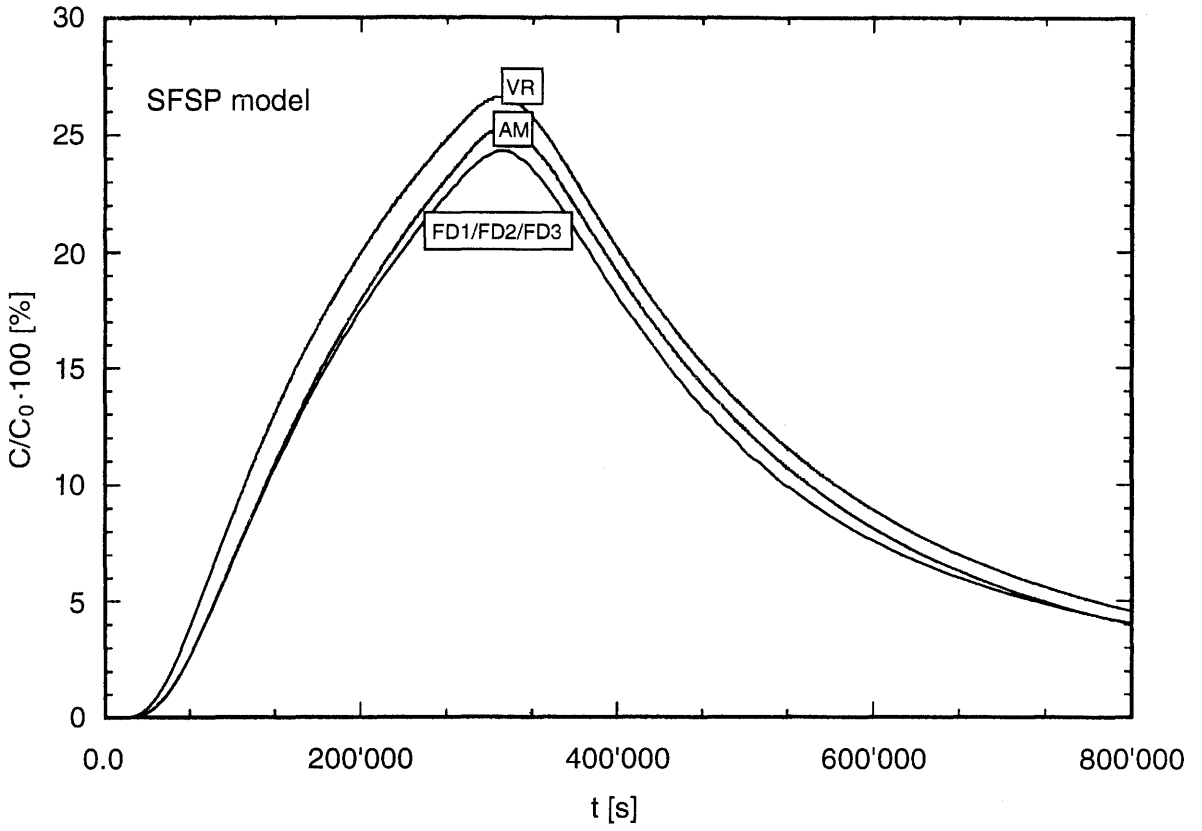

Fig. 6.11: Comparison of models with different discretization and with variable vs. constant flowrates. The very fine discretized SFSP-models FP1 models FD1, FD2, FD3 are close to the model AM, which was the base model accepted for all following solute transport calculations. The maximum difference between these 4 models which assume constant flowrates is smaller than 5 %. Another interesting comparison contrasts model AM with VR that accounts for the measured variable flowrates

6.6 Simulation of solute and thermal transport

6.6.1 Approach

A diagnostic approach, which was based on the simple structural models, given in Figure 6.8 was applied to match the solute and thermal response in BK 15-I2 during test VE 520. The matching procedure consisted of the following steps:

- plot the data in a log(t) representation, which is appropriate for flow model identification, when an inhomogeneous flow-field is expected
- fit the peak arrival time and peak concentration for the solute breakthrough by variation of the relevant flow and transport parameters within the range, given in Tab. 6.5

- improve the match of the early and late time response by increasing the model's complexity (single porosity, preferential flow paths, double-porosity)
- simulate the measured thermal response by applying the simple structural models and the solute transport parameters, derived in the previous step
- bracket the thermal response with single and dual fracture models, respectively, by applying reasonable parameters for the solute transport as derived during the previous calibration excercise.

Due to time constraints it was not possible to perform an extensive analysis of thermal transport for the individual structural models. In particular, no thermal simulations were done for the SFPF model. Emphasis was set on showing the benefit of the thermal transport data when there is not a unique structural model, which serves to reproduce the solute breakthrough. By taking advantage, that solute and thermal transport are controlled by different properties of the flow system, the number of the models considered can be reduced and consequently, a better insight is gained into the actual hydrodynamic behaviour of the formation.

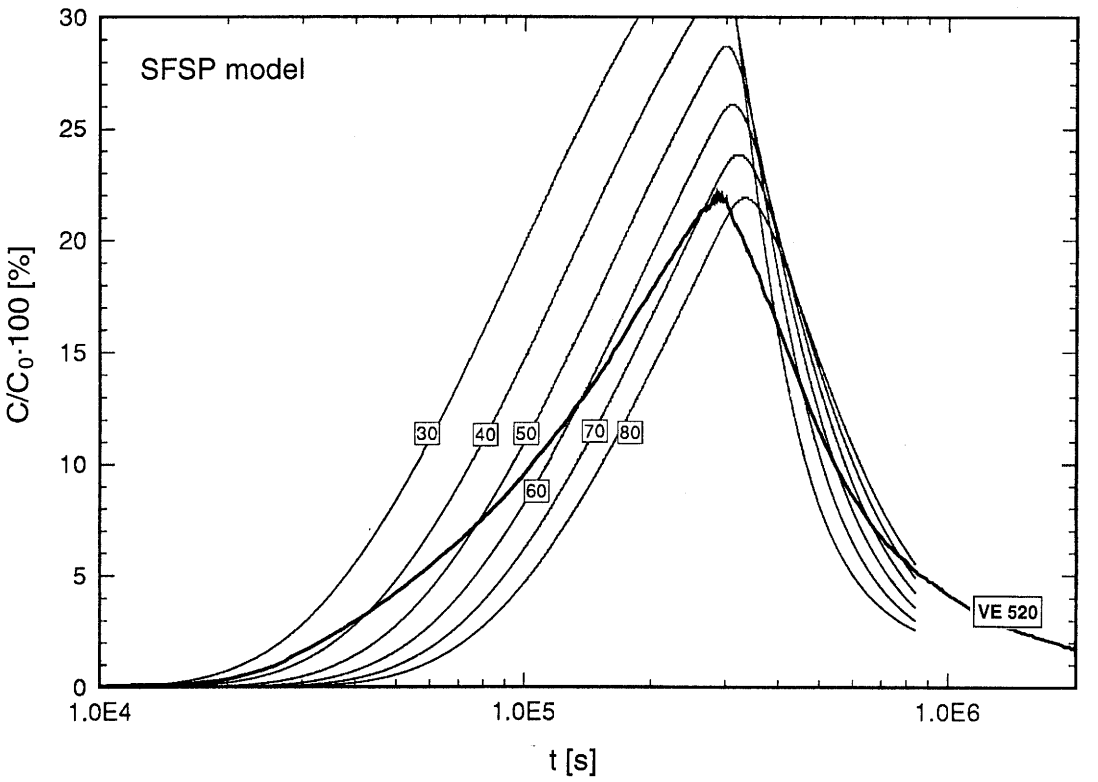

Fig. 6.12: Variation of aperture range for fixed dispersivity lengths (α_L = 2.5 m, α_T = 1.4 m) and 100 % porosity. The apertures are indicated in mm on their labels. VE 520: measurement curve

6.6.2 Solute transport

SFSP model

For this model, the transport depends essentially on the dispersivity length and the fluid particle velocity. Provided that the flowrates are given, the particle velocity distribution is determined by the fracture aperture. The calculations performed indicate rather large apertures and high dispersivity lengths. In Fig. 6.12 the variation of the breakthrough curves for different apertures is shown. Small apertures result in high flow velocities and in a clear peak arrival, whereas the concentration is spread more over the fracture surface for large apertures. To generate the breakthrough curves in Fig. 6.12, a longitudinal dispersivity of 2.5 m and a transverse dispersivity of 1.4 m was applied as proposed by LI & KINZELBACH (1993). It was surprising to find apertures in the range between 60-80 mm, providing the best match of the peak arrival times and the peak concentration. Particularly in the log(t)-representation, however, it becomes obvious, that the fit is poor for the early time period and the tail.

Fig. 6.13 shows the results for the variation of the dispersivities with a fixed aperture of 70 mm. Dispersivity lengths known from literature for small scale tracer tests (α_L = 1 m, α_T = 0.1 m) result in much steeper slopes than measured during test VE 520. Increasing the dispersivities allows a better fit of the early time period, but there is also a tendency of a too short tail. Nevertheless, large dispersivities tend to have a positive effect on the model fit, although they start to have little physical meaning when approaching the same order of magnitude than the presumed travel distance between the injection and extraction interval.

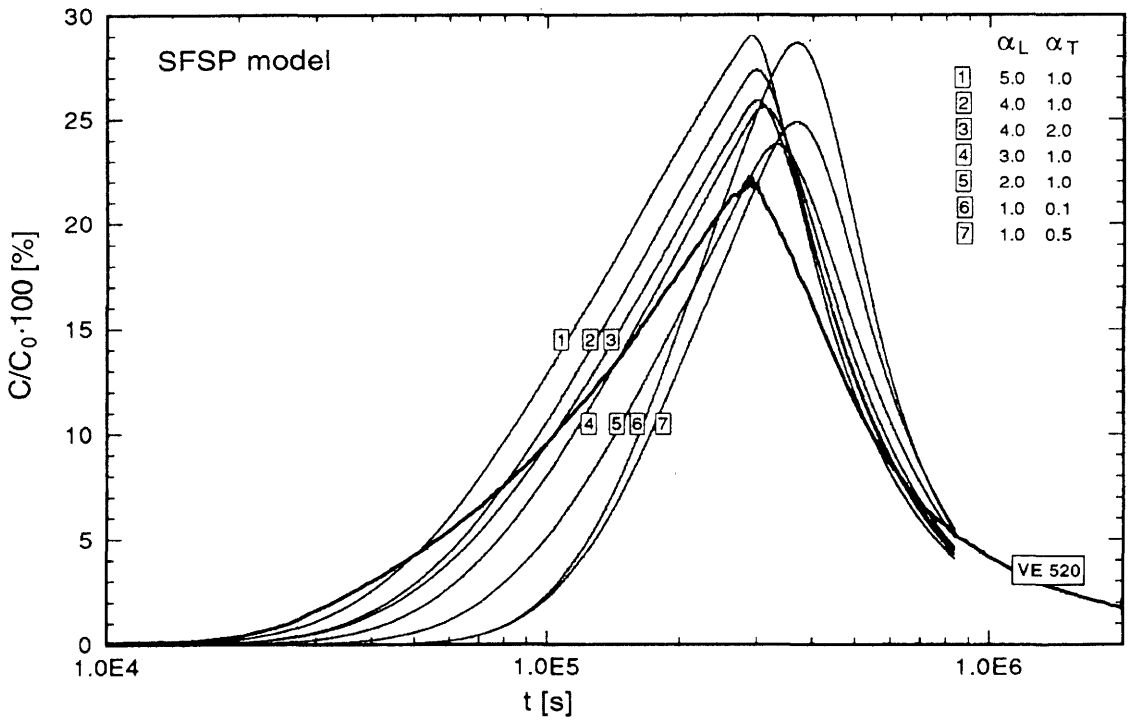

Fig. 6.13: Variation of dispersivity lengths with fixed aperture of 70 mm and 100 % porosity. The dispersivities are given on the Fig. table: mid column - α_L, right column - α_T

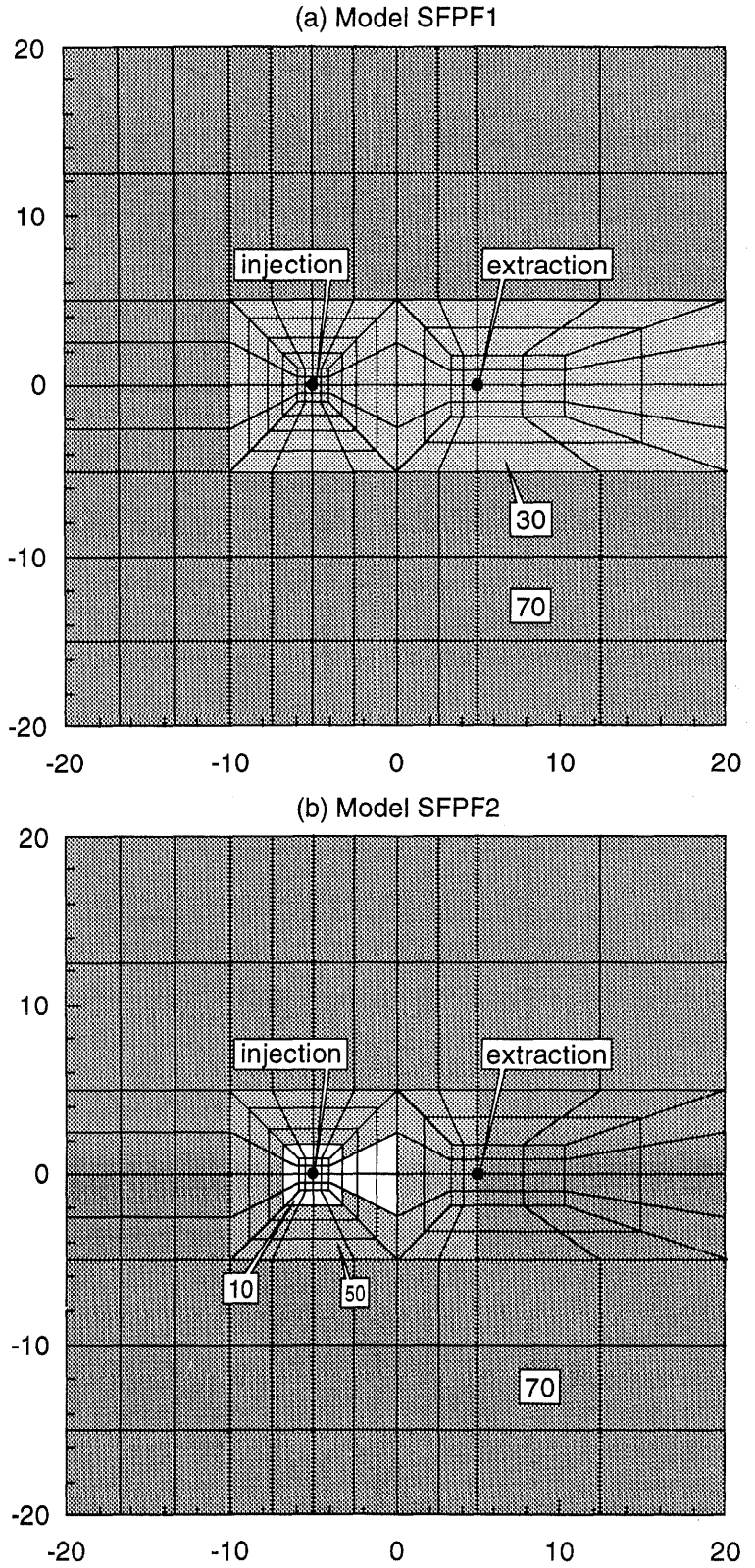

Fig. 6.14: Discretization of the single fracture, preferential flow models PF1 (a) and PF2 (b) with variable apertures in the range between 10 and 70 mm

SFPF model

Preferential flow paths in a single fracture can be explained by the variability of the hydraulic parameters along the fracture or by fracture intersections. Fracture intersections may cause extensive channeling effects, if the transmissivity of the intersecting fracture is high enough to shortcut the dipole flow-field between injection and extraction interval. In a single fracture model, intersecting fractures can be represented by simply increasing the aperture along the trace of the fracture intersection. In the present work, special emphasis was put on models that offer large volumetric flow in the central flow domain between injection and extraction point.

Model SFPF1 (Fig 6.14a): An aperture of 30 mm with a transmissivity of 6.0E-07 m^2/s is assumed for a strip parallel to the dipole axis, which is 10 m wide and ends 5 m behind the injection point. The outer domain has an aperture of 70 mm with a transmissivity of 1.4E-06 m^2/s.

Model SFPF2 (Fig. 6.14b): An aperture of only 10 mm and a transmissivity of 2.0E-07 m^2/s is assumed for a small area in the vicinity of the injection point. This zone is enclosed by a rectangular domain with an aperture of 50 mm and a transmissivity of 1.0E-06 m^2/s which covers both the injection and extraction point. The outermost domain has an aperture of 70 mm and a transmissivity of 1.4E-06 m^2/s.

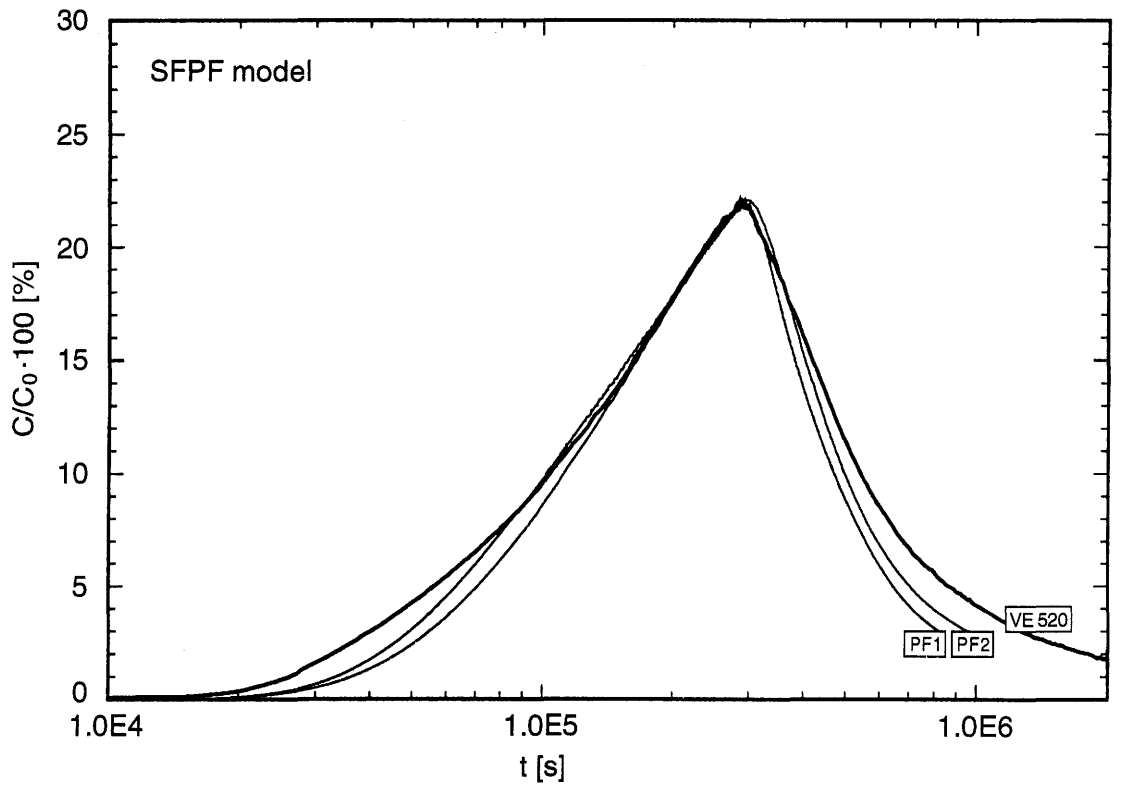

Fig. 6.15: Single fracture, preferential flow model: variation of aperture on the fracture plane. The models are explained in the text

In the course of the present studies, only the transmissivities and the fracture aperture were varied with constant dispersivities (α_L = 2.5 m, α_T = 1.4 m). The most successful models fitted indicate that the injection borehole should not be very well linked to the fracture zone. In fact, the injected fluid would then spread out over a large area and is later recollected by the extraction point. This approach can explain the early arrival but is not able to explain perfectly the tailing. Finally the assumption of variable fracture apertures gives a clear explanation for the large transverse dispersivity lengths. But still there are doubts whether the dispersivities are meaningful, since a rather detailed model should reduce their length. To show the possibilities of this approach the breakthrough curves of two models are shown in Fig. 6.15.

SFDP model

In common double-porosity models, a global transfer coefficient is introduced to describe the solute's exchange between fracture and matrix (see PFINGSTEN 1990). Such models cannot account for dispersive flow in the matrix. FRACTure, however, assigns conductivities not only to the fracture but also to the matrix. The double-porosity model applied for the following simulations consists of three homogeneous domains: The fracture plane, the permeable intermediate layer allowing solute transport and the impermeable matrix, allowing no transport due to very low hydraulic conductivities. When modeling the solute breakthrough curve of test VE 520, the large apertures of the above described single fracture flow models can now be reduced, since the total flow splits into two parts through the permeable layer and the fracture, respectively. With increasing intermediate layer's conductivities the fracture apertures must be further reduced in order not to increase the apparent transmissivity of the total double-porosity system. Five model runs DP1 to DP5 were started, assuming a permeable layer with a thickness of 40 cm and hydraulic parameters given in Tab. 6.5. The breakthrough curves corresponding to these models are presented in Fig. 6.16.

Tab. 6.7: Parameters used for double-porosity simulation

	DP1	DP2	DP3	DP4	DP5
Fracture					
K_f [m/s]	2.E-05	2.E-04	2.E-04	1.E-04	1.E-04
α_L [m]	2.50	2.50	2.50	4.00	4.00
α_T [m]	1.40	1.40	1.40	0.40	0.40
a [m]	30.0E-03	5.0E-03	5.0E-03	5.0E-03	5.0E-03
Intermediate layer					
K_f [m/s]	1.E-10	1.E-07	1.E-08	1.E-08	3.E-08
α_L [m]	0.10	0.10	0.10	0.10	0.10
α_T [m]	0.01	0.01	0.01	0.01	0.01
ϕ [%]	5.00	5.00	5.00	5.00	5.00

The results of the double-porosity simulations can be summarized as follows: as expected, a better fit can be reached than with single porosity models, in particular for the tail of the solute breakthrough (see model DP1 and DP3). Nevertheless none of

the models calculated can reproduce satisfactorily the total breakthrough curve. The small aperture of the fracture tends to fit very well the first 10000 s of the dataset VE 520 (see DP4 and DP5). Small changes of intermediate layer's conductivities may have a dominant effect on transport properties (see breakthrough curves for the models DP4 and DP5 - differing only by the K_f value of the intermediate layer). On the other hand, models with a dominant intermediate layer result in very low peak values as shown in simulation DP2, because solute transport is delayed by the low particle velocity in the intermediate layer.

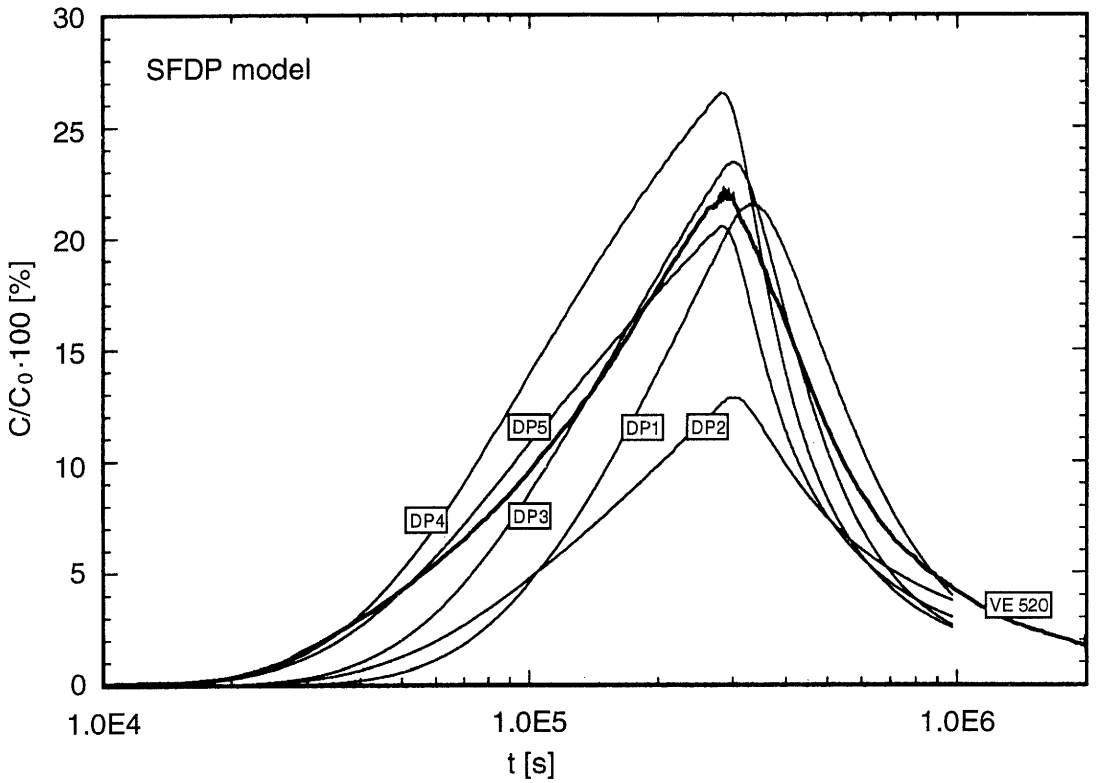

Fig. 6.16: Double-porosity approach: variation of fracture aperture, intermediate layer's permeabilities and dispersivity lengths. The models are described in the text

DFSP model

As mentioned before, the dual fracture, single porosity model can be represented by a SFSP model, when the injection and extraction rates are divided by a factor of two. This is evident, because the distribution of the particle velocity remains unchanged, and thus, solute transport is not affected. For this reason, we have renounced to present an example of solute transport for the DFSP model.

6.6.3 Thermal transport

The simulation of thermal transport was considerably more time consuming than the solute simulations with double-porosity models. Hence, as mentioned, it was not

possible to perform the thermal simulations with the SFPF model. Furthermore, only a few sensitivity runs were carried to study the effect of varying the thermal conductivity of the rock matrix. The simulations showed, that the thermal response will not change essentially, provided that the uncertainties of the thermal conductivity measurements are in a range as given in Tab. 6.6.

SFSP model

The thermal simulations with the single fracture, single porosity model started by applying model parameters, which previously have been used to fit the solute transport (α_L = 2.7 m, α_T = 1.4 m, a = 40-70 mm). The result of the simulations was surprising: the simulated thermal response preceeded the actually measured breakthrough curve considerably (see Fig. 6.17, model SF1 with a = 70 mm). For this reason, the fracture aperture was successively increased to provide a match between simulated and observed thermal breakthrough, regardless to the effect on solute transport. However, as shown in Fig. 6.17 for the model SF2 with a = 140 mm, the apertures required to fit the thermal data became unreasonable. Even with apertures of 200 mm, the simulated response preceeded the observed thermal breakthrough (see KOHL et al. 1994). These simulations indicated clearly, that a single fracture, single porosity model does not serve to explain both, the solute's breakthrough and the thermal response.

SFDP model

Thermal simulations with the single fracture, double-porosity model have been done for parameter sets corresponding to the models DP3, DP4 and DP5 in Tab. 6.6. The models differ considerably with respect to the dispersivities and the transmissivities of the fracture and the intermediate layer. Consequently, the solute breakthrough curves are strongly different, as seen in Fig. 6.16. The thermal breakthrough, however, is practically identical for the three models. Furthermore, the thermal response is very close to the single porosity model SF1. The explanation is that the dispersion in the fracture and the intermediate layer is completely covered by the predominant thermal diffusion. Thermal diffusion is controlled by the area of the interface between matrix and fracture, which is exposed to the advective heat transfer. Provided, that the mass flow in the fracture zone is comparable for single and double-porosity models, the thermal response shows basically no difference, because the volume of rock, accessible to thermal diffusion remains more or less the same.

DFSP model

The thermal transport was simulated for two dual fracture, single porosity models, namely with apertures of 35 and 70 mm (see models DF1 and DF2 in Fig. 6.17). For the solute transport, the models DF1 and DF2 are equivalent to the single fracture models SF1 and SF2, respectively. In the thermal response, the dual fracture models are clearly delayed, when compared with the measured breakthrough. The reason is that the area of the fracture/matrix interface, exposed to the advective heat flow is twice as much as for the SFSP model. Hence, the rock volume, accessible for thermal diffusion has increased considerably.

The thermal response, actually measured during VE 520 is bracketed by these to structural models. Furthermore, a dual fracture model would provide breakthrough curves, which are closer to the actually measured thermal response, when the

distance between the two fractures would be smaller. This is because the thermal diffusion between the two fractures is limited by the finite rock volume.

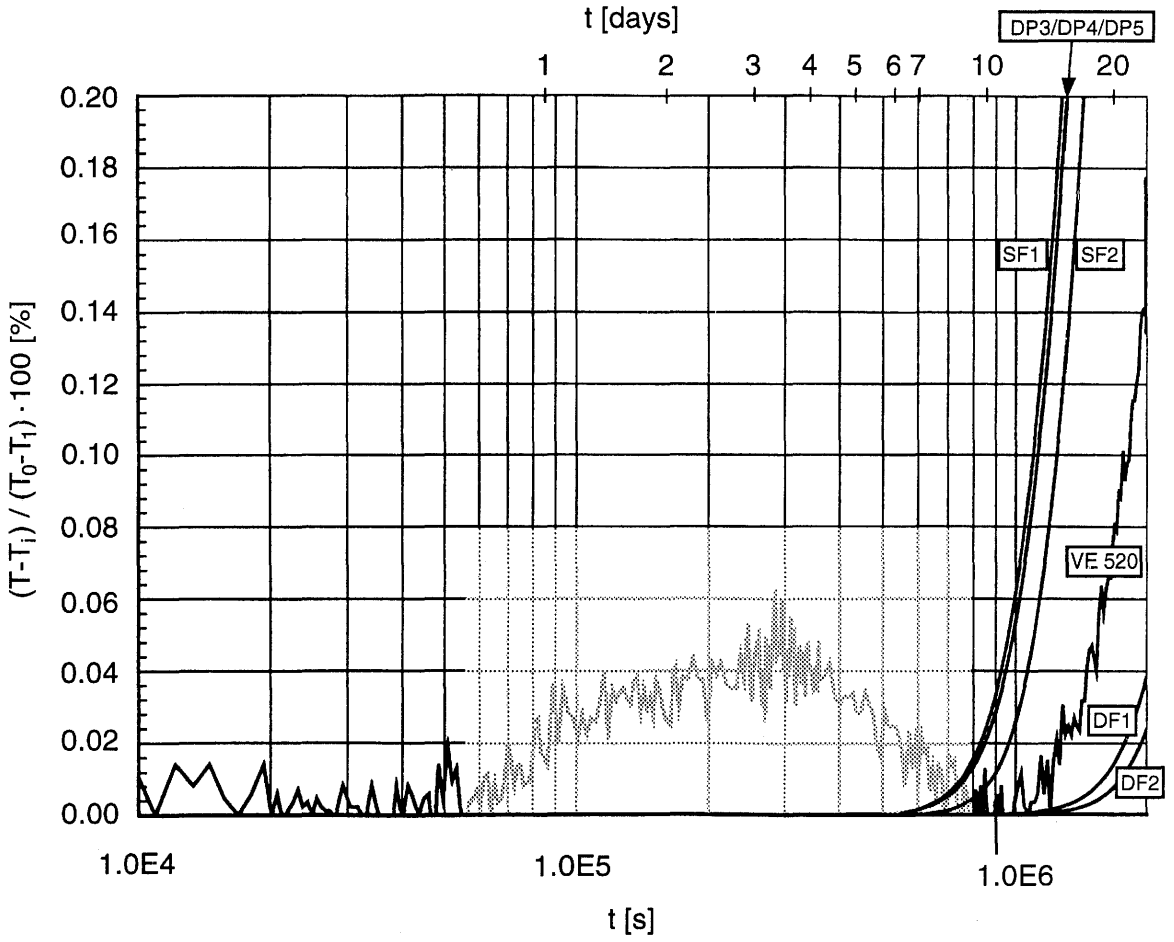

Fig. 6.17: Thermal simulation of VE 520: the curves SF1 and SF2 represent single fracture, single porosity models with apertures of 70 and 140 mm, respectively. The models DP3 to DP5 represent double-porosity models as specified in Tab. 6.7. DF1 and DF2 are dual fracture models with apertures of 35 and 70 mm. The shaded part of the thermal breakthrough curve was disturbed by cross coupling effects with the solute breakthrough

6.7 Discussion of the results

The combined Salt/Heat Tracer Experiment, performed at the BK site represents a novel methodology to characterize flow and transport properties of fractured rock. In the scope of the investigations, equipment components for long term injection of heated water were developed and the applicability of heat as a non-reactive tracer was tested. Furthermore, a simple diagnostic approach was applied to interprete the experiments and the finite element code FRACTure for modeling coupled transport processes was tested. In the following section, the experimental findings and the

results of the modeling approach are discussed with special focus on the combined use of heat and salt as complementary tracers.

Experimental findings

The experimental investigations were carried out as planned, except that the stabilized pressures prior to the test were not as high as expected. As a consequence the extraction rates, proposed by the design calculations could not be realized. Therefore, the test took longer and the response in the extraction interval was less pronounced than initially expected. The experimental findings can be summarized as follows:

- The water heater described in Section 6.3.2 worked reliably and accurately over the whole injection period of more than 16 days. The average power input during the test was about 12 kW, which is only 60 % of the rated power input.

- With the current equipment, it was not possible to isolate the injection tubing thermally. For this reason thermal losses of 60-70 % occured between the heater and the downhole temperature probe. In the framework of future tests, it is recommended to improve the injection equipment by using a PVC injection tubing.

- The dynamic range of temperature measurements during heat tracer tests, which is defined as the ratio of the differential temperature in the injection well and the resolution of the temperature probe in the extraction interval, is estimated to be not more than 1000-2000. To increase the injection temperature to values of more than 20 °C above formation temperature would cause uncertainties due to non-linear flow around the injection borehole, whereas the resolution of the temperature probes under field conditions is in the best case 0.01 °C.

Provided, that the flowrates are in the same range as during test VE 520, reasonable heat tracer tests for conditions similar to the ones in BK to be limited on dipole distances up to about 10 m. By slightly modifying the current equipment, the injection flowrates might be increased by at least a factor of 2 or 3. In case the hydraulic conditions would allow for higher injection rates, it is expected to get reasonable heat tracer test results even for travel distances of 15-20 m. Keeping in mind the restricted dynamic range, for larger distances heat is no longer a suitable tracer, due to the dominant thermal diffusion.

Modeling approach

None of the presented conceptual models can explain entirely the VE 520 test data. Nevertheless, the modeling approach proposed in Section 6.6.1 provides some useful insights into the basic transport behaviour of the fracture zone under investigation:

- When simulating the solute transport with the single porosity model of a single fracture, a match of the test data demands for extremely large dispersivities, which tend to have little physical relevance. The strong spreading might be caused by preferential flow within the fracture (microstructure of the fracture system) or by a distortion of the dipole field due to discrete features, intersecting the fracture. Both models provide potential conceptualizations of the investigation area.

- Double-porosity simulations provide an alternative approach to explain the strong spreading of the solute breakthrough curve. The double-porosity model fits the solute transport better than the single porosity model. It provides more flexibility, when reasonable (i.e. physically meaningfull) estimates for the fracture's dispersivity are required.

- By jointly fitting the solute and the thermal breakthrough, several of the considered conceptual models can be further evaluated and be accepted or rejected. Thus, the single fracture, single porosity model fails, when applied to the thermal transport, because the rock volume, accessible for thermal diffusion, is too small. The simulated breakthrough preceeds the thermal response considerably.

- The single fracture double-porosity model gives almost the same results as the single fracture model, because the heat transfer into the rock matrix is essentially determined by area of the fracture/matrix interface, exposed to the advective heat transfer. This area is not significantly different for the single and double-porosity model.

- A dual fracture model does not affect the solute transport. However, the thermal response is strongly delayed with respect to the measured data. Thus, the measured breakthrough curve is bracketed by the models of a single and a dual fracture system, respectively.

- A plausible approach to interprete the thermal response during the SHT experiment with a dual fracture model is to decrease the distance between the fractures systematically until a good fit with the measured thermal breakthrough is achieved. The distance between the two fractures might be attributed to the thickness of the fracture zone. However, the verification of this approach was beyond the scope of the present investigations.

The finite element code FRACTure worked reliably without any problem. In the scope of the present study, the functional coupling capabilities of FRACTure have not been activated, because the temperature difference between the injected water and the formation water was moderate. Hence the uncertainties, arising from the variability of the hydraulic parameters exceeded the errors, caused by the nonlinear behaviour of thermal transport.

PART V

VISUALIZATION AND FRACTURE ZONE MODELING

7 VISUALIZATION AND CONCEPTUALIZATION OF HYDROGEOLOGICAL DATA IN FRACTURED ROCK

F. Müri (VAW), P. Bossart (Geotechnisches Institut AG), N. Correa (Nagra)

7.1 Introduction and scope

In an advanced phase of site characterization for a potential nuclear waste repository, tunnels and caverns are excavated and a large number of boreholes is expected to be drilled to develop and improve the structural information database for the host rock. In addition, various hydrogeological and rock mechanical tests will be carried out, aimed at hydrogeological and rock mechanical characterization of the geological barrier in the vicinity of the repository. The geometric arrangement of the tunnels, caverns and boreholes can become very complicated. In order to achieve a better understanding of the hydrogeological conditions in the vicinity of the repository, visualization tools are required which translate the geometric, structural and hydrogeological information into a 3D context.

The Fracture System Flow Test in the BK area has been initiated in 1984 with emphasis on flow and transport processes in complex fracture networks. The site was explored with a total of 19 boreholes oriented in different directions. An extensive geological database was created from the petrographical investigation of the borehole cores, producing a list of all observed fracture traces (BRÄUER et al. 1989, MARTEL & PETERSON 1991, PAHL et al. 1992, VOMVORIS & FRIEG 1992). Further detailed hydrological and geophysical observations were made, which were completed with hydraulic tests and tracer experiments. These observations and measurements have been compiled to form a reasonable conceptual model of flow in the BK fracture network as a basis for hydrodynamic modeling (Chapter 8).

7.1.1 Objectives

The large amount of geological, hydrogeological and geophysical data available, as well as the complex geometry of the site, makes it difficult to construct a transparent and consistent conceptual model of flow and transport within the BK fracture network with simple means. In particular, the need for selection and classification of relevant structural data requires an adequate and flexible representation of the information available. Conceptualization of data within the framework of a structural interpretation is greatly assisted by 3D visualization. Therefore, the aim of this task was:

- to test a computer-based 3D visualization tool for its capability to represent various structural data and results of hydrogeological experiments,
- to develop a strategy for derivation of the BK conceptual model which makes use of the above-mentioned visualization tool,
- to apply this strategy to establish a condensed fracture zone model for hydrodynamic modeling of crosshole hydrotests at the BK site.

In Section 7.1, the 3D visualization software AVS is described and the user's extensions developed in the AVS environment to visualize structural and hydrogeological data are explained. In Section 7.2, the spectrum of hydrogeological applications is described, including the visualization of complex geometric structures (e.g. tunnels, caverns, large-scale geological structures), local structural information in the boreholes (petrographical, geological, hydrogeological) and the observed hydrodynamic processes (flow and transport processes during hydrogeological tests). In Section 7.3, a strategy for the derivation of a conceptual flow model in complex fracture zone systems is presented. This strategy is then applied to the BK site, where the 3D visualization is used to derive a reduced network of fractures by jointly interpreting structural data and hydrogeological tests. The experience, gained in the present work and perspectives of 3D visualization are discussed in Section 7.4.

7.1.2 Overview of the 3D visualization program AVS

The program AVS (AVS MANUALS, Advanced Visual Systems, 1992, 1993), which has been applied up to now by Nagra for visualization and animation purposes, was selected as the basis of the present studies. AVS is a commercially available, complex graph software package that is used worldwide. It runs on a series of different platforms, from simple workstations to high-end graphics computers (Convex, DECstations, VAX, HP, IBM RS6000, Kubota (Stardent), Sun workstations). The program is frequently used in computational fluid dynamics and in chemical visualization applications. Up till now, Nagra has used it mainly for the presentation of hydrodynamic calculations.

AVS incorporates a library with an extensive set of modules, each of which performs a complex task (data input, scaling of data, transformation of coordinates etc.). The modules are selected and connected to each other through the network editor, where the information between the modules is transferred through standardized interfaces. A typical module chain begins with data input and ends with the geometry viewer module, which generates an image from geometric objects on the screen.

Usually, geometric objects are generated by the AVS standard modules. Additionally, user-supplied modules can be created in the development environment by the Module Generator. Two libraries in the programming languages C (C++) and FORTRAN provide subroutines for the object generation and take care of the internal data administration. By means of these it is possible to describe the geometric objects in the format that is finally used by the geometry viewer module.

A special AVS module was developed for the present visualization task. This module creates geometric objects directly from an input ASCII file and converts object-related data to geometry-related data. The module was written in the language C. At the moment the module contains about 2000 lines of code (see MÜRI et al. 1993). Its task is to convert the geometric data to a common global coordinate system and to call further subroutines from the AVS geometry library. From the presented data, the library builds the geometric objects, which are finally transferred to the geometry viewer module.

A second module was written for the visualization and animation of transient hydraulic heads, recorded during the Multiple Source Crosshole Tests (see Chapter 5). It resembles the module for static data, but contains additional routines for the presentation of time-dependent heads. With a few modifications, it would be possible to present other time-dependent processes such as material or heat transport.

7.2 Spectrum of applications

In the following section, the different types of structural and hydrogeological data which can currently be visualized are classified. The data requirements and the process of 3D representation are described. Examples from the BK site are given and the sources of data used are specified. Finally the advantage of appropriate visualization is discussed.

7.2.1 Visualization of major structural objects

Visualization aids

Even in a perspective view, information on the third dimension is partly lost when 3D objects are displayed on screen or are printed. Hence, special visualization aids are of great assistance in emphasizing 3D geometric objects. For instance, introducing **auxiliary planes** allows the observer to recognize 3D structures which lie in a plane. This feature is especially useful for visualizing coplanar boreholes. Moreover, the directions of the coordinate system are indicated by an **imaginary cube** enclosing the investigation area. This cube enables front and back to be recognized more easily. All auxiliary planes should be drawn transparently to avoid obstructions of other information.

Geometry of the tunnel system

The geometric data of the tunnel system were taken over from previous studies (VOMVORIS & FRIEG 1992). The whole tunnel was digitized from a map and third-dimension information was added. The resulting finite element (FE) mesh was processed by FED (program for the visualization of FE data by Colenco PC), resulting in a geometric object for AVS. On the majority of the images presented below, only the small BK area is visible from the whole GTS model (total of 11000 triangles with information about normal directions).

The tunnel geometry is considered as a single object consisting of a large number of polygons. AVS is able to smooth the surface of the polyhedral objects so that, despite the rather coarse FE discretization of the BK site, an impression of curved surfaces is obtained. In Fig. 7.1 a plan view of the BK site is shown, including tunnels, caverns and the boreholes.

Geological structures/features

MARTEL and PETERSON (1991) developed a structural model of the BK area from extensive structural analyses (tunnel surface mapping, core inspection) and geo-

physical investigations (seismic crosshole tomography). Following their work, the BK area is divided into different hydrogeological features. Two extended lamprophyres delimit the investigation area. The two lamprophyres shown in Fig. 7.2 correspond to the features MP2 and MP4 of MARTEL and PETERSON (1991). A system of fractures striking from NW to SE represents the fracture zone MP1. The features were further divided into parts 1a, 1b(a), 1b(b), 1b(c), 2a and 2b according to their spatial position.

The positions of the two lamprophyres were deduced from traces at the tunnel surface and in the boreholes. The northern lamprophyre is about 5 m thick and is plainly visible in the main tunnel, in the boreholes BK 85.004, 85.008, 85.010 and deep down in GS 84.041A. The southern lamprophyre is relatively thin and is only observed in boreholes BK 86.002 and 86.003.

7.2.2 Visualization of structural data from boreholes

Location of boreholes and packers

The locations of the boreholes play a predominant role in the whole visualization concept. Most of the hydrogeological and structural information in the BK area was gained from core inspection and borehole measurements.

The location of a borehole is determined by the position of its mouth, its orientation and its length. For all boreholes at the GTS, the positions of the borehole mouths were surveyed in test site coordinates, which correspond to the coordinates of the triangulation mesh of the Swiss Federal Institute of Topography. The orientation of a borehole is specified by its azimuth and elevation angle. The data on the BK boreholes are summarized in BRÄUER et al. (1989) and PAHL et al. (1992). Nagra operates a databank with the relevant geometric data for all boreholes at the GTS.

In the 3D representation, boreholes can be marked using individual colours and labels. Selected parts of the boreholes may be emphasized by drawing an arbitrarily coloured cylinder of variable radius and length at the desired location. This feature is used, for example, for the representation of injection intervals or packer positions during hydrogeological experiments. In the scope of phase III of the BK project, this information was documented in full to ensure future utilization of the BK test data. Brief descriptions of the test arrangements, including the positions of packers for all hydrogeological tests, have been summarized by BLASER (1994).

Petrography of boreholes

Oriented cores were sampled for all boreholes at the BK site during drilling. During subsequent core inspection, the cores were classified into petrographical units as given in Tab. 7.1. Petrographic profiles for the BK boreholes are found in BRÄUER et al. (1989) and PAHL et al. (1992). In the present work, this information was digitized and visualized. An individual colour was selected for each petrographical unit, as demonstrated in Fig. 7.3a for the boreholes in plane D (see Fig. 1.1 and Fig. 1.2).

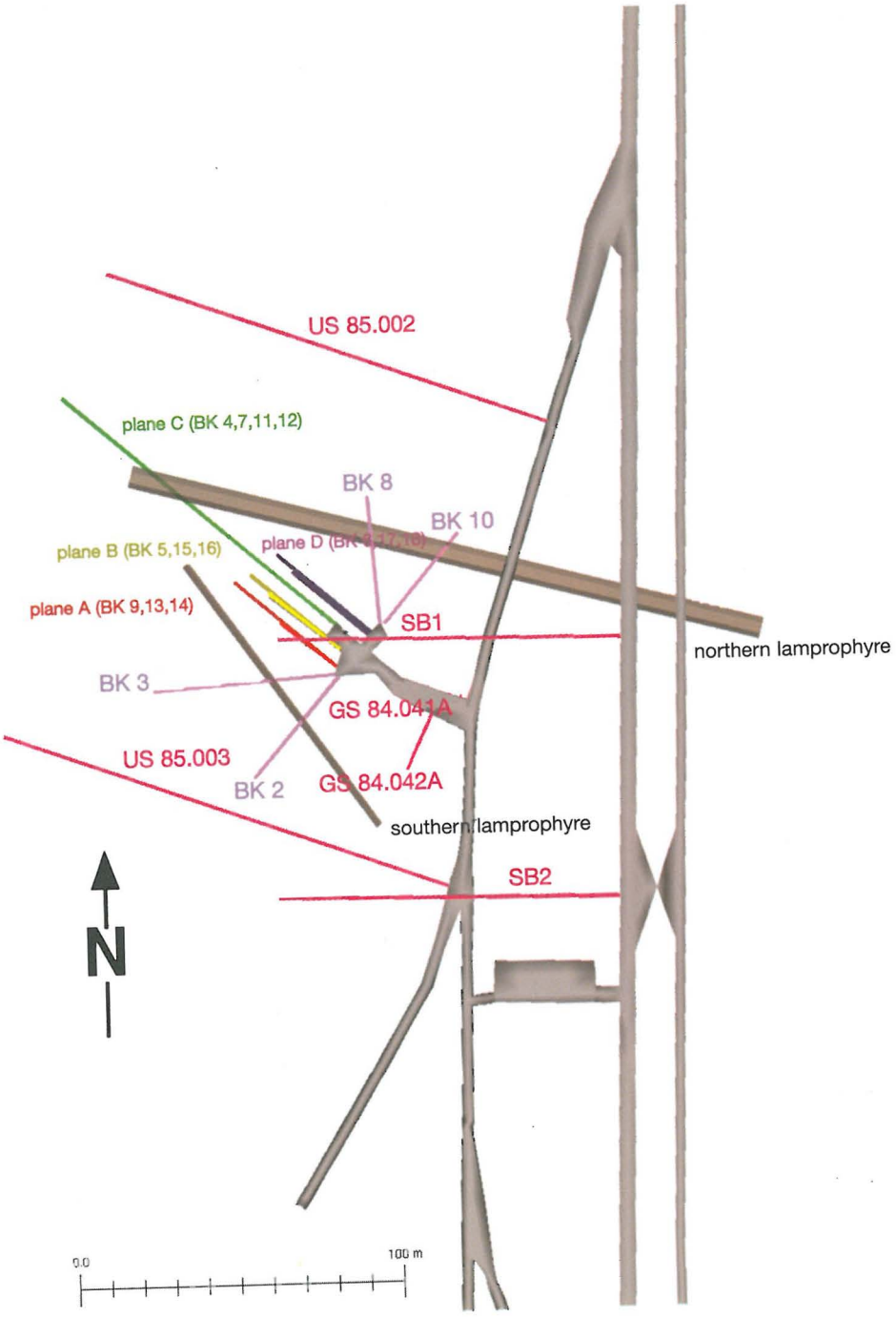

Fig. 7.1: Plan view of the BK site

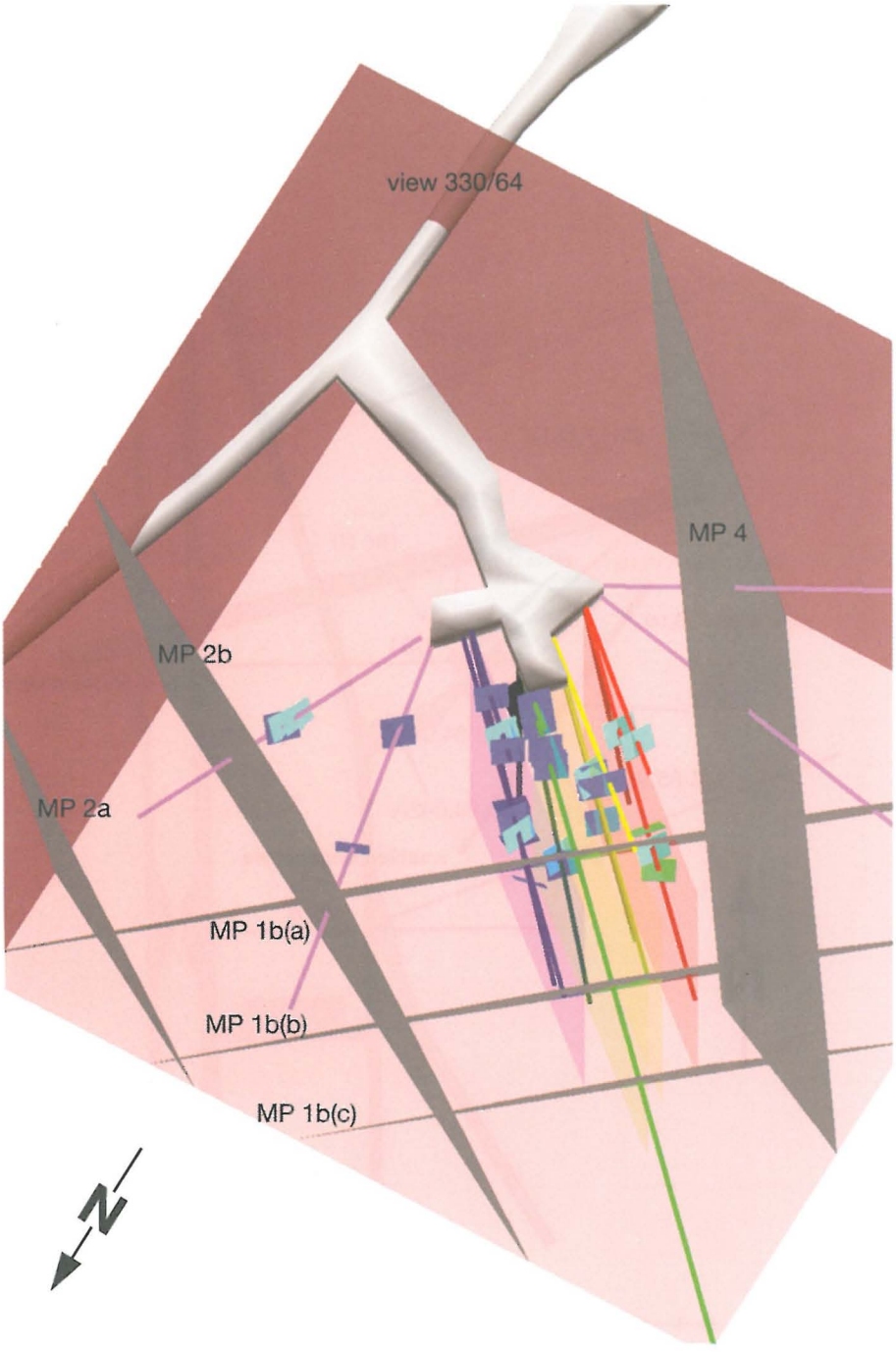

Fig. 7.2: Compilation of structural information at the BK site, out of previous characterization

Fractures along boreholes

An essential aspect of core inspection is fracture mapping. Fractures are structural discontinuities in the broadest sense. Depending on the type of displacement along them, two types can be distinguished: Faults are characterized by major shear deformation along the fracture and mostly contain cataclastic features. Joints, on the other hand, are extensional features characterized by a "pull-apart" movement normal to the discontinuity where little or no shear deformation has occurred. In the following, only the term "fracture" is used. A fracture is characterized by the distance to the top of the borehole and by its orientation (i.e. azimuth and angle of dip). In terms of hydrogeological relevance, fractures can be classified by orientation, water-conducting properties and fracture infill. At the BK site, the dominant orientations belong to the so-called S- and K-systems. Fractures are either open or closed, depending on their rock mechanical and hydrochemical evolution. A comprehensive overview of the structural geology and fracture visualization at the BK site is given in Section 7.3.2 (see also Fig. 7.6).

Tab. 7.1: Petrography of cores, sampled from boreholes at the BK site

Petrographical Unit	Remarks
Central Aare Granite	weak planar fabric
Lamprophyre (Kersantite, Spessartite)	amphibole minerals altered to biotite
Xenolites	basic inclusions, deformed
Zones of hydrothermal alteration	bleached zones, near extension fractures
Quartz-bands	related to ductile shear-zones, recrystallization during metamorphism
mylonitic ductile shear-zones	partly reactivated → fractures

7.2.3 Visualization of hydrogeological test data

Losses of drilling fluid

During the drilling process the boreholes freshwater was used as drilling fluid. When intersecting permeable fractures, some of this water was lost due to penetration into the fractures. For some of the BK boreholes, the amount of water loss was recorded and was documented together with the geological profiles (BRÄUER et al. 1989, PAHL et al. 1992). This is a qualitative measure for the hydraulic transmissivity of the corresponding fracture.

To visualize these data with AVS, the profiles of fluid losses were digitized by hand and brought into tabular form. The table of water losses was then converted into a scale of brightness which can be displayed on the screen (or any other graphical unit) to locate the transmissive zones along the boreholes. In Fig. 7.3b the fluid losses are shown for borehole BoBK6. The light zones represent zones of high fluid losses and are therefore highly transmissive areas. A brightness scale assigns absolute values for water losses to each zone. No data are available for BK 88.018 and 88.017.

Fluid logging

Fluid logging is another powerful method for the detection of hydraulically active fractures or fracture zones. At the BK site, crosshole fluid logging measurements were performed by injecting brine water into borehole BK 85.004 and, afterwards by recording temperature/salinity profiles in boreholes BK 85.005, 85.006, 85.007, 85.008, 85.009, 88.015 and 88.017. The results are described in VOMVORIS & FRIEG (1991). Furthermore, single-hole fluid logging measurements were performed in BK 85.004, 88.014, 88.016 and 88.018 (see Chapter 2).

Inflow locations to a borehole can be visualized by plotting a small slice perpendicular to the borehole axis at the detected inflow point. In some cases, the analysis of fluid logging data does not give a clear indication of inflow points. This uncertainty is accounted for by distinguishing between "inflow" and "possible inflow" locations. Graphically, the difference in data quality is represented by assigning different colours to the slices which mark the inflow points. In Fig. 7.3b, the result of the fluid logging analysis is shown for the boreholes in plane D. The red slices represent the inflow points which have been identified clearly, whereas the green slices indicate possible inflow zones. It should be mentioned that there is a fairly good agreement between the fluid logging results and the losses of drilling fluid in borehole BK 85.006.

a)

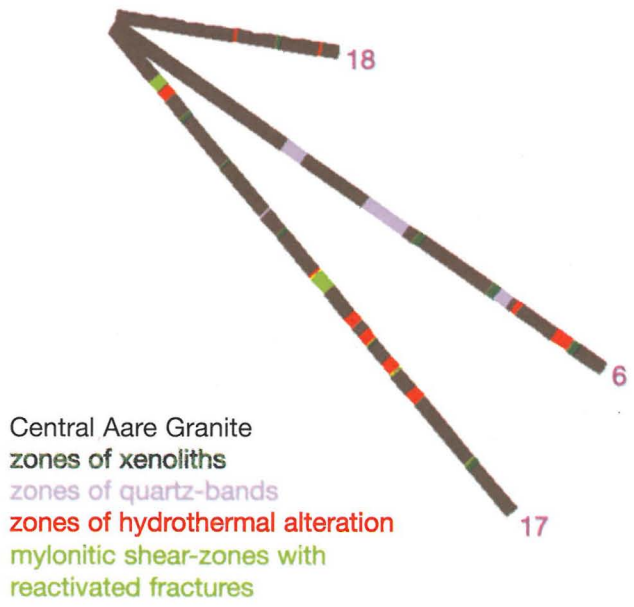

Fig. 7.3: Examples of AVS visualization in BK plane D
a) petrographic data

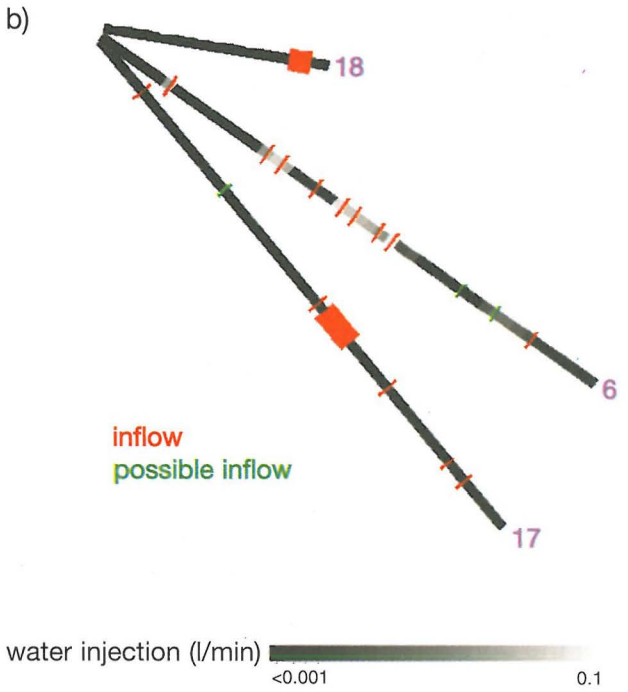

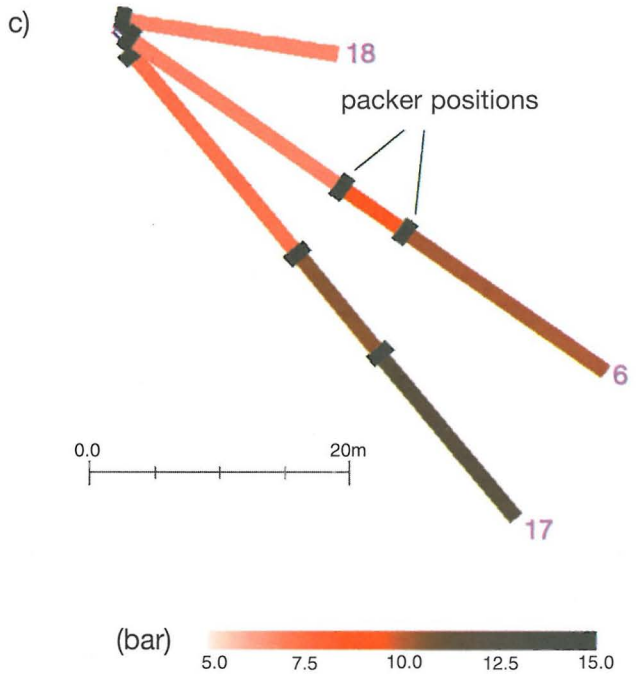

Fig. 7.3: Examples of AVS visualization in BK plane D
b) inflow locations along boreholes, c) pressure build-up and packer positions

Long-term pressure monitoring

Depending on the boundary conditions, the quasi-steady-state (i.e. stabilized) hydraulic head distribution after a pressure recovery period may provide useful hints on the hydraulic connectivity within a fracture network. Particularly in the vicinity of the tunnel, which drains the fracture network, the spatial distribution of stabilized heads is dominated by the orientation of the major fractures. Consequently, knowledge of the head distribution may lead to the identification of hydraulically active fractures.

During test VE 478, the BK boreholes, which were equipped with single- and multi-packer systems, were closed for a period of more than two months (see Chapter 4). Although the heads were not yet completely stable after this period, the spatial distribution of the heads reflects the quasi-steady-state conditions fairly well.

Similarly to the representation of the drilling fluid losses, the head distribution is visualized by converting the measured head values into a scale of brightness or, alternatively, into a rainbow spectrum. The measured heads are assigned to the entire length of the packed-off borehole intervals; each interval is therefore coloured individually corresponding to the measured head. The intervals are separated by short, black cylinders which represent the packers. In Fig. 7.3c, the head distribution at the end of test VE 478 is shown for the boreholes in plane D.

Dynamic processes

AVS provides special animation facilities for visualizing dynamic processes. Within the context of hydrogeological investigations, the propagation of hydraulic disturbances and transport processes are of particular interest. The emphasis of the present studies was the animation of dynamic heads recorded during previous crosshole hydrotests at the BK site. For this purpose, the AVS visualization modules described above had to be slightly modified. The new tool consists of two submodules; the first plots all static objects and the second superimposes the time-dependent information.

A discrete timescale has to be introduced as an additional input parameter. After every time step, the program interpolates between the next two time steps and repaints the picture. The input values need not be structured. This has the advantage that outliers may be eliminated. Time values may be supplied by an AVS standard module, which generates a series of increasing numbers.

The velocity of the sequence of figures is proportional to the computer speed. The desired speed for an animated impression can only be achieved by hardware support. Currently, the AVS module still has some problems with the compatibility of several hardware graphics devices (Sun GS, Titan, Denali).

7.3 Derivation of the conceptual model by 3D visualization

In this section a strategy is outlined to develop conceptual models of flow in fractured rock by a joint interpretation of structural and hydrogeological data. Two different approaches can be followed the fracture network approach or fracture zone approach. In fracture network models, the complex systems of fractures are simulated by their statistical properties (fracture orientation, fracture frequency, fracture extension etc.) and, eventually, by deterministically given major fractures. In fracture zone models,

the multitude of structural and hydrogeological data is comprised and condensed, such that the systems of fractures are represented adequately by a surveyable number of fracture zones with deterministically assigned geometrical and hydraulic properties. In the present investigations, the fracture zone modeling approach was chosen, using the extensive database, collected during the BK project. This is because the fractures at the BK site are not distributed randomly, but they can be assigned to different fracture systems (S- and K-systems). Another reason for the choice of the fracture zone approach is, that less effort is needed to implement it as a numerical model.

3D visualization plays a predominant role in this concept, because it offers a flexible and illustrative means of presenting geometric, structural and hydrogeological data / parameters which are distributed spatially. For the development of a conceptual hydrogeological model, which qualitatively describes all relevant properties of the system, the extensive information "flood" has to be reduced by eliminating less critical data. This can be done by hand, which is always somewhat subjective and very time-consuming. A more reliable method is to analyse the different types of structural and hydraulic data with a visualization tool and then to synthesize (i.e. combine and integrate) the information. The basic procedure for performing this is presented in Section 7.3.1.

The conceptualization approach is then applied to the BK site where an extensive database made up of geological structures (Section 7.3.2) and the results of hydrogeological testing (Section 7.3.3) has been elaborated. These two sources of information are combined in such a way that they characterize the BK system without major contradictions. When uncertainties remain, different hypotheses can be proposed which account for the different investigation methods. The result is one or more conceptual models (Section 7.3.4), the likelihood of which can be tested during the numerical modeling process.

7.3.1 Basic derivation procedure for a discrete fracture zone model

The derived conceptual model, should provide the basis for modeling activities with the following objectives:

- development of a 3D numerical groundwater for the BK site flow model
- calibration of this flow model with in-situ hydrogeological test data

The derivation procedure for the conceptual model is shown schematically in Tab. 7.2. It is important to note that this procedure is valid for the objectives mentioned above. Another objective (e.g. transport modeling) would result in a modified procedure. As can be seen in the table, the procedure is divided into four steps, starting with the compilation of the requirements for structural geology and hydrogeological test sources, followed by the corresponding exploration methods and characterization/interpretation. At the end, the two information sources are synthesized, which results in the final conceptual model. The four steps are now described in more detail.

Data required

The data required (Tab. 7.2) consist on one hand of the geometry of the model domain and structural/petrological data required to characterize the geometric network of fractures and on the other hand of different types of hydrogeological tests to obtain information on the hydraulically connected network. These hydrogeological tests also serve to define a dataset on the hydraulic behaviour of the system for model calibration.

Exploration methods

After having defined the requirements, appropriate methods have to be chosen for obtaining these data. There are different field and laboratory tools mentioned in Tab. 7.2 for collecting the structural information. This is done on different scales: fracture mapping on the km-scale at the surface at one extreme (MARTEL & PETERSON 1991) and definition of porespace on the mm-scale at the other extreme (BOSSART & MAZUREK 1991). On the hydrogeological side there is a variety of tests, some of which were developed and improved in the BK area.

As mentioned above these exploration methods are applied on different scales. Mainly three scales are used, which are indicated in Tab. 7.2 and defined as follows:

- **regional scale:** this scale is in the order of one to several km^3; the underground cavern is included and the major faults and thrusts are identified.

- **local scale:** this scale is in the order of 1,000 to several 10,000 m^3 and includes the specific test site. Fracture mapping at the tunnel surface is performed on this scale.

- **subscale:** this scale is in the order of several dm^3 to 100 m^3 and reflects the vicinity of a borehole. Most of the hydrogeological tests are confined to this scale.

Characterization/interpretation

The most important step follows after consolidating the structural and hydrogeological databases. The structural information serves to identify and locate the main fractures and to establish rules for how fractures are structurally organized within the model domain. Together with the characterization of the porespace geometry (which are the relevant pores where water flows, i.e. grain boundary pores in the matrix, type of infill in the fractures), a geological-structural model of the domain is established.

The hydrogeological database, which basically consists of the results of hydrotests and longterm monitoring of heads and discharge into the tunnel, is now used for model identification. Model identification is defined as selection of the appropriate well-aquifer flow model(s): on one hand the hydraulically connected fracture systems are identified, on the other hand the boundary conditions are addressed. Diagnostic plots, which are compiled out of the test measurements, give information about flow type (e.g. radial or spherical flow in a porous continuum or a double-porosity flow system), and about boundaries (infinite aquifer or limitation by a hydraulic boundary). Such model identification is the basis for the parameter estimation, which is done via analytical and numerical analyses (see Chapters 4 and 5).

Tab. 7.2: The deriviation procedure of the conceptual flow model (VIS = visualization recommended)

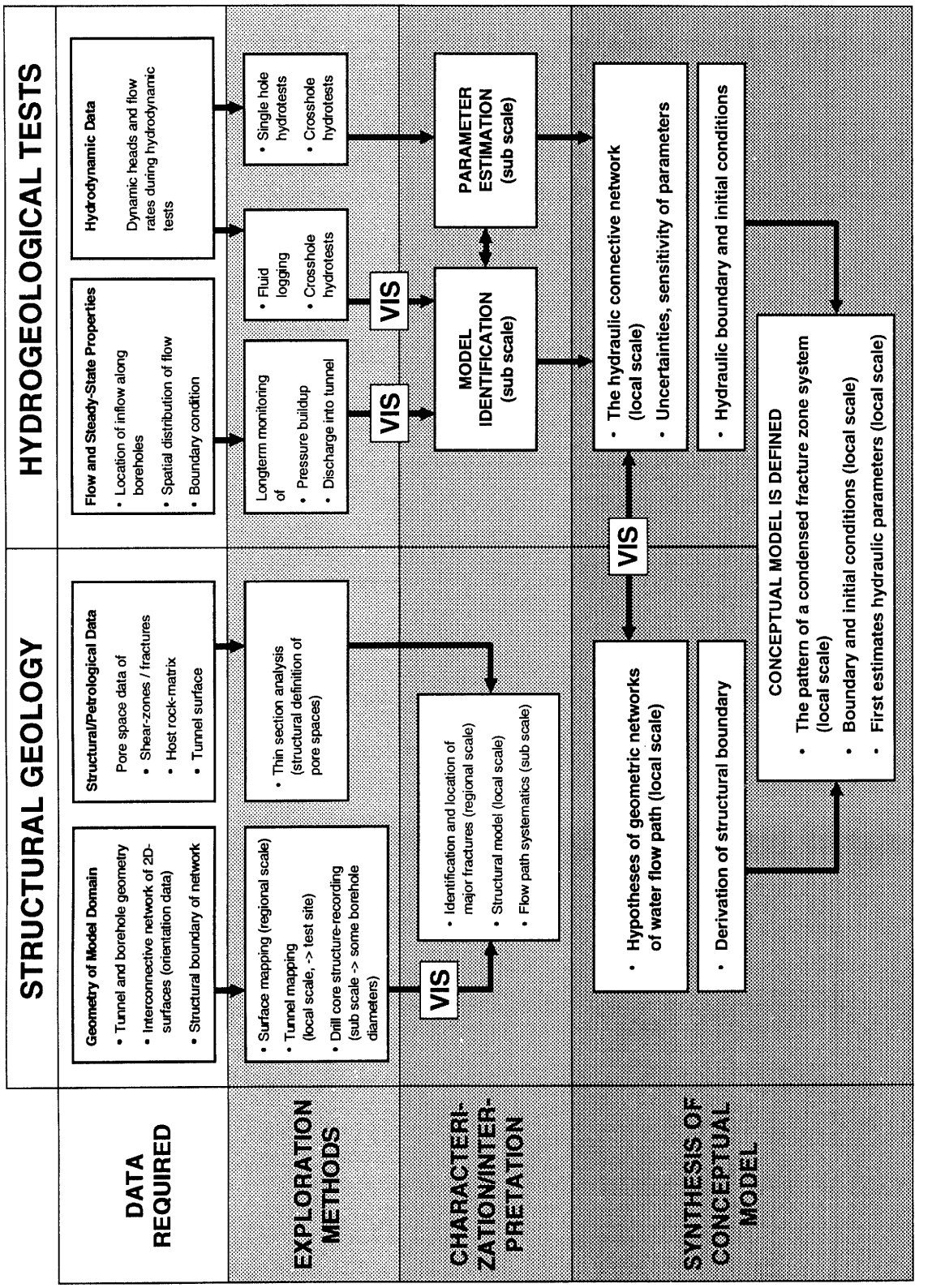

Model identification and parameter estimation are done mainly on the subscale at different locations along the boreholes. This then represents the hydrogeological basis for the synthesis of the conceptual model.

Synthesis of the conceptual model

Conceptualization starts with combining the structural systems of fractures and the systems of hydraulically connected fractures. In this step the normally quite complicated geometric fracture systems are reduced by selecting only those fractures or fracture zones, respectively, which are hydraulically linked and active. This procedure results in a condensed model, consisting of those fractures and fracture zones, which are expected to provide a major contribution to the flow system.

The boundary conditions are obtained in a different way: when a hydraulic boundary is found by model identification, its structural manifestation has to be confirmed or denied. A good example where a hydraulic boundary coincides with a structural boundary is presented at the BK site (Section 7.3.4). Initial conditions are determined from steady-state conditions at the investigation site, normally by the interpretation of pressure build-up tests and discharge measurements into the underground cavern.

First estimates of the hydraulic parameters on a local scale are gained by averaging the test results from the hydraulic tests. Hydraulic parameters required for the conceptual model are transmissivities, storativities and parameter uncertainties. Sensitivity analyses are often performed to obtain the maximum error of the parameters (GUYONNET & LAVANCHY 1992). In general confidence in hydraulic parameters can be improved when the flow path is well-known.

Visualization plays an important role in the characterization and interpretation step. Here the whole flood of numerical data is inspected visually. In Sections 7.1 and 7.2 it was shown that different layers of graphic information are analysed on the screen.

Perhaps the best application of AVS is during the synthesis of the conceptual model: hydraulically active fractures are superimposed graphically onto the structural network. Then, only those structural orientations, which are also hydraulically linked are selected.

In the next sections, the derivation of the conceptual model is applied to Nagra`s Grimsel Test Site (GTS), at the BK site (for location see Fig. 1.1 and 1.2).

7.3.2 Structural geology

Introduction

In crystalline basement rocks such as the Aare Massif, ductile mylonitic shear-zones commonly occur in two sets with opposite shear sense. Such an array of two sets of ductile shear-zones is called a conjugate shear-zone system. At the GTS, these two sets are termed S zones (shear-zones striking WSW-ENE, with counterclockwise shear sense) and K zones (shear-zones striking NW-SE, with clockwise shear sense). Fig. 7.4 shows the formation of such a conjugate shear-zone system, from an undeformed to a deformed state.

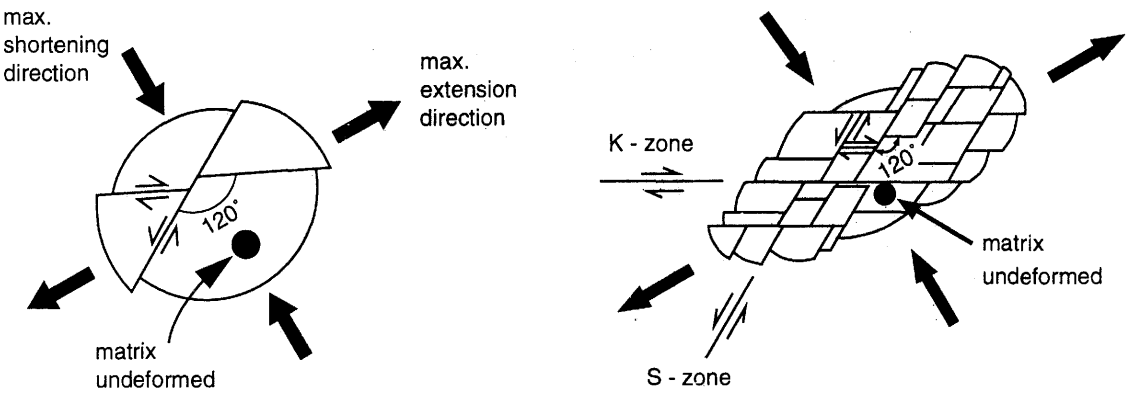

Fig. 7.4: The formation of ductile conjugate shear-zones. a) undeformed state, b) deformed state. The matrix (part inbetween the shear-zones) always remains undeformed

In ductile shear-zones, the density of brittle fractures is significantly increased. This observation is interpreted in terms of the significant mechanical competence contrast between the granitic matrix and the mylonites. The mechanically weak mylonite may act as a focal point for subsequent brittle deformation and brittle deformation associated with regional uplift was thus preferentially accommodated in the mylonitic shear-zones. This fracture system, which has the same geometry as the ductile shear-zones, is now identified as the relevant water flow path network.

Database for the structural fracture systems

In Tab. 7.2 the requirements concerning the objective of the modeling are presented. These are the geometry of the model domain (the construction of a fracture network and its boundary) and structural petrological data for characterizing the flow path in the fractures and matrix. The information is compiled out of geological and structural information and is independent of the hydrotests.

Exploration methods

Previously published reports on the geology at the BK site were collected, reviewed and quality-controlled. Information concerning regional mapping at ground surface, local mapping in the laboratory at the BK cavern, structural analyses of drillcores, fracture and fault zone systematics and the nature of the flow path in the structural elements was compiled from these reports. The information sources used in the present approach are presented briefly below:

- GEOTEST AG 1981 (Sondierbohrungen Juchlistock Grimsel)
  Structural analyses of fractures in boreholes, drilled from the main access tunnel into the area of the future rock laboratory. Identification of major geological structures at the surface: S and K zones, lamprophyres etc.
- NAGRA et al. 1985 (Grimsel Test Site: Overview and Test Programs)
  This report was published after construction of the rock laboratory and contains a geological map of the US/BK site; the major shear-zones around the BK site are identified.

- KEUSEN et al. 1989 (Felslabor Grimsel: Geologie)
  This report summarizes the geological investigations in the rock laboratory conducted between 1980 and 1987. Fracture systematics (different systems of ductile shear-zones and brittle fracture systems) and a 3D structural model of the Juchlistock area (combination of surface and tunnel mapping) are the main topics in this report.
- BRÄUER et al. 1989 (Ingenieurgeologische Untersuchungen zur Interpretation von Gebirgsspannungsmessungen und Durchströmungsversuchen)
  In this report detailed fracture maps of the BK cavern surface are published. Drill-core mapping and profiling of different boreholes (Bohrlochkranz) drilled from the BK tunnel into the highly transmissive S zones are also presented.
- LIEDTKE et al. 1989b (Bohrlochkranzversuch, Anlage 26, "Bräuer Daten")
  The water-conducting zones identified during drilling of the BK boreholes (water losses) are related to the fractures in the drillcores. This document summarizes the orientations and locations of these water-conducting structures, which are also visualized in Fig. 7.2.
- PAHL et al. 1992 (Bohrlochkranzversuch, Durchströmung von geklüftetem Fels)
  Besides hydrogeological testing and modeling work, the rest of the BK drilling campaign (drillcore mapping and profiling) is published in this report.
- BOSSART & MAZUREK 1991 (Structural Geology and Water Flow-Paths in the Migration Shear-Zone)
  In this report the water flow path in and around a brittle reactivated shear-zone is characterized. Special resin injection methods were applied to make the flow path visible. The results obtained are also valid in the S zones of the BK site.
- MARTEL & PETERSON 1991 (Interdisciplinary Characterization of Fracture Systems at the US/BK Site, Grimsel Laboratory, Switzerland)
  In this paper geological and geophysical-tomography information on the BK site is combined in order to provide a structural model for hydrological modeling. The structures in this model are termed "MP-features" (see Fig. 7.2).

Quality control was mainly done by selectively re-examining the orientation of structures in the drillcores and comparing them with orientation data published in the reports. Some of the cores which had already been stored for 10 years were still in such good condition that microscopic inspection of the porespace fractures was possible. The details of reinspection of cores are included in BOSSART et al. (1993). It was concluded, that:

- the fracture dips of the BRÄUER dataset (LIEDTKE et al. 1989b) and the MP model seem to be too flat (range of 40-80°). Practically all fractures dip subvertically between 80 and 90°. This is the reason why the spatial arrangement of the fracture network in our structural model is modified.
- a conjugate ductile shear-zone model with S- and K-directions (Fig. 7.4), which has undergone brittle reactivation, best accounts for the fracture pattern found in the boreholes. Therefore it does not make sense to categorize the fractures into three ductile (S1, S2 and S3) and 6 brittle zones, as is done in several publications.

Characterization/interpretation

The identification and location of the major fracture zones and fractures, respectively, was performed from a regional scale (surroundings of Grimsel laboratory) to a local scale (BK site). On all scales it was found that NE-SW-striking S fractures and NW-SE-striking K fractures define the structural network. It should be noted that the S-directions at the BK site are more pronounced than the K-directions due to the fact that the orientation of most of the boreholes is more or less parallel to the strike of the K zones. Nevertheless well-defined K fractures (fault zones) have been identified by interpreting the fracture map of the BK drift.

Fig. 7.5 shows the S and K fracture system derived by core reinspection (the network has been projected onto the 1730 m asl plane). The revised structural model of the BK area differs from the MP model which is shown in Fig. 7.2 in that the highly transmissive fracture zones in this model strike closer to the BK tunnel than in the MP model. Included in this presentation are "open" S fractures, where the fracture infill material (fault gouge) has been mainly washed out, and "closed" S fractures where the infill is still more or less in place. Locations of high fracture densities are composed to fracture zones. This structural model agrees with the theory of a ductile shear-zone network.

The visualization with AVS clearly showed that there is little point in plotting the total amount of fractures in a 3D perspective view when fractures are clustered and/or hide each other. A much better result was achieved when plotting fractures intersecting with vertical planes containing the individual BK boreholes. As an example, Fig. 7.6 shows the intersection of S and K fractures in plane D containing boreholes BK 88.018, 85.006, and 85.017. With the assumption that fractures are planar on this scale, the structurally linked fractures of the corresponding boreholes could be selected (red S fractures in Fig. 7.6, which are comprised to one L-feature crossing all boreholes as a straight line). This procedure has also been performed in planes A, B and C.

The next step, the synthesis of the geometric network with the hydraulic network and the formulation of the conceptual model, is discussed in Chapter 7.3.4.

7.3.3 Hydrogeological tests

Database required

The hydrogeological database, required to build a conceptual model of the fracture flow system includes:

- the spatial distribution of the steady-state heads
- the detection and quantification of inflow locations along boreholes and tunnels
- dynamic head and flow data derived from hydrodynamic tests

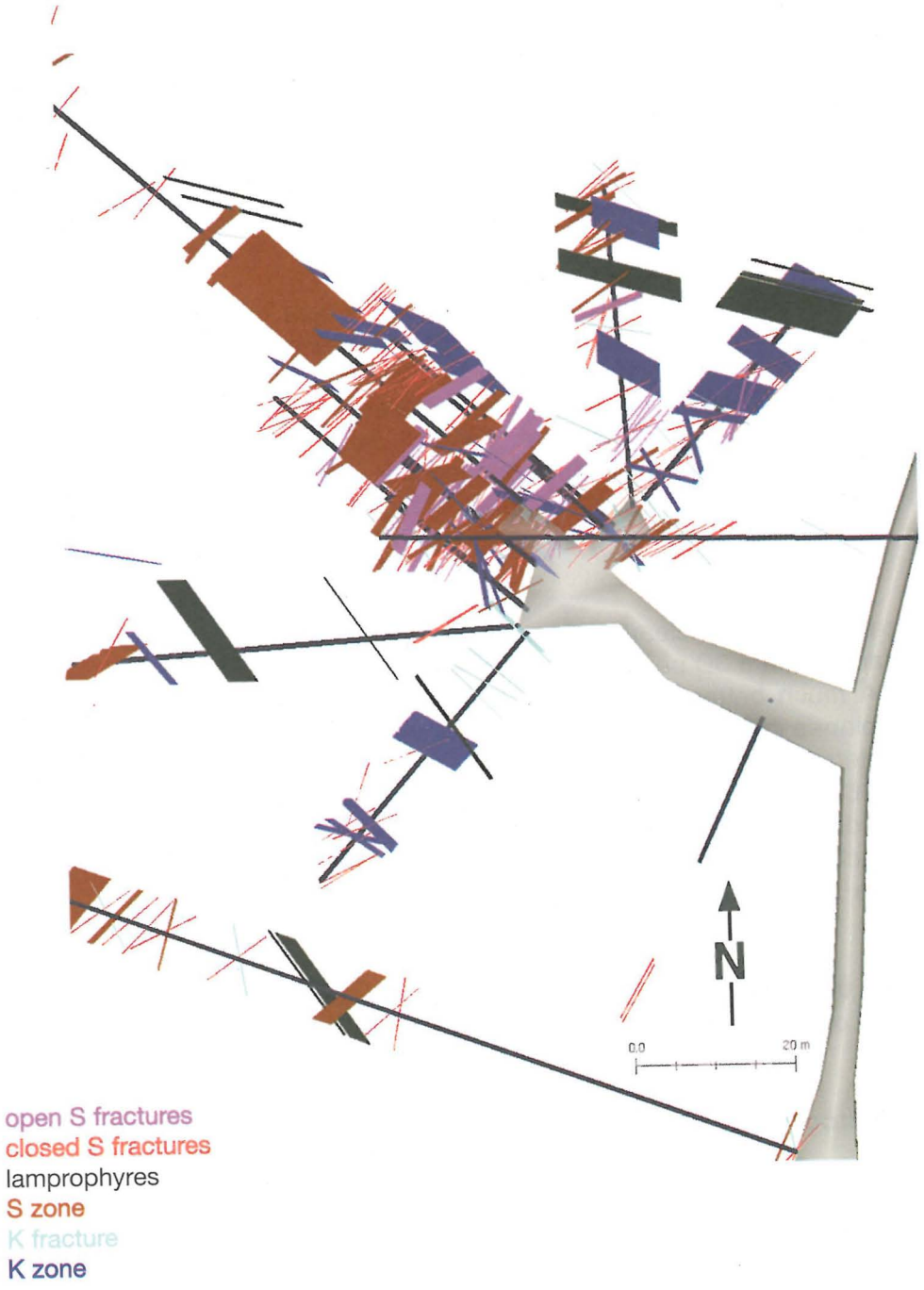

Fig. 7.5: The structural fracture network

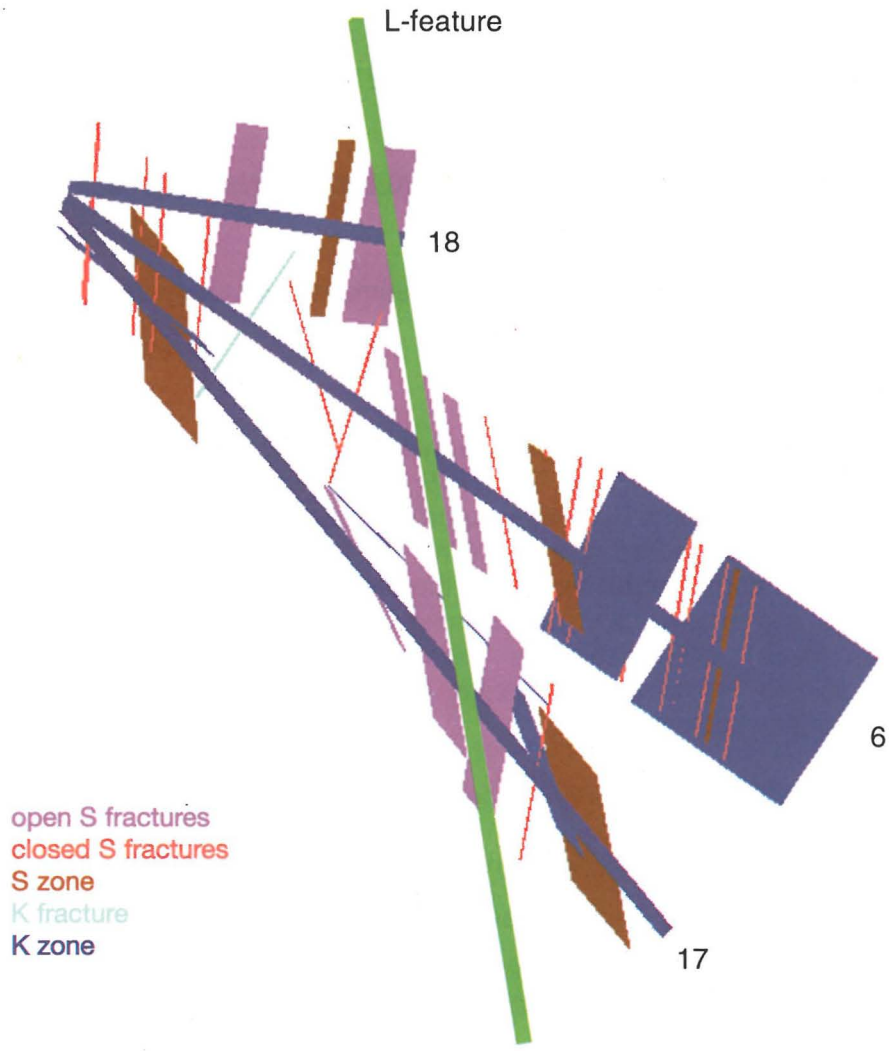

Fig. 7.6: S and K fractures of the structural model in plane D; L is the resulting fracture plane, which links the three boreholes

Exploration methods

Previously numerous different hydrogeological tests were performed to characterize fracture flow at the BK site. The sources used in the present approach are given below:

- single and crosshole fluid logging (KELLEY & LÖW 1992, see also Chapter 2 in this report)
- single and crosshole hydrotests (GUYONNET & LAVANCHY 1992, see also Chapter 4 in this report)
- Multiple Source Crosshole Tests (MARSCHALL & JOHNS 1993, see also Chapter 5 in this report)
- direct measurements of pressure build-up (estimation of steady-state pressure) and water inflow (discharge) into the tunnel.

Characterization/interpretation

Methods for analysing single and crosshole hydrotests which have been developed by MISHRA (1992) and MARSCHALL & JOHNS (1993) were implemented in this step. Both methods are based on a diagnostic approach used to identify the flow model/flow dimension which is best suited to interpreting the test data. Thus, for instance finite skins or linear boundaries in the vicinity of the tested borehole can be detected. The selection of the appropriate flow model using diagnostic plots is the task of model identification. Model identification is then the basis for estimating hydraulic parameters. In the following the results of model identification and parameter estimation are briefly outlined:

Diagnostic plot analyses of single and crosshole tests suggest that:

- The lamprophyres act as no-flow boundaries
- The BK system is probably unconfined (free surface)
- Flow occurs predominantly along individual fractures and fracture zones. There is no indication of a contribution from the matrix.

The results of the parameter estimation are:

- Transmissivities from single-hole and crosshole tests yielded values which range between about 5.0E-7 and 5.0E-5 m^2/s for the area located between the lamprophyres.
- Storativities range between 1E-6 and 1E-3. There is quite a high uncertainty in these parameters.
- Stabilized heads (in the central BK area) range between 86 and 92 m above the 1730 m asl elevation of the drift surface.

7.3.4 The derivation of the deterministic fracture zone model

Basic hypotheses

Due to the fact that most of the BK boreholes cut the S fractures perpendicularly and the K fractures obliquely, the S fractures are predominant and many of the K fractures seem to vanish. This fact is clearly seen in Fig. 7.5. This uncertainty is accounted for by assuming different hypotheses for the structural network (Tab. 7.3).

Hypothesis 1: The geometrical structure of the model is defined by the deterministic fracture network shown in Fig. 7.5.

Hypothesis 2: The geometrical structure is that of hypothesis 1 but combined with additional K fractures. The individual fracture systems are stochastically generated (out of means, deviations and correlation lengths of measured S- and K-orientations).

Hypothesis 3: The geometrical structure of the model is given by a limited number of fractures and fracture zones, which are gained by comprising individual fractures of the structural network and by weighting them with the major fluid logging locations.This results in a condensed fracture zone model.

Although there is uncertainty as to discrete orientations and frequencies of K fractures (hypotheses 1 and 2), their existence in the BK area is clearly confirmed on one hand by the structural fracture map of the BK drift and on the other hand by the crosshole hydrotests. These tests have shown that the pressure response in the observation boreholes can only be explained by the existence of K zones connecting the S zones.

The fracture pattern of a condensed fracture zone model

A simple geometry for the structural model can greatly reduce the mesh construction during numerical modeling. This is one of the reasons why hypothesis 3 is introduced: only those fractures, which have been identified as hydraulically active are selected from the structural model. This selection procedure is done by combining the fluid logging data with the structural model of Fig. 7.5. The procedure, which is split into five steps, is now explained in more detail:

1. Localizing the fluid logging inflows along the observation boreholes. This is done visually in the vertical planes A, B, C and D containing the BK boreholes. An example is shown in Fig. 7.7a, where plane D is shown.
2. Combining the inflow locations with the fracture systems of the structural model. This is also done in the four vertical planes. In Fig. 7.7b, only the vertical plane D is shown.
3. Selection of only those structural orientation data for fractures which correspond to one or more inflow locations. This is done in the vertical planes A-D. The orientation data of this network are given in Tab. 7.4.

4. Expanding the 2D networks (fracture networks in the four vertical planes) to a 3D network. This is done by connecting the four vertical planes with horizontal cuts and selecting those fracture orientations which satisfy all the fluid logging locations.

5. Comprising those hydraulic active fractures, which are more or less coplanar and located close to each other to a major fracture or to a fracture zone. This then results in a condensed fracture zone model (hypothesis 3).

Tab. 7.3: The BK conceptual models (Abbreviations: p = pressure, T = transmissivity, S = storativity, K = Hydraulic conductivity, S_S = Specific storativity)

Model hypotheses →	**1 deterministic fracture network**	**2 stochastic fracture network**	**3 condensed fracture zone system**
Model Structure	• 250 S fractures deterministic orientation • 30 K fractures deterministic orientation • fracture zones limited only by structural boundaries (lamprophyre dikes)	• 250 S fractures stochastically generated • 250 K fractures stochastically generated • S zones limited by boundary K fractures of variable expansion	• 7 S fractures (Fig. 7.8) • 1 S zone • 4 K fractures (Fig. 7.8) • limited model extension inbetween planes A, B, C and D
	Matrix: (3D blocks) • filling up the space inbetween fracture network	• same as hypothesis 1	• same as hypothesis 1
Boundary Condition	• no flow along lamprophyres • prescribed head at outer boundary • p = 0 prescribed discharge at tunnel surface • Prescribed head/discharge at injection borehole free surface	• same as hypothesis 1	• same as hypothesis 1
Initial Condition	• steady-state heads field (closed boreholes)	• same as hypothesis 1	• same as hypothesis 1
First estimates of Hydraulic Parameters	**S and K Fractures:** **S:** T = 5E-6 m^2/s S = 1E-5 **K:** T = 5E-7 m^2/s S = 1E-5 **Matrix:** K = 1E-9 m/s S_S < 1E-5 1/m **Lamprophyre:** K = 1E-10 m/s S_S < 1E-5 1/m	• same as hypothesis 1	**S and K Fractures:** **S:** T = 5E-6 m^2/s S = 1E-5 **K:** T = 5E-7 m^2/s S = 1E-5 **Highly transmissive S zone** T = 5E-5 m^2/s S = 1E-5
Comments	• fracture network of Fig. 7.5 all fractures/fracture zones are considered		• closely clustered fractures are reduced to one highly transmissive fracture
	• rock matrix considered as low permeable continuum	• same as hypothesis 1	• rock matrix can be considered as impermeable; flow occurs mainly in the fractures

This final fracture zone model includes 7 S fractures, 1 S fracture zone and 4 K fractures. Its horizontal cut with the 1730 m level is shown in Fig. 7.8. Most of the S fractures are oriented subparallel. The fracture zone at ca. 10 m distance from the westernmost gallery of the BK drift, which consists of a couple of individual S fractures, is a highly transmissive feature and dominates the hydraulic behaviour of the BK flow system.

Boundary and inital conditions

The northern and southern lamprophyre dykes define the structural boundaries of the BK region (Fig. 7.1, 7.2 and 7.5). Inspection and structural mapping at surface sites also shows that the ductile shear-zones often cut the lamprophyres and not vice versa. Therefore the lamprophyres may reflect a boundary with many shear-zone and also fracture intersections. This fact is also confirmed by the single-hole hydrotests, where permeability variations of several orders of magnitude along the boundary support the quite heterogeneous character of these lamprophyres. Nevertheless, the permeability of the lamprophyres seems to be at least one or two orders of magnitude lower than in the central BK area (see Tab. 5.7, Tests VE 510 and VE 511).

Although there might be flow across the lamprophyres from a geological viewpoint, the hydrotests and the longterm monitoring of hydraulic heads (see Chapter 4) gave a clear indication that these two boundaries at the southern and northern ends of the model domain are completely decoupled and quite tight. Therefore no-flow boundaries along the lamprophyres seem to be justified (see Tab. 7.3).

The constant slope of the pressure build-up data during the longterm monitoring of hydraulic heads indicates that a free surface at the top of the model domain better accounts for the system behaviour. Finally, prescribed heads (or measured discharges if available) should be introduced at the BK drift surface.

For transient flow simulations, initial conditions are needed. It is suggested to use a steady-state head field in the model domain where all BK boreholes are closed. The pressure sink induced by the BK tunnel could be superimposed.

Parameter estimation

For the numerical modeling, first estimates of flow parameters are needed. These first estimates are taken from the model identification and the subsequent parameter estimation on the local scale and include transmissivity and hydraulic conductivity of the fractures and matrix blocks respectively. The numerical modeling also treats transient simulations, so the fracture storativity and the matrix specific storativity have to be estimated. If early-time responses are considered, the coefficient of wellbore storage also has to be estimated.

In a first approach, the granitic matrix can be considered as impermeable. Therefore only the S and K fracture transmissivities and storativities are used. In general the S fractures are more transmissive (especially the highly transmissive zone in Fig. 7.8) than the K fractures. In Tab. 7.3, first estimates of some selected parameters are presented. These parameters were mainly derived by analysis of the crosshole injection tests (MISHRA 1992, GUYONNET & LAVANCHY 1992, GUYONNET & MARSCHALL 1993).

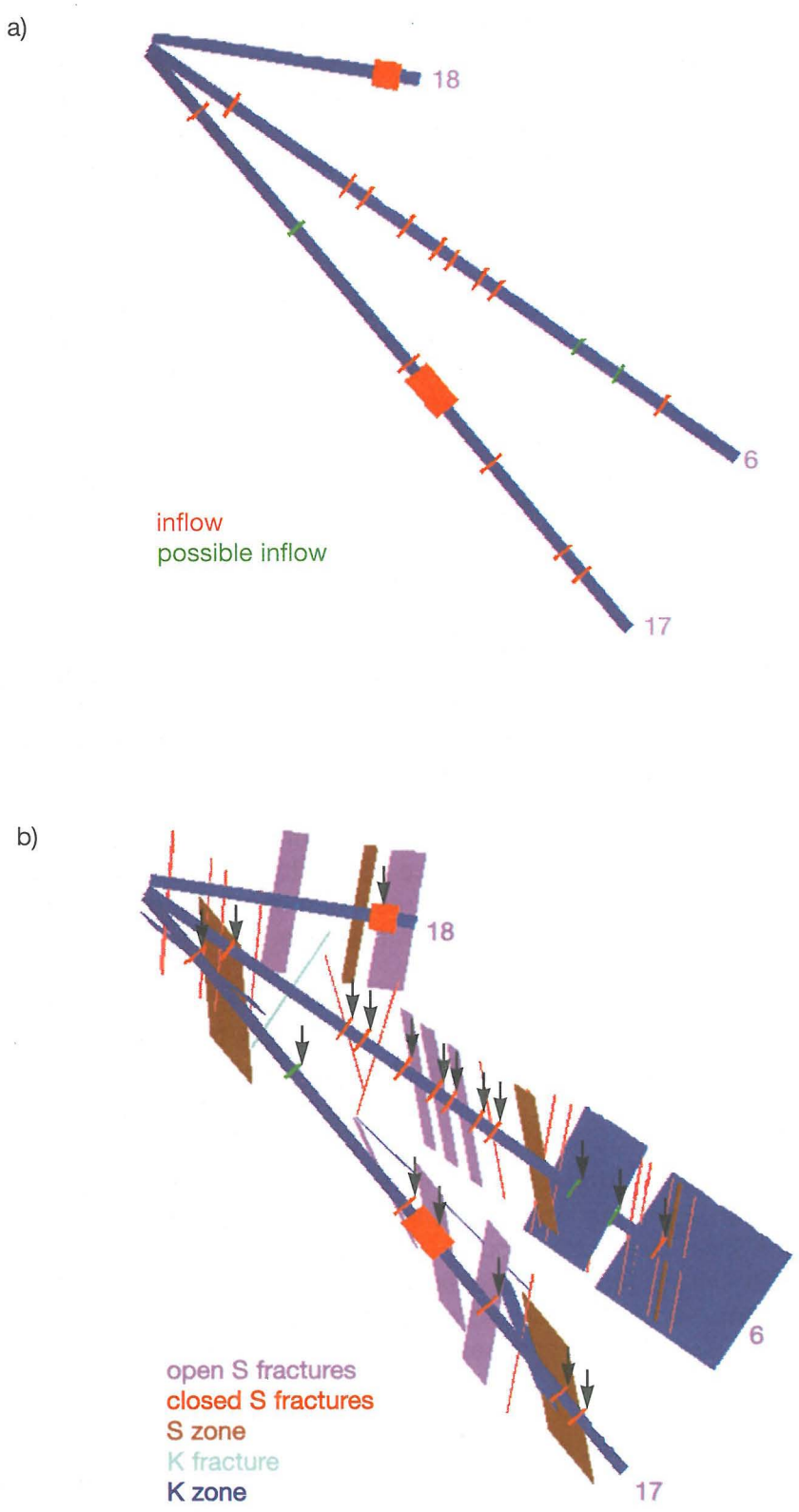

Fig. 7.7: AVS visualization in BK plane D
a) inflow locations, b) structural model combined with inflow locations

Tab. 7.4: Traced inflows along observation boreholes. Injection borehole is BK 85.004 (6.7 - 107 m). ? = the traced inflow could not be linked with any structure (K, S)

Borehole	Structure	Depth [m]	Azimuth of Dip / Angle of Dip
BK 85.004	S	8.0	340/85
	S	32.0	140/80
	S	34.0	140/80
	S	39.0	140/80
	S	44.0	140/80
	S	49.2	140/80
	K	57.0	190/85
BK 85.005	K or S	5.5	215/80 or 150/90
	S	8.5	290/85 and 150/90
	?	12.7	?
	S	16.0	290/80
	S	17.6	310/80
	S	18.2	300/80
	S	18.8	315/80
	S	19.5	315/80
	S	20.7	320/80
BK 85.006	S	6.5	135/90
	S	15.6	135/90
	S	17.0	160/90
	S	20.2	295/85
	S	22.7	315/85
	S	23.9	315/85
	S	26.1	290/85
	S	27.4	315/80
BK 85.007	S	24.6	290/80
	S	27.1	310/75
	S?	30.4	175/80?
BK 85.008	S	13.8	340/75
	?	16.2	?
	K or S	21.8	200/90 or 110/85
	?	24.9	?
BK 85.009	S	18.2	320/90
	S	19.0	325/90
	S	28.3	310/75
BK 88.015	S	25.1	135/85
	S	25.6	140/85
	S	35.7	135/90
BK 88.014	?	9.5	?
	?	11.8	?
	S	17.5 - 18.5	115/85
	S	20.4	125/90
BK 88.016	S	19.3	130/85
	S	22.1	135/90
	S	24.1	130/90
	?	25.2 - 25.5	?
BK 88.017	K or S	5.0	035/80 or 315/90
	K	26.2	045/85
	K and S	27.0 - 29.0	040/85 and 315/80
	S	34.6	160/85
BK 88.018	S	14.5 - 16.0	135/80

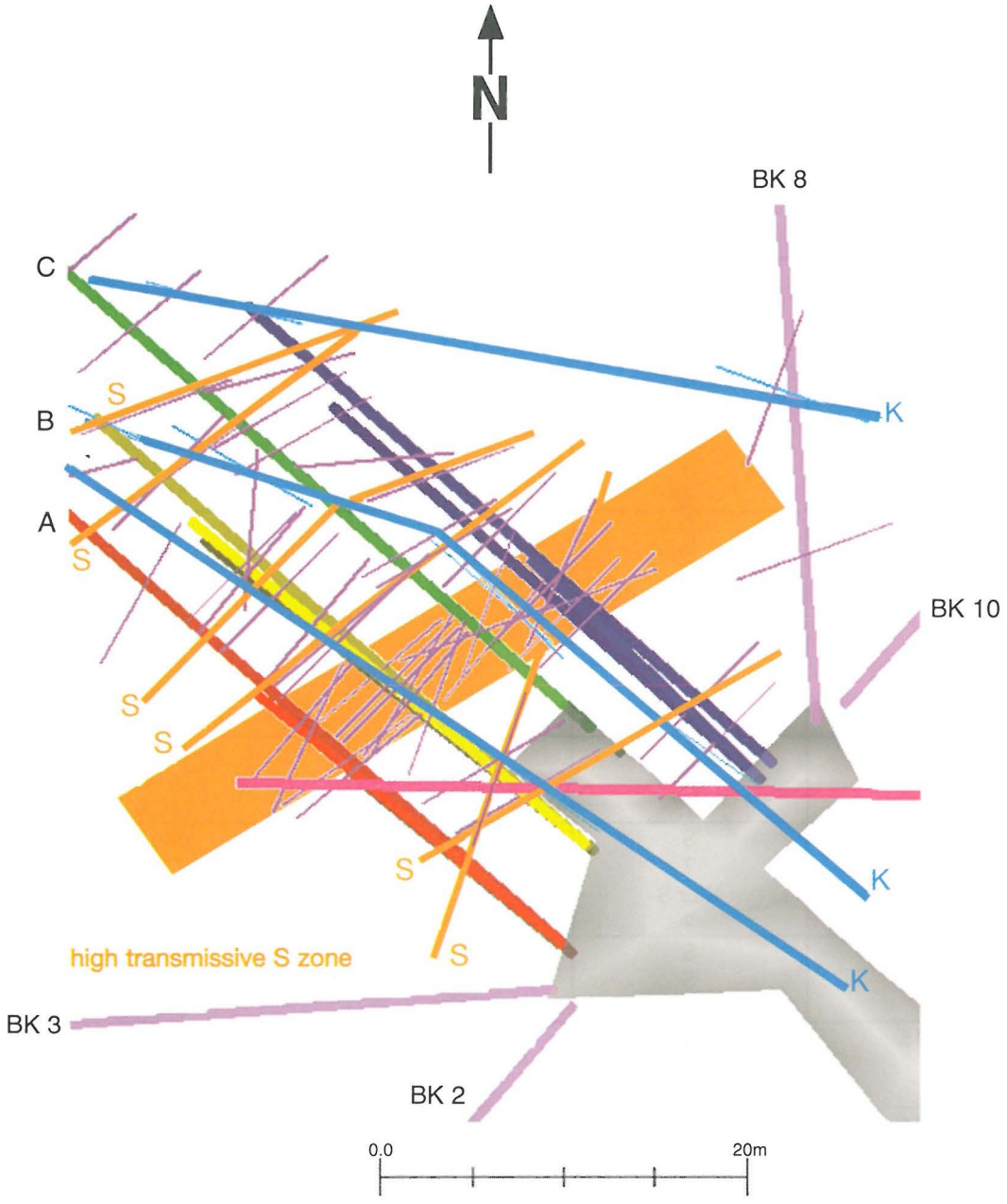

Fig. 7.8: The minimal fracture network (8 S fractures), many of the densely clustered S fractures are linked to 1 high transmissive S zone (horizontal cut at 1730 m)

Consistency with other BK conceptual models

Structural models of the BK site have been developed by MARTEL & PETERSON (1991) and by BRÄUER et al. (1989). As mentioned before, the fracture dips seem to be to flat in both structural models. Hence, the distance of the highly transmissive S zone to the BK cavern is larger than in the present fracture zone model. Nevertheless, there is a great degree of consistency in particular to the BRÄUER model, which explicitly attributes to the relevance of the K fractures in the northern part of the BK and to the more or less coplanar S fractures on the other side of the highly transmissive S zone.

LIEDTKE et al. (1994) presented a discrete fracture transport model to interprete previous tracer tests at the BK site. The model consists of 4 intersecting "fractures". In their concept too, the highly transmissive S zone plays a predominant role. There are any further S fractures, which might contribute to the flow system. To realize a connection between the S zone and the boreholes of the northern part of the BK, the northern lamprophyre acts as a drainage. In the condensed fracture zone model, we have accounted for this hydraulic connection by the K fractures, because the hydrotests (see Chapter 5) suggest, that the lamprophyre is rather tight.

In the condensed fracture zone model, only structural and hydrogeological information was used to derive the model. MARTEL & PETERSON (1991) and LONG (1992) use another approach: they integrate structural and geophysical information (seismic and radar tomography data) into their conceptual model. In our strategy, this "third line" of information could also be integrated and combined with the actual conceptual model.

7.5 Summary and conclusions

In the first part of this chapter the ability of computer-based visualization tools to conceptualize structural and hydrogeological data is demonstrated. The 3D visualization system AVS has been further developed in order to visualize various types of structural and hydrogeological data collected at an underground test site. This visualization tool was then applied at the BK site at the Grimsel Test Site. Examples of data visualization are:

- 3D visualization of complex geometries such as tunnels and caverns or large-scale structures such as geological formations.
- 2D visualization of fracture networks: a complex 3D fracture network is cut by 2D planes of any orientation and the traces of the fractures are then shown.
- 1D visualization of petrographical, structural or hydrogeological information along boreholes.

An especially strong tool is the visualization of 2D cutting planes which contain the traces of different 3D structures. Out of the combination of such cuts, the user quickly obtains an idea of complex 3D geometries. Another strong tool is the visual comparison (or superposition) of different types of data: when a hydraulic fracture network has to be derived, structural data (orientations of fractures) and hydraulical (traced inflow locations from fluid logging) along boreholes are superimposed and those structures, which are hydraulically active are selected.

In the second part of this chapter, the derivation of a conceptual model for numerical flow modeling has been presented. This derivation procedure could be applied at other underground test sites where structural and hydraulic information is available. The derivation procedure, together with the support of the newly developed AVS tools (which are part of the derivation strategy) were applied at the BK site.

The application of the derivation strategy at the BK site results in a condensed fracture zone model. By combining the structural with the hydraulic information, a system of 12 fractures resp. fracture zones with different extensions, orientations and hydraulic properties is obtained. This condensed fracture zone model now serves as a basis for the numerical modeling.

In the derivation procedure of the conceptual model, only geological-structural and hydraulic information is considered. The strategy could also be extended to other information sources such as geophysical data (i.e. borehole tomography). Certainly when processes other than flow in fractured media are considered (i.e. solute transport in fractures and matrix), the derivation procedure presented has to be modified.

8 FRACTURE ZONE MODELING

U. Kuhlmann (VAW), N. Correa (Nagra)

8.1 Introduction

8.1.1 Scope of the investigations

Usually, the final step of hydrogeological site characterization is the simulation of flow (and transport) with numerical models, with the aim of improving the understanding and prediction of the hydrodynamic processes at the site. In fractured formations, the simulation of flow is a particularly challenging topic, which differs greatly from such simulation in common porous media. The derivation of the conceptual model is much more difficult: it requires a detailed knowledge of the site structural geology and modified methods for the hydrogeological test interpretation. In addition, fracture flow modeling requires specific discretization and mesh generation techniques, e.g. to account for an appropriate representation of fracture intersections or to simulate short-circuiting between different fracture zones by intersecting boreholes.

In a fractured rock the spatial distribution of flow is basically restricted to the system of fractures and is therefore discontinuous by definition. A complete structural description of the entire fracture network, as required for a detailed flow model, is almost never available. Thus, the simulation of flow in a fractured formation essentially consists of substituting the real, but very complex network of fractures with more or less unknown structural and hydrodynamic properties using a simplified model which, nevertheless, represents the main characteristics of the flow system within a certain range of accuracy. A strategy for deriving such a conceptual model by jointly analysing structural data and hydrogeological tests has been developed in the present project (see Chapter 7). The approach was applied to establish a numerical flow model for the BK site by analysing drillcore data, fluid logging results and single/crosshole hydrotest results, collected during previous investigation phases: the result was a so-called condensed fracture zone system, containing a set of 14 planar hydraulic features determined by their location, orientation, extent and first estimates for the hydraulic parameters. Furthermore, initial and boundary conditions were derived from longterm observations of the hydraulic head distribution and inflow measurements to the BK cavern.

It became obvious at an early stage of the modeling exercise that it was not possible to include all features of the "condensed fracture zone system" in the numerical model. This was due to the time constraints within the modeling project and due to the immense computational effort necessary to realize the inverse modeling procedure. For this reason, the numerical model was restricted to up to 6 fracture zones (4 fractures plus the 2 lamprophyres), while the "condensed fracture zone system" serves as a basis for the structural model.

8.1.2 Objectives and chapter outlines

Modeling of flow in fractured rock requires specific procedures for conceptualization, model discretization and, finally, for model calibration. The emphasis of the present

study was to obtain more experience with the simulation of flow in fractured formations. In detail, the specific objectives of the fracture zone modeling were defined as:

- to provide new/improved tools and techniques for the discretization of complex fracture zone models (e.g. mesh generation)
- to implement a complex numerical flow model of the BK fracture network based on the conceptual model of a condensed fracture zone system, which was derived in Chapter 7
- to demonstrate the applicability of inverse modeling schemes in the calibration of flow in fracture zone models
- to outline the use of error and sensitivity analysis for improved model structure identification

Various different concepts are available to simulate flow in fractured formations. In essence, the choice of a conceptual model depends on the structural and hydraulic properties of the fracture network. In Section 8.2, some well-known approaches are given and the specific conceptual model selected to simulate the BK fracture flow system is discussed. Furthermore, the hydrotest data used to calibrate the BK numerical model are presented and the data processing is briefly described.

In Section 8.3, the methodology of inverse modeling is summarized.

The process of model discretization is described in Section 8.4, focusing on the discretization of small structures (e.g. boreholes, tunnel) and on the mesh generation procedure. Furthermore, the initial and boundary conditions are defined and the time stepping scheme is briefly described.

Two different structural models and several model variants were constructed to simulate the hydrotest data. In Section 8.5, these models are described and initial estimates for the hydraulic parameters are presented. The results of the model calibration are shown: estimated fracture zone transmissivities, storativities and standard deviations as well as a match between observed and calculated head data for selected boreholes. Finally, a sensitivity analysis is presented with the emphasis on improving the model performance by studying the residuals between observed and calculated heads.

In Section 8.6, the procedure of modeling flow in the BK fracture network is summarized. The problems which arose during mesh generation and time discretization are mentioned. The results of the calibration and sensitivity analysis are reported and conclusions are presented.

8.2 Conceptualization and data selection

8.2.1 Basic concepts

In general, four approaches for the simulation of groundwater flow in fractured rocks are available, each corresponding to a different conceptualization of the problem:

- In the classical approach the medium is considered as a 3D porous **continuum**.This approach is frequently used to describe flow in fractured formations on a regional scale or for highly fractured rock, when the fracture orientations are distributed more or less isotropically.

- In the **discrete fracture** approach the rock matrix is impervious and the flow takes place only within the fractures. The flow in the fractures is described by a continuous approach. Major fractures or fault zones are commonly modeled as 2D features. Frequently, if the formation consists of numerous minor fractures, stochastic approaches are applied to generate a random network of fractures with similar statistical properties (fracture orientations, fracture densities) to the formation.

- A **combination** of the first two approaches consists of explicitly modeling major fracture zones and treating the rock matrix inbetween as a continuum. The latter can be modeled by either 1D connections between highly conductive fracture zones (quasi 3D) or by means of 3D elements (fully 3D).

- The **channeling** approach assumes that water flows mainly through discrete interconnected channels (tortuous 1D features) embedded in the fracture planes/rock matrix.

In Chapter 7, a conceptual model of the BK fracture network was derived, consisting of 8 S fractures and S fracture zones, respectively, 4 K fractures and 2 lamprohyres ("condensed fracture zone system"). When starting the modeling investigations, it was planned to construct a numerical model which was very close to the conceptual model. Unfortunately, the modeling activities were limited in time and computational capacity. Thus it was not possible to implement the entire "condensed fracture zone system" into a numerical model: the number of fractures and fracture zones, respectively, had to be reduced and the free surface, proposed in Chapter 7, could not be simulated. Nevertheless, the "condensed fracture zone system" served as a reference model and it was attempted to avoid contradictions between the "condensed fracture zone system" and the conceptual model actually used for fracture zone modeling. Below, the main features of the modified conceptual model are summarized:

- In the central BK area flow takes place mainly in fracture zones. Thus, the second discrete fracture approach was chosen for the present study. The fractures and fracture zones, respectively, are represented as planar features, each of them determined by its location, extent and orientation. The hydraulic parameters are constant within each feature. Due to the high conductivity of the fractures, the influence of the rock matrix is expected to be negligible.

- The central BK area is bounded by the two lamprophyre dykes which intersect the GTS tunnel north and south of the BK cavern (Fig. 7.2). Both fault zones are oriented so that they mutually intersect probably about 100 m west of the BK cavern. To the east, the system is controled (drained) by the tunnel system of the GTS. The vertical extent of the hydraulic system seems to be restricted by a free surface, which cannot be simulated in the numerical model.

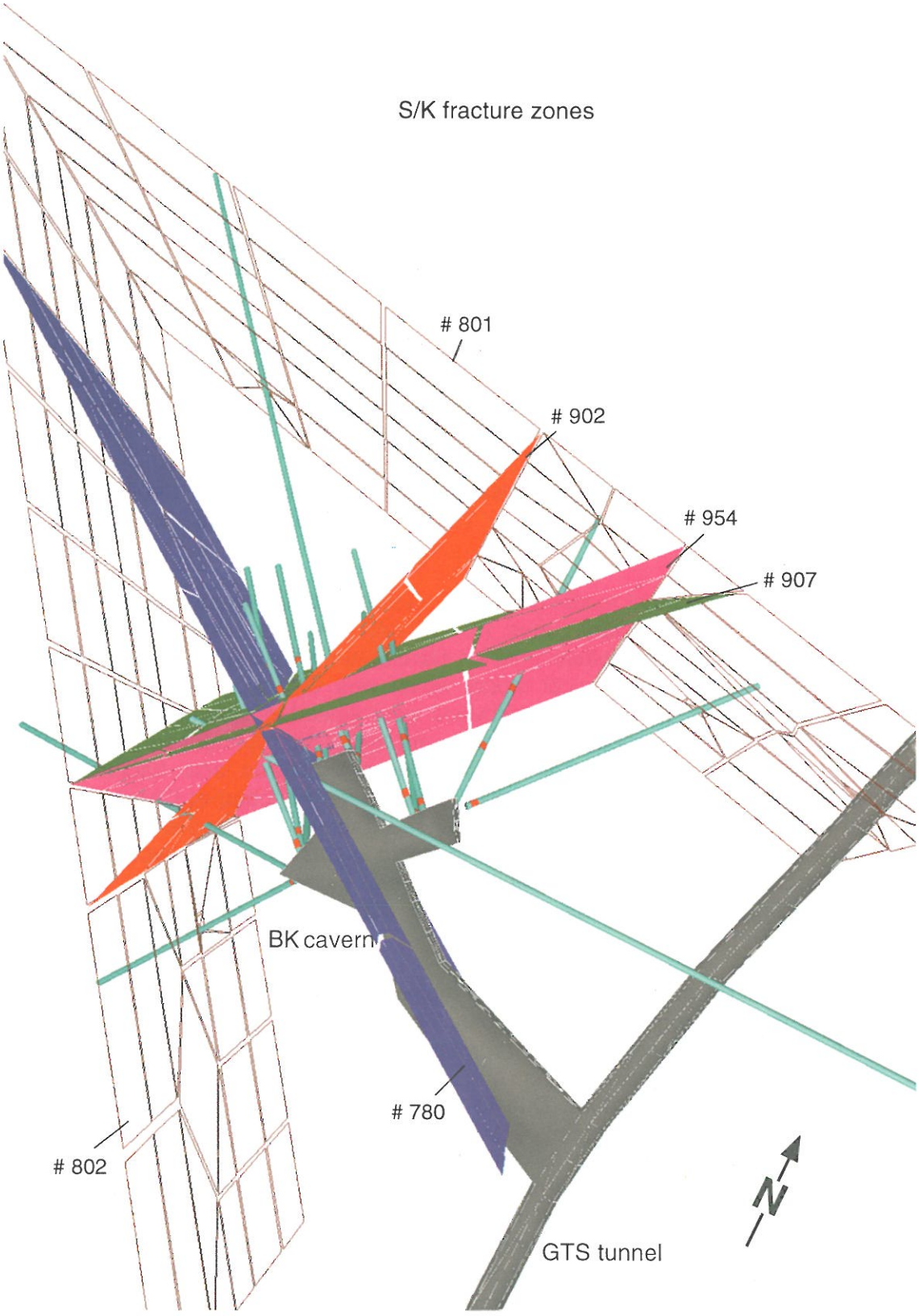

Fig. 8.1: Idealized system of fracture zones in the BK area

- In the BK fracture network three main groups of fractures can be distinguished (BOSSART et al. 1993). According to the orientation, the fracture zones S^+, S^- and K^+ have been identified. While both of the S zones are oriented subparallel to the GTS tunnel the latter K zone intersects almost perpendicularly through the center of the BK cavern.

In summary, this conceptualization relies mainly on the three fracture zones which are represented by two-dimensional features (planes). Compared to the "condensed fracture zone system", given in Chapter 7, it has been considerably simplified. The S^+ and S^- zones represent more or less the large S fracture zone close to the BK cavern as shown in Fig. 7.8. The K^+ zone corresponds to the K zone which is subparallel to plane B. Except for the two lamprophyres, all other features are omitted. The simplification originates from the numerical constraints, because the hydraulic conditions to be simulated (transient crosshole test with relatively high injection rate) require a large numerical load resulting from a very high mesh density as well as small timesteps. A graphical overview of the conceptual fracture zone model is given in Fig. 8.1.

8.2.2 Data selection

Numerous single/crosshole hydrotests were performed during previous field campaigns in the central BK area. The tests VE 451 to VE 457 were performed in 1990 and analysed by GUYONNET & LAVANCHY (1992). The results of these tests in terms of estimated transmissivities and storage coefficients will be used as initial estimates in the following inverse modeling study. The Multiple Source Crosshole Test (MSCT) conducted in 1992 consisted of 15 hydraulic crosshole tests (VE 499 - VE 513). The MSCT was designed in particular to improve the spatial resolution of the distribution of hydrodynamic parameters in a fracture network. During the field experiment, pulse injection tests and injection/withdrawal tests were performed with measured responses in up to 23 observation intervals.

Clearly, the simultaneous interpretation of all crosshole tests performed during the MSCT field experiment would provide the most reliable estimation results. However, because of time restrictions within the present study, only one test has been selected: due to the relatively good quality of the data and the good level of response in most of the observation intervals test VE 513 was chosen to be simulated in the inverse analysis below. During this test a flowrate of 12 l/min was injected in interval BK 85.005.1, creating an overpressure of about 100 m. After 2.4 hours, a shut-in was carried out and the pressure recovery was measured. The total duration of the data recording lasted approximately 6 hours.

8.2.3 Data processing

During test VE 513, several hundred pressure measurements were recorded in each of the packed-off intervals with a sampling interval of 40 to 50 seconds. All data are overlain by a considerable noise component, which originates from the poor performance of the data acquisition system (see Section 5.4.1). Although the inverse modeling scheme used to analyse the head measurements is based on a statistical approach and is therefore appropriate for treating noisy data, data outliers/errors

which do not follow the assumed normal distribution may bias estimation results. Moreover, in order to avoid the expensive numerical reproduction of system responses with sampling intervals of 40 seconds, preprocessing the observed 'raw data' prior to modeling was preferred. The time discretization can thus be fitted to the test

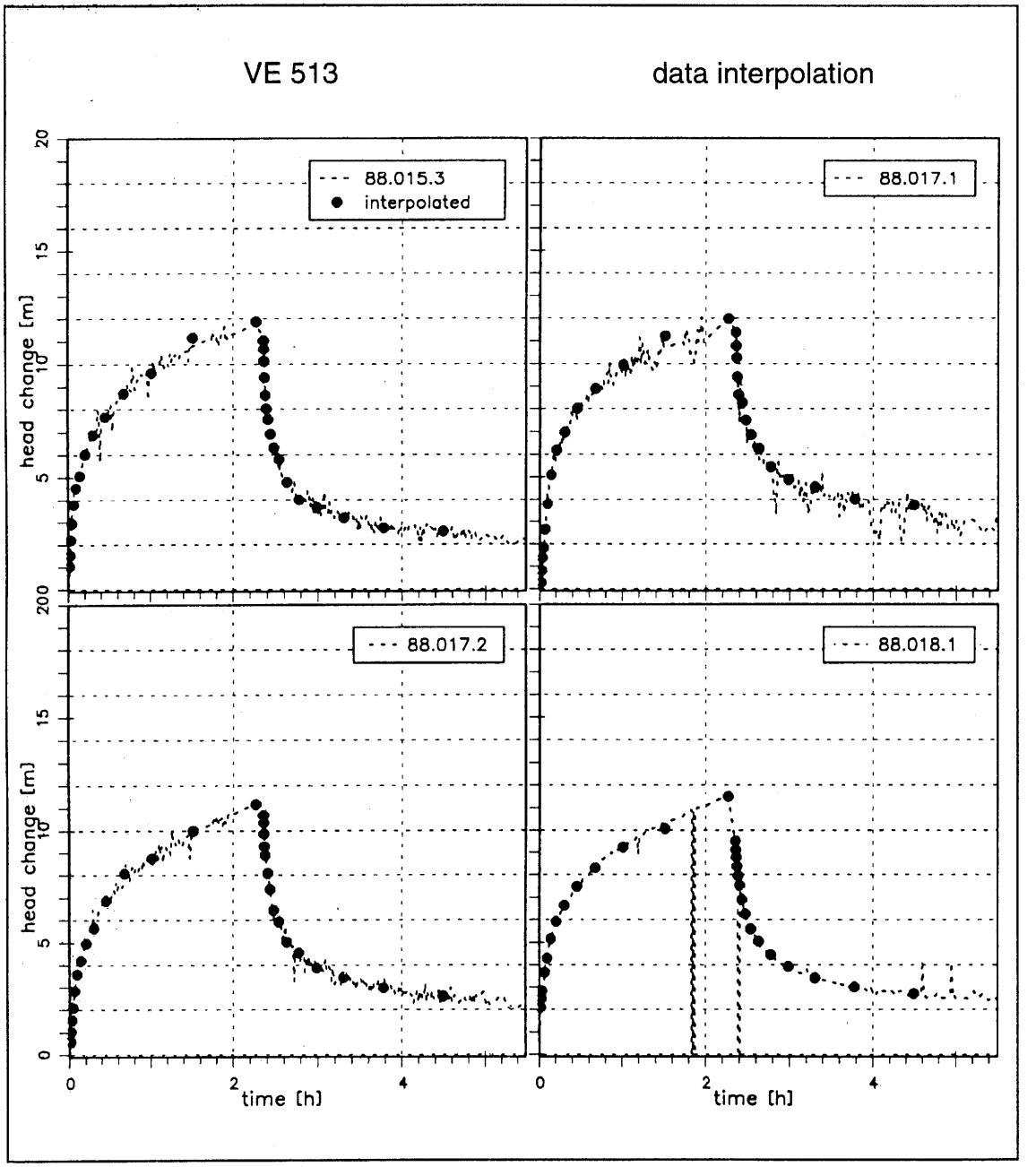

Fig. 8.2: Examples of final observation data processed by 'smoothing interpolation' compared to the original data sets

procedure by reducing the sampling interval when the system response changes rapidly and increasing it otherwise. Three algorithms were applied to obtain the final data for interpretation in a sequential process:

1) detection and removal of data errors (GUERRA & TAPIA 1974);

2) data approximation by 'smoothing' splines using cross-validation (CRAVEN & WAHBA 1979);

3) resampling of the smoothed data at a reasonable sampling rate.

The procedure applied offers the possibility to easily quantify the data noise in terms of its variance. This variance will be considered in the inverse analysis. In addition to smoothing, the absolute head data have been transformed into relative heads by subtracting the initial head prior to the test as an offset from each record. By way of an example, Fig. 8.2 illustrates results of such a 'smoothing' data interpolation as uniformly applied to all of the response curves of test VE 513. The complete data set used within this study, as well as a more detailed description of the methodology, is given in KUHLMANN & CORREA (1993).

8.3 Methodology of inverse modeling

8.3.1 Direct Problem

Numerical modeling in this study has been performed with the CASA code which allows the automatic estimation of the hydrological and hydrogeological model parameters (KUHLMANN 1992). In essence, the computer program searches for optimal parameter values by the repeated solution of the so-called **Direct Problem**. For saturated groundwater flow this consists of solving the following equation which has been simplified according to the problem at hand:

$$\mathrm{div}(T\nabla h) = S\frac{\partial h}{\partial t} + q \qquad (8.1)$$

subject to appropriate initial and boundary conditions. The quantity h [m] represents the hydraulic head, T [m^2/s] is the isotropic transmissivity, S [-] is the storage coefficient and q [m/s] denotes sources and sinks. Equation (8.1) is solved numerically by means of the Galerkin finite element method coupled with implicit finite differences in time. Discretization in space is achieved by applying isoparametric elements with second order shape functions. The difficult problem of hydrogeological parameterization can be treated alternatively using either conventional zonation or defining the hydrogeological properties pointwise in combination with a kriging interpolation scheme.

8.3.2 Inverse Problem

The **Inverse Problem** consists of estimating model parameters from measurements made on the system response and from appropriately weighted prior information on the parameters. In CASA the inverse problem is formulated within the framework of the statistical Maximum Likelihood (ML) estimation method and largely follows an approach proposed by CARRERA (1984). The ML theory leads to the following negative log-likelihood function Z to be minimized with respect to the geohydrological parameters

$$Z = \sum_i \frac{Z_i}{\sigma_i^2} + \sum_i M_i \ln\sigma_i^2 + \sum_i |\mathbf{V}_i| + M \ln(2\pi) \tag{8.2}$$

where bold letters denote vectors or matrices (capital) and

$$Z_i = \mathbf{r}_i^T \mathbf{V}_i^{-1} \mathbf{r}_i \qquad \text{where } i = h, Q, p \tag{8.3}$$

$$M = M_h + M_Q + M_p = \sum_i M_i$$

$$\mathbf{r}_i = \begin{Bmatrix} \mathbf{r}_h \\ \mathbf{r}_Q \\ \mathbf{r}_p \end{Bmatrix} = \begin{Bmatrix} \mathbf{z}_h - \mathbf{z}_h^* \\ \mathbf{z}_Q - \mathbf{z}_Q^* \\ \mathbf{p} - \mathbf{p}^* \end{Bmatrix}$$

(8.4)

M denotes the total number of available measurements and prior estimates and represents the sum of the subsets $\mathbf{M}_i$ where the index i refers to the type of the data subsets $i \in \{h, Q, p\}$ (i.e. head, flowrate, model parameters). $\mathbf{V}_i$ represents symmetric, positive definite matrices, which account for a-priori covariance within the individual groups of data. σ_i^2 denotes positive scalars often taken as unknown statistical parameters to be estimated by the inverse scheme. The sums Z_h und Z_Q (equation 8.3) quantify the discrepancies between the computed performance measures $\mathbf{z}_i$ and the vector of measurements $\mathbf{z}_i^*$ and are often termed as 'fit'-criteria. Z_p (equation 8.3), on the other hand, quantifies the deviations between the actual values of model parameters **p** and their prior estimates **p*** representing a plausibility measure of the estimation results (plausibility or penalty criterion).

If the error structure is assumed to be known i.e. given $\lambda_i = \sigma_h^2/\sigma_i^2$, minimizing the log-likelihood function (equation 8.2) is equivalent to minimizing

$$Z = \sum_i \lambda_i Z_i \tag{8.5}$$

CASA minimizes equation (8.5) by applying alternative optimization algorithms such as the Levenberg-Marquardt algorithm or a Quasi-Newton method. In case a global and unique minimum is detected, those model parameters are estimated which are most likely to reproduce the measurements based on a given model structure. Details

of the approach can be found elsewhere (e.g. CARRERA & NEUMAN 1986a, b, c and KUHLMANN 1992, 1994).

8.4 FE discretization

8.4.1 Groundwater flow into small structures

When modeling groundwater flow, the problem of an adequate representation of relatively small structures such as boreholes or tunnels is often discussed. The extent of the structure (e.g. diameter), the grid density in its vicinity, the order of the shape function in the FE formulation and the type of boundary conditions are the parameters which determine the accuracy of the numerical solution.

Provided that the injection/extraction rates into/from the borehole are known (i.e. flux boundary conditions are given), the corresponding head distribution in the formation can be simulated correctly for the far-field region, regardless of the computational error in the immediate vicinity of the borehole. However, this error has to be taken into account when the computed head in the borehole is used for parameter identification. On the other hand, there are practical hydraulic problems - and this is true in the present case at tunnel/cavern boundaries - where hydraulic heads are known (atmospheric pressure) rather than flowrates. In these cases, it is convenient to specify heads at the structure boundary. However, the computational error of the resulting in- or efflux may affect the overall mass balance of the model.

Singular structure approach

Two alternative approaches are available to overcome the numerical problems described above. One modeling concept is the singular structure approach. In this case, the structure is treated as a single node boundary or - in a 3D model - as 1D line elements. In order to remove the resulting singularity in the solution near the structure, special types of finite elements can be included. Either enriched interpolation functions can be applied in the adjacent elements or analytical solutions can be incorporated locally in the FE model (CHARBENEAU & STREET 1979). In some simple cases (steady-state, regular mesh), sufficient numerical accuracy can also be achieved by adjusting adequately the conductivities of the elements surrounding a singular structure (KUHLMANN 1989).

Modeled structure approach

The most obvious way of representing a small structure, however, is the modeled structure approach. This means that the structure itself is explicitly modeled by discretizing it with finite elements or by just leaving a 'hole' in the mesh. A systematic investigation with the focus on the required mesh density in the vicinity of a borehole showed that, under steady-state conditions, sufficient accuracy (error less than 5 % in heads and/or flowrates) can be achieved if the radial extent of the adjacent elements is less than 5 times the borehole radius.

BK approach

The approach applied in the present study is a combination of the two methods described above. The BK cavern (approximated by a circular cross-section), which

intersects the K fracture zones as well as the northern lamprophyre, is represented by holes in the mesh, specifying appropriate conditions at the corresponding boundary nodes (see Section 8.4.4). The intersections of the boreholes with individual fractures are explicitly modeled by discretizing them with finite elements.

Unfortunately, some of the packed-off sections of the BK boreholes connect individual fractures to each other. As a consequence these intervals may act as a short-circuit between the fractures and represent important flow paths within the model, behaving similarly to an injection/extraction interval. Thus, the actual FE model treats all of the borehole-fracture intersections uniformly, not differentiating between injection and observation intervals. As depicted in Fig. 8.3, the 2D borehole intersection elements consist of triangular elements (second order shape functions) with a high (fictitious) conductivity and a storage coefficient representing the wellbore storage effect. The representation of the tunnel/cavern is illustrated in Fig. 8.4.

As outlined above, an additional mesh refinement around the boreholes is required. Due to the extremely transient conditions at hand (high pressure gradients), it is obvious that the mesh density has to be finer than in steady-state conditions, starting the discretization around the boreholes with less than 2 times their radius (Fig. 8.3).

In addition, the boreholes themselves are incorporated by means of 1D line elements with equivalent 'hydrodynamic' parameters. Thus the hydraulic connections between the individual fractures are realized, the center nodes of the intersection surfaces being linked to the 1D features. To ensure that water flows only within one packed-off section, packers are simulated by means of separate impervious elements.

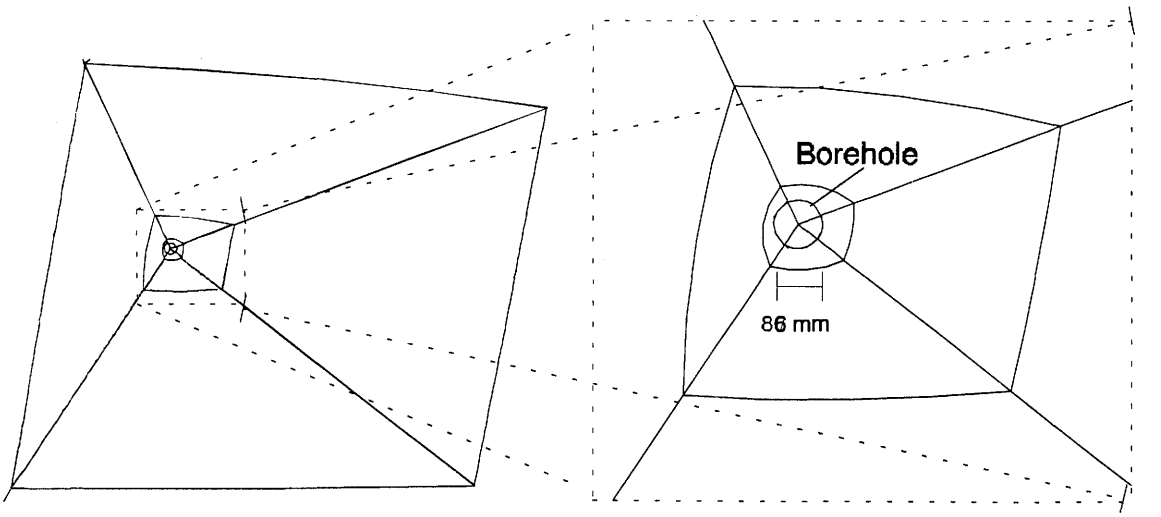

Fig. 8.3: Borehole discretization and corresponding mesh refinement

8.4.2 Mesh generation procedure

When simulating flow in fractured formations, it is a common procedure to investigate alternative hypotheses of the model structure, which account for the uncertainty in the structural description of the fracture network. This requires multiple mesh generation

with flexible discretization capabilities. Due to the geometric complexity with several intersecting fractures penetrated by numerous boreholes, mesh generation and refinement can only be handled automatically. On the other hand, the characteristics of a fracture network are site-specific, each requiring its own approach. In this context, a specific mesh generation procedure has been developed for the BK area. Involving different independent preprocessing tools the proposed approach can be easily adapted to different applications. The following packages were applied and/or developed within the scope of this study:

- FRACMESH (HÜRLIMANN 1994) is suitable for generating fracture networks embedded in a 3D matrix, when structural information such as location and orientation of the fractures is available.

- EQGRID is a preprocessor integrated in the CASA code (see Section 8.5) and has been developed within this study. It is designed to refine and equalize distorted elements of an existing mesh by specifying a maximum edge length or a maximum distortion factor for the elements (Fig. 8.4a, b).

- BHOLE is a preprocessor integrated in the CASA code. The package of subroutines is appropriate for generating 1D borehole elements based on orientation and packer data. Any intersection points with existing fractures are computed and incorporated in both the borehole and the fracture mesh, the latter being locally refined as outlined in the previous section (Fig. 8.3).

To demonstrate the mesh generation in detail, the complete model setup procedure applied in the present study is outlined below. The output of steps 2, 3, 4, 5, 6 involving mesh generation or modification is illustrated in Fig. 8.4a, b, c, d and Fig. 8.5 for the example of one of the K fracture zones (#780). Sequentially, the following steps were carried out:

1) Definition of all structural elements required for the generation of the numerical model.

2) Generation of a 3D fracture network with FRACMESH: discretization of the entire model space as defined in the conceptual model, except for the small structures; removal of the rock matrix inbetween the fracture zones (see Fig. 8.4a).

3) Grid modification by means of EQGRID in order to refine the largest elements (see Fig. 8.4b).

4) Running BHOLE to incorporate the BK cavern (simplified by a circular section) which intersects the K fracture zone (Fig. 8.4c) and the GTS tunnel which intersects the northern lamprophyre.

5) Second homogenization of the mesh applying EQGRID (Fig. 8.4d).

6) Incorporation of borehole elements and intersection surfaces in both the fracture planes and the boreholes; local refinement around the intersection points (preprocessor: BHOLE, see Fig. 8.3 and 8.5).

a) output of FRACMESH

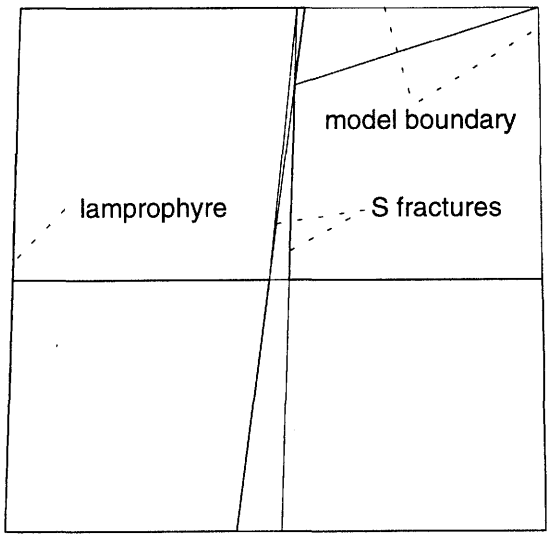

b) output of EQGRID (1)

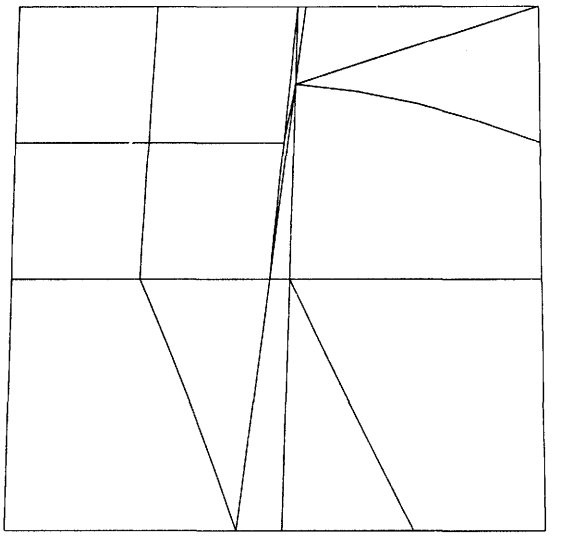

c) output of BHOLE(1)

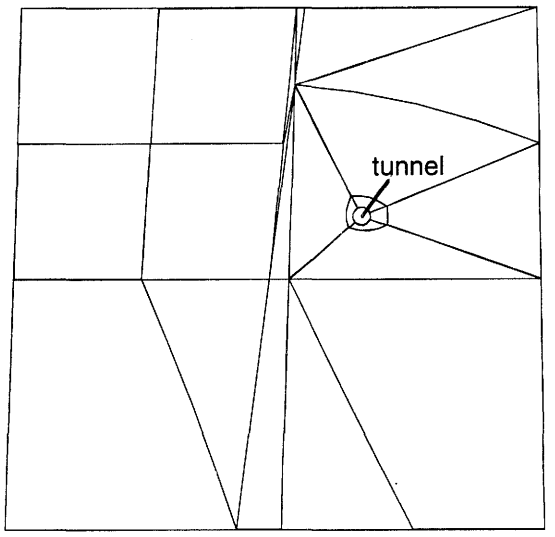

d) output of EQGRID(2)

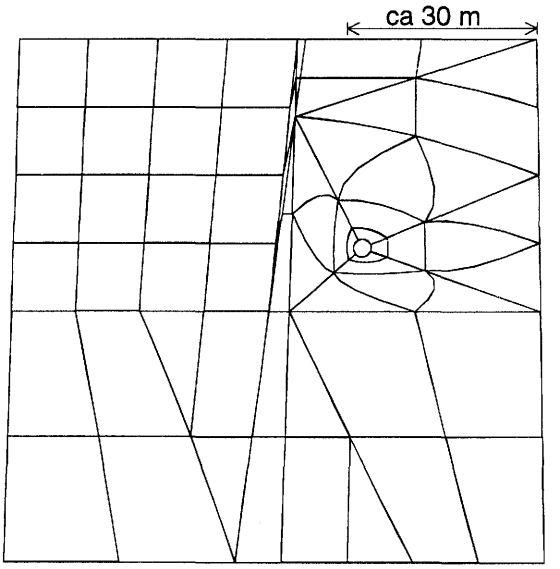

Fig. 8.4: Output of the different mesh generation tools (example of a K fracture, see also Fig. 8.1)

In spite of the conceptual simplicity the generation of the FE-mesh turned out to be a complex task. Difficulties arose from both the fracture location/orientation and packer arrangement in the boreholes. The boreholes had to be incorporated in the model because long packed-off sections hydraulically connect the fracture zones, mutually. The required refinements in the vicinity of fracture/borehole intersections (total 45) resulted in relatively large number of nodes (2000-5000) and often lead to ill-conditioned meshes when the distance between the fracture intersection lines became too small (a few cm).

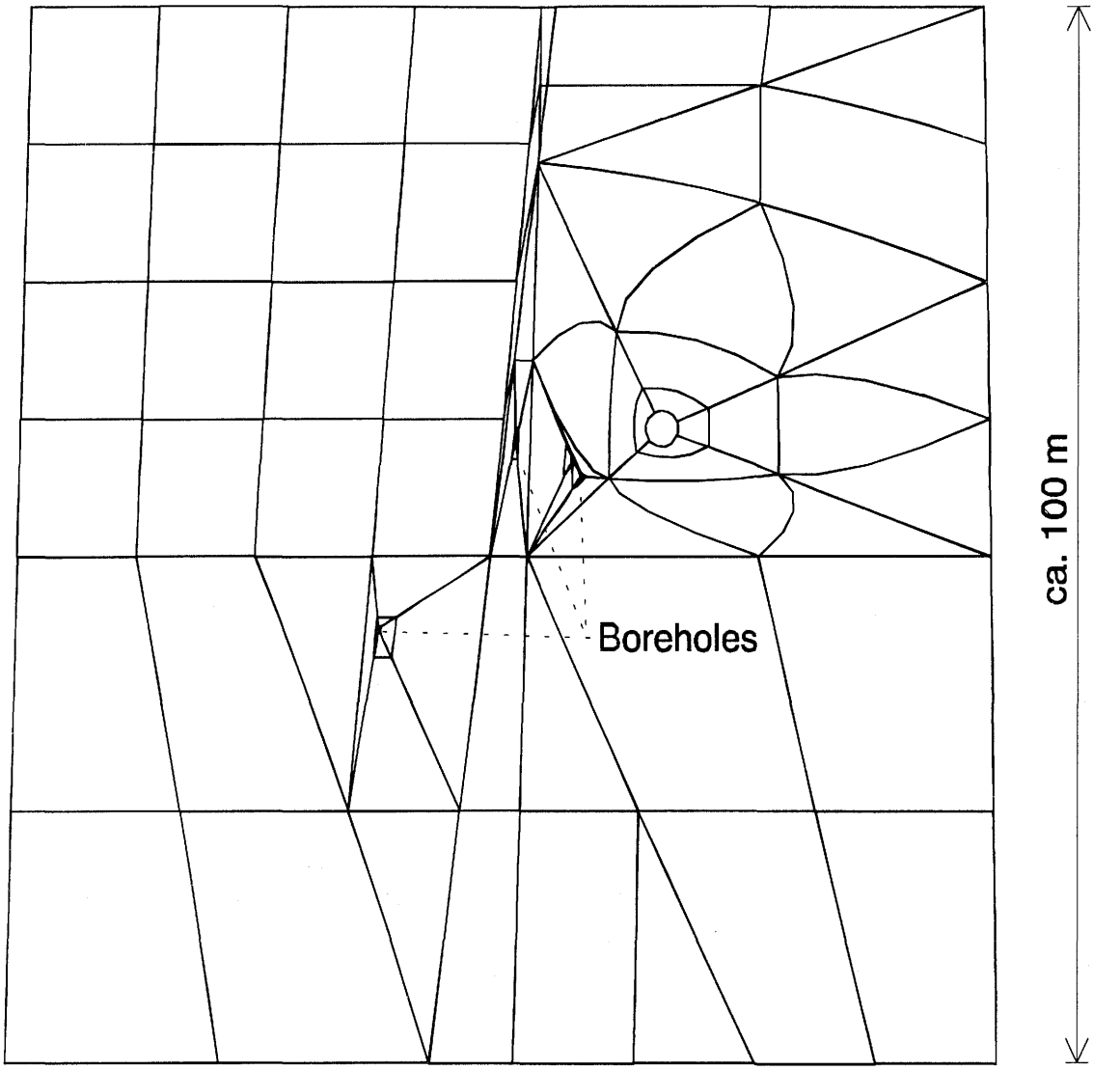

Fig. 8.5: Example of FE mesh for K fracture zone (#780), final mesh as output by BHOLE (2) (borehole refinement see Fig. 8.3)

8.4.3 Initial and boundary conditions

The groundwater flow equation (equation 8.1) is solved, subject to initial conditions

$$h(\mathbf{x},0) = h_O(\mathbf{x}) \tag{8.6}$$

where h_O may be an arbitrarily prescribed function or the solution of the steady-state equivalent of (equation 8.1), whenever the initial heads are assumed to be stationary. In analysing well test data as in the present study, h_O was taken as zero everywhere, so that h was the head variation (i.e. the net response).

The boundary conditions were taken as no-flow type at the outer boundaries of the model due to the relatively short duration of the test VE 513 and due to the lack of other information. At those nodes where the BK cavern intersects the fractures, boundary conditions varied depending on the model structure which was analysed (see Section 8.5.1). In the case where prescribed head conditions were investigated, nodal heads were imposed equal to zero (no head variation, see Section 8.4.3). Injection was simulated by means of a prescribed flow node in the center of the 1D element(s) which represented the injection interval.

8.4.4 Time stepping scheme

The time stepping scheme implemented in CASA is based on weighted finite differences where the nodal state vector **h**(t) is interpolated by means of

$$\mathbf{h}(t) = (1-\Theta)\mathbf{h}^k + \Theta\mathbf{h}^{k+1} \qquad (8.7)$$

where $\mathbf{h}^k$ and $\mathbf{h}^{k+1}$ represent the nodal vectors at times t^k and t^{k+1}, respectively, and Θ is a weighting factor. In the present application, logarithmic time stepping has been used, multiplying the current time step Δt^k by a constant factor larger than 1:

$$\Delta t^{k+1} = \Delta t^k c_i \qquad (8.8)$$

where the initial time step Δt^0 has to be chosen to be sufficiently small. The control factors Θ, c_i and Δt^0 depend on both mesh characteristics and test conditions. Therefore, their choice is specific to the application. For the conditions at hand, the following values have been found to be a feasible compromise between numerical accuracy and computational efficiency.

Θ = 0.66
Δt^0 = 0.001 s
c_i = 1.2

The maximum time step was limited to 120 s. At the shut-in time (8164 s) when recovery started, the time step was reset to the initial one. The total time of simulation lasted about 20,000 s, so that more than 300 steps were needed to obtain the forward solution.

8.5 Calibration and sensitivity analysis

8.5.1 Model structures

Model A

Based on the hydrogeological conceptualization outlined in Section 8.2.1, two different models, Model A and Model B, were generated in terms of the inverse analysis. Initially, Model A consisted of 5 fracture zones representing the northern and southern lamprophyre dykes (#801, #802), the K^+ zone (#780), S^+ zone (#902) and the S^- zone (#954) (see Fig. 8.1). The hydrodynamic parameters were assumed to be homogeneous within each zone; i.e. one transmissivity value and one storage coefficient had to be estimated for each fracture zone (10 model parameters). Preliminary runs showed that the southern lamprophyre is weakly connected to the hydraulic system considered, a fact that can also be observed in the interval BK 86.002.1 which responds insignificantly to hydraulic disturbances in the central BK area. Thus, this fracture zone was considered impervious in one run, the number of unknown parameters reducing from 10 to 8. The five fracture zones contain 34 intersection points with the BK boreholes and intersected 14 packed-off intervals where measurements were available. As shown in Tab. 8.1 some of the test intervals are intersected by both the S^+ and the S^- fracture zones. The total number of measurements to be interpreted amounts to 448 (32 interpolated values per 14 intervals, see Section 8.2.3).

Three variants of model A have been established in order to identify the appropriate boundary conditions. The modified Models A.2 and A.3 are mainly motivated by the discrepancies that Model A.1 produced in the injection interval.

Model A.1: Prescribed head (PH) boundary conditions at the intersection between K zone and the BK cavern (see Fig. 8.5)

Model A.2: No PH conditions anywhere

Model A.3: PH conditions at the BK boundary in the K zone as well as at the intersection of the northern lamprophyre dyke and the GTS tunnel. In addition, a fictitious horizontal feature at the top of the model has been introduced and connected to all of the other fracture zones modeled. Assigning a high storage coefficient to it aims at simulating unconfined conditions.

Tab. 8.1: Computed intersections between fractures and BK boreholes for Model A

Fracture	Interval	Distance[2] [m]	Coordinates[1] X [m]	Y [m]	Z [m]	Observed Data
# 801	85.010.1	34.38	7447.69	9243.94	1710.36	y
"	85.008.2	34.33	7425.82	9249.81	1710.41	y
"	85.004.3	71.14	7370.06	9260.91	1689.37	
#802	86.002.1	21.88	7402.83	9192.95	1717.21	y
"	86.003.1	23.64	7394.15	9205.14	1716.52	
#780	88.015.0	5.73	7412.71	9217.03	1725.57	
"	85.005.0	5.27	7412.08	9217.80	1727.14	
"	88.016.0	10.39	7407.35	9221.50	1728.96	
"	85.009.4	33.04	7393.59	9227.32	1711.20	
#902	88.017.2	39.90	7405.54	9235.30	1699.09	y
"	85.004.2	10.27	7407.69	9228.20	1724.28	y
"	88.015.1	22.70	7404.00	9224.00	1712.78	y
"	85.006.3	28.06	7408.07	9234.53	1714.05	y
"	85.007.2	27.76	7405.06	9230.52	1705.75	y
"	85.005.1	16.09	7405.39	9223.62	1720.93	y
"	88.016.0	11.67	7406.38	9222.30	1728.73	
"	86.003.1	18.18	7398.60	9205.60	1719.65	
"	80.001.1	90.35	7405.75	9218.25	1733.25	y
"	85.009.2	17.01	7403.50	9218.70	1720.39	
"	88.014.1	12.36	7404.51	9217.31	1728.48	y
#954	85.008.2	20.61	7426.60	9238.60	1718.28	y
"	88.017.2	20.16	7415.04	9227.04	1714.30	y
"	85.004.1	2.91	7412.24	9224.24	1728.50	y
"	88.015.0	14.05	7408.44	9220.44	1719.30	
"	88.018.1	12.69	7415.47	9227.47	1728.78	y
"	85.006.2	15.55	7415.81	9227.81	1721.22	y
"	85.007.1	8.68	7412.26	9224.26	1722.28	
"	85.005.1	10.70	7408.72	9220.72	1724.02	y
"	88.016.0	8.84	7408.53	9220.53	1729.23	
"	88.012.1	2.20	7412.21	9224.21	1730.38	
"	80.001.1	89.86	7406.24	9218.24	1733.24	y
"	85.009.1	14.24	7405.21	9217.21	1721.98	
	88.014.1	11.79	7404.95	9216.95	1728.58	y
	88.013.1	23.30	7404.94	9216.94	1710.06	y

1 Coordinates of intersection point of borehole axis with fracture plane
2 Length from the borehole mouth to intersection point of borehole axis with fracture plane

Model B

In addition to the features included in Model A, Model B contains a fracture zone which intersects, among others, the test intervals BK 85.005.2 and 88.015.3 (#907). This additional fracture was added to account for the observations during the Salt/Heat Tracer Tests (see Chapter 6), which showed that these two intervals are connected hydraulically. The transmissivity of the southern dyke as well as the storage coefficient of the northern lamprophyre dyke were fixed in Model B as a result of the sensitivity analysis described in Section 8.5.4. Together with the new transmissivity and storage coefficient for fracture #907, the number of model parameters now comes to 10. The geometric data of the 11 intersection points between the new fracture and the BK boreholes are listed in Tab. 8.2. In summary, a total number of 512 data points was available for the inverse analysis. The boundary conditions for Model B are equivalent to Model A.1.

Tab. 8.2: Additional intersections between fractures and BK boreholes for Model B

Fracture	Interval	Distance [m]	Coordinates X [m]	Y [m]	Z [m]	Observed Data
#907	85.008.2	31.15	7426.00	9247.22	1712.23	y
"	88.017.2	36.46	7407.20	9233.86	1701.74	y
"	85.004.2	11.22	7407.10	9228.71	1723.73	y
"	88.015.3	29.63	7400.45	9226.85	1707.56	y
"	85.006.3	25.06	7409.93	9232.92	1715.77	y
"	85.007.2	29.14	7404.53	9230.97	1704.55	y
"	85.005.2	20.75	7402.51	9226.12	1718.26	y
"	88.016.0	15.47	7403.49	9224.68	1728.07	
"	80.001.1	98.65	7397.46	9218.39	1733.39	y
"	85.009.3	25.41	7398.31	9223.21	1715.58	
"	88.014.1	19.02	7399.45	9221.47	1727.29	y

8.5.2 Prior information

Prior estimates of transmissivities and storage coefficients were determined by averaging data taken from the test analysis of GUYONNET & LAVANCHY (1992). Note that these parameters characterize the behavior of the medium along the whole length of the packed-off sections. Thus, the indicated values represent mean values in cases when more than one fracture intersects the interval. Nevertheless, they are considered as best-guess values for the parameters and will be used in the following inverse analysis; the standard deviations, however, were slightly increased (0.5 related to log values).

The error structure of the residuals between computed and measured head variations is assumed to be known. An explicit estimation of its statistical parameters would have required repeated inverse runs which would have resulted in prohibitively high CPU times. In summary, head errors are assumed to be uncorrelated in space and time. With the exception of the measurements in the injection interval, where the errors have been increased by a factor of 2, standard deviations were taken to be 0.1 m for the remaining test sections.

8.5.3 Calibration results

Model A

The inverse simulation of crosshole test VE 513 minimizing objective function (8.5) leads to the results shown in Fig. 8.6, where measured and computed head variations are compared. As a first impression it can be stated that, qualitatively, the response of the model is in agreement with the measured system response. That means that the shape and order of magnitude of the computed head variations approximately correspond to the experimental data. The most significant deviations are observed in the injection interval BK 85.005.1, where the computed overpressure drops off about 50 m from the measurement. The maximum errors in the remaining intervals are an average of about 10 % of the measured head variation.

Although the boundary conditions were modified for Models A.1 and A.3 both systems behave similarly. In particular, the discrepancies in the injection interval are of the same order. Tab. 8.3 shows values for the sum of weighted residuals (8.5) compared for the three Model A variants. In summary, while the structural modifications are mostly compensated by parameter variations, they all fail to fully explain the observed conditions in the injection interval.

Tab. 8.3: Evaluations of the objective function Z (equation 8.5) for the Model A variants

Model	A.1	A.2	A.3
Z [-]	274000	264000	298000

The hydraulic parameters of the 5 fractures estimated by inverse run A.2 are shown in Tab. 8.4, as well as estimates of the a-posteriori standard deviations. Note that the standard deviations listed were computed without considering prior information. In case parameters don't have much influence, their (a-priori) standard deviations would determine the bounds of the computed confidence interval. Thus, very low sensitivities of the system response to certain parameters would not have become as clearly evident as seen below in Tab. 8.4 (marked values). The unreasonably high a-posteriori errors of the two parameters T-LamN and S-LamS (transmissivity of the southern and storage coefficient of the northern lamprophyre dyke) indicate their negligible influence on the performance measures analysed (see also Section 8.5.4).

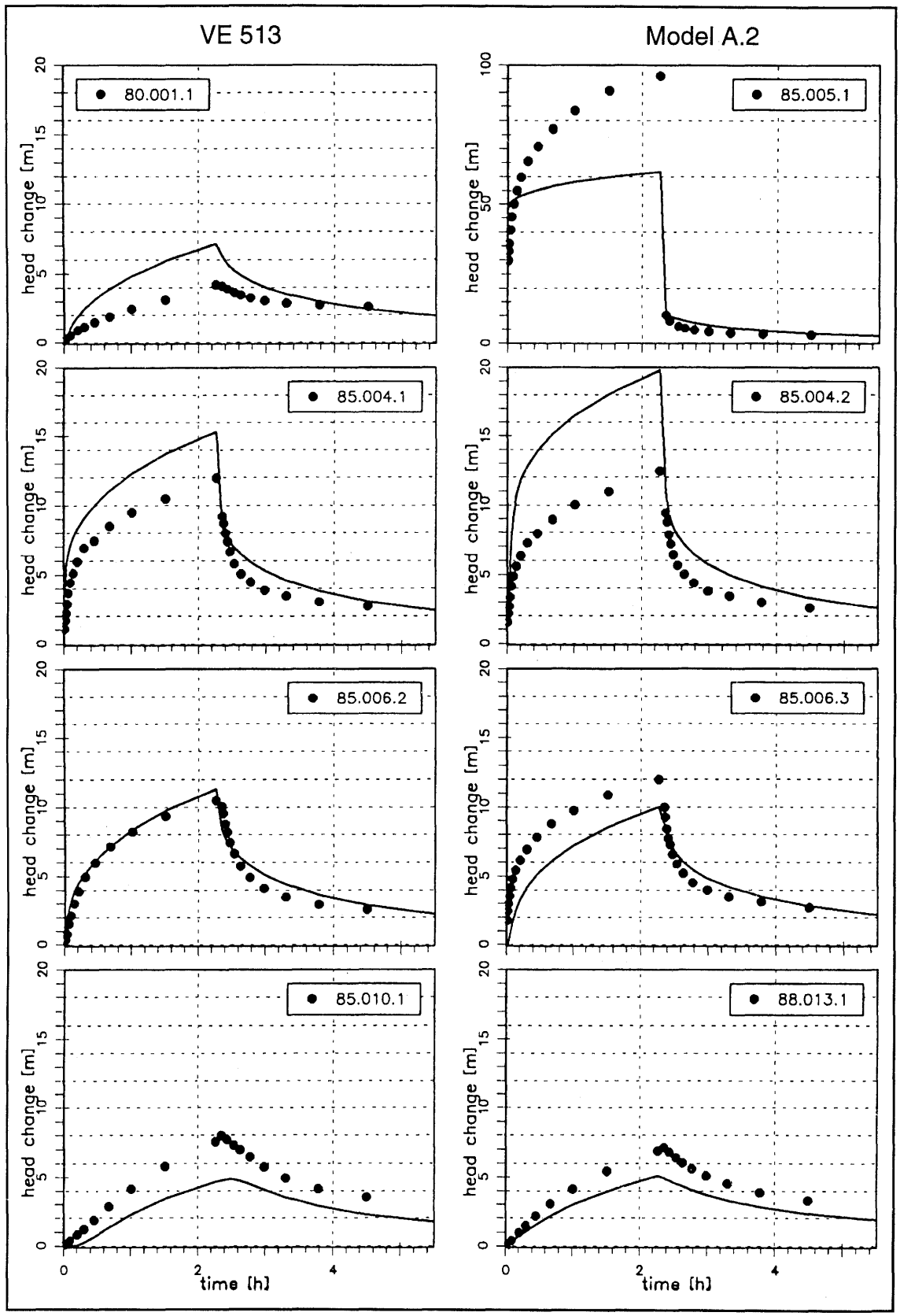

Fig. 8.6: Comparison of computed and measured head variation for Model A.2

Keeping in mind the hypothesis that unsaturated and/or unconfined conditions may be present somewhere in the BK area, the resulting relatively high storage coefficients of S >1.E-04 (LamS, K^+) are at least indicators for the existence of higher storativity features.

Tab. 8.4: Computed parameters, approx. 95 % confidence interval and standard deviations for model A.2

Parameter	Transmissivity [m^2/s]	lower bound of 95 % conf. int. [m^2/s]	upper bound of 95 % conf. int. [m^2/s]	Standard[3] deviation log[m^2/s]
LamN	5.50E-08	4.53E-08	6.68E-08	4.22E-02
LamS	1.91E-03		∞	1.27E+01
K^+	1.05E-06	1.03E-06	1.07E-06	4.38E-03
#902 (S^+)	5.44E-08	5.21E-08	5.68E-08	9.36E-03
#954 (S^-)	1.19E-06	1.19E-06	1.20E-06	6.63E-04
	Storage coefficient [-]	[-]	[-]	log[-]
LamN	5.88E-17	0	∞	5.95E+07
LamS	1.12E-04	4.45E-05	2.83E-04	2.01E-01
K^+	3.25E-04	3.20E-04	3.30E-04	3.32E-03
#902 (S^+)	2.56E-07	2.34E-07	2.81E-07	2.02E-02
#954 (S^-)	3.75E-06	3.65E-06	3.84E-06	5.31E-03

Model B

Results of inverse run B are shown in Fig. 8.7 which compares computed and observed heads for distinct observation intervals. The objective function is computed as Z = 194,000 or as Z = 155,000 when the measurements in the injection interval are not taken into account. Essentially, the additional feature modeled leads to minor improvements in model performance. The computed parameters are given in Tab. 8.5. Note that high storage coefficients as computed in run A.2 do not occur any more, which is an effect of the prescribed head conditions at the tunnel boundary.

[3] related to the log value of the parameter

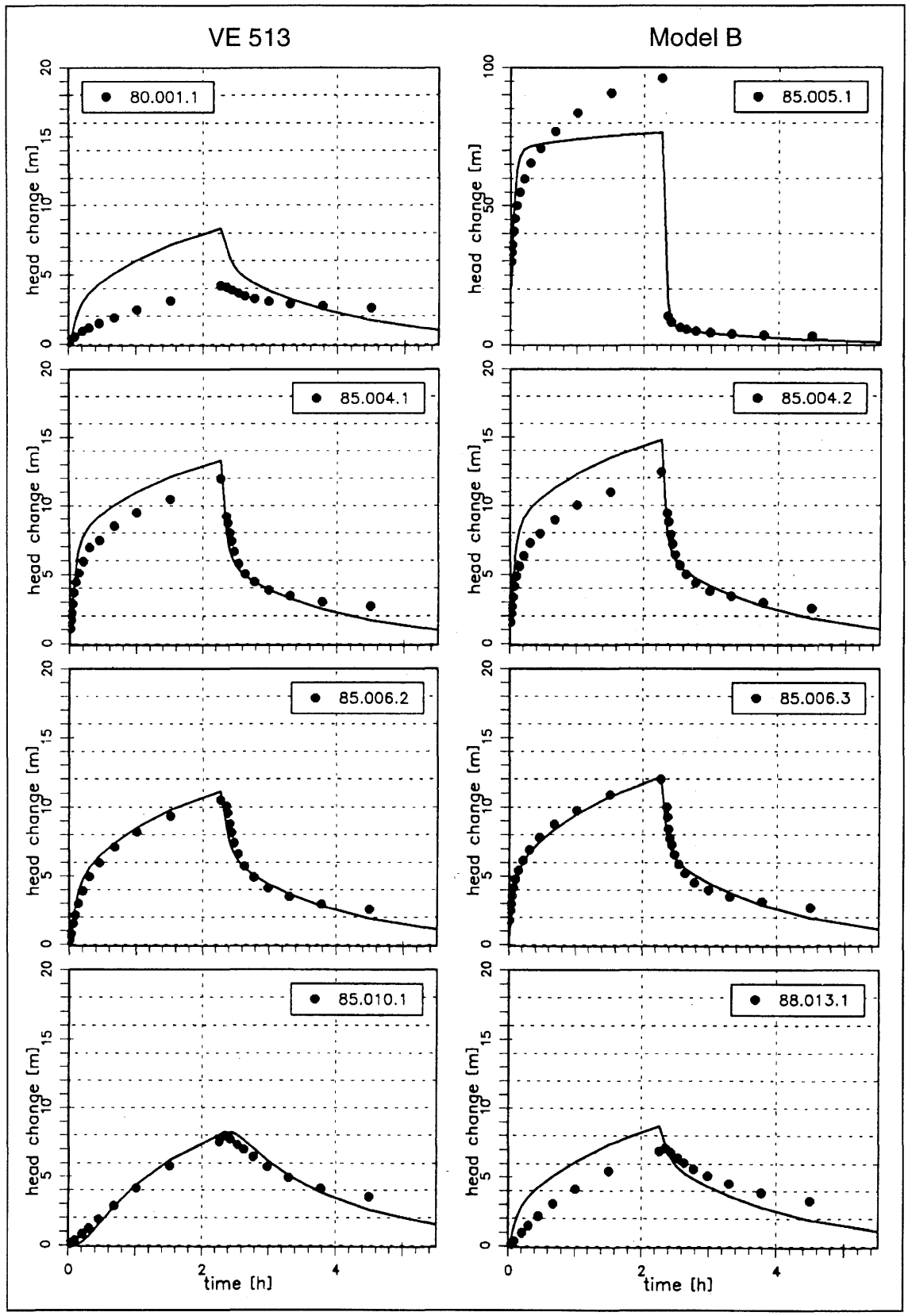

Fig. 8.7: Comparison of computed and measured head variation for Model B

Tab. 8.5: Computed model parameters, approx. 95 % confidence intervals and standard deviations for Model B

Parameter	Transmissivity [m^2/s]	lower bound of 95 % conf. int. [m^2/s]	upper bound of 95 % conf. int. [m^2/s]	Standard[4] deviation log[m^2/s]
LamN	2.57E-07	2.16E-07	3.06E-07	3.78E-02
K^+	2.32E-06	2.28E-06	2.37E-06	4.49E-03
#902	1.21E-06	1.17E-06	1.25E-06	7.10E-03
#954	1.17E-06	1.13E-06	1.22E-06	8.48E-03
#907	4.75E-07	4.47E-07	5.05E-07	1.33E-02
	Storage coefficient [-]	[-]	[-]	log[-]
LamS	2.66E-05	2.59E-05	2.73E-05	5.83E-03
K^+	7.98E-06	7.60E-06	8.37E-06	1.05E-02
#902	3.23E-06	3.03E-06	3.45E-06	1.42E-02
#954	5.05E-06	4.86E-06	5.25E-06	8.41E-03
#907	2.30E-10	0	∞	1.30E+02

8.5.4 Sensitivity analysis

The objective of this section is to give examples of how an insight into the physical behavior of the modeled system can be increased by a sensitivity study. Note that the sensitivity of the model parameters is a by-product of the inverse simulations and does not require much additional computational effort. In a first step, contributions of the individual test sections to the model performance are calculated in terms of the sum (in time) of the weighted residuals (see also equation 8.2 ff):

$$R_m = \sum_{k=1}^{M^t} \rho_m^k \qquad (8.9)$$

m - test/observation interval

M^t - number of observation times

$$\rho_m^k = \frac{r_{hm}^k}{\sqrt{\sigma_h v_{hm}^k}}$$

where index k denotes the values of the corresponding vector at observation time k.

The spatial distribution of these residuals with respect to the individual observation intervals provides a good indication of the localized model performance in different

[4] related to the log value of the parameter

directions of the model area. Large residuals calculated for a specific interval are an indication that the structural model is poorly represented at that particular location and might be improved. In this context, a positive residual means that the response has been overestimated by the simulation. In other words, the hydraulic connection between the observation interval and the test interval is weaker than expected. When the residual is negative, it can be concluded that additional hydraulic features in the vicinity of the observation interval would improve the data match.

In Fig. 8.8, some of the residuals are shown for inverse run A.2. As seen in the Figure the intervals BK 85.004.2, 85.008.2 and 85.010.1 provide the largest contribution to the objective function. It is an interesting fact that those intervals located close to the northern lamprophyre (plane D, BK 85.008 and 85.010) tend to show negative residuals, whereas most of the intervals in the vicinity of the source interval provide positive values. When comparing the structural Model A with the "minimal fracture network" derived in Chapter 7, it becomes clear that those K zones which are oriented subparallel to plane D (see Fig. 7.8) might increase the connectivity of the northern part of the BK site considerably and therefore would cause a better response of the observation intervals. Alternatively another S zone might be added beyond the fractures #902 and #954 as identified within the scope of the Salt/Heat Tracer Test.

The dependence of the residuals R_m on the total set of model parameters

$$G_m = \sum_{j=1}^{N} \frac{\partial R_m}{\partial p_j} \tag{8.10}$$

is illustrated in Fig. 8.9 where the contributions to the gradient of the objective function (see equation 8.3) are summed over time and over the parameters. G_m is an indicator of how much the observations in a certain interval may be influenced by parameter variations. Apparently, the residuals in interval BK 85.004.2 as well as in interval 85.005.1 are most sensitive to parameter variations. In order to determine which of the parameters and which fracture zones affect the heads in these observation intervals most, Fig. 8.10a and b present the computed sensitivities in these test sections summed over time:

$$\Phi_m = \sum_{k=1}^{M^t} \frac{\partial z_{hm}^k}{\partial p_j} \tag{8.11}$$

Multiplying the discrete sensitivities (in time) by the corresponding residuals:

$$g_{mj} = \sum_{k=1}^{M^t} \frac{\partial z_{hm}^k}{\partial p_j} \rho_m^k \tag{8.12}$$

yields the contribution of the test sections to the objective function gradient (Fig. 8.10c, d). Negative bars indicate an improvement of model performance (decreasing objective function) if model parameters are increased, positive bars indicate the opposite. Obviously, increasing the transmissivity of fracture zone #954 (S^-) leads to

significant response reduction in both intervals considered (Fig. 8.10a, b). However, this would cause an improvement of model performance only in 85.004.2 (Fig. 8.10d). Either heterogeneous conditions or an additional fracture intersecting between both test sections may be responsible for this contradictory behavior.

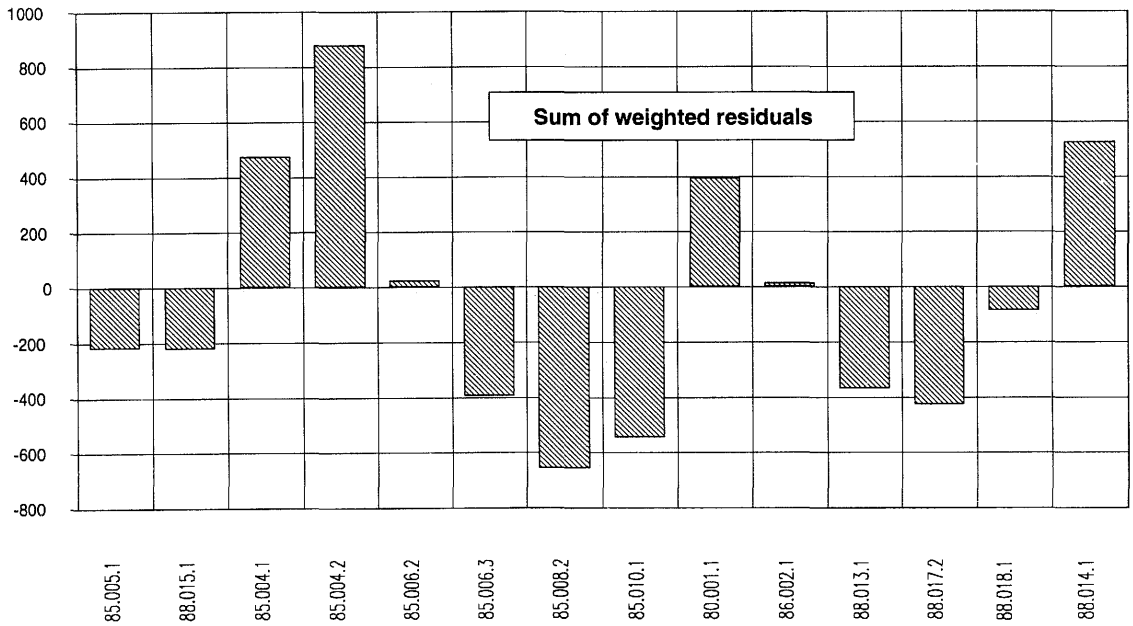

Fig. 8.8: Sums of computed residuals (equation 8.9) for the individual test sections (run A.2)

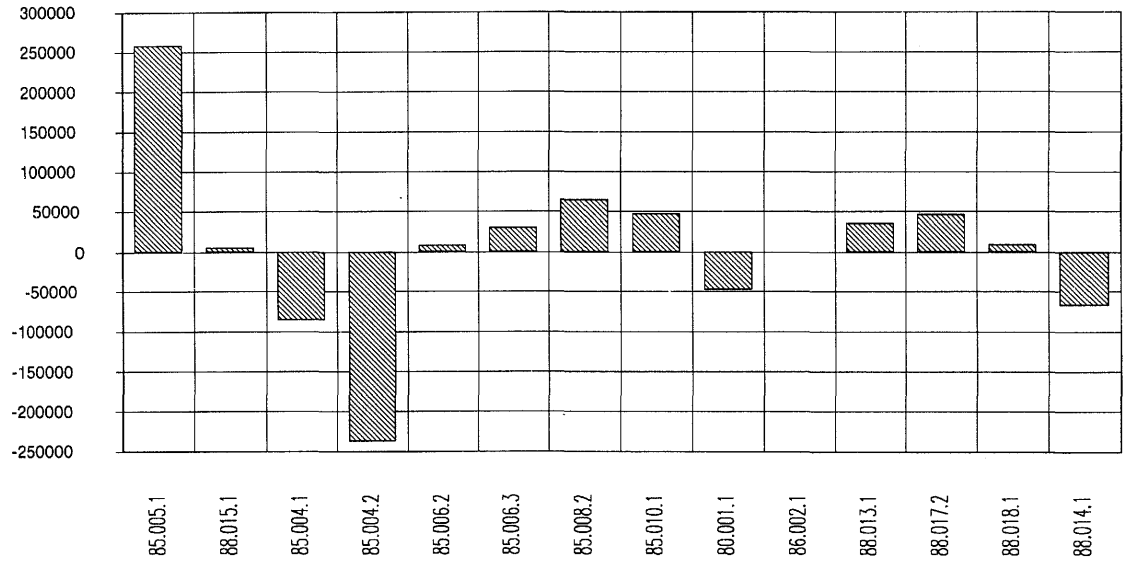

Fig. 8.9: Gradient contributions (equation 8.10) for the individual test sections (run A.2)

a) Sum of sensitivites

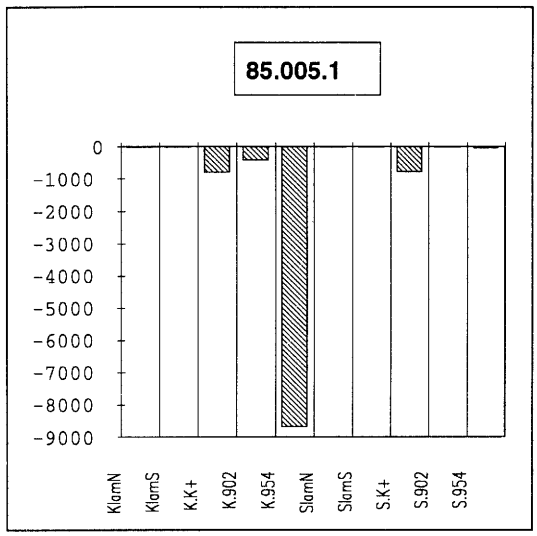

b) Sum of sensitivities

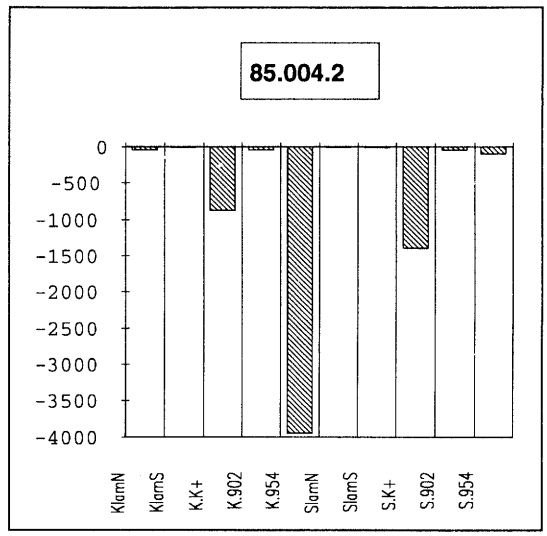

c) Sum of gradient contributions

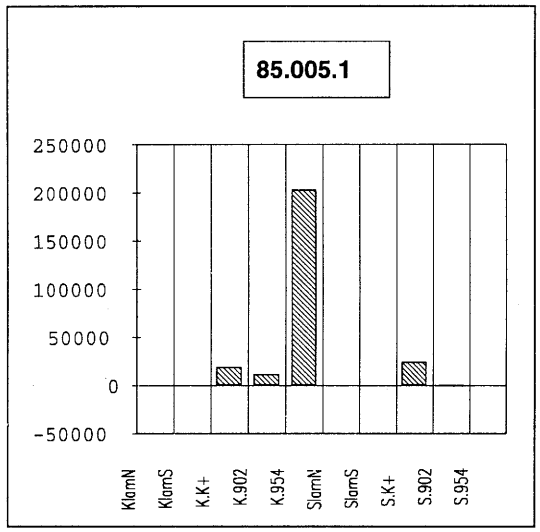

d) Sum of gradient contributions

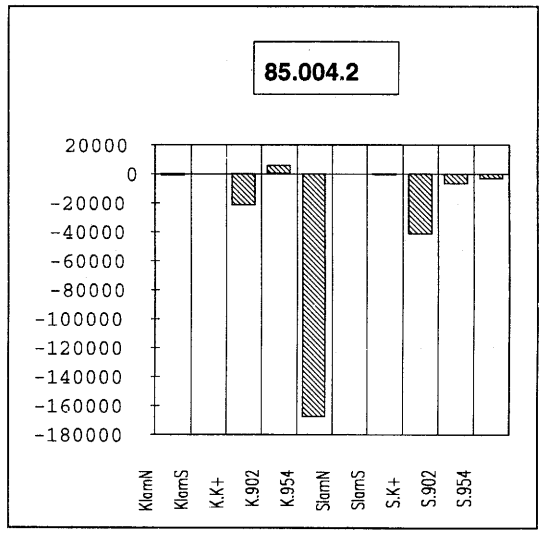

Fig. 8.10: Sums (over time) of sensitivities (equation 8.11) and gradient contributions (equation 8.12) for individual test sections (run A.2)

8.5.5 Run-time environment

The computations were carried out on both a Sun Sparc10 workstation and a Kubota/Stardent vector computer. Due to the iterative matrix solver (PCCG) in CASA, the solution of the FE system depends heavily on the conditions to be simulated (parameters, injection rate). In some interim cases, where the model parameters were unfavorably selected by the optimization algorithm (e.g. step length too large), con-

vergence was very poor so that the maximum number of PCCG iterations was exceeded (the current setting is 250). In its final parameter status, Model A with about 2000 nodes took 10 s per system solution (time step) on the Sun (the Stardent is approximately 30 % slower). One forward solution (direct problem) took about 3000 s (300 time steps). CPU-time needed for parameter estimation is N+1 times the forward solution time if Levenberg-Marquardt minimization is used, where N is the number of model parameters. Thus, one inverse solution took about 2 to 3 days, the number of parameter iterations being 5 to 10.

8.6 Principal findings and conclusions

The emphasis of the present study was to gain experience with the simulation of flow in fractured formations as a final step of site characterization. The selected modeling approach was based on the assumption that the fracture network can be described deterministically by a small number of planar features which intersect each other in a more or less complex manner. The extensive database which was compiled during previous investigation phases was used to develop a conceptual model of flow at the BK site. In this concept, flow takes place exclusively in a network of discrete, planar fractures, which can be localized deterministically by structural analysis of drillcores and by fracture mapping at the tunnel surface. The concept was converted into two alternative numerical models. Data from a crosshole hydrotest previously performed at the BK site were used to calibrate the models in terms of an automatic inverse modeling procedure. Finally a sensitivity study followed the different possibilities to analyse results of an inverse study. The major findings of the fracture modeling activities are summarized below:

- simulation of transient flow in fracture zone systems, in particular in conjunction with inverse modeling, is extremely expensive. The initial conceptual model of the BK site, which had been developed by jointly analysing structural and hydrodynamic data, was too complex to be converted into a numerical model. In the present study, the final conceptual model consisted of 5 and 6 fractures, respectively, instead of 14, as required for a complete representation of the BK fracture system.
- fracture zone modeling requires modified techniques for discretization and mesh generation. In the scope of the present studies, a special preprocessor has been developed to refine and equalize distorted elements of an existing mesh by specifying a maximum edge length or a maximum distortion factor for the elements. Furthermore a sequential mesh generation procedure was developed and tested successfully. In particular, the correct representation of flow into small structures (e.g. boreholes) had to be ensured, because some of the boreholes intersected several fractures and therefore acted as short-circuits between those features.
- model calibration with an automatic inverse modeling scheme has been successfully tested, although it required huge computational effort. Keeping in mind that a very simple structural model was used, the match between the observed and the computed heads is surprisingly good. The estimated hydrodynamic parameters are reasonable and agree rather well with the results of previous investigations. The relatively large storage coefficients, which occur particularly in Model A,

support the presumption of a free surface in the BK flow system, which could not be modeled explicitly.

- The sensitivity study provided some interesting insights into the basic structure of the BK fracture system: although it has not been indicated by the structural analysis, the northern part of the fracture system seems to be more intensively connected than the southern part. This might be due to additional K zones in the vicinity of the northern lamprophyre, which have been postulated by structural geologists but have not been found in the drillcores, because they strike more or less parallel to the orientation of the boreholes.

In summary, the investigations indicated, that the simulation of flow in fractured formations is basically restricted by computer capacity. During this work, we have provided numerical tools to generate a deterministic structural model of the fracture system and optimization procedures to calibrate the numerical model automatically. The results of the inverse modeling procedure were encouraging insofar as the actual field data could be matched fairly well with an extremely simple structural model. Potential future studies should focus mainly on the improvement of the model perfomance by extending the model complexity. The following activities are recommended:

- generating the complete "condensed fracture zone system" as proposed in Chapter 7. The performance of different model variants, including the hypothesis of a stochastically generated K fracture system, should be tested and improved by a sensitivity analysis as proposed in Section 8.5.4.

- analysing Multiple Source Crosshole Tests (MSCT, see Chapter 5) in terms of a joint inversion. This is expected to improve local performance of the calibrated model for different observation intervals.

Pressumably, such calculations would no longer be possible on the computer platform currently used (SUN Sparc 10 workstation). Nevertheless, a detailed simulation of the actual BK flow system, verified by the vast amount of hydrotest data available, would be a convincing example for flow modeling in a fractured formation.

9 HYDROGEOLOGICAL INVESTIGATIONS AT THE BK SITE

Results and benefits at the end of Phase 3

P. Marschall, S. Vomvoris (Nagra)

9.1 Hydrogeological investigations at the BK site: a retrospective

Nearly 10 years of hydrogeological investigations have elapsed, since the BK project was initiated. BGR was the principal investigator in the first two investigation phases. In Phase 3 of the BK program, Nagra reinforced its research activities considerably, motivated by the increased importance which has been ascribed to flow processes in fractured formations during the current site studies for low and high/intermediate level waste disposal. Intentionally, the BK project provides an excellent opportunity to develop and test new equipment, methodologies, interpretations and modeling approaches under well-defined conditions, aiming to transfer this know-how to the actual site investigation programs. Now, at the end of the project, a number of questions inevitably arise, concerning the benefit of the BK research activities: do we now have a reliable procedure for the hydraulic characterization of a fractured formation? Which exploration/investigation methods have been successful and might be transferred to a site program? Which of them failed? Would we start another fracture flow project in the same way?

Undoubtedly, the most valuable information about the internal structure of the BK fracture system was gained by the inspection of borecores and by fracture mapping at the tunnel walls. The large number of boreholes drilled to explore the extent of the site and to investigate the structural setup provided a detailed picture of the boundaries, the main classes of fractures and their relevance for the hydrogeological flow system. Nevertheless, from a hydrogeological point of view, these boreholes considerably disturbed the flow conditions at the site by short-circuiting different hydraulic features. Thus, not only was the global connectivity of the system increased artificially but also the head distribution at the site changed completely. Despite the large number of boreholes available, an important class of fractures (K fractures) has not been detected adequately with respect to its contribution to the BK flow system, as indicated by the analysis of the crosshole tests. This is because most of the boreholes are oriented parallel to the strike of these fractures, which resulted in a reduced probability of intersecting them during drilling. In summary, for a future site exploration concept it is strongly recommended to keep the number of boreholes as small as possible in order to minimize the disturbance of the flow system, and to avoid a preferential orientation of the boreholes which might lead to an unequal weighting of detected fracture orientations. Additionally, a well-structured strategy may help to derive a conceptual model of the fracture system without collecting superfluous data (see Chapter 7). In the case of the BK site, certainly, some of the boreholes need not have been drilled if a concise hydrogeological conceptualization at the BK site had started in an early stage of the exploration phase.

The sophisticated longterm monitoring system with multiple packers in each borehole did not fully accomplish expectations: despite the large number of packers, short-circuits in the boreholes could not be avoided completely during long-term pressure observation, nor during tracer tests or hydrotests. To isolate all hydraulic features individually, the number of observation intervals required would be twice as great

(about 60 instead of 30 intervals), which is no longer realistic from the point of view of cost. Further problems arose: the gas-filled packers had to be checked frequently and they lost gas into the formation. On the other hand, the downhole equipment for pressure monitoring was damaged occasionally by lightning or by failure of the sealings. Thus, one of the main objectives of the longterm monitoring, the determination of stabilized hydraulic heads in the BK system, was hardly achieved because the recovery period at the BK site could never be monitored for longer than about 3 months. However, it should be mentioned that other longterm monitoring systems have been tested at the GTS, which consist of water-filled packers with a surface head monitoring system. These systems have proved to be much more reliable and they fit the requirements of long-term head monitoring.

Unquestionably, the greatest benefit of the BK investigation program was the development of equipment and methodologies for site characterization. As mentioned in Chapter 7, the most important data used to build a conceptual hydrodynamic model of the BK site were obtained by the fluid logging and the hydraulic crosshole testing. The crosshole fluid logging at the end of BK Phase 2 provided useful hints on the connectivity of a fracture network, although a quantitative analysis of such tests is difficult. Besides this, the analysis of the first crosshole hydrotest campaign (VE451-455) increased experience with the interpretation of such tests under conditions of a fracture network. In particular, the novel developments of fluid logging with fixed probes and the Multiple Source Crosshole Test (MSCT) improved the hydrogeological means available for detailed characterization of fractured formations: inflow points and inflowrates can be determined even in inclined boreholes and the structural properties as well as the hydraulic connectivity of a fracture network can be resolved better. Apart from some minor modifications, both developments are expected to be applicable as standard procedures in future site investigation programs.

Another promising experiment was the Salt/Heat Tracer Test. Although this test is far from becoming a routine experiment for site characterization because its applicability is limited due to the long test duration and the relatively weak thermal response, the concept of using complementary flow-fields and complementary tracers to describe the complex flow and transport properties of the fracture network seems to be an extremely challenging topic in hydrogeological research. As a contribution to the safety assessment, the investigations may serve to provide a better insight into the basic processes which determine flow and transport in fractured formations.

In the present studies on hydrodynamic modeling, we have chosen a deterministic approach to deriving a simplified structural model of the BK fracture system. A conceptualization procedure was presented, providing the structural model of the BK fracture system with boundary conditions, initial conditions and prior information. Besides this, tools for a refined mesh generation were developed and an inverse modeling scheme was tested. A calibration exercise and a sensitivity analysis were carried out to gain experience with the numerical and interpretational aspects of model calibration of fracture systems. We are aware that a complete validation of the calibrated flow model has not been performed and that there are some basic open questions left which could not be solved within the framework of this study. Nevertheless, the encouraging first results of the flow simulations showed that this problem is mainly due to the restricted availability of computer capacity and manpower, at least in the case of a sparsely fractured medium - when the main hydraulic features can be described deterministically.

9.2 The current conceptual model of the BK fracture system

In Chapter 7, an extensive study of structural data and hydrodynamic investigations previously performed at the BK site was carried out to derive a conceptual model of the hydrodynamic processes in the BK fracture system. Here we present the findings in a condensed form:

- The BK fracture system is hydraulically restricted by the lamprophyre dykes, which act basically as no-flow boundaries. This was clearly confirmed by the longterm monitoring of hydraulic heads.

- Unless a full pressure recovery is achieved with stabilized pressures (which was hardly ever the case), a free surface is observed in the BK hydraulic system. The actual elevation (above the altitude of the cavern) of the free surface depends on the water balance, which consists of the water recharge across the boundaries into the fracture system and the drainage by the BK cavern.

- The total number of fractures detected using fracture mapping and core inspection was immense. However, only a very limited number of fractures are hydraulically active. A contribution of the matrix to the BK flow system could not be proved.

- Recent crosshole hydrotests have pointed out the importance of the S fractures in the vicinity of the northern lamprophyre for the hydrodynamic model. In previous studies, the contribution of these features was underestimated.

- The microscopic flow pattern along the hydraulic features seems to be rather complex, although the features can be described as planar elements in the conceptual model. Even for transport processes along individual features, the rock volume which is accessible for (thermal) matrix diffusion is considerably larger than expected for a single fracture.

Meanwhile, the hydrodynamic behaviour of the BK site is well understood. Many of the obscure observations, which arose in terms of the hydrotesting and longterm pressure monitoring, can be attributed to the finite extent of the BK fracture system and the existence of a free surface. The simple modeling investigations have shown that we have gained a basic insight into the main hydrodynamic processes at the BK site and the procedure which has been outlined to improve the model performance would definitely increase our knowledge. However, it was never the aim of the BK project to perform an extensive characterization of a specific site but rather to provide an opportunity for application-oriented research within the broad framework of fracture flow investigations.

10 REFERENCES

ABRAMOWITZ, M. & STEGUN, I.A. (1970): Handbook of mathematical functions with formulas, graphs and mathematical tables. Dover Publications, Inc., New York.

AVDEYENKO, V.A. & MALYUKOV, A.A. (1989): A quadrature formula for the Fourier Integral based on the use of a Cubic Spline. U.S.S.R. Comput. Maths. Math. Phys. 29(3).

AVS MANUALS (1992): Developer's Guide; User's Guide; Module Reference; AVS Release 4, Advanced Visual Systems Inc. Waltham, MA 02154, May 1992.

AVS MANUALS (1993): Advanced Visual Systems Inc. Waltham, MA 02154, February 1993.

BARCZEWSKI, B. & SCHMID, G. (1992): Pilotversuch zum Fluidlogging mit stationären Sonden. Unpubl. Ber. Univ. Stuttgart v. Dez. 1992 z.H. der Nagra. Nagra, Wettingen, Switzerland.

BEAR, J., VERRUIJT, A. (1987): Modeling groundwater, flow and pollution. D. Reidel Publishing Company. Dordrecht, NL.

BGR handout (1991a): Bohrlochkranzversuch III. Tischvorlage zur 8. AK-BK Sitzung am 29.08.1991. Unpubl. BGR Rep. Bundesanstalt für Geowissenschaften und Rohstoffe, Hannover, Germany.

BGR handout (1991b): Bohrlochkranzversuch III. Tischvorlage zur 9. AK-BK Sitzung am 29.08.1991. Unpubl. BGR Rep. Bundesanstalt für Geowissenschaften und Rohstoffe, Hannover, Germany.

BGR handout (1993): Bohrlochkranzversuch III. Tischvorlage zur 13. AK-BK Sitzung am 17.08.1993. Unpubl. BGR Rep. Bundesanstalt für Geowissenschaften und Rohstoffe, Hannover, Germany.

BLACK, J.H. & KIPP, K.L. (1981): Determination of hydrogeological parameters using sinusoidal pressure tests: A theoretical appraisal. Water Resour. Res. 17/3.

BLASER, P. (1994): FLG: Bohrlochkranzversuch - Dokumentation der BK-Datenbank. Unpubl. Nagra Interner Bericht. Nagra, Wettingen, Switzerland.

BOSSART, P. & MAZUREK, M. (1991): Grimsel Test Site: Structural geology and water flow paths in the migration shear-zone. Nagra Technischer Bericht NTB 91-12. Nagra, Wettingen, Switzerland.

BOSSART, P., DOLLINGER, H. & MÜRI, F. (1993): Hydromodellierung BK - Konzeptuelles Modell. Unpubl. Memorandum Geotech. Inst. Bern March, 1993 z.H. der Nagra. Nagra, Wettingen, Switzerland.

BRÄUER, V., KILGER, B. & PAHL, A. (1989): Felslabor Grimsel. Ingenieurgeologische Untersuchungen zur Interpretation von Gebirgsspannungsmessungen und Durchströmungsversuchen. Nagra Technischer Bericht NTB 88-37. Nagra, Wettingen, Switzerland.

CARRERA, J. (1984): Estimation of aquifer parameters under transient and steady-state conditions. Diss. University of Arizona, Tucson.

CARRERA, J. & NEUMAN, S.P. (1986a): Estimation of aquifer parameters under transient and steady-state conditions: 1. Maximum Likelihood Method incorporating prior information. Water Resour. Res. 22/2, 199-210.

CARRERA, J. & NEUMAN, S.P. (1986b): Estimation of aquifer parameters under transient and steady-state conditions: 2. Uniqueness, stability and solution algorithms. Water Resour. Res. 22/2, 211-227.

CARRERA, J. & NEUMAN, S.P. (1986c): Estimation of aquifer parameters under transient and steady-state conditions: 3. Application to synthetic and field data. Water Resour. Res. 22/2, 228-242.

CARSLAW, H.S. & JAEGER, J.C. (1959): Conduction of heat in solids. Oxford University Press.

CHARBENEAU, R.J & STREET, R.L. (1979): Modeling groundwater flow-fields containing point singularities: A technique for singularity removal. Water Resour. Res. 15/3, 583-594.

CRAVEN, P. & WAHBA, G. (1979): Smoothing noisy data with spline functions. Numerische Mathematik 31, 377-403.

DORNSTÄDTER, J. (1987): Das Temperaturangleich-Verfahren (TAV), ein Verfahren zur in-situ Bestimmung thermischer Gesteinseigenschaften. Unpubl. Dipl.arb. Univ. Karlsruhe, Germany.

DORNSTÄDTER, J., THRIEMER, T. & WELTER, M. (1993): Rohdatenbericht, Fluidlogging, Bohrungen BK8 und BK15, Felslabor Grimsel. Unpubl. GTC Bericht. GTC, Karlsruhe, Germany.

DRISCOLL, F. (1986): Groundwater and wells. Johnson Division Publ. St. Paul, Minnesota, USA.

DUFFY, C.J. & GELHAR, L.W. (1985): A frequency domain approach to water quality modeling in groundwater: Theory. Water Resour. Res. 21/8.

EARLOUGHER Jr., R.C. (1977): Advances in well test analysis. Soc. of Petrol. Monograph 5 of the Henry L. Doherty Series. Dallas.

ELSWORTH, D. (1986): A model to evaluate the transient hydraulic response of 3D sparsely fractured rock masses. Water Resour. Res. 22/13, 1809-1819.

FRICK, U., ALEXANDER, W.R., BAEYENS, B., BOSSART, P., BRADBURY, M.H., BUEHLER, C., EIKENBERG, J., FIERZ, T., HEER, W., HOEHN, E., McKINLEY, I.G. & SMITH, P.A. (1992): The radionuclide migration experiment. Overview of investigations 1985-1990. Nagra Technischer Bericht NTB 91-04. Nagra, Wettingen, Switzerland.

GEOTEST AG, ZOLLIKOFEN & INGENIEURUNTERNEHMUNG AG BERN, BERN (1981): Sondierbohrungen Juchlistock - Grimsel. Nagra Technischer Bericht NTB 81-07. Nagra, Wettingen, Switzerland.

GIECK, K. (1979): Technische Formelsammlung. Gieck Verlag Heilbronn, Germany.

GRINGARTEN, A. (1984): Interpretation of tests in fissured and multi-layered reservoirs with double-porosity behaviour: Theory and Practice. J. Petrol. Techn., distinguished author series.

GROSSWIG, S., HURTIG, E. & KÜHN, K. (1993): FLG: Bohrlochkranzversuch, Untersuchungen zum Einsatz faseroptischer Temperatur-Messtechnik beim Fluidlogging in kleinkalibrigen Schrägbohrungen. Unpubl. Nagra Interner Bericht. Nagra, Wettingen, Switzerland.

GUERRA, V. & TAPIA, R.A. (1974): A local procedure for error detection and data smoothing. MRC Technical Summary Report 1452, Mathematics Research Center. Univ. of Wisconsin, Madison.

GUYONNET, D. & LAVANCHY, J.-M. (1992): Analysis of single and crosshole tests at the BK site, Grimsel Test Site. In: VOMVORIS, S. & FRIEG B, (eds.): Interpretation of crosshole hydraulic tests and a pilot fluid logging test for selected boreholes within the BK Site. Nagra Technischer Bericht NTB 91-09. Nagra, Wettingen, Switzerland.

GUYONNET, D. & DOMSKI, P. (1993): Raw data report for the Multiple Source Crosshole Test performed at the BK Site, Grimsel Test Site, 25.11.92 to 03.12.92. Unpubl. Colenco Report. Colenco Power Consulting AG. Baden, Switzerland.

GUYONNET, D. & MARSCHALL, P. (1993): GTS: Fracture Flow Test. Interpretation of the Multiple Source Crosshole Test. Unpubl. Nagra Interner Bericht. Nagra, Wettingen, Switzerland.

HARTOG, A. & GAMBLE, G. (1991): Photonic distributed sensing. Physics World 3, 45-49.

HEINEMANN-GLUTSCH, B. & DORNSTÄDTER, J. (1993): Fluidlogging mit stationären Temperatursonden, Interpretation der Meßdaten Bohrungen BK8 und BK15. Unpubl. GTC Bericht. GTC, Karlsruhe, Germany.

HÜRLIMANN, W. (1994): FRACMESH - A program for the generation of finite element meshes for the hydrodynamic modeling of fractured rock. Nagra Technischer Bericht NTB 93-46. Nagra, Wettingen, Switzerland.

HURTIG, E., SCHRÖTTER, J., GROSSWIG, S., KÜHN, K., HARJES, B., WIEFERIG, W. & ORRELL, R.P. (1993): Borehole temperature measurements using distributed fibre optic sensing. Scientific Drilling 3, 283-286.

IMSL LIBRARY REFERENCE MANUAL (1987): FORTRAN subroutines for mathematical applications, Vers. 1.0. Houston, Texas.

JENKINS, G. & WATTS, P. (1968): Spectral analysis and ist applications. Holden Day, San Francisco.

JOUANA, P. (1992): Technical Note: Access to stochastic fractured media characteristics by harmonic hydraulic pumping. Int. J. Rock Mech. Min. Sci. & Geomech. Abstr. 29/1, 83-87. Pergamon Press, Great Britain.

KELLEY, V.A., LAVANCHY, J.-M. & LOEW, S. (1991): Transmissivities and heads derived from detailed analysis of Siblingen 1989 fluid logging data. Nagra Technischer Bericht NTB 90-09. Nagra, Wettingen, Switzerland.

KELLEY, V. & LOEW, S. (1992): Analysis of pilot crosshole fluidlogging tests at the BK Site Grimsel Test Site. In: VOMVORIS, S. & FRIEG, B. (eds.) 1992: Interpretation of crosshole hydraulic tests and a pilot Fluidlogging test for selected boreholes within the BK Site. Nagra Technischer Bericht NTB 91-09. Nagra, Wettingen, Switzerland.

KEUSEN, H., GANGUIN, J., SCHULER, P. & BULETTI, M. (1989): Grimsel Test Site. Geology. Nagra Technical Report NTB 87-14E. Nagra, Wettingen, Switzerland.

KOHL, T. (1992): Modellsimulation gekoppelter Vorgänge beim Wärmeentzug aus heissem Tiefengestein. Ph.D. thesis no. 9802. Eidgen. Technische Hochschule ETH Zürich, Switzerland.

KOHL, T. (1993): Numerische Designstudie Salz-Wärme Dipolversuch. Unpubl. Nagra Interner Bericht. Nagra, Wettingen, Switzerland.

KOHL, T., CORREA, N.R. & RYBACH, L. (1994): FLG: Design and interpretation of a combined salt and heat transfer experiment in the Grimsel rock laboratory. Unpubl. Nagra Interner Bericht. Nagra, Wettingen, Switzerland.

KUHLMANN, U. (1989): Modeling small structures in Finite Elements. Unpubl. Interner Ber. Versuchsanstalt für Wasserbau, Hydrologie und Glaziologie. ETH Zürich, Switzerland.

KUHLMANN, U. (1992): Inverse Modellierung in geklüfteten Grundwasserträgern. Versuchsanstalt für Wasserbau, Hydrologie und Glaziologie, Mitteilung Nr. 120. Zürich, Switzerland.

KUHLMANN, U. (1994): Inverse Modellierung in geklüfteten Grundwasserträgern. Nagra Technischer Bericht NTB 93-19. Nagra, Wettingen, Switzerland.

KUHLMANN, U. & CORREA, N. (1993): Inverse modeling in the central BK-fracture zone area. Unpubl. Nagra Interner Bericht. Nagra, Wettingen, Switzerland.

KUNSTMANN, H. (1994): Inverse zweidimensionale Modellierung des Transports von Tracern in Dipolfliessfeldern eines Kluftnetzwerks. Institut für Umweltphysik, Universität Heidelberg, Diplomarbeit. Heidelberg, Germany.

LANDOLT-BÖRNSTEIN (1982): Physical properties of rocks, Volume I (Subvolume 6). Springer Berlin/Heidelberg/New York.

LI, G.M. & KINZELBACH, W. (1993): Felslabor Grimsel: Bohrlochkranzversuch - Auswertung von Dipol-Tracertests, Programmdokumentation GTTS (Groundwater Tracer Test Simulation). Unpubl. Nagra Interner Bericht. Nagra, Wettingen, Switzerland.

LIEDTKE, L., NAUJOKS, A., BRÄUER, V., SIEMERING, W. & KOHLENBERG, K. (1989a): Bohrlochkranzversuch. BMFT-Forschungsvorhaben Forschungsvorhaben KWA 3504 A5, Archiv-Nr. 106637, Tagebuch-Nr. 10302/90. Bundesanstalt für Geowissenschaften und Rohstoffe, Hannover, Germany.

LIEDTKE, L., NAUJOKS, A., BRÄUER, V., SIEMERING, W. & KOHLENBERG, K. (1989b): Bohrlochkranzversuch (Fracture System Flow Test), Anlage 26 (sog. "Bräuer-Daten"). BMFT-Forschungsvorhaben KWA 3504 A5, Archiv-Nr. 106637, Tagebuch-Nr. 10302/90. Bundesanstalt für Geowissenschaften und Rohstoffe, Hannover, Germany.

LONG, J.C.S. (1992): Evaluation of the US/BK hydraulic test data. Unpubl. Memorandum, LBL, California.

MARTEL, J.S. & PETERSON, J.E. (1991): Interdisciplinary characterization of fracture systems at the US/BK Site, Grimsel Laboratory, Switzerland, Int. J. Rock Mech. Min. Sci. & Geomech. Abstr. 28/4, 295-323.

MARSCHALL, P. & JOHNS, R. (1993): Spectral analyses of hydraulic crosshole tests. Unpubl. Nagra Interner Bericht. Nagra, Wettingen, Switzerland.

MISHRA, S. (1992): Methods for analyzing single- and multi-well hydraulic test data. In: VOMVORIS, S. & FRIEG, B. (eds.): Interpretation of crosshole hydraulic tests and a pilot fluid logging test for selected boreholes within the BK Site, Grimsel Test Site. Nagra, Technischer Bericht NTB 91-09. Nagra, Wettingen, Switzerland.

MOHR, S. (1993): Quick Look Report über den Salz-Wärme-Tracer-Versuch im Felslabor Grimsel vom 22.02.93-24.03.93. Unpubl. Rep. v. 08.06.93 z.H. der Nagra. Nagra, Wettingen, Switzerland.

MÜRI, F., CORREA, N. & BOSSART, P. (1993): Visualisierung hydrogeologischer Informationen des Bohrlochkranzversuchs im FLG. Unpubl. Nagra Interner Bericht Nagra, Wettingen, Switzerland.

MURPHY, H.D. (1977): Fluid injection profiles - A modern analysis of wellbore temperature surveys. Soc. Petrol. Eng., SPE 6783.

MURPHY, H.D. (1982): Enhanced interpretation of temperature surveys taken during injection or production. J. Petrol. Techn., 1313-1326.

NAGRA, BGR & GSF (1985): Felslabor Grimsel - Rahmenprogramm und Statusbericht. Nagra Technischer Bericht NTB 85-34. Nagra, Wettingen, Switzerland.

NEUMAN, S. (1972): Theory of flow in an unconfined aquifer considering delayed response of the water table. Water Resour. Res. 8/4.

NEUMAN, S. (1975): Analysis of pumping test data from anisotropic unconfined aquifers considering delayed gravity response. Water Resour. Res. 11/2.

NIVA, B., OLSSON, O. & BLÜMLING, P. (1988): Radar Crosshole Tomography with application to migration of saline tracer through fracture zones. Nagra Technischer Bericht NTB 88-31. Nagra, Wettingen, Switzerland.

PAHL, A., LIEDTKE, L., NAUJOKS, A. & BRÄUER, V. (1992): Felslabor Grimsel: Bohrlochkranzversuch. Durchströmung von geklüftetem Fels. Nagra Technischer Bericht NTB 91-01. Nagra, Wettingen, Switzerland.

PFINGSTEN, W. (1990): Stofftransport in Klüften mit porösen Gesteinen. Interne Mitt. Heft 73. Institut für Wasserwirtschaft, Hydrologie und landw. Wasserbau der Universität Hannover, Germany.

PICKENS, J., GRISAK, G., AVIS, J., BELANGER, D. & THURY, M. (1987): Analysis and interpretation of borehole hydraulic tests in deep boreholes: Principles, model development, and applications. Water Resour. Res. 23, 1341-1375.

RATZ, U. (1993): Stationary multiprobe-testing at Lawrence Berkeley Laboratory California, USA. Unpubl. Solexperts Rep. Solexperts, Schwerzenbach, Switzerland.

RITZI, R.W., SOROOSHIAN, S. & GUPTA, V.K. (1991): On the estimation of parameters for frequency domain models. Water Resour. Res. 27/5.

SCHELLSCHMIDT, R. & HAENEL, R. (1987): Influx and water loss in open-hole sections of boreholes determined by temperature measurements. Geol. Jb. E39, 101-108.

SCHICKETANZ, D. (1981): Anwendung des Rückstreumessprinzips in der Lichtwellenleitertechnik. Siemens Forschungs- und Entwicklungs-Berichte, 10/1, 53.

SHAPIRO, A.M. & BEAR, J. (1985): Evaluating the hydraulic conductivity of fractured rock from information on fracture geometry. Hydrogeology of rocks of low permeability. Internat. Assoc. Hydrogeologists Memoirs 17, 4633-472.

STIESS, H. (1990): Berechnungen zum Wärme-, Stoff- und Nuklidtransport in einer Einzelkluft mit Hilfe von NAMMU: Theoretische Grundlagen, Verifikation und Berechnung der Wärmeausbreitung in einem zweidimensionalen Kluft-Matrix-System. Unpubl. Nagra Interner Bericht Nagra, Wettingen, Switzerland.

TSANG, C.F. & HUFSCHMIED, P. (1988): A borehole fluid conductivity logging method for the determination of fracture inflow parameters. Nagra Technischer Bericht NTB 88-13. Nagra, Wettingen, Switzerland.

TSANG, C.F., HUFSCHMIED, P. & HALE, F.V. (1990): Determination of fracture outflow parameters with a borehole fluid conductivity logging method. Water Resour. Res. 26/4, 561-578.

VOBORNY, O., ADANK, P., HÜRLIMANN, W., VOMVORIS, S. & MISHRA, S. (1991): Grimsel Test Site. Modeling of groundwater flow in the rock body surrounding the underground laboratory. Nagra Technischer Bericht NTB 91-03. Nagra, Wettingen, Switzerland.

VOMVORIS, S. & FRIEG, B. (eds.) (1992): Interpretation of crosshole hydraulic tests and a pilot fluid logging test for selected boreholes within the BK Site. Nagra Technischer Bericht NTB 91-09. Nagra, Wettingen, Switzerland.

WARREN, J.E. & ROOT, P.J. (1963): The behavior of naturally fractured reservoirs. Soc. Petrol. Eng. J., 245-55.